Springer Series on

Atoms+Plasmas 2

Editors: G. Ecker P. Lambropoulos H. Walther

Springer Series on

Atoms+Plasmas

Editors: G. Ecker P. Lambropoulos H. Walther

Volume 1 **Polarized Electrons** 2nd Edition
By J. Kessler

Volume 2 **Multiphoton Processes**
Editors: P. Lambropoulos and S. J. Smith

Multiphoton Processes

CONF-8409129--

Proceedings
of the 3rd International Conference,
Iraklion, Crete, Greece

September 5–12, 1984

Editors: P. Lambropoulos and S. J. Smith

With 101 Figures

Springer-Verlag
Berlin Heidelberg New York Tokyo 1984

Professor Peter Lambropoulos, Ph.D.
University of Crete, P. O. Box 470, Iraklion, Crete, Greece, and
Department of Physics, University of Southern California, University Park
Los Angeles, CA 90089-0484, USA

Professor Stephen J. Smith, Ph.D.
JILA, Campus Box 440, University of Colorado
Boulder, CO 80309, USA

Series Editors:

Professor Dr. Günter Ecker
Ruhr-Universität Bochum, Institut für Theoretische Physik, Lehrstuhl I, Universitätsstraße 150
D-4630 Bochum-Querenburg, Fed. Rep. of Germany

Professor Peter Lambropoulos, Ph.D.
University of Crete, P. O. Box 470, Iraklion, Crete, Greece, and
Department of Physics, University of Southern California, University Park
Los Angeles, CA 90089-0484, USA

Professor Dr. Herbert Walther
Sektion Physik der Universität München, Am Coulombwall 1
D-8046 Garching/München, Fed. Rep. of Germany

ISBN 3-540-15068-4 Springer-Verlag Berlin Heidelberg New York Tokyo
ISBN 0-387-15068-4 Springer-Verlag New York Heidelberg Berlin Tokyo

Offset printing: Weihert-Druck GmbH, 6100 Darmstadt
Bookbinding: J. Schäffer OHG, 6718 Grünstadt
2153/3130-543210

Preface

The chapters of this volume represent the invited papers delivered at the 3rd International Conference on Multiphoton Processes (ICOMP III) held in Iraklion, Crete, Greece, September 5-11, 1984. The invited papers at a conference like ICOMP cannot possibly cover the whole field which has grown to immense proportions in recent years, overlapping with such diverse areas as atomic and molecular spectroscopy, plasma physics, nonlinear optics, quantum optics, etc. We believe these contributions represent that part of the research activity which has been attracting the most interest in the past year or so, as well as reviews of some of the more established topics. Even within this scope, and given the confines imposed by the finite duration of a conference, important and timely topics are inevitably left out. But then, there will be ICOMP IV.

The collection of articles in this volume, combined with extensive references to related work given by the authors, should provide an introduction to the major problems of the field and its state of the art. The chapters have been arranged according to thematic proximity, beginning with atoms, and continuing on with molecules and surfaces. This classification, however, would not cover all the subject matter even within the limited scope of the conference and of this volume. Multiphoton physics is interdisciplinary and topics dealing with the stochastic properties of the field or with collisions and collective effects, to name a few, are part of the field and part of the conference. We have chosen to group such articles separately since they relate as much to atoms as they do to molecules.

The conference was made possible by financial support from the Greek Ministry of Research and Technology, the U.S. Department of Energy and National Science Foundation, as well as the International Union of Pure and Applied Physics. The support of Lambda Physik and Spectra Physics is also gratefully acknowledged.

Many people have contributed significantly to the success of the conference. In particular, members of the organizing committee and colleagues at the University of Crete must be recognized for their contributions to the programming and organization of the conference. Finally, ICOMP III would not have been the success it was without the dedication of Ms. Lia Papadopoulou who handled every detail with admirable professionalism.

P. Lambropoulos · S.J. Smith

Contents

Part III Multiphoton Processes in Molecules and Surfaces

Introduction

Peter Lambropoulos

University of Crete, P.O. Box 470, Iraklion, Crete, Greece, and

Department of Physics, University of Southern California, University Park Los Angeles, CA 90089-0484, USA

S.J. Smith

JILA, Campus Box 440, University of Colorado, Boulder, CO 80309, USA

Multiphoton transitions are found whenever electrons bound in atoms or molecules interact with sufficiently intense electromagnetic radiation. Multiphoton ionization is the ultimate outcome of multiphoton transitions provided the radiation is reasonably intense, which we will take to mean about 10^6 W/cm^2, or more, at optical frequencies. With intense sources and interaction times of the order of a nanosecond or more, ionization may be expected for atomic, and dissociation with varying degrees of ionization for molecular gases. For still higher intensities (about 10^{13}-10^{14} W/cm^2), ionization of anything in the interaction region can be predicted with certainty.

Although the end result of such interactions is evident, the underlying dynamics and interplay between atomic/molecular structure and radiation is what attracts the interest and defines the problems. Many features set such problems apart from traditional interaction of radiation with atoms and molecules. First of all, the interactions are nonlinear, which brings in a number of new phenomena. Second, a multiphoton transition probes atomic and molecular structure in a more involved and detailed way than can be imagined in single-photon spectroscopy. Third, owing to the high intensities available, one can reach extremely high levels of excitation, thus introducing qualitatively new physics. To these and other features, one should add the possibility of applications such as isotope separation, generation of coherent radiation at wavelengths shorter than ultraviolet, and plasma diagnostics.

Until about three years ago, most studies of multiphoton ionization centered around processes in which one electron was ejected with energy equal to $N\hbar\omega$-W, where N is the minimum number of photons necessary to bridge the ionization potential W. A number of interesting phenomena have emerged from such studies, especially those employing intermediate resonance with real atomic states. Work along these lines will of course continue, especially in view of its usefulness in the study of intermediate states.

Two recent important observations have opened a new dimension and introduced a host of substantively new problems. First, it has been found that photoelectrons with energy higher than the minimum necessary to bridge the ionization potential are ejected under certain conditions, which suggests that absorption of laser photons occurs into the continuum above the first ionization threshold. Second, multiply charged ions have also been found. This means that ionization of the ion remaining after the ejection of the first electron is relatively easy, or that two or more electrons can simultaneously make transitions to the continuum.

The first four articles in this volume deal with these topics. There are experimental situations in which it appears that a single electron continues absorbing photons above threshold and that the doubly ionized species come from subsequent multiphoton ionization of the first ion. On the other hand, experimental results under somewhat different conditions point to the possibility of two-electron transitions as well. Various aspects of this problem are discussed by Crance, by Agostini and Petite, and by Lompré and Mainfray. Under extreme conditions, i.e., higher intensity, there is the possibility that a whole atomic shell absorbs collectively in some sense, as argued by Rhodes. Even with additional absorptions, presumably by a single electron above the first threshold, important questions remain in connection with quantitative interpretation of the heights of the additional peaks.

Thus we have a new set of problems concerned with the understanding of multiphoton absorption in the continuum of an atom when the laser intensity is above 10^{10} W/cm^2, although there is ample evidence that continuum-continuum transitions may also play a role at lower intensities. In any case, when we are dealing with transitions within the continuum the possible role of autoionizing states must be considered. Moreoever, the study of autoionizing states through multiphoton excitation has been pursued for quite some time, independently of the role of autoionizing states in multiple ionization phenomena. A special aspect of this work is presented by Freeman et al. who have made major contributions to the study of this area. Their article deals with the excitation of two electrons via specific channels which are singled out by the appropriate choice of wavelengths in a sequence of transitions. The focus is on the use of this technique to probe the doubly excited states and the relaxation of the intermediate states through which they are reached.

The next two articles deal with somewhat older aspects of multiphoton ionization. Photoelectron angular distributions, discussed by Leuchs, only recently reached the point where quantitative comparison with theory has become possible. Clearly, such experiments are extremely important probes of intermediate states. As discussed by Leuchs, however, significant laser intensity effects are to be expected under certain circumstances. Not only does the angular distribution change because of the ac Stark shift of a pair of fine structure intermediate states, but it appears that Raman type processes may also be playing some role above a certain level of intensity.

The effect of dc fields on highly excited states has received considerable attention during the past few years. The article by Klots and Compton addresses one aspect of this question in the context of multiphoton ionization via two-photon excitation of D states in Cs. In addition to its inherent interest, this problem may be relevant to our understanding of the effect of fields generated by the charge produced in multiphoton ionization on other processes taking place simultaneously, e.g., harmonic generation. Even under the controlled conditions of the experiments reported by Klots and Compton, several questions remain to be answered.

The four articles that follow discuss more general aspects of intense field interactions that can apply to atoms as much as to molecules. Zoller presents a review of the effect of field fluctuations (coherence) on multiphoton processes. The only aspect that matters in usual weak-field single-photon transitions, in addition to the average intensity of the radiation, is its bandwidth, because such processes are linear in the radiation intensity. The nonlinear dependence of a multiphoton process on the intensity makes the picture much more complicated and interesting. Not only the

intensity and bandwith (first-order correlation function), but also high order correlation functions play a role. In other words, not only does a multiphoton process involve more of the structure of the atom/molecule, it also involves more of the structure of the radiation. One might say that through a multiphoton process the radiation sees more of the insides of the atom and the atom sees more of the insides of the radiation.

In this context, a number of very interesting theoretical questions have been answered over the past few years, and some experimental work has also been done. Although the area has reached some maturity, it will continue to play a role as long as multiphoton processes are studied. In addition to reviewing the formalism employed in such studies, Zoller presents some recent results which are likely to be relevant to a new generation of experiments.

Elliott presents the first experiment in which a laser field with controlled phase fluctuations has been employed in two-photon absorption. Although this was an experiment in which the two-photon transition was not saturated (weak field), it opens the door for further studies under stronger fields and/or with fields undergoing controlled amplitude fluctuations. We should see more such experiments in the near future.

As soon as strong lasers became available, one of the first questions was about the interplay between collisions and laser excitation. This question has many facets, some of which have been explored in considerable detail while others must await further developments in either theory or experiment. The three articles in this volume relating to this general area address three specific aspects quite distinct from one another. Rosenberg discusses the problem of electron scattering in the presence of strong laser radiation. Under the assumption that the target is not excited and the photon energy is low (soft photon approximation), theory and experiment are in reasonable agreement. In addition to reviewing the problem in that context, Rosenberg offers some suggestions for going beyond the soft photon approximation.

The article by Burnett and Cooper discusses a diametrically opposed setting. Here the radiation is on resonance with an atomic transition, and the atom is excited in the presence of different atoms with which it can undergo collisions. The objective is to extract information about the collisions by observing the influence on the emitted radiation. The multiphoton aspect enters either indirectly through the Rabi splitting of the excited state (when the field is sufficiently strong to saturate the transition), or directly through the excitation of a multiphoton level system in a collisional environment.

A third aspect is treated in the article by Johnson et al. Atoms undergoing multiphoton ionization via a real intermedate state show a significant dependence of the resonance lineshape on pressure. The surprising feature is that the line narrows with increasing pressure under certain focusing conditions. The same phenomenon has been observed in multiphoton ionization of NO. This type of observation has had a long and turbulent history. The interpretation proposed by Johnson et al. invokes a type of collective behavior. The paper raises a number of other questions, some of which are at least partially answered. This type of problem appears in many contexts, for example, in the well-known suppression of multiphoton ionization in favor of harmonic generation.

Multiphoton processes in molecules and surfaces is the main theme of the following part. Much has been written on this topic over the past 10

years, but until about four years ago, most of the reported work concentrated on infrared transitions along vibrational ladders of molecules (usually large). Isotope separation was one of the main motivations for such studies. The field of infrared multiphoton absorption and decomposition of molecules has thus reached a measure of maturity and is reviewed here by Evans and McAlpine. According to these authors, the field is far from complete, especially insofar as the fundamental dynamics is concerned.

The question of fundamental dynamics is addressed by Taylor in his article on the onset of chaos in nonlinear systems. He provides a general and pedagogical introduction to the problem of quasi-periodic motion and localization in a system with a nonlinear Hamiltonian. The considerations of this article are relevant to a number of situations in which strong radiation is absorbed by a large number of degrees of freedom coupled nonlinearly. The context of molecules is perhaps closer to the spirit of this work than any of the other contributions to this volume. Of course, for the moment, the analysis in Taylor's article is more of an explanatory than a predictive nature.

The four articles that follow represent the most active area in multiphoton ionization of small molecules. With the recent availability of intense UV sources, it has become possible to study three- and four-photon ionization of molecules such as H_2, N_2, NO, and CO. Although there have been experiments on these molecules for some time now, only relatively recently has it become possible to obtain data via selected Rydberg and valence states through resonant multiphoton ionization. According to the Franck-Condon principle, it is expected that ions with selected electronic, vibrational, and rotational states should be produced. It is already apparent, however, that in some cases, departures from Franck-Condon behavior are occurring. Clearly, there must be interesting dynamical explanations, which we do not yet understand, for such behavior.

This is one of the important questions that will be attracting theoretical and experimental interest in the immediate future. The theory of resonant multiphoton ionization in such molecules is discussed by Dixit et al., who have most recently formulated a framework for this problem. Their work has direct bearing on the experiments reported by Dehmer et al. in the paper that follows. Kimura presents a broad review of experimental work along these lines and includes a discussion of autoionization, intramolecular vibrational redistribution and the study of van der Waals as well as hydrogen bonded complexes. The fourth article in this group is more specific and reports high resolution studies of H and H_2 with intense VUV radiation. Welge and Rottke have pioneered the construction of such a source which promises to be a valuable tool.

The final two articles in this volume treat laser interactions with surfaces. In the first, Antonov and Letokhov discuss experimental techniques for the spectroscopy and analysis of surfaces employing multiphoton ionization of surface molecules. At least two mechanisms are possible: either ionization of the molecule on the surface followed by desorption of the ion through repulsive states, or desorption of the molecules by the leading edge of the laser pulse and subsequent ionization. The conditions of intensity and pulse duration are among the factors that are important in determining which of the two dominates. The work of Antonov and Letokhov as well as work recently reported by other groups points to extremely promising developments on multiphoton techniques in surface physics and chemistry.

Farkas and Chin address an old but always pertinent question in this field -- the mechanism of ionization from metal surfaces under strong laser radiation. Unlike the free atom case, electrons in metal surfaces can be ejected by mechanisms other than direct multiphoton ionization or tunneling, e.g., electron heating. Among the important parameters in experiments of this type is the pulse duration which plays a central role in the possibility of tunneling. The authors discuss some evidence for what looks like tunneling from a gold surface, with the promise of further investigations using shorter pulses and higher intensities.

Reflecting on the summary of the contents of this volume, one is struck by the number of important and fundamental questions that run through the articles. Although a considerable body of knowledge and understanding has formed over the past ten years it is a sign of vitality that even more interesting and difficult questions are still emerging. The main problems of a fundamental nature that will unlock some of the present mysteries seem to be: multielectron excitation in atoms, multiphoton excitation and ionization through selected states in small molecules, and collisional effects on multiphoton excitation. We trust that when we meet for the next ICOMP, more of the puzzle will have been fitted together.

Part I

Multiphoton Processes in Atoms

6/7

Multiphoton Ionisation of Atoms in Strong Fields

Michele Crance
Laboratoire Aime Cotton, CNRS II, Bat. 505, F-91405 Orsay Cedex, France

Most of the features observed in strong field multiphoton ionisation cannot be interpreted by perturbation theory applied at the minimum non-vanishing order. When it is realistic to assume that only one electron is involved in the process, experimental results are well reproduced by calculations in which some discrete quasi-resonant states are treated on the same footing as the initial state. These methods are not applicable to complex atoms such as noble gases. We present a simple picture of multiphoton processes which allows an interpretation of the most salient experimental features in multiphoton stripping and electron-energy spectroscopy of noble gases.

I INTERPRETATION of STRONG FIELD EFFECTS

Most experiments on multiphoton ionisation involve strong light fields. When speaking of strong fields, one generally refers to the validity of perturbation theory applied at the minimum non-vanishing order. For an excitation field of frequency ω, n is the smallest integer such that $n\hbar\omega$ be larger than the ionisation potential of the ground state E_o. In weak fields, ionisation probabilities vary as the n-th power of the field intensity I. Power laws are also observed in Above Threshold Ionisation experiments for the emission of electrons which have absorbed more than n photons. The number of electrons with energy $(n+q)\hbar\omega - E_o$ varies as the (n+q)-th power of the laser intensity I. Experimental power laws are in agreement with the predictions of perturbation theory applied at the minimum non-vanishing order. When the intensity is increased, a deviation from power laws is observed. This is measured by the effective order of non-linearity defined as:

$$k = d(LnN)/d(LnI) \qquad (1)$$

N is either the number of ions created or the number of electrons with energy $(n+q)\hbar\omega-E_o$. In weak fields, k is equal to the index observed on power laws (either n or (n+q)). Depending on the atom and the frequency, for excitation in strong fields, k may become smaller or larger than the number of photons absorbed in the process. An analysis, case by case, shows that the deviation of k from n can be explained by considering that a few states are nearly resonant. When the field intensity increases, these resonances shift and broaden. Even if the process is not resonant in weak fields, strong field effects may appear corresponding to the wings of a resonant profile which generally has a complicated structure.[1,2]

Experimental features are well reproduced by calculations which take into account resonant processes. Two equivalent formalisms have been proposed, one consists in resuming the largest contributions, the other one consists in building an effective hamiltonian He acting on the initial state and the quasi-resonant states. He is obtained by using the projection operator techniques. Its matrix elements are multiphoton transition probability amplitudes between discrete or continuum atomic states. Each term is calculated by perturbation theory, applied at the minimum non-vanishing order. Application of such methods

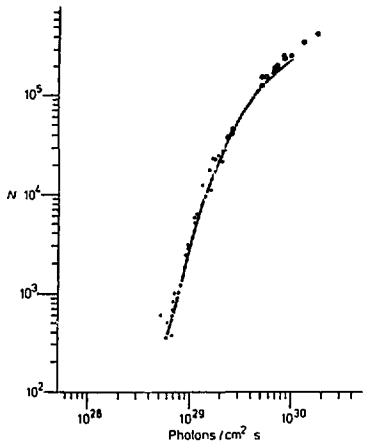

Figure I:4-photon ionisation of Caesium at 9470 cm^{-1}. The number of ions created is plotted as a function of intensity. Solid line: calculation based on effective hamiltonian method (2). Circles: experimental data from (3).

have allowed the interpretation of experiments carried out on alkalies, Atomic quantities are then calculated in the framework of an independent electron model. Only one electron is involved in the ionisation process and powerful methods such as the Dalgarno method or the Green's function method allow precise calculation of atomic quantities. When the detail of experimental conditions (time and space distribution of intensity) is taken into account, experimental data such as number of ions, electron energy spectrum or effective order of non linearity are well reproduced by calculations (2). An example is given in Fig. I.

A recent experiment has provided a crucial test for these methods: angular distributions of electrons emitted after absorption of 4 or 5 photons have been observed when Caesium is irradiated by a Nd-YAG laser. The essential features of angular distributions are in good agreement with the result of calculations based on effective hamiltonian methods (see Fig. II).

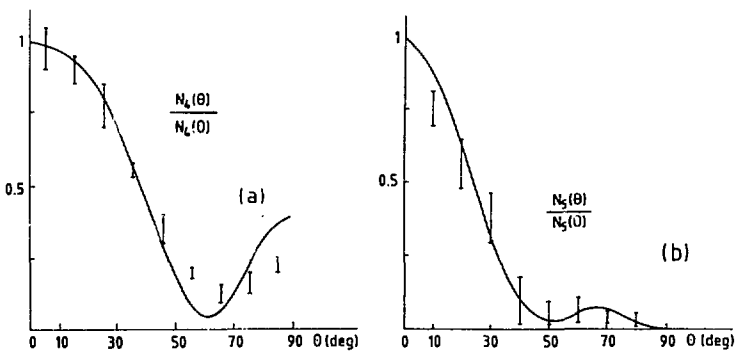

Figure II: multiphoton ionisation of Caesium in a strong field. Angular distribution of electrons emitted after absorption of 4 or 5 photons (4).

In the latter methods, the major assumption is that one electron only is involved in the ionisation process. This is fully justified for alkalis but becomes questionable for more complex atoms. In fact, there is no reliable method to interpret experiments carried out on alkaline earths or noble gases. An attempt at understanding multiphoton ionisation of noble gases based on standard methods mentioned above is presently hopeless. For the experiments carried out in well defined conditions, the number of photons involved is large (6 in Xenon excited at 0.53μ up to 19 in Neon excited at 1.06μ). This defines the minimum order of perturbation expansion to be used. Moreover, a large number of quasi resonant states is involved. A careful calculation in Caesium requires one to introduce about ten quasi resonant states. An equivalent calculation in noble gases would require the introduction of several tenths of states, some of them being unknown experimentally. An additional problem is that atomic states of alkali atoms may be defined as eigenstates of a monoelectronic hamiltonian while noble gases' states are obtained by diagonalisation of large dimension matrices. It is worth trying a somehow qualitative interpretation based on simple considerations such as how ionisation probabilities depend on n, ω, or the size of an atom. In one-photon processes the ionisation cross-section may be interpreted as the size of an atom considered as a target hit by a flux of photons I. For an interaction time τ, the ionisation probability is:

$$P = \sigma I \tau \tag{2}$$

Saturation intensity is defined by:

$$\sigma I_S \tau = 1 \tag{3}$$

An atom ionises if the energy received in the cross-section is equal to the energy of one photon. Multiphoton processes are described through generalised cross-sections $\sigma^{(n)}$. The ionisation probability when an atom is irradiated by a light beam of intensity I during a time τ is

$$P = \sigma^{(n)} I^n \tau \tag{4}$$

Saturation intensity is defined by

$$\sigma^{(n)} (I_S)^n \tau = 1 \tag{5}$$

Generalised cross-sections for different n cannot be compared directly. However, saturation intensities can be compared. Coming back to the above picture of one-photon ionisation, when an atom is excited by a beam of intensity I during an interaction time τ, it appears as a target of size S such that the energy received by an atom in S is n times the energy of a photon:

$$S\, I_S\, \tau = n \tag{6}$$

Equation (6) is a generalisation of (3). The atomic size S is defined by

$$S = \frac{n}{\tau} \left(\sigma(n)_\tau\right)^{1/n} \tag{7}$$

If we want to define a meaningful atomic size, we need to find an intrinsic interaction time. For one-photon ionisation, absorption of one photon is an energy-conserving process and it happens whatever the interaction time is. When the field frequency is smaller than the ionisation potential, absorption of a single photon may happen, but only as a virtual process which cannot last a time longer than the one defined by Heisenberg's relation. So, virtual absorption of any number of photons smaller than n is allowed, provided that it lasts less than

$$T = h/E_o \tag{8}$$

Taking T as an intrinsic interaction time, we define an atomic size of

$$S = \frac{n}{T} \left(\sigma(n)\ T\right)^{1/n} \qquad (9)$$

S obviously depends on the field frequency. Such an approach is certainly not valid for weak fields, when ionisation probability is known to present a complicated structure of resonances. For strong field, resonances are expected to vanish because they broaden and they shift within a pulse when the field intensity increases and decreases. In such a case, what is observed is an average cross-section in which the detail of resonances has vanished. Such quantities should be smoothly varying functions of frequency. Extensive calculations of ionisation cross-sections have been done only in Hydrogen [5]. n=2 to n=8 processes have been studied. Resonances appear on a smooth background of shallow minima. For each value of n, an approximate atomic size can be deduced from this background by using (7). Surprisingly, S evolves slowly with n. The ratio between the largest and the smallest is less than 4. $\sqrt{S}$ is of the order of magnitude of r_o, the mean distance between the electron and the nucleus in the ground state.

3 INTERPRETATION of MULTIPHOTON IONISATION of NOBLE GASES

A series of experiments has been carried out on noble gases excited by a Nd-YAG laser and a frequency-doubled one. Multicharged ions have been observed [6]. Assuming that the ionisation process is related to the size of the atom in its ground state, we extend the previous picture to complex atoms by considering that all the outershell electrons have the same probability to absorb a photon. Ionisation occurs if an electron has absorbed n photons within a time $\hbar/E_o$. A singly charged ion is left. If one of the remaining electrons has absorbed enough photons to reach the second ionisation threshold, a doubly charged ion is created... A simple measure of the size of an atom is S_o

$$S_o = \pi\ r_o^2\ , \qquad (10)$$

r_o being the mean distance between an outershell electron and the nucleus. When p photons are virtually absorbed by an atom, they are shared among all outershell electrons. So the average number of photons necessary for ionisation is larger than n when several electrons are involved in the absorption process. By examining the possible distributions of p photons among the outer shell electrons, we define p_S, which is to replace n in (6) (for noble gases, there are 8 outershell electrons and p_S is about 2n). The equivalent of (6) for noble gases is thus:

$$S_o\ I_S\ T = p_S \qquad (11)$$

Starting from this simple picture, it is possible to describe all the processes observed in multiphoton stripping of noble gases. More precisely, we have calculated the saturation intensity for single ionisation, the ratio of doubly charged to singly charged ions and the charge state distribution in strong fields when several states of charge are observed [7]. For an excitation at 1.06μ, the agreement between experimental data and statistical predictions is fairly good. For an excitation at 0.53μ, experimental saturation intensities are lower than theoretical predictions. In fact, only Xenon and Neon have been studied with excitation at 0.53μ. For an excitation at 1.06μ, ionisation occurs just above the threshold since $n\hbar\omega - E_o$ is much smaller than $\hbar\omega$. Conversely, for excitation at 0.53μ, the emitted electrons have an energy larger than $(\hbar\omega)/2$ This fact explains, at least qualitatively, the discrepancy observed for excitation at 0.53μ [8].

Above Threshold Ionisation can be analysed on the same ground. When the electron energy spectrum is studied for high enough entensity, a series of

peaks appears which correspond to electrons with energies $(n+q)\hbar\omega - E_o$. Peaks are interpreted as resulting from ionisation after absorption of (n+q) photons. By examining the distribution of virtually absorbed photons among electrons, we can predict the probabilities for absorption of n, n+1,... photons. This allows us to rebuild an elctron energy spectrum (see Fig. III). Experiments have been carried out in well-defined conditions for Xenon excited at 1.06μ. Statistical predictions reproduce rather well the experimental spectrum, except for the first peak (q=0) which is overestimated. In fact, one explanation could be related to the shift of the ionisation threshold which is not taken into account in this simple model.

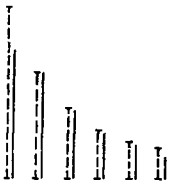

Figure III: Electron energy spectrum in multiphoton ionisation of Xenon excited at 1.06μ. Comparison between experimental results (full lines) (9) and statistical predictions (broken lines) (10).

4 CONCLUSION

The success of such a simple description of multiphoton processes is certainly related to the fact that resonances are wiped out by the A.C. Stark shift when the intensity varies along a light pulse. To go further about strong field effects as well as atomic structure, a number of problems has to be solved first. For strong field effects, a solution has been proposed (11) which in principle could be applied to arbitrary field intensities. Hydrogen has been studied by using a simple representation of the atomic states' whole spectrum. Although this method is very powerful, it may still be too complicated to be applied to processes in which several electrons are involved. New progress in interpretation of noble gases multiphoton ionisation requires a strong improvement of atomic structure calculations both in compactness and flexibility.

REFERENCES

1 L.A.Lompré,G.Mainfray,B.Mathieu,G.Watel,M.Aymar,M.Crance:J.Phys.B13,1799 (1980)
2 M.Crance,M.Aymar: J.Phys.B12, L667 (1979)
3 J.Morellec,D.Normand:Proc.Multiphoton Processes Conference,Benodet (1979)
4 G.Petite,F.Fabre,P.Agostini,M.Crance,M.Aymar:Phys.Rev.A29, 2677 (1984)
5 Y.Gontier,M.Trahin:Phys.Rev. 172, 83 (1968)
6 A.L'Huillier,L.A.Lompré,G.Mainfray,C.Manus:J.Physique 14, 3585 (1983)
A.L'Huillier,L.A.Lompré,G.Mainfray,C.Manus:Phys.Rev.A27, 2503 (1983)
A.L'Huillier,L.A.Lompré,G.Mainfray,C.Manus:J.Phys. B16, 1363 (1983)
7 M.Crance:J.Phys.B17, 3503 (1984)
8 M.Crance:J.Phys.B17, L635 (1984)
9 P.Kruit,J.Kimman,M.Van der Wiel:J.Phys. B14 L597 (1981)
10 M.Crance:J.Phys. B17 L355 (1984)
11 S.I.Chu,W.P.Reinhardt: Phys.Rev.Lett. 39, 1195 (1977)

Multiphoton Transitions in the Ionization Continuum of Atoms

P. Agostini and G. Petite

Service de Physique des Atomes et des Surfaces, Centre d'Etudes Nucleaires de Saclay, F-91191 Gif-sur-Yvette Cedex, France

1 Introduction

Two series of experimental results , which appeared around the middle of the seventies,clearly did not fit into the Hydrogen-model,lowest-order-perturbation frame which had been the standard way of thinking in Multiphoton Ionization (MPI) theory for about ten years.That was the detection in MPI experiments first of electrons with large kinetic energies [1] and second of multiply charged ions[2].

The production of fast electrons was first related to the so-called "ponderomotive force" and eventually lead to the study of Above-Threshold Ionization (ATI) a process by which the electron absorbs more photons than strictly necessary,thus undergoing transitions in the Continuum [3].For a few years,this was observed only in Xenon and,perhaps,in alkaline earths, bringing up the idea that several electrons were simultaneously excited,ie that the structure in the Continuum was playing a major role.Recently, the observation of this process in Cesium [4] where the Continuum has no structure has certainly lessen this conviction,although the fact that ATI is much more important in Xenon than in Cesium could still leave some reason to believe in the influence of two-electron states.(Describing the intensity effects on these autoionizing states has been recently the object of a large number of theoretical works [5]).
Indeed the question of the influence of two-(or more)-electron states arose from the observation of doubly charged ions.Almost from the beginning, two competing mechanisms were considered : either a direct multiphoton transition through the two-electron spectrum up to the escape of two electrons , or a stepwise process involving successively the creation of the singly charged ion and its ionization by the same laser pulse.However, no evidence has been given , so far, of two-electron states as intermediate states ,although such resonances are very likely to occur during a direct double ionization.

This paper contains two main parts: in the first one we briefly summarize our contribution to the study of ATI and discuss the role of the ponderomotive force.For more details the reader is referred to a recent review [6] and to the original papers.In the second one we report new results on multiple ionization of Calcium atoms with picosecond pulses and discuss a possible two-electron resonance.

2 Above-Threshold Ionization versus Ponderomotive Force

In the early MPI experiments detecting electrons,broad spectra extending to several tens of electron-volts were recorded.Such high kinetic energies were correlated to the effect of the ponderomotive force acceleration. The physical interpretation of this classical force is very simple: a free

electron in an inhomogeneous electro-magnetic field has a rapid oscillatory motion due to the Lorentz force plus a secular motion due to the gradient of the field. Thus, an electron in a tightly focused beam will be accelerated towards the low-field region and, under certain circumstances, all its oscillating energy can be converted into translational energy. If the intensity is I ($W.cm^{-2}$) the kinetic energy of the electron in the zero-field region would be increased by $10^{-13}.I$ (eV). Therefore at 10^{13} $W.cm^{-2}$, energies up to 100 eV could be detected [7]. However, as soon as better resolutions were achieved in electron spectrometers used in such experiments, the spectra showed a characteristic structure of lines separated by the photon energy: this was in contradiction with the ponderomotive force explanation and lead to interpretations based on either Inverse Bremsstralhung or on ATI. The Inverse Bremsstralhung, a process in which the free electron absorbs photons during a collision with an ion or an atom, could be easily ruled out: the atomic densities used in MPI experiments is low enough so that no collision can take place during the laser pulse [8].

In the next three paragraphs we summarize our works on ATI going from the simplest situation (Cesium, "low" intensity) to the most complex one (Xenon, high intensity). The effect of the ponderomotive force is too small to be detected in the low-intensity case but it should be visible around 10^{13} $W.cm^{-2}$. However we will see that it could be cancelled by another effect: the Stark shift of the Continuum limit.

2.1 Above-Threshold ionization of Cesium, 1064 nm, 100 $GWcm^{-2}$

The quantum process of ATI is illustrated on Fig. 1: it is a direct coupling of ground state of the atom to the Continuum by absorption of S photons more than the N strictly necessary for ionization.

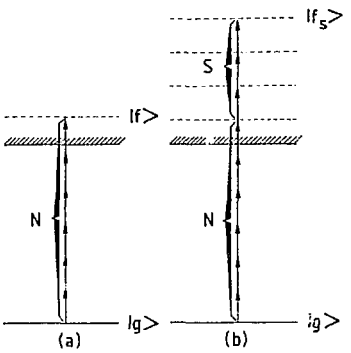

Fig.1-Schematic representation of MPI (a) and ATI (b)

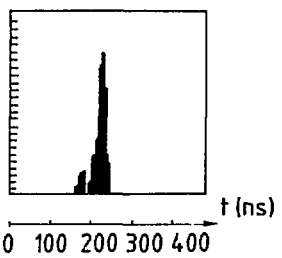

Fig.2 - Time of flight spectrum of electrons produced by ionization of Cesium, 1064 nm, 200 $GW.cm^{-2}$

The cross-sections for such processes have been calculated by a number of authors [9] both for hydrogen and alkali. Their values are quite "normal" and, in this sense, such transitions are <u>not</u> more probable than transitions involving the absorption of the same number of photons in the discrete part of the spectrum. Therefore, in general, ATI will be a small perturbation of MPI which is always of lower order. This can be seen on Fig.2 [4]. The small peak on the left is from the contribution of 5-photon ATI while the peak on the right is from the 4-photon MPI. The intensity dependence of these peaks,

Table 1 - Experimental and calculated values of $K=\partial \ln N_e/\partial \ln I$ (N_e number of electrons). Intensities are between 300 and 600 GW.cm^{-2}.

Source	Ions	Slow Electrons	Fast Electrons
Expt	3.85±0.2	4.2±0.2	4.8±0.2
Theory	4	4.3	5

as shown on Table 1, is as predicted by perturbation theory taking into account the level shifts, which can be quite important at such intensities [4]. (This is the reason for the 4.3 value corresponding to a 4-photon process).

One important consequence of the fact that ATI is a direct process starting from the ground state of the atom is that it saturates when the population of the ground state is depleted. This is illustrated by Fig.3 showing the intensity dependence of the ratio of the 5-photon ATI signal to the 4-photon MPI signal [4]. Clearly the maximum relative contribution of ATI is observed around 60 GW.cm^{-2}, the saturation intensity I_s. It means that the higher the saturation intensity the higher the probability of ATI. Precisely, the ratio of (N+1)-photon ATI to the N-photon MPI probabilities at the saturation intensity is proportional to I_s. For a sufficiently high saturation intensity, this ratio can be close to 1 even with "normal" cross sections. This can be achieved, for instance with picosecond pulses since I_s is proportional to the reciprocal of the N-root of the pulse duration. Note here that the excellent agreement between theory and experiment has been achieved by taking into account the laser parameters as well as the stong distorsion of the atomic spectrum [4]. At our maximum intensity (600 GW.cm^{-2}) the ponderomotive force would increase the electron energy by 60 meV which is too small to be detected in this experiment.

2.2 Above-Threshold ionization in Xenon, 532 nm, 100 GW.cm^{-2}

Fig.4 shows a typical spectrum of the ejected electrons when Xenon is ionized by the second harmonic of a YAG laser. The number and the amplitudes of the peaks make this spectrum strikingly different from the one on Fig.2. It shows the absorption of up to four photons above the ionization threshold for the series leaving the ion in the $^2P_{1/2}$ state. The other series, leaving the ion in the $^2P_{3/2}$ state is also significant althouh of lesser impor-

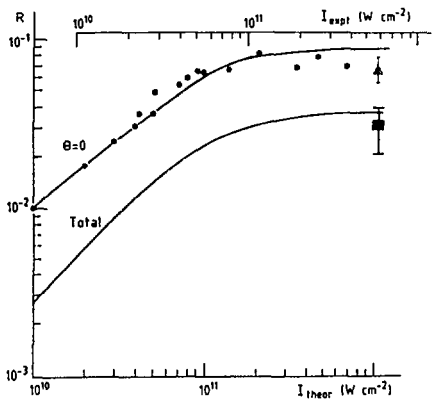

Fig.3 - Ratio N_5/N_4 as a function of intensity. The dots are experimental and the line is calculated. For details see [4]

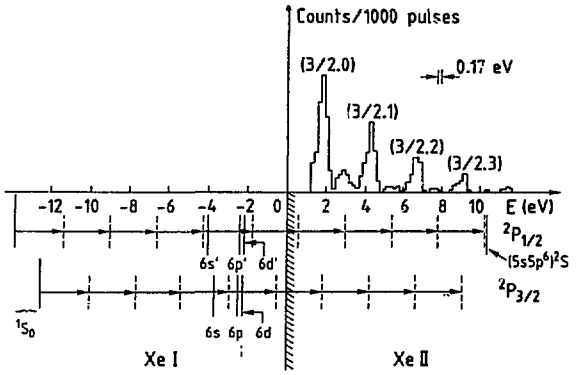

Fig.4 - Energy spectrum of photoelectrons produced in MPI of Xenon,532 nm 100 GW.cm^{-2}

tance.Trying to understand why Xenon is different from Cesium (as far as ATI is concerned),one could speculate that the Continuum part of the transition is enhanced by resonances on two-electron states in Xenon and not in Cesium.But if one looks at what is known of the two-electron spectrum of XeI,it appears that only the most energetic electrons reach the energy of these states.Therefore,they are highly non resonant and it is difficult to believe that they are playing a major role in the difference between these two atoms.A more likely interpretation is to be found in the values of the saturation intensity and of the ratio of consecutive-order cross-sections. This ratio is approximately constant [11] and is 10^{-33} cm^2.s for Cesium but 10^{-31} cm^2.s for Xenon [10].The saturation intensity for Xenon (at 532 nm) is about twice that of Cesium (at 1064 nm) .This is probably enough to account for the difference between the spectra of Fig.2 and Fig.4.The quoted value for the Xenon constant is experimental.For Cesium,this value is very close to the Hydrogen one (Gontier and Trahin [9]).As mentioned above,there is a good agreement between the experimental and theoretical values.

Table 2 - Experimental and theoretical values of $\partial \ln N_e / \partial \ln I$

Line	1/2,0	1/2,1	1/2,2	3/2,0	3/2,1	3/2,2
N+S Expt		7.3±.1	7.8±.3	5.5±.7	6.5±1.6	5.7±1.8
N+S Theo	6	7	8	6	7	8

As a conclusion,it seems after all that the single-electron,perturbation-theory picture is still usable for Xenon at 532 nm.Unfornunately such a calculation is well beyond the reasonable.

Again,the ponderomotive force would give,in this experiment,a contribution much less than the widths of the peaks and could not have been detected.

2.3 Above-Threshold ionization of Xenon,1064 nm,3000 GW.cm^{-2}

Fig.5 shows a typical photoelectron spectrum under these conditions.Each peak is the superposition of two unresolved components generated by the 11-photon ionization of the $^2P_{3/2}$ core and the 12-photon ionization of the $^2P_{1/2}$ core.The peaks are separated by the photon energy 1.17 eV.Altough the

number of photons absorbed in the Continuum is about twice that of the previous case,the maximum energy reached is about the same.The intensity dependence of these peaks has been found to scale like I^N and not I^{N+s} like predicted by perturbation theory [12].However,recent results tend to contrast with this finding and to bring back the perturbative scheme [13].The explanation for the high relative values of the probabilities would be the same as above:namely the increase of the saturation intensity.In [12] the effective intensity is estimated to be between 20 and 70 TW.cm^{-2}.The ponderomotive force effect would then be to increase the electron energy by 2 to 7 eV.But no shift seems to be observable either in [12] or in [8].This question is addressed in the next paragraph.

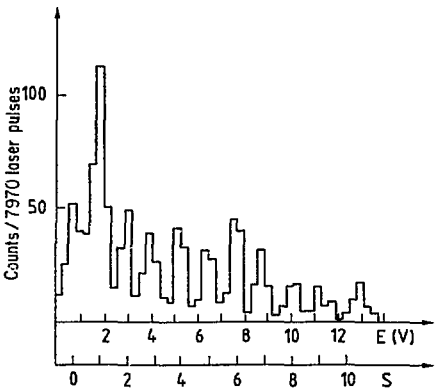

Fig.5 - Energy spectrum of photoelectrons produced by MPI of Xenon at 1064 nm,3 TW.cm^{-2}

2.4 Ponderomotive Force in MPI

One very attractive scenario has been recently proposed to interpret this result [14],[15].To understand it,one should recall first that the ac Stark shift of Rydberg states induced by an electromagnetic field of optical frequency $\omega_L$is given by

$$E_v = e^2F^2_L/2\, m\omega^2_L \qquad (1)$$

where $F_L$is the amplitude of the laser electric field [15] provided that $\hbar\omega_L >> E_L$ where E_L is the energy separation of the atomic levels.The physical interpretation of this energy is very simple.It is the kinetic energy of the electron oscillating in the incident electromagneetic field.This shift of all the levels close to the Continuum limit can be interpreted as an increase of the effective mass $mc^2=E_v$.As a consequence the ionization potential of the atom,E_i,is changed by an amount equal to the sum of the Starkshift of the ground state,ΔE_g,and the the energy E_v.The energy of the outgoing electron is then given by

$$E_k = N\hbar\omega_L - (E_i + E_v - \Delta E_g) > 0 \qquad (2)$$

But,before being detected,the electron has to leave the electromagnetic field and,during its journey to the detector,it will experience the ponderomotive force,which,under most circumstances,will increase the electron energy by exactly E_v.Three experimental facts support this scenario:

(i) The Stark shift of the Rydberg states has been independently measured for the transition 5s-48p in Rb and found in qualitative agreement with (1) [17].

(ii) Spectra like the one on Fig.5 do not show any shift but only a broadening of the peaks[12].

(iii) The increase of the ionization potential could be such that an N-photon ionization would become impossible.In the corresponding spectra the first peak would then be suppressed.This is indeed what has been observed [12] and,later, been supported by a non perturbative calculation of the photoionization of a model atom[15].

However the following points should also be considered:

(i) In[12] the Continuum shift and the ponderomotive force effect are estimated using an N-photon effective intensity while these effects depend linearly on the intensity.Using the average intensity (which is one order of magnitude less)the the maximum shifts would be 0.7 eV which is barely detectable.

(ii) In previous experiments at 10^{15} W.cm^{-2} [7],low resolution spectra extend to 100 eV while according to the above explanation there should be a cutoff for electrons under roughly 100 eV.

To gain a complete conviction in this matter,the best way would be to do a good photoelectron spectrum at such an intensity.Both conditions are easy to fulfill with up-to-date technology.

3 Multiple Ionization of Calcium with Picosecond Pulses [1]

The double ionization of alkaline earth elements by a laser pulse was first reported in 1975 [2].Although it was clear that ions were produced only by the interaction of the laser radiation with the atoms,two different mechanisms were proposed which could explain the double ionization:either a direct process of simultaneous excitation of two electrons through the two-electron spectrum up to the double ionization limit;or a two-step process involving the creation of the singly charged ion and its ionization by the same laser pulse.A first suggestion of the predominance of the direct process was given by the ratio A^{++}/A^{+} which was found larger by 13 orders of magnitude than the prediction for the cascade process [18].However,subsequent experiments [18],[19],although emphasizing the resonant character of the double ionization,did not definitely prove that two-electron states were important in the process.Even more, some authors concluded to stepwise double ionization [19].More recently,multiple ionization of rare gases at fixed laser frequencies were reported [21],[22].Based on arguments similar to the one above it was concluded either to the direct process or to the stepwise process depending on the wavelength and intensity of the laser,but,again,direct evidence of the influence of two-(or more)-electron states could not be obtained.We report here preliminary observations of simple,double and triple ionization of Calcium atoms at 1064 nm,532 nm, and 560-568 nm.Calcium was chosen because its spectrum has been extensively investigated [22] and also because it was reported to be very difficult to double-ionize [18],which seemed to isolate it from the other akaline earths. We have used picosecond pulses to increase saturation intensities,thus increasing the rates of higher order processes.

3.1 Multiple ionization of Calcium at 1064 nm and 532 nm

The experiment is as follows: a 10pps YAG laser delivers single 50 psec pulse with a peak power of 1 GW.We have used successively the fundamental

1 - This is part of paper which has been submitted for publication to J.Phys.B Letter to the editor

frequency output,the second harmonic (P.P$\sim$0.3 GW) and the output of a dye laser to ionize an effusive atomic beam of Calcium.The dye system consists of a Littman oscillator,sychronously pumped by the frequency-doubled output the YAG oscillator,followed by two amplifiers,longitudinally pumped by the single pulse of the amplified,frequency-doubled YAG.Its pulse duration and spectrum have been independently measured and,with Rhodamine 6G,it delivers transform-limited 50 psec pulses with a peak power of 10 MW.The beams are focused by a 200 mm focal-length spherical lens.The produced ions are charge-analyzed in a time-of flight spectrometer [4] and detected by a electron multiplier tube.The EMT signal is fed into a boxcar integrator whose output is sent to the Y input of an X-Y recorder.A computer,when necessary,scans the laser wavelength and the X input of the X-Y recorder.Wavelengths are measured with a calibrated spectrometer and the average power of the laser is monitored with a Scientech power meter.

At 1064 nm simple,double and triple ionization of Ca are easily observed as shown on Fig.6,for average laser power in the range 10 mW to 1 W.This corresponds to intensities in the range .7 to 70 TW.cm^{-2} with a beam cross-section at the best focal plane of 3.10^{-5} cm^{-2}.(This intensity is known with an accuracy of about 50%). It can be seen that not only Ca^{++} ions are produced but they are created with a rate which is almost equal to that of Ca^{+} ions.This is not really in contradiction with [18] since the authors had a field strength of "only" 10 MV.cm^{-1} (250 GW.cm^{-2}).It simply proves once again that if one can increase enough the intensity before reaching saturation,otherwise undetectable processes become visible.Furthermore,the intensity dependences on Fig.6 are somewhat similar for the two ion species: both these facts suggest,according to [18] and [21],that double ionization is reached by a direct process.However,this argument,based on values of "typical" cross-sections must be taken with some precaution since special situations may arise due to quasi-resonances,as established for Barium [23].

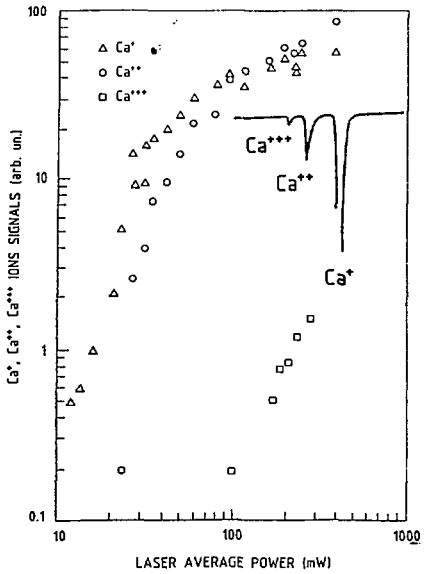

Fig. 6 - Intensity dependences of Ca^{+},Ca^{++},Ca^{+++} ions signals at 1064 nm (the insert shows a typical ion spectrum)

The Ca^{+++} signals,albeit small, are significant.They have been identified by careful measurements of times of flight.The fact that 3 electrons can be "easily" removed from Ca is in agreement with recent observations of double ionization of Sodium and Potassium [24].This is the first time,to our knowledge,that triple ionization of alkaline earths is reported.

At 532 nm,up to triple ionization of Ca is observed with a laser average power of 20 mW.But results suggest a stepwise process for the double ionization since the Ca^{++} signal appears only above the saturation intensity. In rare gases also [20] it was observed that,when the wavelength is decreased,the stepwise channel becomes dominant.However,this dependence may not be universal since,again Ca^{3+} are detected with a ratio Ca^{3+}/Ca^{2+} larger than observed at 1064 nm.Note also that the intensity is about one order of magnitude lower than at 1064 nm.

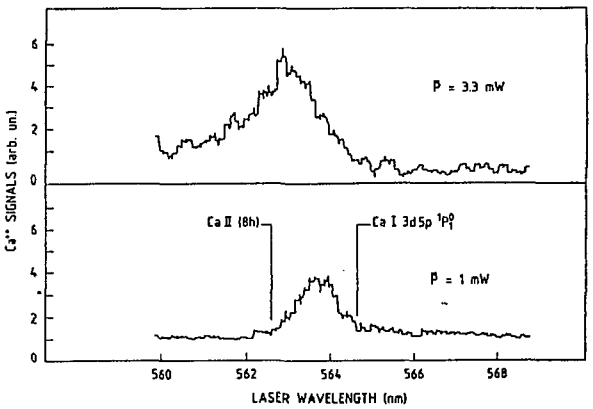

Fig.7 - Wavelength dependence of Ca^{++} signal for two laser powers

3.2 Dicussion of a possible two-electron resonance

With the dye laser,the intensity is presumably much lower.The average power is between 0.1 and 2 mW but no focal cross-section measurement was carried out.Making a conservative estimate of 10^{-4} cm^{-2} for this cross-section, the maximum intensity would be 0.2 $GW.cm^{-2}$.Again singly and doubly charged ions are observed with quite comparable rates at some wavelength around 562.5 nm.Figure 7 shows the wavelength dependence of the Ca^{++} signal at two different powers,clearly displaying a resonance shifting with intensity.In the same wavelength range,the Ca^{+} signal only shows a slow increase towards the long wavelengths.Extrapolated linearly to zero-intensity,the wavelength of the resonance is 564.6 nm (in air).A scan of the same range with circular polarization gives a similar resonance,attesting that it is allowed with circular polarization.Measurements of the slopes (intensity dependences in Log-Log coordinates) show strong variations around 563.7nm. No exactly resonant states can be found either in the neutral atom nor in the ion spectra.Table 3,where the best candidates are collected,shows that the interpretation of the observed resonance is not easy.

Table 3.

Transition	# of photons	Wavelength(nm)	Allowed in Circ.Pol
$4s^2\ {}^1S_0$-$3d5p\ {}^1P_1^o$	3	564.81	No
$4s\ {}^2S_{1/2}$-$3p^6\ {}^1S_0$ 6s	4	565.7	No
$4s\ {}^2S_{1/2}$-$3p^6\ {}^1S_0$ 8f	5	562.6	No
$4s\ {}^2S_{1/2}$-$3p^6\ {}^1S_0$ 8h	5	562.7	Yes

Only the last transition is allowed in circular polarization but its position is relatively far from the observed resonance.However,it should be noted that the extrapolation made to obtain the zero-intensity position is not very accurate.The resonance on the two-electron state is ruled out,not only by the polarization test,but by the observed linewidth,which is much less than the autoionizing width of this sate [18].Line narrowing due to the intensity effect on the configuration interaction [25] or strong modification of the Fano profile [26] are not very likely to occur here.Furthermore,no resonance is observed on the Ca^+ signal.It is therefore very likely that the double ionization is produced,in this case,by a stepwise process.First a 3-photon ionization of Ca then a 5-photon resonant,6-photon ionization of Ca^+,the resonance being on the ion 8h state.Feldman et al.[19] came to the same conclusion concerning resonances observed in the double ionization of Srontium.To conclude the presentation of these preliminary results on multiple ionization of Ca with picosecond pulses,we would like to emphasize the following points:

(i) it is not certain to conclude to a single step process because sinly and doubly charged ions appear before saturation or because the rates are comparable.Both conditions are fulfilled here and,nevertheless,the analysis concludes to a stepwise process.

(ii) the slopes are not what is expected either for the direct nor for the two-step process.

(iii) It seems to us that the signature of the process will be found in the electron energy spectra.Here the direct process would probably correspond to a continuous spectrum extending up to 1.94 eV while the two-step process would give two peaks at .52 eV and 1.42 eV.Of course this simple picture could be complicated and obscured by ATI.

4 Concluding remarks

The physics of ATI is well understood,at least when a single electron is involved.The measurements reasonably agree with calculations (when they are possible) even under strong distorsion of the atomic spectrum.The cross-sections are "normally" decreasing with the order and it must be stressed that high probabilities do not necessarily mean high cross-sections but,often,a high saturation intensity.

A very interesting hypothesis has been proposed to explain how the ponderomotive force acceleration is cancelled by the shift of the Continuum limit.However a quantitative check of the shift of Rydberg states is still to be done and a good measurement of electron spectrum at 10^{15} $W.cm^{-2}$ seems to be necessary to reach a definitive conclusion.

Multiple ionization of akaline earths is still a puzzling problem since it is not clear how the direct double ionization competes with the two-step process.The role of two-electron state as intermediate states in a supposed direct double ionization has still to be proved.Photoelectron spectroscopy is very likely to shed some light on this question.

So far,the basic theoretical guideline has been the time-dependent perturbation theory:situations where atoms are making transitions between (even relatively strongly perturbed) states are well under control.But situations where the level shifts could be of the order of the ionization potential itself are far from being understood.The same can be said of situations where the laser field is strong enough to either excite the the inner shells of the atom or to induce collective response of the electrons. Describing precisely such situations seems a good challenge for the MPI physicist of the eighties.

References

1 E. a. Martin and L. Mandel Appl. Opt.: 15,2378 (1976)
2 V.V. Suran and I.P. Zapesochnyi:Sov. Tech. Phys. Lett. 1,420 (1975)
3 P. Agostini,F. Fabre,G. Mainfray,G. Petite and N. K. Rahman:Phys. Rev. Lett. 42,1127(1979)
4 G. Petite,F. Fabre,P. Agostini,M. Crance and M. Aymar:Phys. Rev. A 29, 2677 (1984)
5 P. Lambropoulos and P. Zoller in Multiphoton Ionization of Atoms.S. L. Chin and P. Lambropoulos ed.,Academic Press (1984)
6 P. Agostini,F. Fabre and G.Petite in Multiphoton Ionization of Atoms S. L. Chin and P.Lambropoulos ed.,Academic Press (1984)
7 M. J. Hollis:Op. Commun. 25,395 (1978)
8 F. Fabre,G. Petite,P. Agostini and M.Clement:J. Phys.B 15,1353 (1982)
9 W. Zernik and R. W. Klopfenstein:J. Math. Phys. 6,262(1965);E. Karule J. Phys. B 11,441(1978);S.Klarsfeld and A. Maquet:Phys. Lett. 78A,40(1980); M. Aymar and M. Crance:J. Phys.B 14,3585(1981);Y. Gontier and M.Trahin: J. Phys.B 13,4381(1981).Many other references can be found in these papers.A calculation of the 4-photon and 5-photon ionization cross-sections of Cesium at 1064 nm is in Ref 4.
10 F. Fabre,P. Agostini and G. Petite:Phys. Rev. A 27,1682 (1983)
11 J. Morellec,D. Normand and G. Petite:Adv. At. Mol. Phys 18,97 (1982)
12 P. Kruit,J. Kimman,H.G. Muller and M.J. Van Der Wiel:Phys. Rev. A 28, 248 (1983)
13 H.L'Huillier,L.A. Lompre,G. Mainfray and Y.J. Fan:Postdeadline paper Int. Conf. Mult. Phot. Proc. Iraklio (1984)
14 F.Fabre:These de Doctorat Paris 1983 (unpublished)
15 H.G. Muller,A. Tip and M.J. van der Wiel:J. Phys. B 16,L679 (1983)
16 P. Avan,C. Cohen-Tannoudji,J. Dupont-Roc,and C. Fabre:J. Phys.(Paris) 37,993 (1976)
17 S. Liberman and J.Pinard:Phys. Rev. A 20,507 (1979)
18 N.B. Delone,V.V. Suran,B. A. Zon:Multiphoton Ionization of Atoms.S. L. Chin and P. Lambropoulos ed.,Academic Press (1984)
19 D. Feldman,H.J.Krautwald and K.H. Welge:Multiphoton Ionization of Atoms S.L. Chin and P. Lambropoulos ed.,Academic Press (1984)
20 A. L'Huillier,L.A. Lompre,G. Mainfray and C.Manus:J.Phys.B 16,1363 (1983)
21 T.S. Luk,H. Pommer,K.Boyer,H. Shadidi,H.Egger and C.K. Rhodes Phys.Rev. Lett.51,110 (1983)
22 J. Sugar and C.Corliss:J. Phys. Chem. Ref. Data 865 (1979)
23 J.I. Bondar,A.J. Gomonay,N.B. Delone,I.P. Zapesochnyi and V.V. Suran: J. Phys. B 17,2049 (1984)
24 S.L. Chin,H.K. He and F. Yergeau:J. Opt. Soc. Am. B 1,505 (1984)
25 Y.S. Kim and P. Lambropoulos:Phys. Rev. Lett. 49,1698 (1982)
26 P. Lambropoulos and P. Zoller:Multiphoton Ionization of Atoms. S.L. Chin and P. Lambropoulos ed.,Academic Press (1984)

Multiply Charged Ions Produced in Multiphoton Ionization of Rare Gas Atoms

L.A. Lompré and G. Mainfray

Service de Physique des Atomes et des Surfaces, Centre d'Etudes Nucléaires de Saclay, F-91191 Gif-sur-Yvette Cedex, France

1 Introduction

Multiphoton ionization of atoms is a typical example of one of the new fields of investigation in atomic physics that lasers have opened up. The different aspects of the multiphoton ionization of one-electron atoms have been well understood these last few years. They can be correctly described by rigorous theoretical models in the framework of perturbation theory when only one electron is assumed to be involved in the ionization [1-5]. Alkaline atoms which have only one valence electron, and of course atomic hydrogen, are the examples that best satisfy this condition. For example the different aspects of multiphoton ionization of cesium atoms now form a well developed field. Accurate measurements of absolute values of the two and four-photon ionization cross sections of cesium atoms are in good agreement with calculated values, and clearly emphasize the validity of perturbation theory [6]. In the same way, there is also a good agreement between theoretical and experimental results on resonance effects in multiphoton ionization of cesium atoms in the moderate laser intensity range, 10^7-10^9 W.cm^{-2} [7]. Resonance effects emphasize the important role played by laser-induced atomic level shifts. Destructive interference effects, which give rise to minima in the multiphoton ionization cross sections of atoms, have been investigated with a high degree of accuracy in the two-photon ionization of Cs atoms [8]. This effect has been successfully used to check the validity of different calculation models. Furthermore, laser temporal-coherence effects induced by chaotic fields increase the non-resonant N-photon ionization rate by N!, in good agreement with theoretical calculations. The resonance curves obtained by incoherent laser pulses are shifted and broadened with regard to those induced by coherent pulses with the same average intensity [9]. Finally, absorption processes above the first ionization threshold have been investigated recently in Cs atoms at 1064 nm, in the 10^{10} - 10^{11} W.cm^{-2} range. Cs atoms which can be ionized by the absorption of 4 photons can also absorb 5 photons. The ratio of the 5-photon to the 4-photon absorption rate, which is about 10^{-2}, is in good agreement with a calculation performed in the framework of the perturbation theory [10].

The present paper will be devoted to multiphoton ionization of many electron atoms in the outer shell, as rare gases. It induces removal of several electrons and the production of multiply charged ions. The production of doubly charged ions has been investigated in detail. Doubly charged ions can be produced, either by simultaneous excitation of at least two electrons, or by a stepwise process via singly charged ions. This depends mainly on the laser intensity and the photon energy. The basic interaction processes involved are considerably more complicated than for one-electron atoms. A new theoretical model will have to be developed to take into account electron correlation effects.

2 Experimental Results

Recent experiments have emphasized the production of multiply charged ions by multiphoton absorption in rare gas atoms [11-14]. A mode-locked Nd-YAG laser is used to produce a 50-psec pulse, which is amplified up to 5 GW at 1064 nm. The second harmonic can be generated at 532 nm up to 1.5 GW when needed. The laser pulse is focused into a vacuum chamber by an aspheric lens corrected for spherical aberrations. The vacuum chamber is pumped to 10^{-8} Torr and then filled with a spectroscopically pure rare gas at a static pressure of 5×10^{-5} Torr. At this pressure, no collisional ionization occurs, and no complications from charge exchange reactions are expected. Only collisionless multiphoton ionization occurs. The ions resulting from the laser interaction with the atoms in the focal volume are extracted with a transverse electric field of 1 kV.cm^{-1}, separated by a 20 cm length time-of-flight spectrometer, and then detected in an electron multiplier. The laser intensity is adjusted in order to produce 1 to 10^5 ions. The experiment consists of the measurement of the number of ions corresponding to different charges formed as a function of the laser intensity.

2.1 Multiphoton Ionization of Xe at 532 nm

Figure 1 is a typical result of the multiphoton ionization of Xe at 532 nm [13]. Up to Xe^{5+} ions are formed. Let us analyse the different processes which occur when the laser intensity I is increased. Figure 1 can be divided into two parts. The first part ($I < 1.5 \times 10^{12}$ W.cm^{-2}) is characterized by a laser-neutral atoms interaction, while in the second part ($I > 1.5 \times 10^{12}$ W.cm^{-2}) a laser-ions interaction occurs. In the first part, the absorption of 6 photons by an atom leads to the removal of one electron and the formation of a Xe^+ ion. This process appears in Fig. 1 through experimental points joined by a straight line with a slope 6 because the 6-photon ionization rate varies as I^6. When the laser intensity is increased further, approaching the I_S value, the absorption of 15 photons by an atom induces the simultaneous removal of two electrons and the production of a Xe^{2+} ion. This process appears in Fig. 1 through experimental points joined by a straight line with a slope 15. The 6-photon and 15-photon ionization processes deplete the number of atoms contained in the interaction volume. A marked change appears in the slope of the curves for both Xe^+ and Xe^{2+} ions beyond the laser intensity I_S. This saturation is a typical effect, which occurs in multiphotonionization experiments when all the atoms in the interaction volume are ionized. The intensity dependence of both curves of Xe^+ and Xe^{2+} ions just beyond I_S arises from ions produced in the expanding interaction volume when the laser intensity is increased further.

The second part of Fig. 1, for $I > 1.5 \times 10^{12}$ W.cm^{-2}, describes the interaction of the laser radiation with ions, because the interaction volume is filled up with Xe^+ ions in place of atoms. A sudden increase in the number of Xe^{2+} ions occurs when the laser intensity is increased further. This comes from the absorption of 10 photons by a Xe^+ ion. This removes one electron from the Xe^+ and produces a Xe^{2+} ion. This appears in Fig. 1 through experimental points joined by a straight line with a slope 10. When the laser intensity is increased further, the 10-photon ionization of Xe^+ ions also saturates and Xe^{3+}, Xe^{4+} and Xe^{5+} ions are formed, most likely through stepwise processes. This means Xe^{3+} ions are produced from Xe^{2+} ions by absorbing 14-photons. In the same way, Xe^{4+} ions are produced from Xe^{3+} ions by absorbing 20 photons, and likewise for Xe^{5+} ions. To sump up, Fig. 1 is a clear picture of the response of the elec-

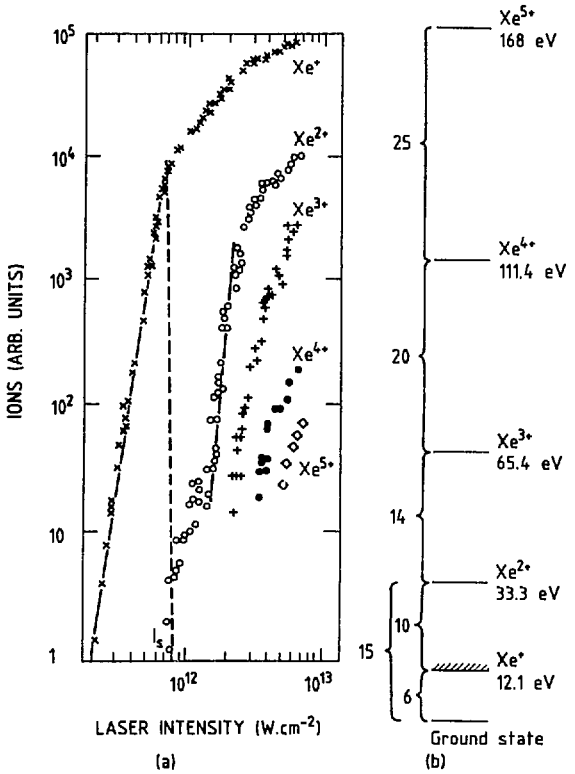

Fig. 1 - (a) A log-log plot of the variation in the number of Xenon ions formed at 532 nm as a function of the laser intensity. (b) Schematic representation of the number of photons involved in the production of multiply charged ions.

trons of Xe atoms to a high laser intensity. Each step of increased intensity gives rise to the removal of an additional electron.

It should be noted that the 10-photon ionization of Xe^{+} ions which produces Xe^{2+} ions can be investigated in a well-defined laser intensity range. The corresponding 10-photon ionization cross section is measured to be $10^{-297\pm1}$. The uncertainty in this measurement comes mainly from the uncertainty of the laser intensity in absolute values. It should be recalled that a generalized N-photon absorption cross section is expressed in cm^{2N} s^{N-1} units when the laser intensity is expressed in number of photons cm^{-2} s^{-1}. It is initially amazing to find that a multiphoton ionization cross-section of a singly charged ion can be measured so easily while very few examples of measurements of photoionization cross-section of ions are found in existing literature. Here the measurement is easy because it is the same laser pulse which produces both a clean Xe^{+} ion target with a 10^{12} cm^{-3} density, and induces the 10-photon ionization of Xe^{+} ions.

2.2 Multiphoton Ionization of Ne at 532 nm

Figure 2 shows in a log-log plot the variation of the number of Ne^+ and Ne^{2+} ions produced as a function of the laser intensity [13]. The Ne^+ ion curve has a slope of ten, which is characteristic of a non-resonant 10-photon ionization of Ne atoms. Ne^{2+} ions are produced in a laser intensity range far beyond the saturation intensity value I_S, that is when the interaction volume is filled up with Ne^+ ions and no longer with any Ne atoms. This requires that Ne^{2+} ions are produced through an 18-photon ionization of Ne^+ ions. This is confirmed by the slope 17 ± 2 measured on the Ne^{2+} ion curve. Here, the probability of production of Ne^{2+} ions by a simultaneous excitation of two electrons is much two low to be measured.

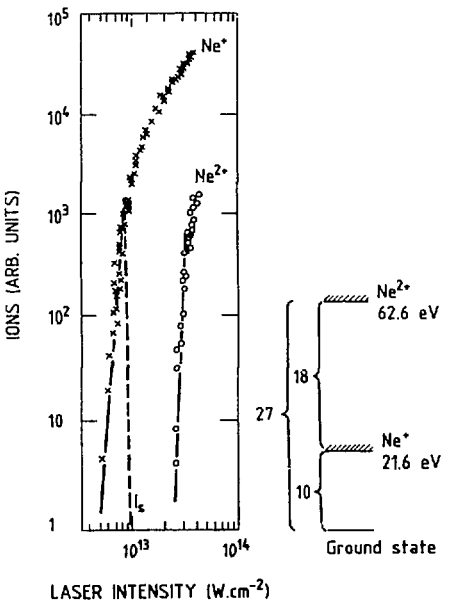

Fig. 2 - The laser intensity dependence of Ne^+ and Ne^{2+} ions formed at 532 nm.

2.3 Multiply Charged Ions Produced in Rare Gases at 1064 nm

The production of multiply charged ions has also been investigated in the five rare gases at 1064 nm [12]. Let us consider here the two most different examples : Xe and He. Figure 3 shows the variation of the number of Xe^+, Xe^{2+}, Xe^{3+}, Xe^{4+} and Xe^{5+} ions as a function of the laser intensity. The general behavior is similar to that observed at 532 nm, except for two points. First, the two different processes of production of Xe^{2+} ions, namely the simultaneous two-electron removal from Xe atoms, and the one-electron removal from Xe^+ ions, are not so well separated than at 532 nm. Second, the probability of creating Xe^{2+} ions through a simultaneous two-electron removal from Xe atoms is 30 times larger here than at 532 nm, at the reference intensity I_S. At saturation intensity $I_S = 1.2 \times 10^{13}$ W.cm^{-2} at 1064 nm the proportion of Xe^{2+} to Xe^+ ions is 1.5×10^{-2}, whereas it is only 5×10^{-4} at $I_S = 8 \times 10^{11}$ W.cm^{-2} at 532 nm.

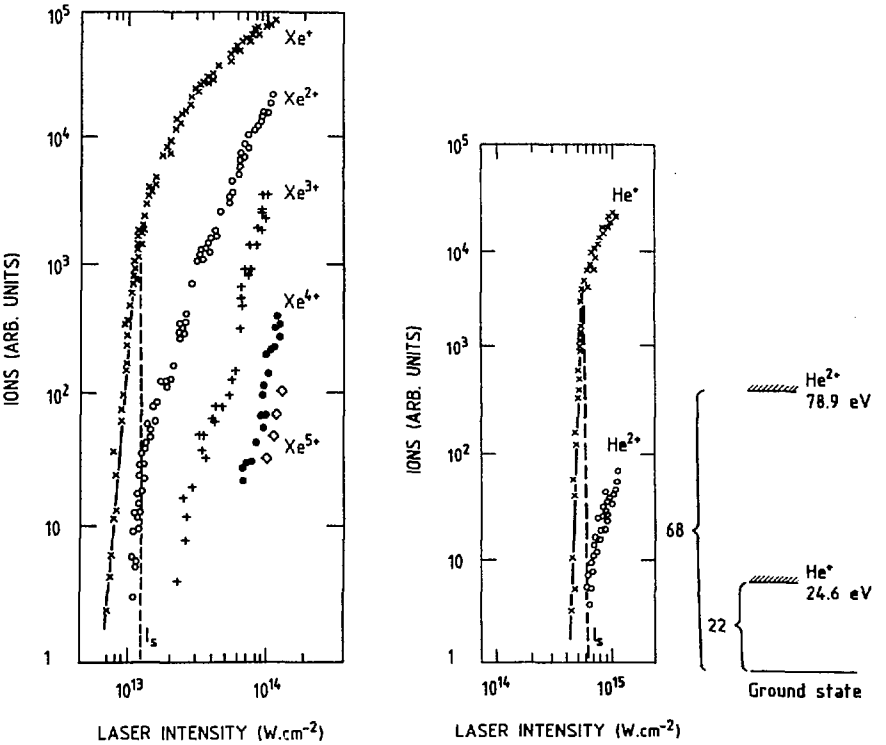

Fig. 3 - The laser intensity dependence of Xenon ions formed at 1064 nm.

Fig. 4 - The laser intensity dependence of He^+ and He^{2+} ions formed at 1064 nm.

Figure 4 shows the variation of the number of He^+ and He^{2+} ions produced as a function of the laser intensity. 68 photons at least have to be absorbed by He to produce H^{2+} ions which most probably come from a simultaneous excitation of the two electrons. This conclusion is supported by the fact that saturation of both He^+ and He^{2+} ions occurs at the same laser intensity I.

3 Discussion

The theoretical one-electron model which has been used successfully to describe one electron removal in multiphoton ionization of atomic hydrogen and alkaline atoms in the past few years cannot be applied to explain the production of multiply charged ions induced in many-electron atoms. In this respect, the following example of the production of doubly charged ions is very convincing. The one-electron removal in Xe atoms through 11-photon absorption at 1064 nm requires a laser intensity of 10^{13} W.cm^{-2}. The 29-photon absorption corresponding to the production of Xe^{2+} ions at 1064 nm would require a laser intensity of 10^{15} W.cm^{-2}, a value anticipated from the lowest order perturbation theory in the one-electron model. This is

at variance with experimental results (Fig. 3) which show that a laser intensity of 1.5 x 10^{13} W.cm^{-2} is enough to produce Xe^{2+} ions. Figure 3 also shows in other terms that the 29-photon absorption rate giving Xe^{2+} ions is only 100 times less than the 11-photon absorption rate giving Xe^{+} ions at 1.5 x 10^{13} W.cm^{-2}. In contrast, the 29-photon ionization rate anticipated from the lowest-order perturbation theory in the one-electron model would be about 10^{40} times less than the 11-photon ionization rate.

This suggests that multiphoton ionization of a closed shell such as a rare gas atom cannot be described in any circumstances by considering the interaction of the laser field with only one electron of the shell. A collective response of the atomic shell irradiated by the laser pulse should be considered. The absorption of a large number of photons may involve several electrons. The absorbed energy can be redistributed between electrons by means of electron correlations which need to be included in this picture.

The production of multiply charged ions through multiphoton absorption emphasizes both atomic properties and laser characteristics such as intensity, photon energy, pulse duration, etc... The difficult point is that these parameters are not independent. For example, changing the laser photon energy leads to change in the nonlinear order of the interaction, i.e. to change the number of photons required to reach first and second ionization limits, and consequently the laser intensity required to produce singly and doubly charged ions.

The photon energy seems to play an important role in the production of doubly charged ions through the simultaneous excitation and removal of two electrons. For example, the probability of production of Xe^{2+} ions through a simultaneous two-electron removal from Xe atoms is 30 times less at 532 nm at 10^{12} W.cm^{-2} than at 1064 nm at 10^{13} W.cm^{-2}, as shown by a comparison of Figs. 1 and 3. This result can more likely be explained in terms of laser wavelength than in terms of laser intensity, as exemplified by Fig. 2. This figure shows that at 532 nm and at high laser intensity (10^{13} W.cm^{-2}) no Ne^{2+} ions are produced below the saturation intensity I_S by a simultaneous excitation of two electrons. The longer the laser wavelength, the higher the simultaneous two-electron removal probability. Such a wavelength dependence in the simultaneous removal of two electrons looks like the well known wavelength dependence in the photoionization cross section of excited atoms. This wavelength dependence could be amplified further because here, we deal, not with a singly excited state, but with a multiply excited atom.

Figure 5 shows the variation of the maximum ion charge states produced in the five rare gases, as a function of the atomic number Z, at 1064 and 193 nm at 10^{14} W.cm^{-2}. The 193 nm data are derived from the literature [15]. Figure 5 also emphasizes the important role played by the photon energy. He^{2+} and Ne^{2+} ions are produced at 1064 nm through a simultaneous removal of two electrons. This process is very sensitive to the laser wavelength. Its rate decreases dramatically when the laser wavelength is decreased. It is expected to have a rate too low at 193 nm to be observed. Ne^{2+} ions have been observed recently at 193 nm at a much higher intensity of 10^{15} W.cm^{-2} [16]. They are most likely produced through multiphoton ionization of Ne^{+} ions. The Z dependence shown in Fig. 5 is very sensitive at 193 nm and not so important at 1064 nm. Finally, a large amount of energy can be transmitted to a many-electron atom through multiphoton absorption processes. For example, at least 250 eV have been absorbed by a Xe atom when Xe^{6+} ions are produced.

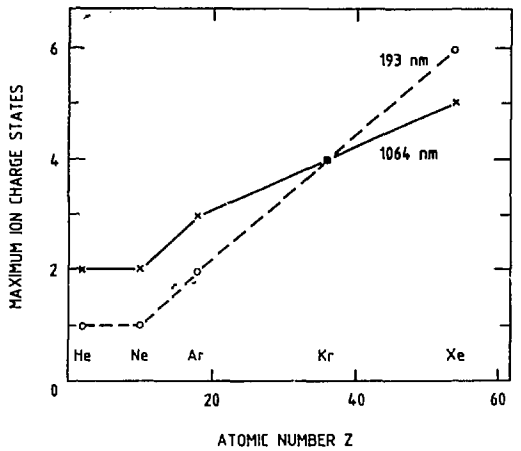

Fig. 5 - The maximum ion charge states produced in the five rare gases at 193 and 1064 nm as a function of the atomic number Z, at I = 10^{14} W.cm^{-2}.

The production of multiply charged ions has been reported in alkaline-earth atoms [17-18] and in rare gas atoms. All many-electron atoms are expected to behave similarly. There exists no quantitative theoretical model to understand these processes. Going beyond the one-electron model of multiphoton ionization is the first step towards such understanding. This requires taking into account, first, electron correlation effects, and second, doubly excited states for the alkaline-earth atoms. For rare gas atoms, the situation is still more complex because this requires the inclusion of multiply excited states. In addition, laser intensity effects on doubly or multiply excited states should be taken into account [19]. Finally, for rare gases with high Z, core excitation could become important.

As there exists no quantitative theoretical model yet, we can attempt to suggest the following tentative picture derived from the preceding experimental observations. Let us consider first the simplest example, i.e. He atom, at 1064 nm. When the laser intensity is low enough so that no ionization occurs, the two electrons can absorb many photons through laser-induced virtual doubly-excited states. Such states could be detected only by fluorescence measurements. When the laser intensity is increased, the two electrons absorb enough energy from the laser field, so that one of the two electrons is released and a He^+ ion is produced in its ground state or in an excited state. This picture could look like the well known autoionization process. When the laser intensity is increased further, the electrons absorb enough energy so that both are released simultaneously, and a He^{2+} ion is produced. For a many-electron atom, this picture should be extended to all the electrons of the outer shell, and also including possibly inner shells, to explain the production of multiply charged ions observed in rare gases. This picture seems to prevail when a long wavelength laser radiation is used. On the other hand, this picture could be quite different if a short wavelength laser radiation is used. This is because the minimum number of photons absorbed by the atom to release the first electron is much smaller. As a consequence the laser intensity required to ionize the atom is also much smaller, typically

10^3 times less. This lower intensity would not favor the production of multiply-excited states in the neutral atom. In particular, doubly charged ions would be produced only from multiphoton ionization of singly charged ions, and never through a simultaneous removal of two electrons of the neutral atom. Obviously, such a picture should be corroborated by further experimental and theoretical data.

4 Conclusion

The interaction of an intense laser field with a many-electron atom is quite an open field because the observation of multiply charged ions produced in rare gas atoms raises a number of stimulating questions which cannot be answered at the present time. The production of multiply charged ions is most likely induced by a collective response of the atomic shell. Multiply excited states are expected to play an important role. Furthermore, at 1064 nm at least 68 photons, equivalent to 79 eV, have to be absorbed by a He atom to explain the production of He^{2+} ions. The basic absorption mechanism of such a large number of photons is not yet understood. Further data on electron energy distributions and on fluorescence from excited states would be useful to understand the basic processes involved in the interaction of an intense laser field with a many-electron atom. Finally, an increase in the data concerning atomic and ionic spectroscopic behaviour can be expected.

References

1 P. Lambropoulos : Adv. At. Mol. Phys. 12, 87 (1976)
2. J. Eberly and P. Lambropoulos : Multiphoton Processes (John Wiley and Sons, New York 1978)
3 Y. Gontier and M. Trahin : Phys. Rev. A 19, 264 (1979)
4 J. Morellec, D. Normand and G. Petite : Adv. At. Mol. Phys. 18, 97 (1982)
5 G. Mainfray : J. Physique 43, C2-367 (1982)
6 D. Normand and J. Morellec : J. Phys. B 13, 1551 (1980)
7 G. Mainfray and C. Manus : Appl. Optics 19, 3934 (1980)
8 J. Morellec, D. Normand, G. Mainfray and C. Manus : Phys. Rev. Lett. 44, 1394 (1980)
9 L-A. Lompré, G. Mainfray, C. Manus and J-P. Marinier : J. Phys. B 14, 4307 (1981)
10 G. Petite, F. Fabre, P. Agostini, M. Crance and M. Aymar : Phys. Rev. A 29, 2677 (1984)
11 A L'Huillier, L-A. Lompré, G. Mainfray and C. Manus : Phys. Rev. Lett. 48, 1814 (1982)
12 A. L'Huillier, L-A. Lompré, G. Mainfray and C. Manus : J. Phys. B 16, 1363 (1983).
13 A. L'Huillier, L-A. Lompré, G. Mainfray and C. Manus : Phys. Rev. A 27, 2503 (1983)
14 A. L'Huillier, L-A. Lompré, G. Mainfray and C. Manus : J. Physique 44, 1247 (1983)
15 T. Luk, H. Pummer, K. Boyer, M. Shahidi, H. Egger and C.K. Rhodes : Phys. Rev. Lett. 51, 110 (1983)
16 K. Boyer, H. Egger, T. Luk, H. Pummer and C.K. Rhodes : J. Opt. Soc. Am. B1, 3 (1984)
17 I. Aleksakhin, I. Zapesochnyi and V. Suran : J.E.T.P. Lett. 26, 11 (1977)
18 D. Feldman, J. Krautwald, S.L. Chin, A. von Hellfeld and K. Welge : J. Phys. B 15, 1663 (1982)
19 Y.S. Kim and P. Lambropoulos : Phys. Rev. Lett. 49, 1698 (1982).

Studies of Collision-Free Nonlinear Processes in the Ultraviolet Range

C.K. Rhodes

Department of Physics, University of Illinois at Chicago, P.O. Box 4348
Chicago, IL 60680, USA

The collision-free response of atomic systems generated by intense irradiation at 193 nm exhibits several unusual properties. The behavior observed for the dependencies on atomic number, intensity of illumination, frequency, and polarization are discussed. The experimental evidence points to collective atomic motion involving several electrons and implicates a possible role for a Coster-Kronig mechanism, enabling rapid energy transfer among atomic subshells.

1. Introduction

Studies of atomic and molecular absorption, conducted under collision-free conditions at ultraviolet wavelengths, have exhibited unexpected and unusual characteristics. The initial studies [1,2] of the Z-dependence of collision-free multiphoton ionization of atoms at 193 nm clearly exhibited anomalous behavior in terms of the gross rate of energy transfer. The general class of physical processes studies in these experiments was

$$N\gamma + X \rightarrow X^{q+} + qe^{-} \quad . \tag{1}$$

A prominent feature of these studies was the unusually strong nonlinear coupling found, characteristic of certain heavy materials. These experiments clearly demonstrated that standard theoretical techniques were incapable, by a discrepancy as great as several orders of magnitude, of describing those results. Subsequent work [3], as well as other studies [4,5] conducted at a wavelength of 1.06 μm and 0.53 μm, has confirmed the anomalous nature of the coupling strength.

For the studies of multiple ionization conducted since the earlier studies [1,2] were completed, the 193 nm ArF* laser used for irradiation [6] (∿ 5 nsec, ∿ 3 GW) was focused by an appropriate lens to generate intensities in the range of 10^{15} - 10^{17} W/cm^2 in the experimental volume. In order to produce the highest intensities used, an f/2 aspheric focusing element was necessary. The ions are created in a vacuum vessel which is evacuated to a background pressure of ∿ 10^{-8} Torr.

In contrast to the earlier work [1,2], the ion analyzer had a greatly extended time-of-flight drift region which permitted significantly superior mass and charge discrimination [7]. This enabled the isotopic signature of heavy atoms to be readily distinguished [8]. This aspect provided a clear identification of the signal and enabled unambiguous separation of the desired ion cur-

rent from any spurious signals originating from the background gas. For example, the characteristic isotopic pattern observed for Xe^{5+} and Xe^{6+} corresponded closely to the strengths expected on the basis of the isotopic natural abundance [9].

2. Discussion of Results

The primary information obtained by observation of the ion spectra pertains to the scale of the energy transfer, for both average and peak values, communicated to the target atom X by the radiation field and an examination of the Z-dependence of the average energy transfer is informative. Figure (1) illustrates the dependence observed at 193 nm for an intensity of irradiation in the range of 10^{15} - 10^{16} W/cm^2. Specific notice is called to the comparison in the average energy absorbed for the adjacent elements, I (Z = 53) and Xe (Z = 54), which is remarkable. This difference, which is approximately a factor of four, cannot reasonably be attributed to experimental error, since only the strong easily registered ion signal components figure appreciably in the calculation of the average energy. Furthermore, since the two elements are close in atomic mass, the ion velocities of the two materials, for a given charge state, are nearly identical, rendering corrections in the sensitivity of the channel plate detector due to differences in velocities negligible. The relatively weak response of the light materials as well as certain heavy atoms, such as Eu and Yb, is also apparent. These data support the significant conclusion that some factor involving the basic atomic structure of the materials must account for the observed differences in energy transfer and that this factor can vary rapidly in atomic number.

Another salient feature of the data is the clear influence of atomic shell structure [1] on the observed ion spectra. This dependence is manifested prominently in the behavior of the heavier

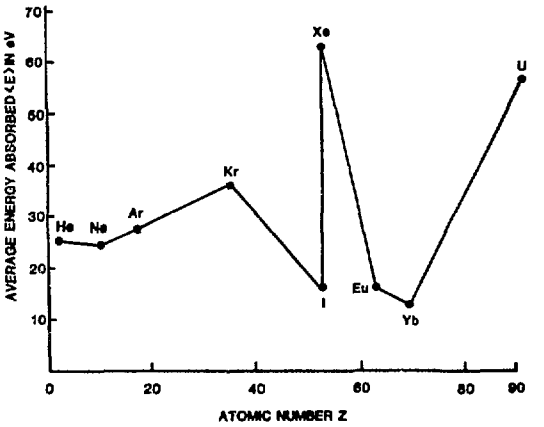

Fig. (1): Average energy absorbed per atom under collision-free conditions for irradiation at 193 nm with an intensity range of 10^{15} - 10^{16} W/cm^2.

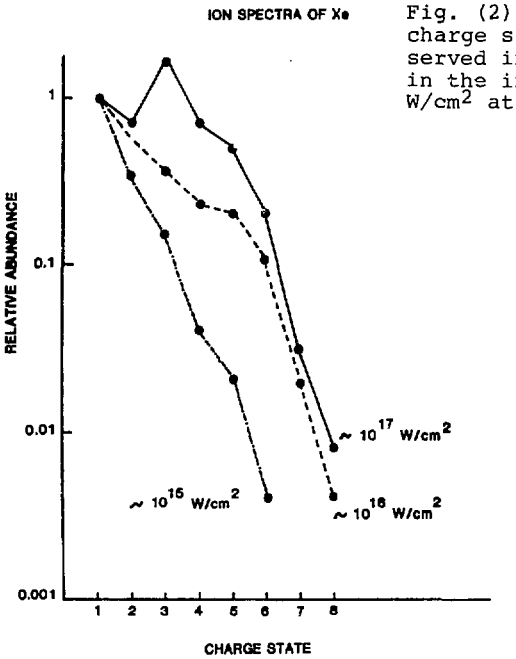

Fig. (2): Relative abundance of charge state distributions observed in the ion spectra of xenon in the intensity range 10^{15} - 10^{17} W/cm^2 at 193 nm.

rare gases. For Ar, Kr, and Xe, the maximum charge states observed would correspond to the complete removal of certain atomic sub-shells. Indeed, for these materials they are the 3p, the 4p, and both the 5s and 5p shells, respectively.

The intensity dependence of these ion spectra has also been preliminarily examined, and Figure (2) illustrates the nature of this response for xenon. Over the range of intensities studied ($\sim 10^{15}$ - 10^{17} W/cm^2), higher intensity translates generally into an increased yield of ions of a particular charge, although not necessarily an increase in the maximum charge state observed. For example, the ion Xe^{8+}, with closed shell ground state [10] configuration $4d^{10}$, is the greatest charge state detected at $\sim 10^{16}$ W/cm^2, and, although its abundance increases at $\sim 10^{17}$ W/cm^2, no Xe^{9+} appears at the higher intensity. The average energy communicated to the atom also increases at the higher intensities, although clearly not as rapidly as the intensity. In the case of xenon shown in Figure (2), the average energy increased only by approximately seven-fold, although the intensity had changed by a factor of approximately one-hundred. From the observed behavior, the average energy appears to scale more closely to the square root of the intensity than the linear power.

The frequency dependence of the coupling has also been examined by comparison of our results at 193 nm with other studies performed [4,5] at 1.06 μm and 0.53 μm. The comparison, conducted at an intensity of $\sim 10^{14}$ W/cm^2 for both krypton and xenon, indicates that the average energy absorbed is reduced at the longer wavelengths.

The influence of polarization has been studied for xenon. With the use of a quarter-wave plate, the linearly polarized radiation normally produced by the 193 nm source [6] can be conveniently transformed into a circularly polarized field. The ion spectra observed for xenon were found to be negligibly modified by the change from linear to circular polarization. This result is in contrast to that expected on the basis of perturbation theory analyses [11,12] in the single electron picture of the interaction. In that case, for high order processes, the much greater abundance of available channels for linear polarization produces a substantially greater ionization rate in comparison to that characteristic of circular polarization.

Qualitatively, several aspects of the basic interaction emerge clearly. With reference to xenon, for example, a one hundred-fold increase in 193 nm intensity from $\sim 10^{15} - 10^{17}$ W/cm^2 does not drastically increase either the maximum charge state observed or the average energy transferred. Over this range, the maximum charge state observed advances from $q = 6$ to $q = 8$, and the average energy transferred in the interaction increases by approximately a factor of seven. Within the experimental uncertainty over this range of intensity, the average energy appears to grow approximately in direct proportion to the magnitude of the radiative electric field, or equivalently, to the square root of the intensity. Furthermore, since the charge state does not increase beyond the apparent removal of the full 5p and 5s subshells, tentatively we can conclude that the $n = 5$ shell is an important agent coupling the xenon atom to the 193 nm radiation field. It is also known, however, particularly from photoionization studies involving multiple electron ejection [13,14], that the 5p, 5s, and 4d shells exhibit substantial intershell coupling and behave in a collective fashion in a manner resembling a single supershell [15]. An immediate consequence of this type of behavior is an increase in multiphoton coupling resulting directly from the larger magnitude of the effective charge involved in the interaction. In this way, a multielectron atom undergoing a nonlinear interaction responds in a fundamentally different fashion from that of a single electron atom. The motion envisaged [1] has a nuclear counterpart known as the giant dipole [16], a phenomenon which can also be manifested in higher multipoles [17].

Several theoretical methods are available for comparison with these data. Among them are standard perturbative multiphoton analyses [11,18,19], nonperturbative treatments [20-22], and static pictures based on a Thomas-Fermi atomic model [23]. All fail to adequately describe the experimental findings. The customary procedures based on a single electron model do not produce a sufficient coupling strength, as described earlier [1,2]. The tunneling model, such as that developed by KELDYSH [22], is found to give neither the correct dependence on intensity nor the observed relationship on atomic number. The Thomas-Fermi picture, since it is a static model, gives a result rigorously independent of frequency of irradiation, a conclusion contrary to the experimental facts obtained in separate studies [1,4,5] at 1.06 μm, 0.53 μm, and 193 nm.

The data strongly indicate that a collective response of an entire shell, or a major fraction thereof, is directly involved

in the nonlinear coupling. Collective responses of atomic shells, as noted above, have been discussed in relation to the mechanism of single photon photoionization. These studies simply point to a nonlinear analog of this basic electronic mechanism. With this picture, the outer atomic subshells are envisaged as being driven in coherent oscillation by the intense ultraviolet wave. We note that an oscillating atomic shell, quantum mechanically, would be represented by a multiply excited configuration.

At sufficiently high intensity, a relatively simple physical model can be envisaged. At an intensity of $\sim 10^{19} - 10^{20}$ W/cm^2, which we anticipate will be available soon with the use of femtosecond rare gas halogen lasers, the peak ultraviolet electric field is more than ten-fold e/a_0^2, so that loosely bound outer electrons could be approximately modelled as free particles. In this case, the problem reduces to that of the acceleration of electrons in focused laser fields [24], an issue that, incidentally, is related to the acceleration of cosmic rays by rotating neutron stars [25]. In this case, we imagine an atom composed of two parts, (a) an outer shell of electrons driven in coherent oscillation by the radiative field and (b) an atomic core. The outer electrons could, through inelastic "collisions," transfer energy to the core. Simple estimates indicate that for intensities of that magnitude, the outer electrons would approach relativistic velocities ($\sim$ 50 - 100 keV) and that oscillating atomic current densities j on the order of $10^{14} - 10^{15}$ amps/cm^2 could be established as a result.

In this high intensity limit, it is possible to formulate an estimate of the coupling of the coherently driven outer electrons with the remaining atomic core by a relatively simple procedure. Since the electron kinetic energies are considerably above their corresponding binding energies, it appears possible to use a first order Born approximation [26] in a manner similar to that used to the study of electron collisions for K- and L-shell ionization [27] and shell specific ionization processes in highly charged ions [28, 29]. Indeed, in the case of xenon ions, cross sections for electron impact ionization are available [30]. In this simple classical picture, we can write the transition rate R as

$$R \simeq \frac{j}{e} \sigma_e \qquad (2)$$

in which e is the electronic charge and σ_e is the cross section characterizing the excitation of the atomic core by inelastic electron collisions arising from the ambient current density j. If $j \sim 10^{14}$ amps/cm^2 and $\sigma_e \sim 10^{-19}$ cm^2, then $R \sim 6 \times 10^{13}$ sec^{-1}. Furthermore, if the coherently driven current density j is damped by electron emission in a time τ on the order of $\sim 10^{-14}$ sec, an approximate time scale characterizing autoionization, the overall transition probability $P \sim R\tau \sim 0.6$, indicating a significant probability of energy transfer.

Naturally, alternative procedures can be used to estimate the energy transfer to the atom. One is an estimate based on inverse bremsstrahlung [31] that could possibly occur in the outer region (a) of the simple atomic model described above. In this case, the increase in the kinetic energy of the electrons in the outer region accounts for the absorption and none is transferred to the core.

In xenon, such an estimate [31] gives a result in excess of 1 keV/atom for an intensity of $\sim 10^{16}$ W/cm^2 at 193 nm for an interaction time $\tau \sim 10^{-14}$ sec.

Both of the simple pictures sketched above imply the existence of energy transfers in the kilovolt range or, equivalently, processes that involve the interchange of more than one hundred quanta. The electron spectra of the inverse bremsstrahlung case, however, should differ appreciably from that involving significant energy transfer to the interior of the atom. Rather distinct Z-dependencies are also expected.

The strong variation in average energy transfer exhibited in Figure (2) deserves comment. These data indicate a complex and rapidly varying Z-dependence for heavy materials. It has not been possible to formulate a reasonable explanation of this behavior solely on the basis of the systematics of valence shell properties [1,2,8]. These results again point to the significance of intershell couplings. Such couplings are manifested in an obvious way, for example, in Coster-Kronig processes [32]. Indeed, if we consider, as specific cases, Giant Coster-Kronig (gCK) processes of the type

$$n\underline{s} \rightarrow n\underline{p}^2 nd, \varepsilon d \qquad (3)$$

and Super Coster-Kronig (sCK) processes like

$$n\underline{p} \rightarrow mf, \varepsilon f \ , \qquad (4)$$

it is well established that strong perturbations [33] are present and that the single electron picture seriously breaks down [34]. These processes are sensitive to systematics of the shell energy levels and, therefore, can exhibit sharp variation in their dependence on atomic number. In particular, many-electron effects are prominent when there is a degeneracy between single and double vacancy states that are strongly coupled. These requirements are commonly fulfilled and strong collective behavior arises, for example, in single photon photoionization [15,35,36]. Significantly, in comparison with the data shown in Figure (1), these effects are known to be of importance [34,37] over certain regions of the atomic number from argon to the heavier part of the periodic table. In this regard, it is significant to recall that degeneracies of single and multiple hole states occur at particular values of the atomic number [33,38]. Indeed, such strong intersubshell couplings are known [39], for example, to produce discontinuous behavior in the L_α and $L_{\beta 1}$ satellite fractions as well as in the $L_{\beta 3,4}/L_\alpha$ and $L_{\beta 1}/L_\alpha$ intensity ratios as a function of atomic number Z in the region $Z \approx 50$. The discontinuous behavior in Z characteristic of satellite fractions has a striking similarity to that exhibited in Figure (2). Similarly, sharp variations in atomic number have been calculated in the Auger width associated with a 2s vacancy [40].

Normally, relaxation mechanisms involving intershell coupling, such as Coster-Kronig and Auger processes, are experimentally observed by initially producing an inner-shell vacancy which subsequently relaxes, generally producing multiple vacancies and excitation in outer shells. In principle, the initial vacancy can be

produced with radiative excitation [41,42], electron collisions [43,44], beam foil methods [45], ion collisions [46], and nuclear decay processes such as K-capture [47,48]. To these alternatives, the results of these experiments suggest that multiquantum processes may now conceivably be added. Furthermore, the nature of Coster-Kronig processes provides a hint at the mechanism that could make this possible. In simple terms, this can be viewed as a reverse Coster-Kronig process [34] in which multiple excitations in outer shells generate excitations in more tightly bound shells. In this fashion we use the term "excitation" in a broad sense to include both bound excited levels and continuum states (vacancies). For double and single excitations or vacancies, this mechanism is basically represented by the reverse reactions of processes (3) and (4), namely,

$$ns \leftarrow np^2nd,\varepsilon d \qquad (3')$$

$$np \leftarrow nd^2mf,\varepsilon f \ . \qquad (4')$$

Indeed, since these intershell couplings are sensitive to the systematics of the shell binding energies, resonance effects [34,49] are expected in certain regions of atomic number Z for the reasons stated above. In summary, the similarity of the discontinuous character of the data represented in Figure (1) and that manifested by Coster-Kronig processes suggests a common origin for this general type of behavior, namely, the possibility that the electrons involved in the nonradiative relaxation of an atom in the forward reaction (3) could, in the reverse process (3'), if driven by coupling to a sufficiently intense radiation field, generate a corresponding transfer of energy into an atom.

3. Conclusions

The nonlinear coupling of 193 nm radiation to a range of atomic systems has been studied up to a maximum intensity on the order of 10^{17} W/cm^2. Studies of ion production, under collision-free conditions, exhibit anomalous behavior which implicates the atomic shell structure as the principal determinant in the observed response. On the basis of the coupling strength observed and the measured Z-dependence, the experimental evidence points to a collective coherent atomic motion involving several electrons, possibly an entire shell, as the main physical mechanism enabling the scale of the energy transfers seen. In quantum mechanical language, states representing multiple excitations appear to play a central role in the coupling, a consideration that fundamentally distinguishes the nonlinear interaction of a multielectron atom from that of a single electron system. In this context, it is interesting to consider analyses [50] which explore the atomic number dependence of the transition from collective to independent-particle motion in outer atomic shells. Furthermore, it is postulated that the sharp variations in Z noted for the heavy materials may be due to a reverse Coster-Kronig mechanism in which inner-shell excitations are produced by interaction with multiply excited outer shells. Comparison with standard theoretical treatments of nonlinear processes, of either perturbative or nonperturbative nature, does not produce agreement with the experimental findings.

4. Acknowledgements

The author wishes to acknowledge the collaboration of H. Pummer, H. Egger, T. S. Luk, K. Boyer, W. Müller, and U. Johann and the expert technical assistance of M. J. Scaggs, J. R. Wright and D. M. Gustafson. This work was supported by the Air Force Office of Scientific Research under contract number F49630-83-K-0014, the Department of Energy under grant number DeAS08-81DP40142, the Office of Naval Research, the National Science Foundation under grant number PHY81-16626, the Defense Advanced Research Projects Agency, and the Avionics Laboratory, Air Force Wright Aeronautical Laboratories, Wright Patterson Air Force Base, Ohio.

References

1. T. S. Luk, H. Pummer, K. Boyer, M. Shahidi, H. Egger, and C. K. Rhodes: Phys. Rev. Lett. 51, 110 (1983)

2. T. S. Luk, H. Pummer, K. Boyer, M. Shahidi, H. Egger, and C. K. Rhodes: Excimer Lasers - 1983, AIP Conference Proceedings No. 100, edited by C. K. Rhodes, H. Egger, and H. Pummer (American Institute of Physics, New York, 1983) p. 341

3. A. L'Huillier, L-A. Lompré, G. Mainfray, and C. Manus: Multiply charged ions produced by multiphoton absorption in rare gas atoms. Proceedings of the Conference on Laser Techniques in the Extreme Ultraviolet (AIP, to be published)

4. A. L'Huillier, L-A. Lompré, G. Mainfray, and C. Manus: Phys. Rev. Lett. 48, 1814 (1982)

5. A. L'Huillier, L-A. Lompré, G. Mainfray, and C. Manus: Phys. Rev. A27, 2503 (1983)

6. H. Egger, T. S. Luk, K. Boyer, D. F. Muller, H. Pummer, T. Srinivasan, and C. K. Rhodes: Appl. Phys. Lett. 41, 1032 (1982)

7. W. C. Wiley and I. H. McLaren: Rev. Sci. Instr. 26, 1150 (1955)

8. H. Egger, T. S. Luk, W. Müller, H. Pummer, and C. K. Rhodes: Collision-free multiple ionization of atoms and XUV stimulated in krypton at 193 nm. AIP Conference Proceedings, Laser Techniques in the Extreme Ultraviolet, Boulder, Colorado, 5-7 March 1984 (to be published); H. Pummer, H. Egger, T. S. Luk, and C. K. Rhodes: SPIE 461, 53 (1984)

9. Table of Isotopes, Seventh Edition, C. Michael Lederer and Virginia S. Shirley (John Wiley and Sons, New York, 1978)

10. J. Blackburn, P. K. Carroll, J. Costello, and G. O'Sullivan: J. Opt. Soc. Amer. 73, 1325 (1983)

11. P. Lambropoulos in Advances in Atomic and Molecular Physics, Vol. 12, edited by D. R. Bates and B. Bederson (Academic Press, New York, 1976) p. 87

12. H. R. Reiss: Phys. Rev. Lett. 29, 1129 (1972)

13. M. J. Van der Wiel and T. N. Chang: J. Phys. B11, L125 (1978)

14. M. Ya. Amusia in Advances in Atomic and Molecular Physics, Vol. 17, edited by D. R. Bates and B. Bederson (Academic Press, New York, 1981) p. 1

15. M. Ya. Amusia and N. A. Cherepkov in Case Studies in Atomic Physics 5, edited by E. W. McDaniel and M. R. McDowell (North-Holland, Amsterdam, 1975) p. 47

16. G. C. Baldwin and G. S. Klaiber: Phys. Rev. 71, 3 (1947), and 73, 1156 (1948); M. Goldhaber and E. Teller: Phys. Rev. 74, 1046 (1948)

17. Giant Multipole Resonances, edited by F. E. Bertrand (Harwood Academic, London, 1980)

18. H. B. Bebb and A. Gold: Phys. Rev. 143, 1 (1966)

19. Y. Gontier and M. Trahin: J. Phys. B13, 4384 (1980); Y. Gontier and M. Trahin: Phys. Rev. 172, 83 (1968)

20. H. R. Reiss: Phys. Rev. A1, 803 (1970); ibid.: Phys. Rev. Lett. 25, 1149 (1970); ibid.: Phys. Rev. D4, 3533 (1971); ibid.: Phys. Rev. A6, 817 (1972)

21. H. S. Brandi and L. Davidovich: J. Phys. B12, L615 (1979)

22. L. V. Keldysh: Zh. Eksp. Teor. Fiz. 47, 1945 (1964) [Sov. Phys. - JETP 20, 1307 (1965)]

23. John C. Slater: Quantum Theory of Atomic Structure, Vol. I (McGraw-Hill, New York, 1960) p. 480

24. Marc J. Feldman and Raymond Y. Chiao: Phys. Rev. A4, 352 (1971).

25. James E. Gunn and Jeremiah P. Ostriker: Phys. Rev. Lett. 22, 728 (1969)

26. N. F. Mott and H. S. W. Massey: The Theory of Atomic Collisions (Oxford University Press, London, 1965); H. S. W. Massey and E. H. S. Burhop: Electronic and Ionic Impact Phenomena, Vol. 1 (Oxford University Press, London, 1969); H. A. Bethe, An. der Phys. 5, 325 (1930); N. M. Kroll and K. M. Watson: Phys. Rev. A8, 804 (1973)

27. James H. Scofield: Phys. Rev. A18, 963 (1978)

28. L. B. Golden, P. H. Sampson, and K. Omidvar: J. Phys. B11, 3235 (1978)

29. L. B. Golden and D. H. Sampson: J. Phys. B13, 2645 (1980)

30. D. C. Gregory and D. H. Crandall: Phys. Rev. A27, 2338 (1983); C. Achenbach, A. Müller, E. Salzborn, and R. Becker: J. Phys. B17, 1405 (1984)

31. Yaakov Shima and Haim Yatom: Phys. Rev. A12, 2106 (1975)

32. E. J. McGuire in Atomic Inner-Shell Processes, Vol. I, edited

by B. Crasemann (Academic Press, New York, 1975) p. 293; D. Chattarji: The Theory of Auger Transitions (Academic Press, New York, 1976)

33. T. Åberg in Photoionization and Other Probes of Many-Electron Interactions, edited by F. J. Wuilleumier (Plenum Press, New York, 1976) p. 273

34. G. Wendin: Breakdown of the One-Electron Pictures in Photoelectron Spectra, Structure and Bonding Vol. 45 (Springer-Verlag, Berlin, 1981); S. Lundquist and G. Wendin: J. Elec. Spectrosc. Rel. Phenom. 5, 513 (1974)

35. G. Wendin in Vacuum Ultraviolet Radiation Physics, edited by E. E. Koch, R. Haensel, and C. Kunz (Pergamon/Vieweg, Braunschweig, 1974) p. 225

36. G. Wendin in Photoionization and Other Probes of Many-Electron Interactions, edited by F. J. Wuilleumier (Plenum Press, New York, 1976) p. 61; H. P. Kelly and S. L. Carter: Phys. Scr. 21, 448 (1980)

37. J. A. R. Samson and G. N. Haddad: Phys. Rev. Lett. 33, 875 (1974); J. A. R. Samson in Photoionization and Other Probes of Many-Electron Interactions, edited by F. J. Wuilleumier (Plenum Press, New York, 1976) p. 419

38. Ken-Ning Huang, Michio Aoyagi, Mau Hsiung Chen, Bernd Crasemann, and Hans Mark: At. Data Nucl. Data Tables 18, 243 (1976)

39. B. L. Doyle and S. M. Shafroth: Phys. Rev. A19, 1433 (1979)

40. B. F. Rozsnyai, V. L. Jacobs, and J. Davis: Phys. Rev. A21, 1798 (1980)

41. T. A. Carlson, W. E. Hunt, and M. O. Krause: Phys. Rev. 151, 41 (1966)

42. T. S. Axelrod: Phys. Rev. A13, 376 (1976); T. Åberg in Proceedings of the International Conference on Inner-Shell Ionization and Future Applications, edited by R. W. Fink, S. T. Manson, J. M. Palms, and P. V. Rao, CONF-720 404 (Natl. Tech. Information Service, U.S. Dept. of Commerce, Springfield, VA, 1972); John W. Cooper in Atomic Inner-Shell Processes, Vol. I, edited by B. Crasemann (Academic Press, New York, 1975) p. 160

43. T. A. Carlson, W. E. Moddeman, and M. O. Krause: Phys. Rev. A1, 1406 (1970)

44. L. M. Middleman, R. L. Ford, and R. Hofstadter: Phys. Rev. A2, 1429 (1970); K. Ishii, M. Kamiya, K. Sera, S. Morita, H. Tawan, M. Oyamada, and T. C. Chu: Phys. Rev. A15, 906 (1977)

45. I. Martinson in Beam-Foil Spectroscopy, edited by S. Bashkin (Springer-Verlag, Berlin, 1976) p. 33

46. D. H. Madison and E. Merzbacher in Atomic Inner-Shell Pro-

cesses, Vol. I, edited by B. Crasemann (Academic Press, New York, 1975) p. 1; U. Fano and W. Lichten: Phys. Rev. Lett. 14, 627 (1965); M. Barat and W. Lichten: Phys. Rev. A6, 211 (1972); P. Ziem, R. Bruch, and N. Stoltefoht: J. Phys. B8, L480 (1975); J. M. Hansteen in Advances in Atomic and Molecular Physics, Vol. 11, edited by D. R. Bates and B. Bederson (Academic Press, New York, 1975) p. 299; P. H. Mokler and F. Folkmann in Structure and Collisions of Ions and Atoms, edited by I. A. Sellin (Springer-Verlag, Berlin, 1978) p. 201

47. Robert J. Walen and Chantel Briançon in Atomic Inner-Shell Processes, Vol. I, edited by B. Crasemann (Academic Press, New York, 1975) p. 233; M. S. Freedman in Photoionization and Other Probes of Many-Electron Interactions, edited by F. J. Wuilleumier (Plenum Press, New York, 1976) p. 255

48. W. Bambynek, H. Behrens, M. H. Chen, B. Crasemann, M. L. Fitzpatrick, K. W. D. Ledingham, H. Genz, M. Mutterer, and R. L. Intemann, Rev. Mod. Phys. 49, 77 (1977)

49. C. -O. Almbladh and L. Hedin in Handbook on Synchrotron Radiation, Vol. 1b, edited by Ernst-Eckhard Koch (North-Holland Publ. Co., Amsterdam, 1983) p. 607

50. C. E. Wulfman and R. D. Levine: Phys. Rev. Lett. 53, 238 (1984)

Multiphoton Excitation of Doubly Excited States of Two-Electron Atoms

R.R. Freeman and L.A. Bloomfield
AT & T Bell Labs., Murray Hill, NJ 07974, USA
W.E. Cooke
Physics Department, University of Southern California,
Los Angeles, CA 90089, USA
J. Bokor and R.M. Jopson
AT & T Bell Labs., Holmdel, NJ 07733, USA

One of the outstanding problems in atomic physics is to better understand the dynamics of highly excited two-electron systems. In 1977, I.C. PERCIVAL [1] coined the term "planetary atoms" to describe these atoms in which both of the electrons are so highly excited that their mutual perturbations are large enough to introduce dramatic angular correlations in their motion. He introduced a semiclassical method-quantizing classical two-electron orbits-to predict some scaling laws. Others have attempted to solve this problem from a purely quntum mechanical approach. HERRICK and SINANOGLU [2] have employed group theory methods to classify energy levels for the He $3\ell 3\ell'$ Their approach was strongly suggestive that these atoms vibrated and rotated with the electrons localized on opposite sides of the nucleus--more like a "molecular atom". FANO and others [3] have analyzed the problem using hyperspherical coordinates and found that, at least for the case of near threshold ionization, both electrons are highly correlated in angle as they move along a "Wannier ridge", a local maximum in the potential energy surface.

On the experimental side, single photon excitation studies [4] have been limited to relatively low-lying states in He, while electron scattering experiments do not adequately resolve individual states [5]. This paucity of experimental data is due to three general characteristics of these highly excited double electron states: 1) they have high energies, usually greater than 1 Ryd, since two electrons are excited; 2) they have little overlap with the ground state; and, consequently, 3) single photon excitation will not efficiently excite these states. It is the purpose of this paper to discuss the multiphoton excitation of these special states in two-electron systems.

Our experimental approach relies upon a technique developed by COOKE and GALLAGHER [6], commonly referred to as Isolated Core Excitation (ICE). JOPSON,FREEMAN,COOKE and BOKOR [7] have recently discussed the multiphoton generalization of ICE, demonstrating how the use of multiphoton techniques allow the investigation of relaxation "shake-up" processes in multi-electron atoms. The excitation of the atoms using ICE is in two parts: Two lasers are used to prepare barium atoms in an atomic beam in a highly excited Rydberg state. (We use barium atoms because of their convenient visible transitions; the characteristics of the highly excited double electron states of barium should be largely insensitive to the xenon-like Ba++ core.) These Rydberg states consist of primarily one single configuration which has one valence electron in the ground, 6s, state and one electron in a highly excited $n\ell$ state. These bound states have been well characterized spectroscopically [8] and are easily resolvable with our pulsed lasers. This initial excitation isolates the core, insofar as further optical fields only affect the remaining 6s core electron, since the Rydberg electron is moving too slowly to respond to a rapidly oscillating field. Furthermore, since the Rydberg electron is localized far from the 6s

electron, the 6s electron responds to frequencies very near to those that excite the 6s core electron to an ns excited state in Ba+. This step can be accomplished stepwise, through a real intermediate state, using two lasers; or it can occur using two photons from one laser in which a virtual intermediate state is used.

Figure 1 shows the two method for exciting the isolated 6s core to a 7s state. In either case, spectra is obtained by tuning the *core laser* frequencies and monitoring the production of doubly excited states, while the first lasers remain *fixed* to a specific Rydberg state. This produces spectra for the 6snℓ → msn'ℓ transitions where n and n' need not be the same, although ℓ does not change.

Figure 2 shows a typical spectrum obtained in this kind of experiment: barium atoms were prepared in a 6s29d ($^1D_2$) state, then two photons from a single laser drove the isolated core 6s electron to the 7s state. The satellite peaks surrounding the "diagonal" 6s29d → 7s29d transition reflect the non-orthogonality between the 6snd states and the 7snd states. This non-orthogonality is a consequence of the 7s core size being larger than the 6s core size so that the quantum defect of the 29d Rydberg electron is different in the two cores.

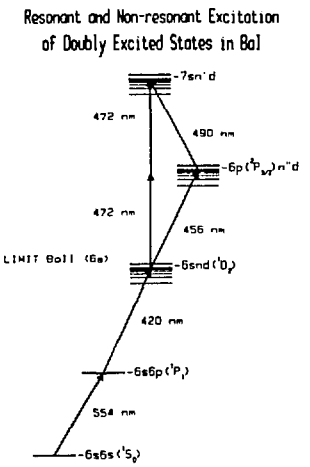

Fig. 1 Schematic of the multiphoton excitation schemes used in ICE

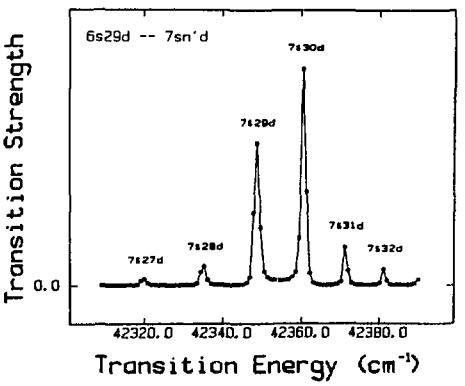

Fig. 2 Low resolution view of the excitation spectrum of the 7sn'd states in Ba

A spectrum that should be qualitatively similar to the spectrum in Fig. 2 could be obtained using the step-wise, two laser technique in which the first laser is tuned to be nearly resonant with one of the intermediate $6p(^2P_{3/2})n''d$ states, and the second laser completes the $6pn''d$ → $7sn'd$ transition. However, it is also clear that the observed "shake-up" spectrum in this case will be different than in the single laser, off-resonance case, because the Rydberg electron will have time to partially readjust to the changing size of the core. That is,from the point-of-view of the Rydberg electron, while the off-resonance two-photon transition can be considered "sudden", as the detuning from a real intermediate state is reduced, the transition appears more and more "adiabatic". Moreover, because there now exists two paths to the same final state, in general for any

given detuning, the two-photon transition moment will evidence *interferences between the direct (sudden) and intermediate-state (adiabatic) processes.*

Figure 3 shows typical data, and highlights the differences between the off-resonance and intermediate resonance cases. In this figure, the x-axis is measured in energy, in this case labeled by the continuous variable n' (in the sense that the binding energy is given by $E=-(1/2)(n'-\delta)^{-2}$ where δ is the quantum defect for the 7s core state). The y axis in each case is the relative transition strength. In case (a) two photons from one laser drive the $6s \rightarrow 7s$ isolated core electron, and the spectrum reflects the "sudden" change in the quantum defect of the 24d electron. In the cases (b)-(d), the first laser of the two-step process is tuned to the n"= 23,24,25 $6p(^1P_{3/2})n''d$, respectively, and the second laser is swept over the same final states as in case (a). Note how these spectra, obtained for small detunings from the 6p24d intermediate-state resonance, differ significantly from the case of far off-resonance in (a).

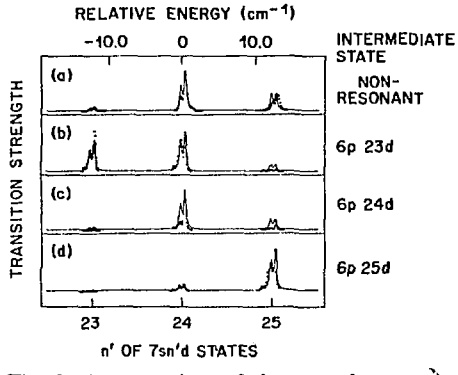

Fig. 3 A comparison of theory and experiment for the observed doubly excited spectra for the two-photon transition 6S24d → 7sn'd. Experimental results are the points, the solid line is the theory described in the text. In (a), the detuning from intermediate-state relaxations are negligible. For (b) - (d) the detunings are small, and the various intermediate-state relaxations play a large role in determining the observed intensity pattern.

A physical description of what is going on may be obtained from considerations of second-order perturbation theory. In two-photon excitations, the "time" that a system spends in a real intermediate state is proportional to $1/\Delta\omega$, where $\Delta\omega$ is the detuning from the state. Now, the readjustment time of a Rydberg wave function due to a change in the potential is given by the inverse of the energy-spacing between adjacent levels; this time is $3\times10^{-16}n^3$. Thus, for far enough detuning from the relevant intermediate states, the transition will appear "sudden" to the Rydberg electron.

This qualitative description may be made quantitative using second order perturbation theory [9], allowing total relaxation for each intermediate state, and summing each state's contribution weighted by the time the atom spends in that intermediate state. That is

$$RATE = \frac{2\pi}{\hbar}|T|^2 A(\Omega) \qquad (1)$$

where $A(\Omega)$ is the density of final states and

$$T = \sum_{n''} \frac{<6snd|\mu_1 E_1|6pn''d><6pn''d|\mu_2 E_2|7sn'd>}{\left[\Delta\epsilon_{n''} + \frac{i\Gamma_{n''}}{2}\right]} \tag{2}$$

where $\Delta\epsilon_{n''} = \epsilon_{n''} - \hbar\omega_1$, and $\epsilon_{n''}$ and $\Gamma_{n''}$ are the energy and width of the intermediate states $6pn''d$. This expression may be written in an isolated core approximation [6]:

$$T = \left[<6s|\mu_1 E_1|6p><6p|\mu_2 E_2|7s>\right]_{ion} \sum_{n''} \frac{<n|n''><n''|n'>}{\left[\Delta\epsilon_{n''} + \frac{i\Gamma_{n''}}{2}\right]} \tag{3}$$

Ba^+ ion wavefunctions, and the Rydberg wavefunctions $|n>$, $|n''>$, and $|n'>$ are hydrogenic, with effective quantum numbers appropriate for the 6s, 6p, and 7s cores, respectively. The analytical expression for the Rydberg overlap integrals is [10]:

$$<n|n''> = \frac{2\sqrt{n^* n''^*}}{\left[n^* + n''^*\right]} \frac{\sin\pi\left[n^* - n''^*\right]}{\pi\left[n^* - n''^*\right]} \tag{4}$$

where n^* and n''^* are the effective quantum numbers of the n and n'' states, respectively.

In the far off intermediate resonance case, $\Delta\epsilon_{n''}$ is large for all n'' and does not vary appreciably in the sum. Under these conditions, Eq.(3) may be evaluated as

$$T = \frac{<n|n'>}{\Delta\epsilon}\left[<6s|\mu_1 E_1|6p><6p|\mu_2 E_2|7s>\right]_{ion} \tag{5}$$

This is just the prediction that far off intermediate resonance, where the transition is fast compared to intermediate state relaxations, the shake-up spectrum will depend only on the direct overlap of $|nd>$ and $|n'd>$. When $\Delta\epsilon_{n''}$ becomes small, then intermediate state relaxation begins to play a role, and T is given by Eq. (3).

The evaluation of T in Eq. (3) is complicated by the fact that all the $6pn''d$ intermediate states are coupled to several continua and are thus autoionizing. This coupling has the effect of making all of the energies of the $6pn''d$ states complex, and the overlap integral in Eq. (4) must be evaluated using complex effective quantum numbers. Physically this represents the additional phase that the electron accumulates in going through the intermediate states, over and above the phase introduced by the detuning from resonance. The proper way to treat this problem is by using multichannel quantum defect theory (MQDT) where the coupling of the $6pn''d$ states is taken into account at the outset.

An analytical summation of Eq. (3) has been performed using MQDT techniques yielding [11]:

$$T = T'_{ion} \cdot \Big\{ <n|n'>\left(A(\omega_1) + B(\omega_2)\right) - <n'|n_p> A(\omega_1) C(n_p, n) - <n|n_p> B(\omega_2) C(n_p, n') \Big\} \tag{6}$$

here $T'_{ion} = \frac{2\pi}{\hbar}[<6s|\mu_1 E_1|6p><6p|\mu_2 E_2|7s>]_{ion}$, $A(\omega_1) = [2\hbar(\Omega^{ion}_{(6s-6p)} - \omega_1)]^{-1}$, $B(\omega_2) = [2\hbar(\omega_2 - \Omega^{ion}_{(6p-7s)})]^{-1}$, $C(n_1^*, n_2^*) = (n_1^*/n_2^*)^{3/2} \cdot [\sin\pi(n_2^* + \delta_i + i\Gamma_i)]$ / $[\sin\pi(n_1^* + \delta_i + i\Gamma_i]$, δ_i and $n^{*3}\Gamma_i$ are the quantum defect and width of the intermediate $6p_{3/2}n''$d states, Ω^{ion}_{6s-6p} is the frequency of the $6s-6p_{3/2}$ ion transition, $<n_1|n_2>$ is given by Eq. (4), and n_p is the effective quantum number corresponding to the energy to which ω_1 is tuned $[1/(2n_p^2) = \Omega^{ion}_{(6s-6p)} + 1/(2n^{*2}) - \hbar\omega_1]$. For tunings of ω_1 far away from the ion $6s-6p_{3/2}$ transition, $<n'|n_p> = <n|n_p> = 0$ and T depends solely upon $<n|n'>$ in agreement with Eq. (5). Further, this expression demonstrates explicitly that near intermediate resonance, $|T|^2$ will evidence *interferences between the direct and intermediate state processes.*

We have used Eq 6. to calculate the expected intensity pattern for the data in Fig 3. The solid curve is that calculation; good agreement between experiment and theory is obtained, apart from the ratio of the intensities in the doublet structure for each 7sn'd peak. What is important here is to note that there is substantial asymmetry between detunings on the high frequency side of the 6p24d intermediate-state resonance and on the low side. This asymmetry is a reflection of the interference between the "sudden" and the "adiabatic" processes.

Using Eq. 6., we have calculated how this interference between the "sudden" and "adiabatic" contributions to the over-all transition moment depends upon detunings. This result is shown in Fig. 4. As in Fig. 3., the initial state was 6s24d, and the "intermediate tuning" refers to the continuous value of n" of the real intermediate state 6pn"d.

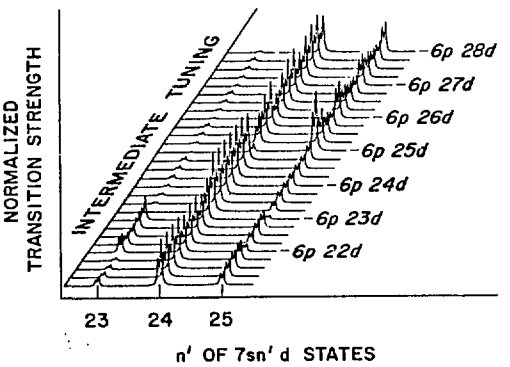

Fig. 4 A calculation of the doubly excited spectra 7sn'd for various detunings from the 6p24d state. In this figure, the integrated transition strength for each intermediate detuning has been normalized to 1

The results of this work show that multiphoton excitation of highly excited two-electron systems is a powerful technique to probe these special doubly excited states. We have used this technique in a rather extensive investigation of "planetary atoms"[12]. This work also demonstrates, however, that intermediate-state relaxations can play a significant role in determining the observed spectra. By varying the detunings from the intermediate states, the time allowed for the intermediate state to undergo relaxation is changed. The spectra and theory presented here clearly show how relaxation dynamics during the multiphoton transition can affect the observed excitation profile.

We are indebted to U. Fano, P. Citrin, and P.F. Liao for helpful suggestions during the course of this work. One of us (W.E.C.) acknowledges the support of the NSF (contract # PHY-7916444) and the Alfred P. Sloan Foundation.

References

1. I. C. Percival: Proc. R. Soc. Lond. A *353*, 289 (1977).
2. D. R. Herrick and O. Sinanoglu: Phys. Rev. A *11*, 97 (1975).
3. U. Fano: Rep. Prog. Phys. *46*, 97 (1983); G. Hose and H. Taylor: Phys. Rev. Lett. *51*, 947 (1983).
4. R. P. Madden and K. Codling: Astrophys. J. *141*, 364 (1965); P. R. Woodruff and J. A. R. Samson: Phys. Rev. Lett. *45*, 110 (1980).
5. S. J. Buckman, P. Hammond, F. H. Read, and G. C. King: J. Phys. B *16*, 4039 (1983).
6. W. E. Cooke and T. F. Gallagher: Phys. Rev. Lett. *41*, 1648 (1978).
7. R. M. Jopson, R. R. Freeman W. E. Cooke and J. Bokor: Phys. Rev. Lett. *51*, 1640 (1983).
8. J. R. Rubbmark, S. A. Borgstrom, and K. Bockasten: J. Phys. B *10*, 421 (1977).
9. J. E. Bjorkholm and P. F. Liao: Phys. Rev. Lett. *33*, 128 (1974).
10. S. A. Bhatti, C. L. Cromer and W. E. Cooke: Phys. Rev. A *24*, 161 (1981).
11. C. Cromer, Ph.D Thesis, Dept. of Physics, USC (unpublished); W. E. Cooke, unpublished.
12. L. A. Bloomfield, R. R. Freeman, W. E. Cooke and J. Bokor: submitted to Phys. Rev. Lett. (Aug 1984).

Multiphoton Ionization Via Rydberg States and Effects of High Laser Intensity

G. Leuchs*

Joint Institute for Laboratory Astrophysics, University of Colorado and National Bureau of Standards, Boulder, CO 80309, USA

1. Introduction

A photoionization experiment is characterized by the initial bound state of the atom, the polarization, frequency, intensity and also temporal distribution of the ionizing radiation, as well as the partial waves describing the final continuum state. The basic observable is the total ionization rate which can be differentiated with respect to the kinetic energy of the emitted photoelectrons yielding total and partial photoionization cross-sections. Additional information can be extracted if the angular distribution of either electron emission [1,2] or spin polarization is measured [3]. The angle-resolved measurement reveals interference effects which average to zero whenever the signal is integrated over all angles, quite analogously to the angular correlations observed, e.g., in γ-γ cascades or scattering of particles.

At a high enough laser intensity the atom may be ionized by simultaneous absorption of several photons and photoionization is observed below the threshold for one-photon ionization [4-6]. The actual light intensity required to produce such a signal strongly depends on whether or not an excitation step is in resonance with an atomic transition. The least intensity is required if photons of different frequencies are present in the light beam, each in resonance with atomic frequencies, leading to resonant stepwise ionization. Depending on the quantum numbers of the resonant intermediate states, the angular distribution may exhibit rather high anisotropy. By varying the polarization and frequency of the photons, one can excite different intermediate states and study their influence on the ionization signal [2] (Sec. 3). In this context we will also address the question of how well photoionization of Rydberg states can be described using the electric dipole approximation.

As the intensity is increased, multiphoton processes like saturation and ac-Stark broadening and shift will become increasingly important [6]. The ionization signal will change drastically whenever the ac-Stark shift becomes comparable to the detuning from resonance (Sec. 4). When one of the intermediate states is nearly degenerate with other states, not directly accessible in the excitation process, Raman coupling may mix these degenerate states.

As the intensity is increased further, above-threshold ionization may occur, giving rise to several peaks in the photoelectron energy spectrum, each having a characteristic angular distribution [7]. At even higher intensities, multiple photoionization has been observed where the remaining

*Heisenberg Fellow of the Deutsche Forschungsgemeinschaft.

ion is multiply charged [8]. These effects, however, will not be further discussed in this paper.

2. Angular Distribution of Photoelectrons

Angular distributions of photoelectrons in N-photon ionization may exhibit quite high anisotropy, since with each absorbed photon anisotropy may be transferred to the atom. We will now make the simplifying assumptions that the atom in its initial state is spatially isotropic (in an ensemble all magnetic substates are equally populated), that each photon-atom interaction is well described by the electric dipole approximation, and that the directions of polarization of the different photons in the laser beam are parallel with respect to each other. Under these conditions the photoelectron angular distributions can be written as expansions in even Legendre polynomials [2,9]

$$A(\theta) \propto 1 + \sum_{n=1}^{N} \beta_{2n} P_{2n}(\cos\theta) \quad , \tag{1}$$

where θ describes the angle between the direction of linear light polarization and electron emission.

It is obvious that the angle-integrated signal does not depend on the parameters β_{2n}. Information about interference between different ionization amplitudes, and, therefore, on scattering phases of the outgoing partial waves, is contained only in the β_{2n}, underlining the importance of angular distribution measurements.

A typical experimental setup for the measurement of photoelectron angular distributions is shown in Fig. 1. Two or more colinear laser beams intersect a thermal atomic beam at right angles. Two electrically grounded metal plates surround the interaction region to ensure field free conditions. The photoelectrons emitted in the direction mutually perpendicular to both atom and laser beam are detected using a secondary electron multiplier. The detector acceptance angle used varies from 10^{-2} to 10^{-1} sr. Since the electrons travel through a field free region of a few cm there will be a dispersion in the arrival time at the detector, so that moderate resolution time-of-flight spectra can be obtained.

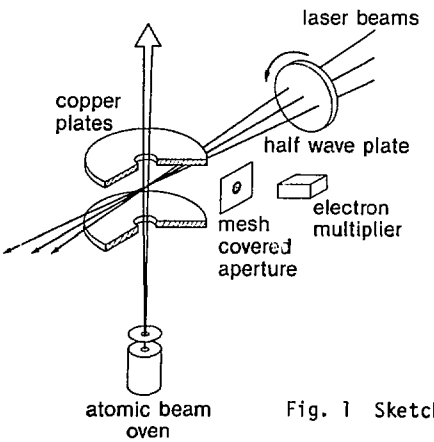

Fig. 1 Sketch of the experimental setup.

The photoelectron angular distribution in the plane perpendicular to the direction of the laser beam is monitored by synchronously rotating all linear polarizations of the laser beams. This procedure has the advantage that nothing has to be moved inside the vacuum chamber. As a result, the measurement is rather insensitive to small residual electric or magnetic fields. However, when one also wants to study possible azimuthal dependence, the detector has to be moved. It is then crucial to carefully avoid stray electric or magnetic fields in the interaction region.

3. Resonant Multiphoton Ionization

The shapes of photoelectron angular distributions are readily described by straightforward application of angular momentum algebra and they resemble angular patterns of one-electron-atom orbitals. However, in the alkaline earth atoms, for example, different independent particle configurations can be strongly mixed. This is sensitively detected in rather drastic changes of the angular distributions [10]. Also, if outgoing partial waves interfere in the continuum the electron angular distribution is influenced strongly and ratios of radial matrix elements of bound-free transitions including their phases can be determined through the data analysis.

Figure 2a shows polar diagrams of photoelectron angular distributions in resonant three-photon ionization of barium atoms via the 6s19d $^1D_2$,$^3D_2$ and 6s15s $^1S_0$ states [11,12]. In these experiments the ionizing Nd:YAG laser pulse at 1.06 μm was time-delayed in order not to perturb the resonant excitation by the dye laser pulses. Using time-of-flight discrimination, only ionization into the 6s continuum is observed. The drastic dependence of the distributions on intermediate state quantum numbers is apparent. The 6s19d and 6s15s configurations are relatively unperturbed. Consequently, the shape of the corresponding electron angular distributions can, at least quantitatively, be understood in simple terms. The angular part of the $^1S_0$ wave function is the isotropic spherical harmonic Y_{00}. In the final ionization step the orbital angular momentum quantum number is increased by one and the angular distribution should be proportional to $|Y_{10}|^2 \propto \cos^2\theta$. The non-zero waist diameter at $\theta = 90°$ found in the experiment is largely due to final state spin-orbit interaction [12]. Consider now the distributions via the $^1,^3D_2$ states. Owing to the linear

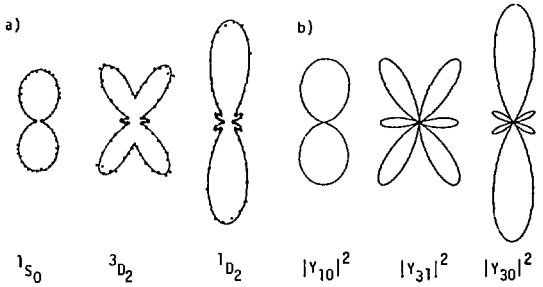

Fig. 2 a) Polar diagrams of electron angular distributions in three-photon ionization of barium via the 6s15s $^1S_0$, 6s19s $^1D_2$, and 6s19s $^3D_2$ states. All linear laser polarizations are vertical [11,12]. b) Polar plots of absolute squares of spherical harmonics.

laser polarization only m = 0 magnetic substates can be populated. If only the $\ell = 3$ partial wave is taken into account, neglecting the weaker $\ell = 1$ partial wave, spin-orbit coupling, and configuration interaction, the photoelectron angular distributions via the $^1D_2$ and the $^3D_2$ states are expected to be $|Y_{30}|^2$ and $|Y_{31}|^2$, respectively (Fig. 2b). Indeed, this qualitatively explains the shape of the observed distributions.

3.1 Unresolved Structure of the Intermediate State

Consider the case where several nearby intermediate states, for example, hyperfine states, are not resolved in the excitation process owing to finite laser bandwidth. The photoelectron angular distribution may then be sensitive to the time duration Δt of the laser pulse, if Δt^{-1} is comparable to or smaller than the frequency-splitting between the nearby states not resolved in the optical excitation [2,13].

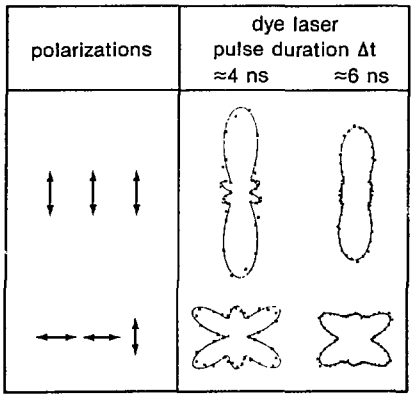

Fig. 3 Polar diagrams of electron angular distributions in three-photon ionization via the $3^2P_{3/2}$ and 20 ^2D intermediate states for two different durations of the dye laser pulses. The arrows from left to right indicate the polarization directions of the lasers for the first, second and third step [11,14].

An example of this is three-photon ionization of sodium atoms via the $3^2P_{3/2}$ and 20 ^2D resonant intermediate states [11,14]. As in the barium experiments discussed above, sodium atoms in the aligned 20 ^2D states are ionized by a Nd:YAG laser pulse, time-delayed so as not to overlap with the dye laser pulses exciting the first two steps. The $3^2P_{3/2}$ state consists of several hyperfine states, the dominant ones being separated by 60 MHz. According to the condition mentioned above, an observable effect of the hyperfine interaction may be anticipated whenever the pulse duration exceeds a few nanoseconds. Figure 3 shows polar diagrams of angular distributions measured for different dye laser pulse durations. The polarizations of the two dye laser pulses for the first two excitation steps have been adjusted both parallel and perpendicular with respect to the polarization direction of the ionizing Nd: YAG laser pulse. The change in the angular distribution when going from 4 ns to 6 ns dye laser pulse duration is quite noticeable and the trend is towards a more isotropic shape. Physically speaking, the spatial anisotropy initially excited in the intermediate state evolves in time [15]. Therefore, this effect can

be avoided, in principle, by exciting all magnetic substates of the nearby intermediate states equally, resulting in a stationary spatial isotropy.

3.2 Validity of the Dipole Approximation for Photoionization Out of Rydberg States

For transitions between bound states of the valence electron the electric dipole term in the interaction operator always dominates higher multipole terms, if it is allowed by symmetry and angular momentum considerations. This is not necessarily true for absorption of high energy radiation whose wavelength is comparable to the atomic dimensions, $k \cdot r \gtrsim 1$. Problems with the dipole approximation can be envisioned not only when going to high photon energies but also when going to large atomic dimensions.

If the atom is excited to a high-lying Rydberg state, the linear dimension of the atom increases as the square of the principal quantum number times the Bohr radius, $r \approx n^2 a_0$. Accordingly, the applicability of the dipole approximation is not obvious for photoionization with light wavelength $\lambda \lesssim n^2 a_0$ [14]. We will now try to get some physical insight by taking a classical view of the problem, known to give good qualitative estimates for many properties of Rydberg states [16].

The emission and absorption of radiation by a moving charge is proportional to the square of its acceleration $\partial^2 \vec{r}$. If the Rydberg electron is in an eccentric low ℓ orbit, the acceleration is greatest at the point of closest approach r_ℓ (perihel) between electron and ion core. This suggests that the region around r_ℓ will dominantly contribute to the radial matrix element for the bound-free transition. Consequently, r_ℓ has to be used instead of $r_n = n^2 a_0$ when comparing the atomic dimension with the wavelength of the ionizing radiation. For high principal quantum numbers r_ℓ is calculated by setting the sum of centrifugal and Coulomb potential energy equal to zero

$$\hbar^2 \ell^2 / (2m\, r_\ell^2) - e^2 / (4\pi\, \varepsilon_0 r_\ell) = 0 \quad ,$$

yielding $r_\ell = \ell^2 a_0 / 2$. As a result r_ℓ is independent of n. Therefore, the ratio Q of the quadrupole and the dipole radial matrix element $Q = \langle k | k \cdot r^2 | n\ell \rangle / \langle k | r | n\ell \rangle$, which is a measure of the deviation from the dipole approximation, will only depend on ℓ. Q should be of the order of unity if $k \cdot r_\ell \approx 1$. For Nd:YAG laser radiation with a wavelength of 1.06 μm this condition implies $\ell \approx 80$, in quite good agreement with a numerical calculation of Q by ZOLLER [17] who obtained $Q \approx 10^{-2}\, \ell$ for photoionization of hydrogen Rydberg states.

Special techniques have to be applied to selectively excite atoms to high ℓ orbits [18-20]. Therefore, the following discussion will be restricted to $\ell = 2$ states. In particular, resonant three-photon ionization of atomic sodium via the $3^2P_{1/2}$ and $n^2D_{3/2}$ states will be studied. The $3^2P_{1/2}$ intermediate state is chosen since it is spatially isotropic when exciting with linearly polarized light, thus avoiding the hyperfine structure effects discussed in the preceding section. The dye laser in resonance with the second step $3^2P_{1/2} \rightarrow n^2D_{3/2}$, has an intensity high enough to also produce ionization. In this case, the quadrupole-dipole ratio is Q = 0.036 (LAMBROPOULOS [21]). The angular distribution of photoelectrons calculated using the dipole approximation [14,22] is $A(\theta) \propto 0.2\text{-}0.4 \cos^2\theta + \cos^4\theta$. Figure 4 shows a three-dimensional polar plot of this distribution. The laser light is linearly polarized parallel to the z-axis and it propagates along the x-axis. If a detector is moved in the x-y plane, the

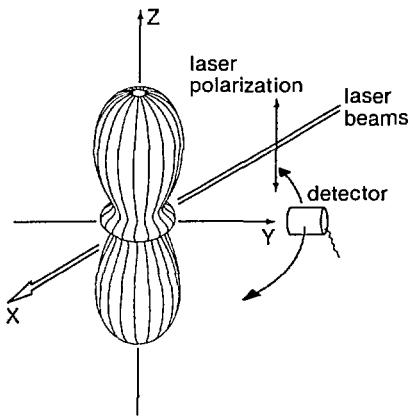

Fig. 4 Projection of a three-dimensional polar diagram of the electron angular distribution in photoionization via a sodium $^2D_{3/2}$ state. The geometry for measuring the ratio of the quadrupole and dipole radial matrix element is shown.

electron signal is independent of the detector position. A nonnegligible quadrupole contribution, however, will lead to a ϕ-dependence of the signal [21], $A(90°,\phi) \propto 1+0.75\ Q \cos\phi$. With $Q = 0.036$ the electron signals at $\phi = 45°$ and $\phi = 135°$ differ by 4% which should be observable. Note that the predicted ϕ distribution is peaked towards $\phi \approx 0$ (positive x-values), in accordance with the picture that the photon momentum is transferred to the photoelectron [23,24]. The experiment is presently under way. Summarizing this section, photoionization of low ℓ Rydberg states of atoms is well described using the electric dipole approximation. For photoionization of high ℓ states, however, higher multipoles can be expected to contribute significantly.

4. High-Intensity Effects in Resonant Multiphoton Ionization

As the intensity of the laser radiation is increased higher-order processes become important and the resonant intermediate states are shifted and broadened [6]. This ac-Stark effect can be observed not only by monitoring the ionization signal as a function of detuning and intensity [4], but also by measuring the photoelectron angular distribution [2]. The latter case is especially interesting if the intensity induced shift and broadening becomes comparable to the splitting between nearby states. In the following we will discuss the influence of the laser intensity on three-photon ionization of sodium for two different cases, $3^2S_{1/2} \rightarrow \rightarrow 4^2D_{3/2,5/2} \rightarrow k$ and $3^2S_{1/2} \rightarrow 3^2P_{1/2} \rightarrow n^2D_{3/2} \rightarrow k$.

In the first case, a 6 ns long dye laser pulse is tuned to the $3s \rightarrow \rightarrow 4d$ resonance, the same pulse also producing ionization. Owing to the nearly Fourier limited bandwidth of 130 MHz of the laser the two fine structure states $4^2D_{3/2}$ and $4^2D_{5/2}$ could be resolved. Angular distributions of photoelectrons were measured by rotating the direction of linear polarization as described in Sec. 2. The polar diagrams in Fig. 5 show the experimental data taken at a number of different intensities [25]. The laser was first tuned to either the $4^2D_{3/2}$ or $4^2D_{5/2}$ resonance at a low intensity (unperturbed atomic transition). Without changing this frequency setting the intensity was then increased to the desired value and the data were taken.

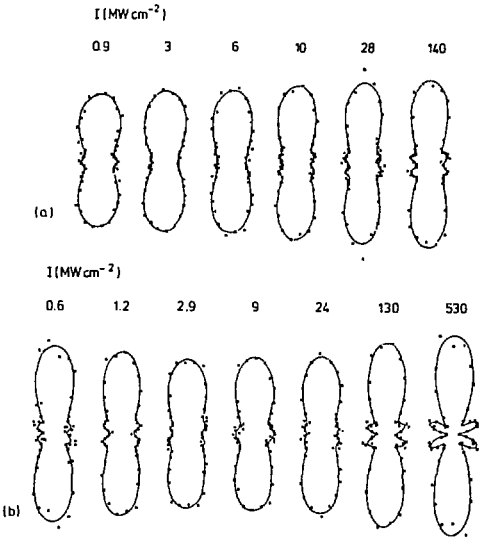

Fig. 5 Photoelectron angular distributions in two-photon resonant three-photon ionization of sodium via the (a) $4^2D_{3/2}$ and (b) $4^2D_{5/2}$ intermediate states for different laser intensities [25].

The intensity dependence has been calculated for these angular distributions by DIXIT and LAMBROPOULOS [26] and there is qualitative agreement between theory and experiment. As the intensity is increased the 3s ground state and the 4d states are shifted differently. If, e.g., the $4^2D_{5/2}$ state is in resonance with the laser radiation at low intensity, it will be shifted out of resonance as the intensity is increased and the $4^2D_{3/2}$ state will be shifted into resonance. At even higher intensities both ac-Stark shifted 4d states are out of resonance. In agreement with this picture the angular distribution changes from a double side lobe to a single side lobe and back to a pronounced double side lobe, which are the characteristic shapes for the $4^2D_{5/2}$, $4^2D_{3/2}$ and unresolved 4d intermediate states.

A quantitative comparison between experiment and theory, however, shows small but significant discrepancies. It turns out that the hyperfine structure of the ground state has to be included. The laser pulse does not couple the two ground hyperfine states, as long as the detuning of the laser frequency from the 3s → 3p resonance is large compared to the hyperfine structure of the 3p states. As a result, the atoms of the thermal beam are either in the F = 2 or F = 1 ground hyperfine state, forming two non-interacting groups of atoms. At a low enough intensity only one of the groups will be resonantly excited. As soon as ac-Stark shift and broadening become comparable to the ground state hyperfine splitting, the other group of atoms, initially out of resonance with the radiation, will also contribute to the signal, and consequently change the angular distribution of photoelectrons [27]. Figure 6 shows angular distribution parameters a_{2n}, determined from the $4^2D_{3/2}$ data in Fig. 5, and also the theoretical values obtained with and without inclusion of ground state hyperfine structure. The experimental data favor, as expected, the theory that includes ground state hyperfine structure.

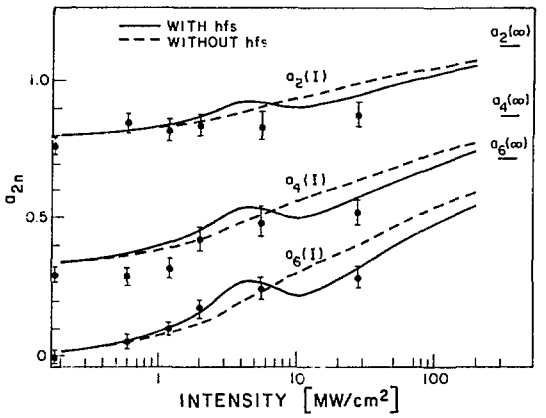

Fig. 6 Experimental anisotropy parameters determined from the distributions shown in Fig. 5 are compared with theoretical values (solid and dashed lines) [27]. The a_{2n} are the coefficients of $\cos(2n\theta)$ in the Fourier function expansion describing the angular distribution [28].

As a last example we now consider the all resonant three-photon ionization of sodium, $3^2S_{1/2} \rightarrow 3^2P_{1/2} \rightarrow n^2D_{3/2} \rightarrow k$. This scheme is similar to the one already discussed in Sec. 3.2; the difference being that here the excitation proceeds via the $3^2P_{1/2}$ state, just to avoid the unresolved structure effects. Again two dye laser pulses prepare the sodium atoms in a $n^2D_{3/2}$, $m = \pm 1/2$ state from which they are ionized by a time delayed Nd:YAG laser pulse. Because of this time delay the angular distribution is not expected to depend on the intensity of the ionizing laser, not even if the ionizing step is highly saturated, i.e., all atoms being ionized during the first part of the laser pulse. The electrons will just be emitted with their characteristic distribution.

In contrast to this we find significant changes in the angular distribution as the intensity is increased [29]. We attribute this to two-photon Raman coupling between the $n^2D_{3/2}$ state and other nearby states, which are not directly accessible in the three-photon ionization process (Fig. 7). For low principal quantum numbers n, the $^2D_{3/2}$ state can be Raman coupled to the $^2D_{5/2}$ state and for higher n, for which the distance to higher ℓ states becomes small, the $^2D_{3/2}$ state may also be coupled to these higher ℓ states (g,i,...). This Raman coupling between nearly degenerate states has also been taken into account in the theoretical description of, for example, two-photon resonant three-photon ionization [26] and quantum beats in photoionization [30,31]. Such effects have not been observed in the experiments on $^1S_0$ and $^1D_2$ states of barium described in Sec. 3, since there is no fine structure splitting and since the 6snd states are farther away from higher ℓ states than are the sodium nd states, owing to the larger quantum defect.

Since the photoionization cross section decreases as n^{-3} for a fixed wavelength of the ionizing radiation, there is always the temptation to increase the laser intensity to compensate for the signal loss. In this case, one must be aware of the intensity effect discussed in the last paragraph. Even when recording an ionization spectrum at a constant intensity the influence of Raman coupling to nearby states could become

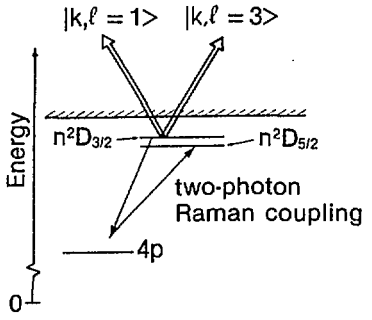

Fig. 7 Energy level diagram showing one-photon ionization out of aligned Rydberg states of sodium. At higher intensities, two-photon Raman coupling populating other nearby Rydberg states becomes important.

more significant with increasing principal quantum number, since the frequency mismatch between the coupled levels decreases as n^{-3}.

Acknowledgments

I would like to thank Dr. Stephen J. Smith for his hospitality and gratefully acknowledge financial support by the Deutsche Forschungsgemeinschaft.

References

[1] S. L. Chin, P. Lambropoulos (eds.): "Multiphoton Ionization of Atoms," Academic Press, Toronto, Orlando, San Diego, 1984.
[2] G. Leuchs and H. Walther in Ref. 1.
[3] J. Kessler: "Polarized Electrons" Springer Verlag, Berlin, Heidelberg, New York, 1976.
[4] G. Mainfray and C. Manus in Ref. 1.
[5] Y. Gontier and M. Trahin in Ref. 1.
[6] M. Crance in Ref. 1.
[7] P. Agostini, F. Fabre and G. Petite in Ref. 1.
[8] N. B. Delone, V. V. Suran and B. A. Zon in Ref. 1.
[9] P. Lambropoulos, Adv. At. Mol. Phys. 12, 87 (1976).
[10] E. Matthias, P. Zoller, D. S. Elliott, N. D. Piltch, S. J. Smith and G. Leuchs, Phys. Rev. Lett. 50, 1914 (1983); and O. C. Mullins, R.-L. Chien, J. E. Hunter III, J. S. Keller and R. S. Berry, to be published.
[11] G. Leuchs, in "Laser Physics" (J. D. Harvey and D. F. Walls, ed.), pp. 174-194, Lecture Notes in Physics, Vol. 182, Springer-Verlag, Berlin, Heidelberg, New York and Tokyo (1983).
[12] G. Leuchs and S. J. Smith, submitted to Phys. Rev. A.
[13] J. A. Duncanson, M. P. Strand, A. Lindgard and R. S. Berry, Phys. Rev. Lett. 37, 987 (1976).
[14] G. Leuchs and S. J. Smith, International School on Lasers and Applications, Vilnius 1981 , V. S. Letokhov (ed.), published by Institute of Physics, Moscow, 1983.
[15] G. Leuchs, S. J. Smith, E. E. Khawaja and H. Walther, Opt. Commun. 31, 313 (1979).
[16] C. Fabre, Ann. Phys. (Paris) 7, 5 (1982).
[17] P. Zoller, private communication (1982).
[18] R. G. Hulet and D. Kleppner, Phys. Rev. Lett. 51, 1430 (1983).

[19] R. G. Rolfes, D. B. Smith and K. B. McAdam, J. Phys. B 16, L533 (1982).
[20] D. Richards, J. Phys. B 17, 1221 (1984).
[21] P. Lambropoulos, private communication (1981).
[22] P. Lambropoulos, Appl. Opt. 19, 3926 (1980).
[23] A. Sommerfeld and G. Schur, Ann. Phys. (Leipzig) 4, 409 (1930).
[24] W. Bothe, Z. Physik 26, 59 (1924).
[25] W. Ohnesorge, F. Diedrich, G. Leuchs, D. S. Elliott and H. Walther, Phys. Rev. A 29, 1181 (1984).
[26] S. N. Dixit and P. Lambropoulos, Phys. Rev. Lett. 46, 1278 (1981); and Phys. Rev. A 27, 861 (1983).
[27] S. Geltman and G. Leuchs, to be published.
[28] G. Leuchs and S. J. Smith, J. Phys. B 15, 1051 (1982).
[29] G. Leuchs and S. J. Smith, unpublished material.
[30] A. T. Georges and P. Lambropoulos, Phys. Rev. A 18, 1072 (1978).
[31] P. L. Knight, Opt. Commun. 32, 261 (1980).

Dup

Effects of dc Electric Fields on Multiphoton Ionization Spectra in Cesium*

Cornelius E. Klots and R.N. Compton
Oak Ridge National Laboratory, Oak Ridge, TN 37831, USA

1. Abstract

The three-photon (one frequency) ionization of cesium atoms is greatly enhanced when the second photon is resonant with a Rydberg nd level. Enhancement by the ns levels is comparatively small. Three-photon ionization is also observed when the first photon excites a quadrupole transition to 5d. This occurs when either (a) the first photon is resonant with one of the 5d spin-orbit states, or (b) when the second photon is resonant with the 7f state.

A dc electric field introduces a number of new features: (a) high Rydberg states can be field-ionized, (b) the photoionization cross sections of the ns levels are greatly enhanced, (c) two-photon access to the np and nf series is induced, and (d) two-photon access to 7g (via a virtual quadrupole transition to 5d) is observed.

These effects have been quantified, the role of laser polarization documented, and a useful scaling law (as a function of the effective principle quantum number) has been demonstrated.

2. Introduction

The multiphoton ionization (MPI) of atoms is scarcely new, and dc electric field effects in atomic spectroscopy

*Research sponsored by the Office of Health and Environmental Research, U.S. Department of Energy under contract DE-AC05-84OR21400 with Martin Marietta Energy Systems Inc.

constitute a standard topic in elementary texts. We describe experiments made at the intersection of these two domains, the effects of static electric fields on MPI. For the most part they can be understood in terms of well-established constructs. The present work serves, however, to illustrate and quantify these constructs in a simple and coherent fashion.

The apparatus we have used is relatively simple. A parallel-plate ionization chamber was housed in a stainless steel enclosure pumped by a 400-l/s vacion pump to a base pressure of 10^{-8} torr. An oven provided an effusive source of cesium atoms which passed through a collimating hole into the ionization region. A Molectron (model UV24) nitrogen laser was used to pump a Molectron (model DL14) dye laser to provide a tunable source of radiation throughout the 6300-7000 Å range studied. The output was linearly polarized and, on passing through a double Fresnel rhomb, the plane of polarization could be rotated.

The laser beam was focussed by a 4 cm lens to a power density $\sim 10^8$-10^9 W/cm^2. It intersected the cesium beam at right angles. Any ions produced were extracted by a variable electric field along the axis perpendicular to each incident beam into a low-resolution time-of-flight mass spectrometer. After amplification, the output of the channelplate detector was monitored with a Princeton Applied Research (model 162) box-car integrator.

3. Field Ionization

In all of this work the energy of the first photon fell in the gap between the 6p and 7p levels. Although other states lie in this region, they are irrelevant except as noted later. It is the 6p level which acts overwhelmingly as the virtual state for most of what we describe.

As illustrated elsewhere [1], large numbers of ions are found when the second photon is resonant with an nd Rydberg level. The spin-orbit components are resolved only for $n \lesssim 17$. The signal drops off roughly as $(n^*)^{-8}$, where n^* is the effective principle quantum number. This

is consistent with a constant two-photon oscillator strength density, and a cross section for ionization by a third photon which varies as $(n^*)^{-5}$.

The MPI signal reappears again at still higher energies where this third photon is no longer needed. The onset for this is quite sharp, but is shifted to below the normal two-photon ionization limit. We attribute this to field ionization, the first of the dc field effects which we discuss.

The effective potential seen by an electron near a singly charged nucleus, immersed in a dc electric field of magnitude F, can be written (in atomic units) as:

$$V = -1/\rho - F\,\rho\cos\theta + (m/\rho\sin\theta)^2/2 \qquad (1)$$

where ρ is the radial distance of the electron from the nucleus, θ is the angle between this radial vector and the field, and $m\hbar$ the conserved component of angular momentum around the field direction. By requiring that the total energy exceed the maximum in this potential for ionization to be effected, the predicted shift is given by [2,3]:

$$\Delta = -2F^{1/2} + mF^{3/4}/2 + \cdots \quad . \qquad (2)$$

We observe $\Delta = -1.90\ (\pm 0.03)\ F^{1/2}$ when the $\bar{E}$ vector of the photon beam is parallel with the applied field, and hence when m=0. When the vectors are perpendicular, a shift to a higher ionization threshold is observed, as illustrated in Fig. 1. The magnitude of the shift is again consistent with Eq. (2).

The structure indicated in the figure above the field-ionization threshold is real. It persists to above the normal two-photon ionization limit; this is already well-known for the case of one-photon ionization [4,5].

4. State Mixing at Low Fields

An applied electric field also changes the character of the MPI spectrum at lower energies. We find that resonances at the np and nf levels become readily

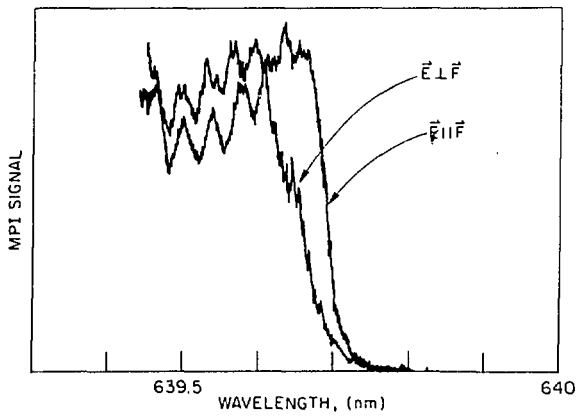

Fig. 1. Effect of polarization orientation on field ionization threshold at ≃500 V/cm.

apparent, while resonances at the ns levels, only barely discernible at zero field, increase in magnitude. We illustrate these in Fig. 2. Their appearance has been ascribed to two complementary sources [1]. In the absence of any field, two photons provide access to the ns and nd levels. The photoionization cross-sections of the ns series are expected to be quite small, however. An electric field mixes into a given s state its neighboring p levels, and it is these components which are more readily ionized. Conversely, the mixing of the

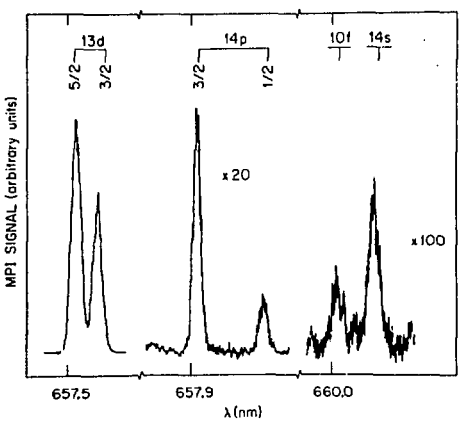

Fig. 2. Composite spectrum of field-induced MPI resonances in cesium at F≃1.1 keV/cm.

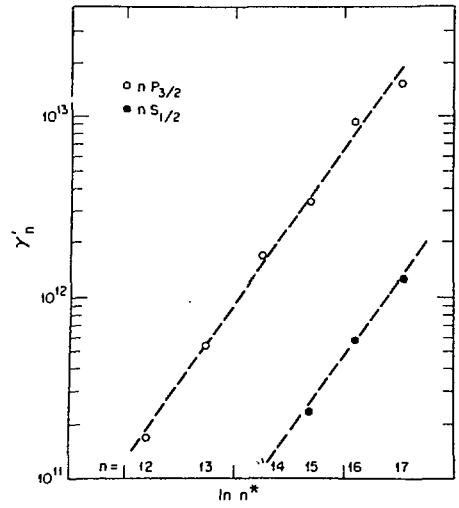

Fig. 3. Log-log plot of coefficient (defined in the text) for field-induced MPI vs effective principle quantum number.

ns and nd series into the p and f levels provides two-photon access to the latter.

We find for $R[np_{3/2}/(n-1)d_{5/2}]$, the ratio of MPI strength via an $np_{3/2}$ state to that via an $(n-1)d_{5/2}$ state:

$$R[np_{3/2}/(n-1)d_{5/2}] = \gamma'(np_{3/2}) \cdot F^2 \qquad (3)$$

The coefficient $\gamma'(np_{3/2})$, when F is in atomic units, is the strongly increasing function of n illustrated in Fig. 3. Similarly:

$$R[ns/(n-1)d_{5/2}] = \gamma_0(ns) + \gamma'(ns) \cdot F^2 \qquad (4)$$

with γ_0 (ns) only a weak function of n, and ≃0.004. The coefficients γ'(ns) are also shown in Fig. 3. Those describing the growth of the nf series with field strength are of comparable magnitude.

These results can be understood with a remarkably simple model. We treat the effects of an electric field with first-order perturbation theory, further simplified

by considering only the mixing between adjacent p and d levels. One then has [6] for a perturbed wave function:

$$|np'\rangle = |np\rangle + a[np,(n-1)d]|(n-1)d\rangle \qquad (5)$$

where $|np\rangle$ and $|(n-1)d\rangle$ are unperturbed wave functions, and:

$$a[np,(n-1)d] = \langle np|ez|(n-1)d\rangle F/[E_{np} - E_{(n-1)d}] \qquad (6)$$

with F the magnitude of the dc field along the z-axis. The energy difference in the denominator on the right-hand side of Eq. (6) clearly scales with $(n^*)^{-3}$; the dipole-matrix element in the numerator will scale roughly [7] as $(n^*)^2$. One then expects

$$\gamma'(np) \sim (n^*)^{10} Q_i(np)/Q_i[(n-1)d]$$

where Q_i indicates a photoionization cross section. We have already remarked that $Q_i(nd)$ are "normal," i.e., that they scale approximately as n^{*5}. If $Q_i(np)$ exhibits the same functional dependence, then $\gamma'(np) \sim (n^*)^{10}$. The dashed lines in Fig. 3 illustrate this relation. The data are seen to conform to it quite well.

The coefficients given in Fig. 3 were obtained when the applied electric field was parallel with the electric field vector of the polarized light. Their functional dependence on the angle between the two vectors has been described elsewhere [1].

It is noteworthy that, for a given np level, the ratio of field-induced signals for the spin-orbit components is ≃4.5:1. While not "statistical" it is much more nearly so than the ratio of one-photon oscillator strengths from the ground state [8].

These relations were obtained at sufficiently low field strengths so that first-order perturbation theory should still be valid. At larger field strengths, higher order processes become evident. We illustrate in Fig. 4 the resonances observed in the wavelength region where, at lower fields, only 16s and 12f were observed. The

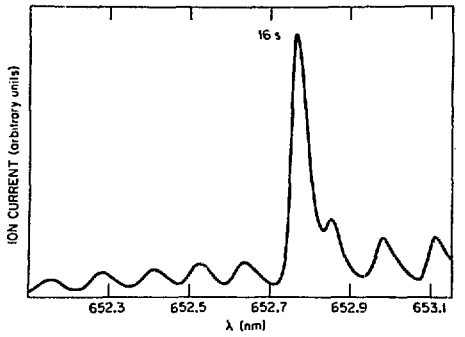

Fig. 4. MPI spectrum in 12f/16s region at 2.7 keV/cm.

field-induced MPI signal via the 12f has been dispersed among all the higher members of the Stark manifold. Note that 16s has not entered into this, being buffered from it by the absence of nearby p and d levels.

5. Role of Quadrupole Transitions

We now consider more carefully the one-photon wavelength region. Between 685 and 690 nm two real states exist, the spin-orbit components of 5d. Between them we expect to find, on the basis of what has been discussed so far, only a single weak resonance, corresponding to the first step of the two-photon transition to 11s. The bottom scan of Fig. 5, obtained at vanishing electric field, is quite different. In addition to 11s there are, to begin

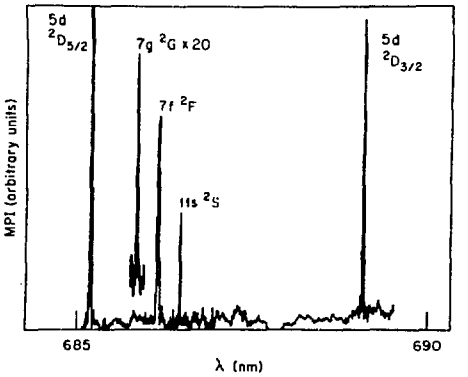

Fig. 5. Quadrupole-induced MPI resonances; 7g resonance obtained at 2 keV/cm.

with, the two components of the dipole-forbidden 5d state. They must arise via a quadrupole transition, with subsequent two-photon ionization. More interesting is the appearance of 7f. We interpret this as arising formally via a near-resonant quadrupole transition, followed by dipole-allowed absorption to 7f, with subsequent photoionization.

This same quadrupole enhancement mechanism accounts for the extremely weak MPI via 6f and 8f which we also can detect. Interestingly, we find no evidence for MPI via 10p or 11p, although they might have arisen via the same mechanism.

Having access to 7f with no dc field, we now expect to reach 7g upon application of such a field. The upper scan of Fig. 5 shows this to be the case. The 7g signal, relative to 7f, grows as the square of the field strength, instead of via the higher-order processes required at larger values of the principle quantum number. Formally the mechanism comprises a nonresonant quadrupole transition, followed by a dipole transition to the field-induced 7f component of the 7g level.

Our topic so far has been dc-field effects. We close by citing a remarkable ac power effect. The bottom scan of Fig. 6 shows the 11s/7f region in greater detail. It was obtained with vanishing dc field and at low laser

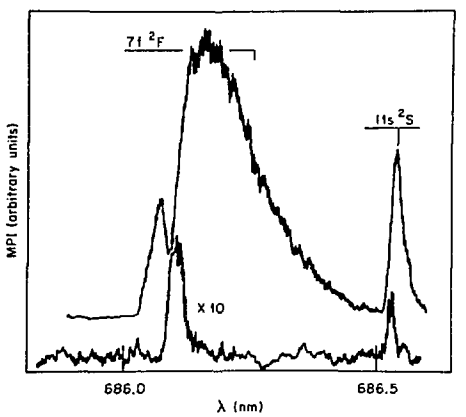

Fig. 6. Effect of a.c. power increase on 7f resonance.

power. Increasing the laser power by a factor of 3 yielded the upper scan. The 11s signal has increased in strength and broadened slightly, with shading to the red. This is typical of the ac Stark effect on the MPI signals we have studied. The behavior of 7f is seen to be quite different. It has split. One component has shifted to the blue and is of normal line shape. The second component has bloomed dramatically and moved to the red. The intimations of structure near its peak are reproducible. There is clearly much here to be understood.

References

1. C. E. Klots and R. N. Compton (to be published).
2. W. E. Cooke and T. F. Gallagher, Phys. Rev. A 17, 1226 (1978).
3. M. G. Littman, M. M. Kash, and D. Kleppner, Phys.Rev. Lett. 41, 103 (1978).
4. R. R. Freeman and N. P. Economou, Phys. Rev. A 20, 2356 (1979).
5. A.R.P. Rau, J. Phys. B 12, L193 (1979).
6. R. Zimmerman, T. W. Ducas, M. G. Littman, and D. Kleppner, Optics Comm. 12, 198 (1974).
7. H. A. Bethe and E. E. Salpeter, QUANTUM MECHANICS OF ONE- AND TWO-ELECTRON ATOMS, Academic Press (New York, 1957).
8. J. M. Raimond, M. Gross, C. Fabre, S. Haroche, and H. H. Stroke, J. Phys B 11, L765 (1978).

Part II

Field Fluctuations and Collisions in Multiphoton Processes

Field Fluctuations and Multiphoton Processes

Peter Zoller

Institute for Theoretical Physics, University of Innsbruck
A-6020 Innsbruck, Austria

1. Introduction

The original motivation to formulate and solve theories which account for laser field fluctuation effects in multiphoton processes are our attempts to understand the large class of experiments performed with noisy lasers [1-16]. High power multimode lasers, for example, are known to exhibit strong amplitude fluctuations which must be taken into account in a qualitative as well as quantitative theoretical analysis of such experiments; even well stabilized single mode lasers, on the other hand, have some residual fluctuations of the phase and amplitude (one of the limitations of precision experiments) which must be understood and should be incorporated in a realistic theory.

The origin of all field fluctuation effects in multiphoton processes is the nonlinearity inherent in any process where many photons are absorbed or emitted: an atom absorbing a number of photons is sensitive not only to the mean intensity and bandwidth of the light, but also to the kind and details of the fluctuations, i.e. the higher-order statistics of the radiation field.

A theory of field fluctuation effects in multiphoton transitions consists of essentially two elements [1]. First, we must specify a noise model to describe the light fluctuations. Usually on the experimental side only information on the mean intensiy and the spectrum (i.e., the first order correlation function) is available [9,14]. Based on our physical understanding of the laser light fluctuations we must therefore parametrize the higher order correlation functions in terms of the experimentally known quantities. These light models can either be purely phenomenological or can be derived from some underlying theory (laser theory, for example) [17,18]. The second, and usually much more difficult problem is to solve the atomic density matrix equations with a stochastic driving field (a system of multiplicative stochastic differential equations). For near resonant processes at high intensities (in the saturation regime) a perturbation theory treatment of the interaction is no longer valid, and non-perturbative techniques must be developed to solve the atom-stochastic field interaction.

During the past few years we have gained a considerable theoretical understanding of amplitude, bandwidth and laser lineshape effects. This has initiated a new generation of experiments ("controlled noise experiments") which are set up to quantitatively test the theoretical predictions by measuring multiphoton processes, in fields with controlled and varying amplitude fluctuations, bandwidth and spectral line shape. Examples include the experiment performed by the Saclay group to study resonant multiphoton ionization in a multimode/single mode laser field [9]; Close to a theorist's ideal are the recent experiments at JILA, where the output of a dye laser is modulated by Gaussian noise to simulate accurately the light models on which the theory is based [15].

Below we summarize some aspects of how to formulate and solve the problem of resonant multiphoton processes in stochastic fields (Sec. 2). In particular we

give an outline how to deal with nonlinear noise fields. In Sec. 3 we discuss some of our recent results.

2. General Considerations

We consider an atom strongly driven by an external fluctuating radiation field. Quite generally we have to distinguish the two limiting cases of fast and slow amplitude-, frequency- and/or phase-fluctuations. When the coherence time of the light is faster than the timescale of the atomic response to the field (the large bandwidth limit, for example), the atom effectively averages over the field fluctuations. Mathematically speaking, this is the limit which can be treated by perturbation theory (fast fluctuation expansions) where only a few low order noise correlation function enter the picture. In the slow fluctuations limit, on the other hand, the atom follows the field fluctuations adiabatically and the atomic averages can be found by integrating the solutions of the atomic density matrix equations over the field distribution functions. Most difficult is the treatment of the intermediate parameter regime, where a nonperturbative solution of the stochastic atomic density matrix equations is required.

A tractable treatment of the interaction of atoms with noise fields, valid for all values of the field coherence times, can so far only be given for fields with Markovian light statistics. Below we summarize the basic ideas and equations of the different variants found in the literature from a common point of view. Mathematically speaking, we are faced with the problem to solve nonperturbatively a linear system of multiplicative stochastic differential equations (Optical Bloch Equations, Heisenberg Equations) of the form

$$\dot{u}(t) = A(\varepsilon(t),t) \tag{1}$$

with u(t) a vector of variables, $A(\varepsilon(t),t)$ a matrix governing the time evolution of our system and $\varepsilon(t)$ a stochastic Markovian driving field amplitude. By definition the Markov property implies that the n-th order distribution function factorizes according to [17]

$$P(\varepsilon_1,t_1,\ldots,\varepsilon_n,t_n) = P(\varepsilon_1 t_1 \,|\varepsilon_2 t_2) \ \ldots \ P(\varepsilon_{n-1}\, t_{n-1}\,|\varepsilon_n t_n)P(\varepsilon_n t_n) \tag{2}$$

for $t_1 \geq \ldots \geq t_n$. Here $P(\varepsilon t|\,\varepsilon' t') \xrightarrow{t=t'} \delta(\varepsilon-\varepsilon')$ is the conditional density to find ε at time t given ε' was realized at time t'. An immediate consequence of the defining property (2) is that the conditional density obeys the differential Chapman-Kolmogorov Equation [17], which for a single variable ε reads

$$\frac{\partial}{\partial t} P(\varepsilon t|\varepsilon' t') = \left[-\frac{\partial}{\partial \varepsilon} a(\varepsilon) + \frac{1}{2}\frac{\partial^2}{\partial \varepsilon^2} b^2(\varepsilon)\right] P(\varepsilon t|\varepsilon' t')$$
$$- \int d\bar{\varepsilon} W(\bar{\varepsilon} \leftarrow\!\!- \varepsilon) P(\varepsilon t|\varepsilon' t') + \int d\bar{\varepsilon} W(\bar{\varepsilon} \leftarrow\!\!- \varepsilon) P(\bar{\varepsilon} t|\varepsilon' t')$$
$$\equiv L(\varepsilon) P(\varepsilon t|\varepsilon' t') \tag{3}$$

i.e., the Markov property restricts the class of admissable light models to diffusion processes with continuous realization as a function of time (described by the Fokker-Planck operator on the RHS of equ. (3) and jump-processes. Returning to the problem of solving equ. (1), we define a marginal average $u(\varepsilon,t) = \langle\delta(\varepsilon-\varepsilon t)u(t)\rangle$ (which gives the average of u(t) and finding a particular value of ε realized at time t). Note that $\langle u(t)\rangle = \int d\varepsilon u(\varepsilon,t)$. Suppose now that we convert the SDE (1) into an integral equation and attempt a formal solution for $u(\varepsilon t)$ by an infinite expansion in powers of A. Due to the factorization property (2) this series can be summed exactly into the integral equation

$$u(\varepsilon,t) = P(\varepsilon t)\ \langle u(0)\rangle + \int_0^t dt' \int d\varepsilon' P(\varepsilon t|\varepsilon' t') A(\varepsilon', t') u(\varepsilon', t) \qquad (4)$$

which in view of (3) is equivalent to

$$\frac{\partial}{\partial t} u(\varepsilon,t) = [L(\varepsilon) + A(\varepsilon,t)]\, u(\varepsilon,t). \qquad (5)$$

The simplification which occurs in solving (5) due to the Markov assumption is that we only have to consider an equation for the marginal densities involving a single time. Formally, we may view the effect of field fluctuations as introducing a field dependent damping operator $L(\varepsilon)$ in the equation of the driven atom. Practically all the work on field fluctuation effects in multiphoton processes done so far is based on variants of Equ. (5) or its integral version (4).

The choice of a light model (within the limits of Equ. (3)) is a compromise between an attempt to give a realistic (and therefore usually too complicated) description of the fluctuation properties and the necessity of still being able to solve Equ. (5). One expects that a realistic description of laser noise properties should be based on a statistical theory of the light source; in practice, however, technical fluctuations in laser systems are quite often the dominant noise source, so that even models taken from laser theory quite often have only a phenomenological meaning. In this sense it seems to be difficult in our context to draw a border line between a purely phenomenological description of laser fluctuations as opposed to one based on first principles. Laser models are usually formulated in terms of Langevin equations, which model the light fluctuations as a diffusion process (which includes Gaussian processes, for example).

Gaussian light models: Phase and amplitude fluctuations of a single mode laser are described by a slowly varying complex amplitude $\phi(t) = [\varepsilon_0+\varepsilon'(t)]\exp(-i\phi(t))$ with the phase $\phi(t)$ obeying the phase diffusion equation (phase diffusion model; PDM)

$$d\phi(t) = \sqrt{2b}\ \ dW_\phi(t) \qquad (6)$$

and $\varepsilon'(t)$ ($\varepsilon_0 >> \varepsilon'$) real amplitude fluctuations obeying

$$d\varepsilon'(t) = -\lambda\varepsilon'(t)dt + \sqrt{2\lambda\langle\varepsilon'^2\rangle}\ \ dW_{\varepsilon'}(t). \qquad (7)$$

In Eqs. (6) and (7) $dW(t)$ are Wiener increments; b may be identified with the bandwidth of the Lorentzian frequency spectrum, while λ is the inverse intensity correlation time. In practice the assumption of a δ-correlated frequency $\dot{\phi}(t) = \nu(t)$ (leading to a Lorentz spectrum) is quite often unrealistic and leads to artificial results far off resonance [2]. Equ. (6) is easily generalized to

$$d\nu(t) = -\beta\nu(t)dt + \sqrt{2b\beta}\ \ dW_\nu(t) \qquad (8)$$

where the parameter β for $\beta >> b$ plays the role of a cutoff of the Lorentzian frequency spectrum. The present experimental work at JILA is based on simulating the model (8) by frequency modulation techniques [15]. A multimode laser with a large number of independent modes M, $\varepsilon(t) = \Sigma\, \varepsilon_j \exp(-i\omega_j t - i\phi_j)$, becomes according to the central limit theorem a chaotic field, i.e., a complex Gaussian field. The simplest version of a Gaussian Markov field is described by

$$d\varepsilon(t) = -b\varepsilon(t)dt + \sqrt{2b\langle|\varepsilon|^2\rangle}\ (dW_1(t) + i\,dW_2(t)) \qquad (9)$$

with b the bandwidth of the Lorentzian spectrum.

Non-Gaussian (nonlinear) diffusion processes: Linear Langevin equations as(6), (7) and (8) describe Gaussian Markov processes. Nonlinear Langevin equations lead to non-Gaussian diffusion processes [17]. A nonlinear noise model of partially coherent light which contains both the chaotic field (9) and the PDM (6) as limiting cases is the Rotating Wave Van der Pol Oscillator (RWVPO) as given by [17]

$$d\varepsilon(t) = [a\varepsilon(t) - |\varepsilon(t)|^2\varepsilon(t)]dt + 2(dW_1(t) + i dW_2(t)). \qquad (10)$$

For large positive values of the "pump parameter" a linearization of Equ. (10) shows that the light is approximately coherent and diffusion shows rapid small amplitude fluctuations and a slow phase diffusion (compare Eqs. (6) and (7)); for $a < 0$ the light becomes chaotic. An interesting example of multiplicative noise in a nonlinear system are pump fluctuations in a single mode dye laser, described by [18]

$$\dot{\varepsilon}(t) = [a + \zeta(t)]\,\varepsilon(t) - |\varepsilon(t)|^2\,\varepsilon(t) \qquad (11)$$

with a the constant part of the laser pump parameter and $\zeta(t)$ fluctuations. In the simplest version $\zeta(t)$ is assumed to be a white noise force; more realistic theories assume a Gaussian process with finite correlation time. One of the features of the noise described by Equ. (11) is that it can have intensity fluctuations stronger than a chaotic field (super bunched light); this is of particular interest in multiphoton processes which are very sensitive to strong intensity fluctuations.

Jumplike Markov processes, where the amplitude, phase and/or frequency of the light are assumed to jump according to given rates have been suggested by Burshtein and coworkers; Burshtein's master equation is a special case of Equ. (5). Shore and Wodkiewicz et al have recently summarized and extended these techniques which have the advantage of being simple from a numerical point of view. [16]

Let us finally discuss techniques of solving the atomic equation of motion (5). For Gaussian Markov fields (7), (8) and (9) we have solved the dynamical equation (5) of the atom-laser system by expanding the dependence of $u(\varepsilon,t)$ on the electric field variables in the complete biorthogonal set of eigenfunctions of the corresponding Fokker-Planck operator L. For complex Gaussian processes, such as the chaotic field, these eigenfunctions are proportional to Laguerre polynomials; for real Gaussian processes (8) these eigenfunctions are Hermite or Fourier functions. Owing to the special properties of these functions and the polynomial structure of the atom field coupling in $\varepsilon(t)$, the expansion coefficients of $u(\varepsilon,t)$ in these basis states obey tridiagonal recursion relations, allowing closed form solutions for the atomic averages in terms of matrix continued fractions. For nonlinear processes, such as described by the Langevin equations (10) and (11), we do not know in general the eigenfunctions of L analytically; in addition, the matrix elements of $A(\varepsilon,t)$ between these eigenfunctions cannot be expected to have a tridiagonal structure. Risken and coworkers, [17] however, have developed techniques for solving nonlinear Fokker-Planck equations by expanding the probability functions $P(\varepsilon,t)$ in a complete basis set (usually Laguerre of Hermite functions for the amplitude and Fourier functions for the phase), not generally related to the eigenfuntions, leading in may cases to continued fraction expansions for the field moments and correlation functions. To solve Equ. (5) for the marginal density with L describing a nonlinear noise field, we can combine our previous method for Gaussian processes with Risken's technique. We expand $u(\varepsilon,t)$ in a suitably chosen basis set (where the underlying Fokker-Planck equation can be solved) so that the atomic averages again be expressed in terms of continued fractions: Physically, this corresponds to constructing the nonlinear light statistics at the same time we calculate the atomic response to the field. As an example, let us consider the RWVPO (10). Chosing the basis functions:

$$P_{n\nu}(I,\phi) = e^{-x}\, x^{|\nu|/2}\, L_n^{|\nu|}(x)\, e^{i\nu\phi}$$
$$\phi_{n\nu}(I,\phi) = \frac{n!}{(n+|\nu|)!}\, x^{|\nu|/2}\, L_n^{|\nu|}(x)\, \frac{1}{2\pi}\, e^{i\nu\phi} \qquad (12)$$

with $x = \alpha I = \alpha|\varepsilon|^2$ and α an arbitrary scaling parameter, we have the matrix elements of the corresponding Fokker-Planck operator [17]

$$\begin{aligned} L_{n\nu,n'\nu'} &= (2n+|\nu|)(n+|\nu|+1)\alpha\, \delta_{n+1,n'}\, \delta_{\nu,\nu'} \\ &+ [(2n+|\nu|)a - 2n(3n+3|\nu|+1)\alpha - |\nu|(|\nu|+1)]\, \delta_{n,n'}\, \delta_{\nu,\nu'} \\ &+ n\left[(6n+3|\nu|-2)\alpha - 2a - \frac{4}{\alpha}\right] \delta_{n-1,n'}\, \delta_{\nu,\nu'} \\ &- 2n(n-1)\alpha\, \delta_{n-2,n'}\, \delta_{\nu,\nu'} \end{aligned} \qquad (13)$$

and the dipole interaction

$$(\phi_{n0}, \sqrt{x}\, e^{i\phi} P_{n1}) = (\delta_{n,n1} - \delta_{n,n1+1})\delta_{\nu\nu'} \qquad (14)$$

which both are seen to be bandstructured in the intex n and ν. Similar considerations apply to Equ. (11) [18]. The result of these continued fraction expansions should - at least in principle - be independent of the scaling parameter α. In practice, however, a careful examination of the numerical results obtained as function of α is necessary before a numerical value can be accepted. In Ref. 6 we discussed the calculation of an atomic absorption spectrum in noisy phase-locked radiation along the lines indicated above.

3. Examples of Light Fluctuation Effects

Among the problems studied in the last couple of years are saturation of atomic transitions, ac-Straksplitting, multiphoton ionization, Raman scattering, four-wave mixing and potential scattering [1-16]. For a summary of earlier work we refer to Ref. [1]. Below we dicuss examples from our more recent work.

In resonant multiphoton ionization the nonlinearity of the dynamics causes the maximum of the distored resonance curve not to be shifted by the mean Stark shift (as in a coherent field); instead the observed shift depends on the statistics of the intensity fluctuations, the bandwidth and other parameters charaterizing the process. Lompre et al. [9] have measured the enhancement of the Starkshift in three-photon resonant four-photon ionization of Cs in multimode laser fields. Figure 1 compares their experimental results with the theory, assuming a finite bandwidth chaotic field to model the multimode radiation, and for comparison, a zero bandwidth multimode pulse with a finite number of modes M. For the experimental parameters the bandwidth dependence turned out to be small. The data points are seen to fall between the M = 5 and M = ∞ (chaotic field) curves in agreement with theory [7]. A characteristic feature of the effect of intensity fluctuations on the resonance profile is the asymmetric washing out of the resonance structure. In addition the fluctuations in the ion signal, an intrinsic feature of multiphoton experiments performed with noisy lasers, are asymmetric over the resonance in agreement with experimental observations. Quite generally, it seems to be worthwhile to study not only mean values of the experimental observables but also their fluctuations in experiment and theory.

So far, theoretical model calculations have predicted only changes of the heights, widths and shifts of atomic lines due to phase and amplitude fluctuations.

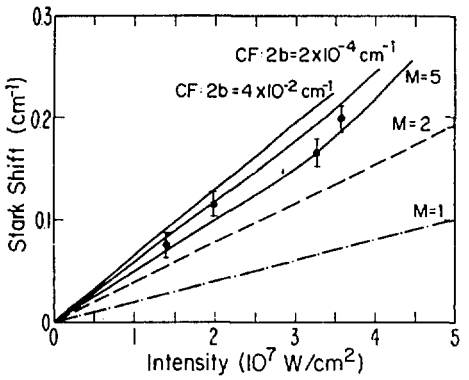

Fig. 1: Effective Starkshift as a function of the laser intensity in three-photon resonant four-photon ionization [7,9].

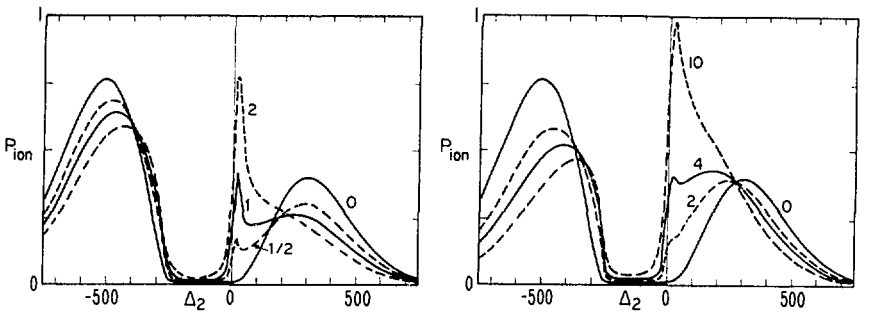

Fig. 2: Ionization probability (in arbitrary units) for a real Gaussian field in double optical resonance [5] as a function of the detuning (MHz) for different (MHz). a) real Gaussian field; b) jumplike Markov processes with Gaussian distribution.

Figure 2 gives an example of laser fluctuation-induced line splitting in the dynamic Stark effect, which is a consequence of the highly nonlinear dynamics of the atomic evolution rather than any structure in, for example, the spectrum of the exciting light [5]. Figure 2a shows the ionization probability in a double optical resonance (DOR) configuration in Na for different values of the coherence time $1/\lambda$ of the fluctuations in a real Gaussian field: ac-Stark splitting of the resonant line $3s^2S_{1/2}$ - $3p^2P_{3/2}$ in a slightly detuned real Gaussian field is probed as a function of the detuning Δ_2 of a second weak laser, inducing population in the $4d^2D_{3/2}$, which is then ionized by the first laser. For λ large the line near shows motional narrowing, while in the static limit $\lambda = 0$ this line is washed out by the strong amplitude fluctuations. The transition between both regimes is so abrupt that the line is split into two components. Note that this line splitting is surprising since it occurs in a parameter regime where the adiabatic result is still expected to be valid. This line splitting appears in a parameter regime, where the model dependence is expected to be most pronounced and, therefore, provides an ideal testing ground for investigating the sensitivity of model predictions. It is remarkable, however, that a jumplike Markov process with Gaussian distribution function gives practically the same results - apart from a rescaling of the intensity correlation time (Figure 2b) [5].

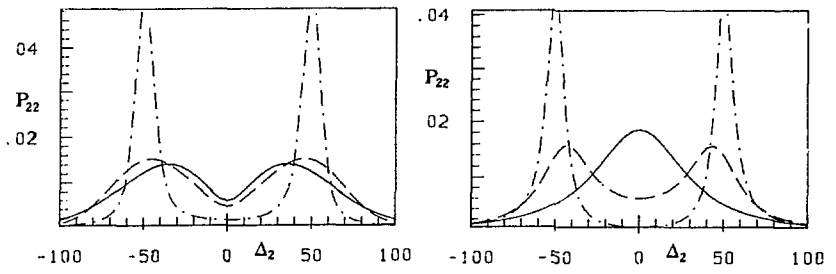

Fig. 3a,b. On-resonance AC-Stark splitting in a double optical resonance configuration induced by a RWVPO for a = -10 (solid line), a = 0 (dashed line) and a = 10 (dot-dashed line) a) zero bandwidth; b) finite bandwidth

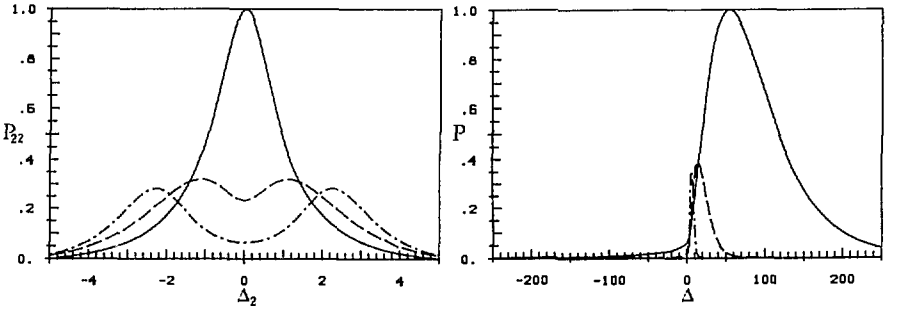

Fig. 4: On-resonant AC-Stark splitting in pump-modulated dye laser light [18]. The light intensity distribution function has the form

$P(I) = N(1+qI)^{a/2q-1+1/2q^2}\, e^{-\frac{1}{2}\cdot I/q}$ with I the scaled light intensity, a the coherent part of the pump and q a measure of the pump fluctuations. The parameters are a = 200; q = 1000 (solid line) q = 100 (dashed line) and q = 10 (dot-dashed line).

Fig. 5: Resonance profile of three-photon resonant four-photon ionization in pump-modulated dye laser light. The detuning Δ is measured in units of the mean ionization rate γ_1 from the resonant state. The ratio $\delta\omega/\gamma_1$ with $\delta\omega$ the mean Starkshift is equal to five. The parameters of the light distribution function are the same as in Fig. 4.

In Figs 3,4 and 5 we show preliminary results of calculations for nonlinear noise fields. In Fig. 3a the on-resonance spectrum of DOR is plotted for a RWVPO in the limit of slow field fluctuations (zero bandwidth). For a = 10 the light is almost coherent. Decreasing a, the amplitude fluctuations of the light become stronger and wash out the doublet of AC-Stark splitting. For finite coherence time, AC-Stark splitting disappears below threshold (a = -10) due to the large bandwidth (Fig. 3b); above threshold the RWVPO exhibits fast but small amplitude fluctuations, leading to a motional narrowing of the spectrum in comparison with Fig. 3a which, however, is compensated from finite bandwidth of the exciting light. For off-resonance excitation the wellknown reversed peak asymmetry is found again which has been discussed previously for the chaotic field and PDM [2]. For (zero bandwidth) dye laser radiation with a δ-modulated pump AC-Stark splitting in DOR disappears for strong modulation (Fig. 4); this reflects the fact that the light has

amplitude fluctuations stronger than a chaotic field since - quite generally - the sideband structure in DOR is related to the amplitude distribution function of the exciting light. In a similar way the resonance profile of three-photon resonant four-photon ionization for the same light parameters shows a strong increase when compared with coherent light; at the same time we note that the enhancement factor of the Starkshift is much larger than in a chaotic field. This suggests that multiphoton transitions constitute a sensitive probe for these nonlinear noise fields. (Fig. 5)

References

1. For a review and references to earlier papers see: J.H. Eberly, in: "Laser Spectroscopy IV", H. Walther and K.W. Rothe, eds., Springer, Berlin (1979), p. 80; P. Zoller, in: "Laser Physics", Proc. of the Second New Zealand Summer School in Laser Physics, D.F. Walls and J.D. Harvey, eds., Academic, New York (1980), p 99; P. Lambropoulos and P. Zoller, Proc. of the Second International Conference on Multiphoton Processes, Budapest (1980), p. 193; A.T. Georges and P. Lambropoulos, Adv. Elect. Electron Phys. 54, 191 (1980); P. Zoller, in: "Coherence and Quantum Optics V", L. Mandel and E. Wolf, eds., Plenum Press, New York (1984), p. 383
2. S.N. Dixit, P. Zoller and P. Lambropoulos, Phys. Rev. A 21, 1289 (1980); P. Zoller, G. Alber and R. Salvador, Phys. Rev. A 24, 398 (1981) and references cited
3. A.T. Georges and S.N. Dixit, Phys. Rev. A 23, 2580 (1981)
4. V.Yu Finkelshtein, Phys. Rev. A 27, 961 (1983)
5. M. Helm and P. Zoller, Opt. Commun. 49, 324 (1984)
6. P. Zoller and J. Cooper, Phys. Rev. A 28, 2310 (1983)
7. P. Zoller, J. Phys. B 15, 2911 (1982); M. Levenstein, P. Zoller and J. Mostowski, J. Phys. B 16, 563 (1983 and references cited
8. J.J. Yeh and J.H. Eberly, Phys. Rev. A 24, 888 (1981)
9. L.A. Lompre, G. Mainfray, C. Manus and J.P. Marinier, J. Phys. B. 14, 4307 (1981)
10. K. Rzazewski and J.H. Eberly, Phys. Rev. A 27, 2026 (1983)
11. J. Dalton and P.L. Knight, J. Phys. B 15, 3997 (1982)
12. G.S. Agarwal and C.V. Kunasz, Phys. Rev. A 27, 996 (1983)
13. R. Danielle and G. Ferrante, J. Phys. B 14, L653 (1981)
14. D.E. Nitz, A.V. Smith, M.D. Levenson and S.J. Smith, Phys. Rev. A 24, 288 (1981)
15. D.S. Elliot, R. Roy and S.J. Smith, Phys. Rev. A 26, 12 (1982); D.S. Elliot, M.W. Hamilton, K. Arnett and S.J. Smith, Phys. Rev. Lett. 53, 439 (1984); see also the contribution by D.S. Elliot in the present volume
16. L.D. Zusman and A.I. Burshtein, Sov. Phys. JETP 34, 520 (1972); B.W. Shore, JOSA B 1, 176 (1984); K. Wodkiewicz, B.W. Shore, J.H. Eberly, JOSA B 1,398(1984)
17. H. Risken, "The Fokker-Planck Equation: Methods of Solution and Applications", in: Springer Serien in Synergetics, H. Haken, ed., Springer, Berlin (1984)
18. A. Schenzle and H. Brand, Phys. Rev. A 20, 1628 (1979); S.N. Dixit and P.S. Sahny, Phys. Rev. Lett. 50, 1273 (1983); P. Jung and H. Risken, submitted to Phys. Rev. Lett. A; and references cited

Two-Photon Absorption from a Phase Diffusing Laser Field

D.S. Elliott

School of Electrical Engineering, Purdue University
West Lafayette, IN 47907, USA

In this report, I will discuss a recent experiment [1] in which we measured the influence of field frequency fluctuations on unsaturated two-photon absorption. The statistical properties of the frequency fluctuations in this experiment are carefully controlled, and the laser lineshape is nearly Lorentzian. This experiment provides direct confirmation of theoretical results of MOLLOW [2] on the linewidth of two-photon absorption by a phase-diffusing field. This report is organized as follows. The first section presents the background of the experiment, including Mollow's results for two-photon absorption from a phase diffusing field, and a simple extension of his work to include the effect of the finite correlation time of the fluctuations. The next unit describes the manner in which the experiment was conducted, and a discussion of the results appears in the final section.

1. Theoretical Background

The study of the effect of laser bandwidth on nonlinear optical phenomena must be based upon the fundamentals of the interaction of light with an atomic system. At present, generalizations of these effects cannot by made between different nonlinear processes or between differences among the statistical properties of the laser radiation. Many models of laser fields have been developed and used over the years to aid in the theoretical study of laser bandwidth effects. While applying only in idealized cases, these models provide a foundation for understanding qualitatively the nonlinear interaction of atoms with more realistic laser fields. Two of the more notable of these models are the phase-diffusion model and the chaotic field model.

The chaotic field is characterized by a fluctuating field amplitude, with a mean value of zero. A thermal source emits chaotic light, and the field of a multi-mode laser approximates the chaotic field if the number of modes is sufficiently high and the modes are statistically independent of one another. Because high power lasers usually operate on several modes, the results of the chaotic field studies are widely applicable to many measurements of nonlinear optical effects.

The field of interest in this report is the phase diffusion field, characterized by a constant amplitude and fluctuating (Gaussian) frequency. This model closely approximates the field produced by a stabilized cw laser. In the model used by MOLLOW [2] and many others [3], the frequency fluctuations are delta-correlated:

$$\langle \omega(t)\,\omega(t+\tau)\rangle = 2b\,\delta(\tau). \tag{1}$$

The parameter b is the spectral density of the fluctuations, as will be discussed later, and $\omega(t)$ is the deviation of the frequency from the mean frequency. The angular brackets denote an ensemble averaging procedure, and $\delta(\tau)$ is the Dirac delta function. The phase of this field is analogous to the position of a particle undergoing Brownian motion, leading to the term phase-diffusion. The correlation function of the Gaussian frequency fluctuations determine unambiguously the laser power spec-

trum, and it can be shown that (1) corresponds to a Lorentzian laser power spectrum of full width at half maximum (FWHM) 2b. A Lorentzian lineshape is noted for its relatively high level of power in the far wings, and this feature is responsible for theoretical predictions of interactions at large detunings, which are larger than intuitively expected for more realistic laser fields.

A modified correlation function in which the frequency fluctuations are exponentially correlated addresses this problem. This correlation function is written

$$\langle \omega(t)\,\omega(t+\tau)\rangle = b\beta \exp\{-\beta|\tau|\}, \tag{2}$$

where the correlation time of the fluctuations is β^{-1}, and b is the same as in the case of delta-correlated frequency fluctuations(1). The lineshape of the laser depends upon the relation between b and β. If the fluctuations are very fast and small in magnitude ($\beta \gg b$), the correlation function is similar to (1), and the laser lineshape is nearly Lorentzian for frequencies within β of linecenter. For larger frequencies, the lineshape falls off much faster than Lorentzian, leading to more realistic results for calculations employing this model. When the fluctuations are slow and large in magnitude ($\beta \ll b$), the laser frequency has a long memory, so that the phase changes significantly before the frequency changes. In this case the phase does not diffuse in a strict sense, but common usage is to regard this as one aspect of the phase diffusion model. The power spectrum of the laser is nearly Gaussian in shape, with FWHM $2\sqrt{2\ln 2\, b\beta}$, reflecting the probability distribution of the frequency fluctuations directly. This report will be concerned only with the near-Lorentzian laser power spectrum.

Linear absorption, of course, depends only upon the laser bandshape and intensity, but nonlinear effects depend upon higher-order correlations of the optical field—information which is not given by the laser bandshape alone. Perhaps the simplest nonlinear effect which can be considered is that of a two-photon absorption process in a weak field. The lineshape for unsaturated two-photon absorption from an arbitrary field was shown by MOLLOW [2] to be given by the following Fourier transform:

$$W_2 = 2|g(\omega_o)|^2 \int_{-\infty}^{\infty} dt \exp\{2i\omega_f t - \kappa_f|t|\}\, G^{(2)}(-t,-t;t,t). \tag{3}$$

In this expression, ω_f and κ_f are the frequency and natural width (FWHM) of the atomic transition, respectively, and $g(\omega_o)$ is the transition moment of the two-photon transition. As there is no resonant intermediate level the transition moment is independent of the laser frequency, and we will not consider its form any further. Finally, the statistical properties of the optical field of interest in this study are contained in the two-time second-order correlation function of the optical field $G^{(2)}(-t,-t;t,t)$. For a single-mode field, this correlation function is defined

$$G^{(2)}(-t,-t;t,t) = \langle E^*(-t)\,E^*(-t)\,E(t)\,E(t)\rangle. \tag{4}$$

MOLLOW [2] applied (3) to the cases of the chaotic field and the phase diffusion field. In both cases the laser power spectrum employed and the absorption spectrum calculated were Lorentzian in shape. For the chaotic field the width of the absorption spectrum was predicted to be twice the width of the laser plus the natural width of the transition. But for the phase diffusion laser the calculation predicted that the absorption width should be four times the laser width plus the natural linewidth. This is a graphic example of the incompleteness of the information about the field provided by the laser power spectrum.

In order to evaluate the differences expected for the two-photon absorption with the two different frequency correlation functions (1) and (2), Mollow's result for the

absorption profile (3) can be applied to the case of the phase-diffusion model with exponentially correlated fluctuations, (2). The second-order correlation function is found to be

$$G^{(2)}(-t,-t;t,t) = \exp\{-4i\omega_o t - 8b(|t| + [\exp(-2\beta|t|)-1]/2\beta)\}. \quad (5)$$

This expression reduces to the correlation function derived by Mollow, $\exp\{-4i\omega_o t - 8b|t|\}$, in the case of a very short correlation time, i.e. $\beta >> b$. Numerical integration of the Fourier transform of (5) will provide the lineshape of the two-photon absorption from this field.

The experiment described here measured the dependence of the linewidth of the absorption profile on the laser bandwidth for the case of exponentially correlated frequency fluctuations. It will be seen that the difference from the case of delta-correlated fluctuations in our experiment is not significant.

2. Experiment

The technique for creating the phase-diffusing field has been partially reported previously [1,5], and a complete description will be provided in a future publication [6]. The technique is based on the random frequency and phase-modulation of the radiation generated by a highly stabilized cw tunable dye laser. Wide-bandwidth acousto-optic and electro-optic modulators are used for this purpose. For technical reasons, frequency modulation is found to be advantageous for the low frequency region of the fluctuations, while phase-modulation is preferred for high frequencies.

The source of the fluctuations was a diode operating in the avalanche mode. By carefully shaping the power spectrum of this noise to a Lorentzian with maximum at zero frequency, the fluctuations of the optical frequency can be made to follow the correlation function given by (2). The spectral density of the fluctuations is given by b, while the correlation time, β^{-1}, corresponds to the frequency at which the spectral density of the noise is reduced to one half the maximum value. The fluctuations are controlled for frequencies as high as 1 GHz. By avoiding saturation of the amplifiers used here, the Gaussian nature of the voltage fluctuations were preserved. This was verified by calculating the moments of the fluctuations with an experimentally obtained probability distribution of the voltage fluctuations.

The modulated laser beam was directed through a vapor cell containing the atomic sodium, and reflected back on itself in a geometry typical of previous Doppler-free two-photon absorption measurements [7]. We chose to observe the $3^2S_{1/2}(F=2) \rightarrow 5^2S_{1/2}(F=2)$ transition in atomic sodium. The absorption lineshape was obtained by monitoring the 330 nm fluorescence radiated at right angles to the laser beams as the laser was tuned through the region around one half the transition frequency. This fluorescence corresponds to the second step in the relaxation of the sodium by way of the 4^2P state. The absorption profile consists of an intense Doppler-free peak on top of a low-level Doppler-broadened background. An interference filter and spatial filter between the interaction region and the photomultiplier served to discriminate against scattered laser radiation. An example of the absorption profile is shown in the lower half of Fig. 1. The dark current background rate was decreased using a fast pulse discriminator, and photo-electric pulses were counted by a 45 MHz scaler interfaced to a PDP-8 minicomputer. Typical maximum count rates were 10 kHz and the pulses of 20 nsec duration, making overlap errors negligible.

The linearly polarized light used in the experiment is able to induce $\Delta F=0$, $\Delta m_F=0$ transitions. The $3^2S_{1/2}(F=1) \rightarrow 5^2S_{1/2}(F=1)$ transition is separated from the transition observed in this experiment by ~800 MHz, and less intense by a

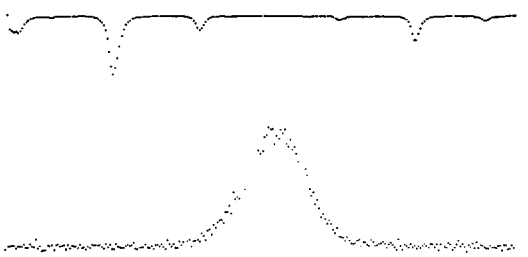

Fig. 1. The lower data shows a typical spectral profile of the two-photon absorption process, while the upper trace is the transmission of the Fabry-Perot interferometer used to calibrate the scan of the laser frequency. The scan is approximately 60 MHz wide.

factor of 3/5 due to the difference in population of the two hyperfine components of the ground state. The population of the intermediate 3^2P state is insignificant since this transition from the ground state is approximately 370 cm^{-1} from resonance with the laser frequency. The attenuation of the laser intensity while propagating through the sodium vapor cell is estimated to be 10^{-6}, so that the laser statistics are unaffected by the absorption. The laser intensity (5 W/cm^2) was three orders of magnitude less than that needed for saturation of the two-photon transition. The cell temperature was maintained at a temperature slightly higher than that of the cold finger where the sodium was condensed (160 ° C). The vapor density of sodium at this temperature is about $10^9 atoms/cm^3$.

The frequency scan of the laser was calibrated by passing a portion of the unmodulated laser beam through a Fabry-Perot interferometer (FSR ~500 MHz). Because of the non-confocal geometry of the interferometer, the intensity of the radiation transmitted by the interferometer consisted of a series of transverse mode fringes separated by a spacing of 35.7 MHz. In addition, a traveling wave electro-optic phase modulator was used for the laser scans of shorter range to produce sidebands of 10MHz spacing. The upper curve in Fig. 1 shows an example of the frequency marker. The two larger peaks are separated by 35.7 MHz, and each are flanked by smaller peaks produced by the phase modulation.

A PDP-8 minicomputer was used to control the scan of the laser frequency, and to record the fluorescence count rate, the frequency fringe marker, and the output of a photodiode which monitored the laser intensity. The laser frequency scan was stepped through 256 increments, and the range varied between 50 and 200 MHz. The counting time was adjusted for each run to give a total count of between 200 and 500 fluorescence photons at the peak of the resonance curve, and ranged from 50 to 300 msec/step.

The linewidth of the absorption profile was typically 4 MHz in the absence of the frequency fluctuations. This is due to the natural relaxation rate of the 5S state (2 MHz) and broadening due to collisions with a foreign gas in the vapor cell. Other broadening mechanisms were kept to a minimum. The laser beam passed through the vapor cell unfocussed (1.3 mm diameter) so that transit time broadening (due to the finite time the thermal atoms spent in the interaction region) is calculated to be about 500 kHz. The ionization rate of the 5S state is estimated [8] to be about 200 Hz at the laser intensity used. Broadening due to the Zeeman effect is insignificant since the g-factor is the same for the initial 3S state and final 5S state. And the fluctuations of the laser were determined to have a root mean square value of about 150 kHz from the error signal produced by the stabilization electronics.

The power spectrum of the modulated laser beam was monitored by projecting a portion of the modulated and unmodulated laser beams onto a fast avalanche photodiode and observing the beat frequency resulting from the mixing of the two beams. The power spectrum is recorded directly by a r.f. spectrum analyzer.

3. Results

Figure 2 shows the dependence of the absorption linewidth on the linewidth of the laser. Absorption profiles for the two-photon process were obtained for Lorentzian laser power spectra of widths ranging from 1 to 14 MHz ($\beta/2\pi$ = 100 MHz and 0.5 MHz < $b/2\pi$ < 7 MHz). The data points are the average of typically eight to ten measurements of the absorption width determined as described above. The vertical error bars represent the single standard deviation of the mean, calculated from the scatter of the data. The horizontal error bars represent a calibration uncertainty in the spectral width measurement of the laser.

The solid straight line of slope four represents the results of Mollow. The only adjustable parameter here is the intercept, or the absorption width in the absence of the imposed frequency fluctuations, and is chosen to be 4 MHz in the figure. The agreement between the experimental results and Mollow's theory is very good.

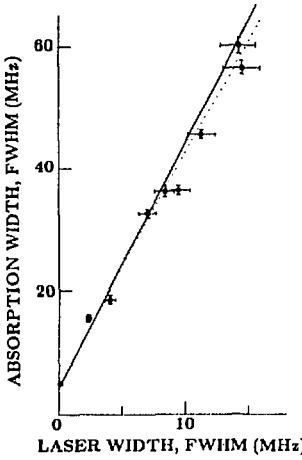

Fig. 2. The points are the data determined in this experiment, showing the dependence of the absorption width on the laser spectral width. The solid line is the expected behavior for delta-correlated frequency fluctuations. For the exponentially-correlated fluctuations used in the experiment, the expected behavior is shown by the dotted line.

The dotted line in Fig. 2 shows the effect expected due to the finite correlation time of the frequency fluctuations, β^{-1}. These linewidths are determined by a numerical integration of the Fourier transform of the correlation function given by (5). It can be seen that for the range of laser bandwidths used here, the difference is not significant. For larger laser bandwidth, however, the laser becomes less Lorentzian and more Gaussian in shape, and the departure from Mollow's results is expected to increase.

In conclusion, we have measured the dependence of the two-photon absorption linewidth on the laser linewidth for a phase diffusion field having a nearly-Lorentzian lineshape. The departure from the behavior expected for the case when the frequency fluctuations are delta-correlated is calculated to be insignificant in our case. A future report will consider the effect of having a Gaussian laser power spectrum, and the effect of applying two fields to the atomic sample, with varying degrees of correlation between them.

The work reported here was a joint effort with M.W. Hamilton, K. Arnett and S.J. Smith, and was carried out at the Joint Institute for Laboratory Astrophysics at the University of Colorado and the National Bureau of Standards. Useful conversations with J.L. Hall, G. Leuchs and K. Wodkiewicz have contributed to this work in a significant way, and are greatly appreciated. This work was supported by the U.S. Department of Energy, Office of Basic Energy Sciences.

References

1. D.S. Elliott, M.W. Hamilton, K. Arnett and S.J. Smith: Phys. Rev. Lett. 53, 439 (1984)
2. B.R. Mollow: Phys. Rev. 175, 1555 (1968)
3. For example, P. Zoller and P. Lambropoulos: J. Phys. B13, 69 (1980); and G.S. Agarwal: Phys. Rev. A1, 1445 (1970)
4. For example, S.N. Dixit, P. Zoller and P. Lambropoulos: Phys. Rev. A21, 1289 (1980); and J.J. Yeh and J.H. Eberly: Phys. Rev. A24, 888 (1981)
5. D.S. Elliott, R. Roy and S.J. Smith: Phys. Rev. A26, 12 (1982); and D.S. Elliott, R. Roy and S.J. Smith: in *Spectral Line Shapes*, Volume 2, edited by K. Burnett (de Gruyter, Berlin, New York, 1983), pp. 989-998
6. M.W. Hamilton, D.S. Elliott, K. Arnett and S.J. Smith: in progress
7. For example, D. Pritchard, J. Apt and T.W. Ducas: Phys. Rev. Lett. 32, 641 (1974); F. Biraben, B. Cagnac and G. Grynberg: Phys. Rev. Lett. 32, 643 (1974); and M.D. Levenson and N. Bloembergen, Phys. Rev. Lett. 32, 645 (1974)
8. A.V. Smith, J.E.M. Goldsmith, D.E. Nitz and S.J. Smith: Phys. Rev. A22, 577 (1980)

Electron Scattering in the Presence of Laser Radiation

Leonard Rosenberg
Department of Physics, New York Unive.sity, New York, NY 10003, USA

I. HISTORICAL INTRODUCTION

Rather than attempting to survey the considerable amount of work done during the past few years on the problem of electron scattering in a radiation field I thought it would be more useful to focus on a particular aspect, concerned with infrared radiation, and describe in some detail what appears to me to provide a proper theoretical framework for such problems. (More comprehensive treatments can be found in recent reviews [1-2].) I will, however, just to set the stage, give a brief rundown of some of the very early work bearing on this topic.

The development of the subject began with the introduction, by VOLKOV [3], of a closed-form solution of the Dirac equation for the motion of an electron in an external electromagnetic field; the field is assumed to have a well-defined direction of propagation but arbitrary spectral composition. The structure and gauge-transformation properties of the electron Green's function was examined some years later by SCHWINGER [4]. Modified Volkov solutions accounting for the effect of the anomalous magnetic moment have been developed [5]. Numerous applications of the Volkov solution to physical processes, such as photodisintegration and high-intensity Compton scattering, have been made over the years, with REISS [6], NIKISHOV and RITUS [7], and BROWN and KIBBLE [8] providing an early impetus. Still earlier, BLOCH and NORDSIECK [9], concerned with the infrared divergence problem of QED, provided a nonperturbative solution of the Dirac equation which allowed not only for an external beam of photons but for spontaneous emission and absorption as well. To obtain a closed-form solution it was necessary to replace the components of the electron momentum operator -- in this case the Dirac matrices -- by c-numbers. Such an approximation is appropriate in dealing with very low-energy photons since electron recoil effects are then negligible. It should be emphasized that electron-field states involving different numbers of soft photons but the same electron momentum are nearly degenerate and ordinary perturbation theory breaks down. One understands this physically by recognizing that in asymptotic states there is plenty of time available and the electron energy is well defined. On the other hand the energy is not well defined during the collision if the collision time is short compared to characteristic periods of the field. In this interval, then, near-singularity problems do not arise and low-order perturbation theory is adequate in many cases of interest. (If there are scattering resonances present that argument is not obviously valid and special care is required. The presence of long-range Coulomb interactions also raises questions about the validity of the asymptotic dominance idea; I will return to this point later on.) The near-degeneracy of the asymptotic states has the consequence that the effective coupling strength between the electron and the field is given by the ratio of the interaction energy to the photon energy (this will be verified

later) and nonperturbative solutions are required, even for fields not intrinsically strong, if the frequency is low enough. The low-frequency domain is also interesting by virtue of its relation to the classical limit. Bloch and Nordsieck, for example, showed that the energy radiated into the low-frequency modes of the field is just what would be expected classically, assuming an instantaneous collision and straight-line trajectories of the electron before and after the collision. There are, furthermore, several interesting soft-photon theorems. The one most relevant to our topic is due to LOW [10] who showed, for single-photon bremsstrahlung, that the first two terms in an expansion of the amplitude in powers of the photon frequency could be determined exactly from a knowledge of the physical (on-shell) amplitude for scattering in the absence of the field. A version of this theorem appropriate to scattering in a low-frequency external field was derived by BROWN and GOBLE [11] as part of a study of soft photons and the classical limit. (The crucial role played by analyticity and gauge-invariance requirements in these investigations should be emphasized.)

The long-range Coulomb interaction between the electron and a charged target particle arises, of course, from the exchange of soft photons. In 1970 KULISH and FADDEEV [12], generalizing to QED earlier work by DOLLARD [13] which dealt with nonrelativistic Coulomb scattering, gave a proper mathematical description of scattering theory which allowed for soft-photon interactions before and after the collision. This powerful and elegant approach provides a justification for the Bloch-Nordsieck solution of the infrared divergence problem and clearly shows that this problem is removed, along with Coulomb divergence difficulties, by a correct dynamical description of the motion of the electron in asymptotic states. In what follows I will describe a simplified, nonrelativistic version [14] of the Kulish-Faddeev theory. The situation where the low-frequency radiation field is external -- an incident photon beam -- is included as a special case. One simply assumes an initial state with a large photon occupation number in one or more of the field modes. This simplified treatment will, I hope, provide insight into the Dollard-Kulish-Faddeev method and will also serve as an introduction to recent theoretical work on nonrelativistic scattering in a radiation field. For most of the discussion I will ignore the internal structure of the target, assuming the electron-target interaction to be given by a local potential $V(r)$, with $V \sim g/r$ for $r \to \infty$; that is, I allow for the presence of a Coulomb tail.

II. THE ASYMPTOTIC HAMILTONIAN METHOD

Recall that in the usual development of time-dependent scattering theory [15] one introduces a Hamiltonian H and the operator $\exp[-iH(t'-t)/\hbar]$ describing the evolution of the system from time t in the remote past to time t' in the distant future. One forms the matrix element of this operator with respect to the plane-wave states representing the system before and after the collision. The time-evolution operator can be expressed in terms of the resolvent $G(z) = (z-H)^{-1}$ as

$$\exp[-iH(t' - t)/\hbar] = (2\pi i)^{-1} \int_C dz \exp[-iz(t' - t)/\hbar]G(z) ,$$

the contour surrounding the real axis. Due to the rapid oscillations of the integrand for large times only the singular part of the resolvent contributes, and the singularity can be isolated by expanding the resolvent (with the aid of the Lippmann-Schwinger integral equation, for example) in terms of the resolvent of the unperturbed system. One must rethink this standard text-book development if there are long-term interactions before

and after the collision. Otherwise one runs into trouble, such as divergences; ordinary Coulomb scattering provides a familiar example of the potential pitfalls that exist. The remedy lies in the replacement of the plane waves by asymptotic states which provide a more realistic description of the dynamics. Thus, suppose the Hamiltonian is of the form

$$H = H_0 + V + H_{eF} ,$$

where $H_0 = H_e + H_F$ is the sum of the electron kinetic energy and the free-field Hamiltonian. In writing down the form of the electron-field interaction energy H_{eF} we separate off the dominant contribution arising from soft-photon effects, since this will have to be treated nonperturbatively along with the Coulomb tail. The soft-photon contribution to the vector potential (in the dipole approximation for simplicity) is written as

$$\vec{A}_S = \sum_{j=0}^{s} \left(\frac{2\pi\hbar c^2}{\omega_j L^3}\right)^{1/2} \vec{\lambda}_j (a_j + a_j^\dagger) ,$$

where L^3 is the quantization volume, $\vec{\lambda}_j$ is the polarization vector of the j'th mode, a_j and $a_j^\dagger$ are the usual photon annihilation and creation operators, and the sum includes soft-photon modes only. We now write

$$H_{eF} = -\frac{e}{mc}(-i\hbar \vec{\nabla}\cdot\vec{A}_s) + \Delta H_{eF} ,$$

where the residual interaction ΔH_{eF} includes A^2 contributions as well as the effects of the hard photons.

The initial unperturbed state is characterized by a set $\{n_1, n_2, \cdots, n_s\}$ of photon occupation numbers (denoted collectively as n) and the electron momentum $\vec{p}$. The state of the system before the collision, including the effect of the long-range interactions, is represented as

$$|\Phi_{n\vec{p}}(t)\rangle = U_{as}(t)|n\rangle|\vec{p}\rangle .$$

The asymptotic evolution operator satisfies the Schrödinger equation

$$i\hbar \frac{d}{dt} U_{as}(t) = H_{as} U_{as}(t) ,$$

with $H_{as} = H_0 + H_{as}'$. The asymptotic interaction energy

$$H_{as}' = -\frac{e}{mc}\left(-i\hbar \vec{\nabla} \cdot \vec{A}_s\right) + \frac{g}{r}$$

accounts for soft-photon and Coulomb effects. Let us look for a solution of the form

$$U_{as}(t) = \exp(-iH_0 t/\hbar) Z(t) .$$

One finds, in the usual way, that $Z(t)$ must satisfy the Schrödinger equation in the interaction representation. This has the formal solution

$$Z(t) = T \exp\left[-i/\hbar \int^t H_{as}'(t_1) dt_1\right] ,$$

where T is the time-ordering operator. The asymptotic interaction $H_{as}'(t)$ now has a time-dependence generated by the free Hamiltonian H_0, so that $a_j(t) = a_j \exp(-i\omega_j t)$ and $r(t) = |\vec{r} + \vec{p}t/m|$. If the domain of integration in the above formula for $Z(t)$ is restricted to times in the remote past,

when soft-photon interactions dominate and electron recoil effects are negligible, we may replace $-i\hbar\vec{\nabla}$ by $\vec{p}$ to good approximation (in close analogy with the Bloch-Nordsieck model). Furthermore, in the Coulomb potential, we have $r(t) \equiv p|t|/m$. These approximations simplify the problem enormously. There still remains the task of carrying out the time-ordering operation; but note that

$$Q(t_1,t_2) \equiv [H'_{as}(t_1),H'_{as}(t_2)]$$

is a c-number. According to a well-known theorem [16] we may then ignore the T-instruction, provided we include the extra phase factor

$$\exp[-\frac{1}{2}\int^{t}\frac{dt_1}{\hbar}\int^{t_1}\frac{dt_2}{\hbar}\,Q(t_1,t_2)] \equiv \exp[-i\,\Delta_{\vec{p}}^{+}\,t/\hbar] \ .$$

In evaluating the double integral we drop contributions from the lower limits. One can verify that this prescription [12] corresponds to imposing the proper initial conditions; it also avoids having to include contributions from finite times during which our soft-photon approximation breaks down. One obtains in this way the "level-shift"

$$\Delta_{\vec{p}}^{+} = \sum_{j=0}^{s}\hbar\omega_j\rho_{j\vec{p}}^{2} \ ,$$

with

$$\rho_{j\vec{p}} = \frac{1}{\hbar\omega_j}\,(-\frac{e}{mc})\,(\frac{2\pi\hbar c^2}{\omega_j L^3})^{1/2}\,\vec{p}\cdot\vec{\lambda}_j \ .$$

The level-shift arises from the emission and absorption of virtual photons. It can be interpreted classically as a radiation reaction effect; the work required to accelerate the electron from rest to momentum p exceeds $p^2/2m$ by an amount equal to the energy radiated during the acceleration and this is just $\Delta_{\vec{p}}^{+}$. (The shift is rather small in the nonrelativistic case considered here and could be neglected.) The parameters $\rho_{j\vec{p}}$ provide a measure of the effective strength of the electron-field interaction. They each have the form of an interaction energy divided by a photon energy. The appearance of the frequency in the denominator is the mathematical origin of the important role played by soft photons, requiring nonperturbative treatment even when the intrinsic interaction strength is not large.

We may now write

$$Z(t) \equiv \exp\{-i/\hbar\,[\int^{t}H'_{as}(t_1)dt_1 + \Delta_{\vec{p}}^{+}t]\} \ .$$

The remaining integrals are easily done, giving

$$-i/\hbar\int^{t}(-\frac{e}{mc})\,\vec{p}\cdot\vec{A}_s(t_1)dt_1 = \sum_{j=0}^{s}\rho_{j\vec{p}}\,(a_j e^{-i\omega_j t} - a_j^{+}e^{i\omega_j t}),$$

where again the contribution from the lower limit of the time integration has been dropped, and

$$-i/\hbar\int^{t}\frac{mg}{p|t_1|}\,dt_1 = i\xi\ell n(4E|t|/\hbar) \ ,$$

where $E = p^2/2m$ and $\xi = mg/\hbar p$ is the Sommerfeld parameter. The fact that the Coulomb integral diverges for large $|t|$ is a clear indication that the effect of the Coulomb tail must be accounted for nonperturbatively. The

choice of integration constant in the Coulomb integral has been obtained by the following prescription: consider a wave-packet solution in configuration space for the asymptotic motion of the electron in a Coulomb field. The center of the packet follows a classical trajectory. With $\vec{r}$ replaced by $\vec{p}t/m$ the wave-packet solution has a logarithmic phase identical to that shown here. (Ref. [13] should be consulted for a more thorough discussion.)

Let us emphasize that inclusion of the Z-factor is crucial in avoiding infrared divergences due to soft-photon exchange between electron and target (Coulomb tail) and emission and reabsorption of soft photons by an isolated electron. Furthermore, in the presence of an external field, which is intrinsically strong, or effectively so, due to the $(\hbar\omega_j)^{-1}$ factor, the nonperturbative treatment is essential. Individual terms in the perturbation expansion will be finite but working to low order will give poor results in general.

Collecting results we have

$$|\Phi_{n\vec{p}}> = \exp[-iE_{n\vec{p}}t/\hbar + i\xi\ell n(4E|t|/\hbar)]|\psi_{n\vec{p}}> ,$$

where $E_{n\vec{p}} = E + E_n + \Delta_{\vec{p}}$ (E_n is the photon energy in state $|n>$). We have introduced the coherent state

$$|\psi_{n\vec{p}}> = W_{\vec{p}}\ |n>|\vec{p}> .$$

with

$$W_{\vec{p}} = \exp[\sum_{j=0}^{s} \rho_{j\vec{p}}(a_j - a_j^\dagger)].$$

We expect that the coherent state should satisfy the time-independent Schrödinger equation

$$[H_0 - \frac{e}{mc}\vec{p}\cdot\vec{A}_s]|\psi_{n\vec{p}}> = E_{n\vec{p}}|\psi_{n\vec{p}}> .$$

This may be verified using the commutation relation

$$[a_j,\ W_{\vec{p}}] = -\rho_{j\vec{p}}W_{\vec{p}}$$

and its adjoint. Thus the wave-operator $W_{\vec{p}}$ builds in the effect of the soft-photon interaction and the logarithmic phase accounts for the effect of the Coulomb tail.

Suppose that the j'th mode has a large occupation number; $n_j >> 1$. Then, ignoring the commutator $[a_j, a_j^\dagger] = 1$ as well as photon depletion effects we have

$$\exp[\rho_{j\vec{p}}(a_j - a_j^\dagger)]|n_j> \cong \sum_{\ell=-\infty}^{\infty} J_\ell(2\rho_{j\vec{p}}\sqrt{n_j})|n_j - \ell> ,$$

as can be verified by expansion of the exponential and comparison with the series representation of the Bessel function. One also verifies that this series expansion is precisely what is obtained by summing the appropriate perturbation expansion for the state of the electron-field system.

With the asymptotic states determined, the initial and final time variables may be extended to infinity. To pick out the singularities in the resolvent we define

$$H_{\vec{p}} = H_0 - \frac{e}{mc}\vec{p}\cdot\vec{A}_s + V \ ;$$

then, with $G_{\vec{p}}(z) \equiv (z - H_{\vec{p}})^{-1}$ we introduce the resolvent identity

$$G = G_{\vec{p}} + G(H - H_{\vec{p}})G_{\vec{p}}$$

which can be further expanded as

$$G = G_{\vec{p}} + G_{\vec{p}}\cdot(H - H_{\vec{p}})G_{\vec{p}} + G_{\vec{p}}\cdot(H - H_{\vec{p}}\cdot)G(H - H_{\vec{p}})G_{\vec{p}} \ .$$

The residues at the initial- and final-state singularities can be expressed in terms of the eigenfunctions

$$|\psi^{(\pm)}_{n\vec{p}} > = W_{\vec{p}}|n>|u^{(\pm)}_{\vec{p}}> \ ,$$

where $u^{(\pm)}_{\vec{p}}$ is the wave function for scattering in the potential V satisfying either outgoing-wave (+) or incoming-wave (-) boundary conditions at infinity. We have

$$H_{\vec{p}}\ |\psi^{(\pm)}_{n\vec{p}}> = E_{n\vec{p}}|\psi^{(\pm)}_{n\vec{p}}> \ .$$

With the passage to an infinite time domain the S matrix takes the form of a product of an energy conserving δ-function and the transition-matrix

$$M_{n'\vec{p}';n\vec{p}} = <\psi^{(-)}_{n'\vec{p}'}|H-H_{\vec{p}}|\psi^{(+)}_{n\vec{p}}> + <\psi^{(-)}_{n'\vec{p}'}|(H-H_{\vec{p}'})G(E_{n\vec{p}})(H-H_{\vec{p}})|\psi^{(+)}_{n\vec{p}}> \ .$$

The effect of the "strong" part of the interaction has been built into the distorted waves, leaving the perturbation

$$H - H_{\vec{p}} = -\frac{e}{mc}(i\hbar\vec{\nabla} - \vec{p})\cdot\vec{A}_s + \Delta H_{eF} \ .$$

We drop the residual interaction ΔH_{eF} in the following and work to first order in the first term (which evidently corrects for the effect of electron recoil). After accounting for the orthogonality of the Coulomb wave functions for $\vec{p}' \neq \vec{p}$ we obtain, as a form of distorted-wave Born approximation,

$$M_{n'\vec{p}';n\vec{p}} \cong -(\frac{e}{mc}) <n'|W^{\dagger}_{\vec{p}'}\vec{A}_s W_{\vec{p}}|n> \cdot <u^{(-)}_{\vec{p}'}|-i\hbar\vec{\nabla}|u^{(+)}_{\vec{p}}> \ .$$

Note that the free-free atomic matrix element is just that for single-photon bremsstrahling, with field effects appearing as an isolated factor, an important simplifying feature of this approximation. The fact that we have ignored target structure can be justfied if the external electric-field strength is small compared to internal (atomic) field strengths. Even with this restriction the external field can, as a consequence of the appearance of the near-singularities mentioned earlier, have profound effects on the motion of the projectile so the remark [17] is not a trivial one.

Let us assume that ΔE, the net amount of infrared radiation emitted by the electron, is small compared to its initial energy. Then the bremsstrahlung matrix element can be evaluated approximately by recognizing that the dominant contribution comes from the asymptotic domain in configuration space. (The singularity which develops for $\Delta E \to 0$ can only arise from an infinite domain of integration.) The approximation procedure, while complicated in its details, can be summarized briefly as follows [18]. One expands in partial waves and replaces the radial Coulomb function by its asymptotic form (or rather, for improved accuracy, by the

first two terms in its asymptotic expansion). This can be expressed in terms of the field-free scattering phase shifts. Only those terms which are slowly varying at infinity are retained. The radial integration can be done and the sum over partial waves is performed with the help of the closure relation for the spherical harmonics. This in turn simplifies the remaining angular integrations. The result is of the form

$$< u^{(-)}_{\vec{p}'} \; | -i\hbar\vec{\nabla} | u^{(+)}_{\vec{p}} > = (\vec{p}' + \vec{p})\, C_+ + (\vec{p}' - \vec{p}) C_- \; ,$$

where

$$C_- = \left(\frac{1}{\Delta E} - \frac{\pi\xi}{4E} \right) t \quad + \cdots \; ,$$

$$C_+ = \frac{-i\xi}{2E} \left[\ell n \left(\frac{\Delta E}{4E} \right) + 1 + \gamma \right] t \quad + \frac{1}{2} \frac{\partial t}{\partial E} + \cdots \; .$$

Here $\gamma = 0.577 \cdots$ is the Euler constant and t is the on-shell scattering amplitude evaluated at an energy midway between the initial and final electron energies. This represents a nonrelativistic version of the theorem of LOW [10], generalized to include the effect of the Coulomb tail. The derivation outlined here can also be applied to potential scattering described by the Dirac equation. We have assumed that the scattering amplitude varies smoothly with energy. If there are resonances present the derivation must be modified [19]. The results are of some interest since they may be of use in determining resonance parameters. This was the motivation of the analysis of single-photon bremsstrahlung given some time ago by FESHBACH and YENNIE [20].

Let us look more closely at the leading term in the expression for the bremsstrahlung matrix element. We take $C_- \cong (\Delta E)^{-1} t$ and $C_+ \cong 0$. Then, using the eigenvalue equation for the coherent state derived earlier, along with the addition formula $W^{\dagger}_{\vec{p}'} W_{\vec{p}} = W_{\vec{p}-\vec{p}'}$, we find

$$M_{n'\vec{p}';n\vec{p}} \cong < n' | W_{\vec{p}-\vec{p}'} | n > t \; .$$

(The external-field version of this result was derived by BUNKIN and FEDOROV [21] and then improved, through inclusion of corrections of higher order in the frequency, by KROLL and WATSON [22].) The cross section is then

$$\frac{d\sigma}{d\Omega} \cong | < n' | W_{\vec{p}-\vec{p}'} | n > |^2 \frac{d\sigma^{(0)}}{d\Omega} \; ,$$

where $d\sigma^{(0)}/d\Omega$ is the field-free cross section. By virtue of the unitarity property of the operator $W_{\vec{p}-\vec{p}'}$ the sum over final photon states gives unity for the field-dependent factor. As observed by Bloch and Nordsieck, this solves the infrared divergence problem since at this stage one can go to the continuum limit (quantization volume $L^3 \to \infty$) without encountering divergences. (A divergence does appear in the expression for the average number of photons radiated during the collision. But this is a physical divergence, consistent with the prediction of vanishing probability for the emission of only a finite number of photons.)

The external-field version of the sum rule has apparently been verified experimentally [23]. An improved version of this sum rule can be obtained by including higher order corrections in the bremsstrahlung matrix element. This result, a relativistic version of which was first given by BROWN and GOBLE [11], has an interesting classical interpretation. That is, to calculate the average energy transferred to the field by the electron, one calculates the energy lost by the electron assuming it follows a classical

trajectory in the field before and after the collision. The collision is assumed to take place instantaneously and without influence from the field. The result depends on the phase of the field at the instant of collision and the energy loss is averaged over the phase in addition to being weighted by the collision probability. The appearance of on-shell scattering parameters only is, of course, in agreement with the classical picture in which no off-shell scattering is involved. Note the analogy with the Bloch-Nordsieck sum rule for the energy loss, mentioned earlier, which can be interpreted in the language of classical radiation theory.

III. BEYOND THE SOFT-PHOTON APPROXIMATION

The simplifying feature of the soft-photon approximation is that particle-field interactions during the collision can be treated perturbatively. To go beyond this approximation requires some honest hard work. A start has been made by SHAKESHAFT [24] who essentially solves the Lippmann-Schwinger integral equation for the resolvent. This is done using the time-honored technical device of replacing the local scattering potential V(r) (assumed to be short-ranged) by a sum of nonlocal separable potentials. Inclusion of a Coulomb tail and allowance for the interaction between the field and the target system will raise substantial difficulties. (An approach to the "Coulomb problem", based on the introduction of a screening parameter, has been suggested recently [25].) It should also be mentioned (as mentioned to me by Shakeshaft) that the existence of scattering resonances introduces new computational problems in the form of numerical instabilities. One way to deal with such problems would be to separate off these resonance effects using standard projection-operator methods developed for nuclear reaction studies. Integral equations for the smooth background amplitudes could then be solved as in the nonresonant case. Such calculations have not been attempted thus far. One specific motivation for doing so would be to examine more closely (perhaps along the lines described recently [26]) several multiphoton ionization calculations [27-29] in which final-state interactions are evaluated in a resonance-dominance approximation, that is, ignoring the effect of the field on the smooth background amplitude.

This work was supported in part by the United States National Science Foundation and the Office of Naval Research.

REFERENCES

1. M.H. Mittleman: Theory of Laser-Atom Interactions (Plenum, New York, 1982)
2. L. Rosenberg: Adv. At. Mol. Phys. 18, 1 (1982)
3. D.M. Volkov: Z. Phys. 94, 250 (1935)
4. J. Schwinger: Phys. Rev. 82, 664 (1951)
5. W. Becker and H. Mitter: J. Phys. A 7, 1266 (1974)
6. H.R. Reiss: J. Math. Phys. 3, 59 (1962)
7. A.I. Nikishov and V.I. Ritus: Sov. Phys. -- JETP (Engl. Transl.) 19, 529 (1964)
8. L.S. Brown and T. W. B. Kibble: Phys. Rev. 133, A705 (1964)
9. F. Bloch and A. Nordsieck: Phys. Rev. 52, 54 (1937)
10. F.E. Low: Phys. Rev. 110, 974 (1958)
11. L.S. Brown and R.L. Goble: Phys. Rev. 173, 1505 (1968)
12. P.P. Kulish and L.D. Faddeev: Theor. Math. Phys. (USSR) 4, 745 (1970)
13. J. Dollard: J. Math. Phys. 5, 729 (1964)
14. L. Rosenberg: Phys. Rev. A 26, 132 (1982)
15. M.L. Goldberger and K.M. Watson: Collison Theory (Wiley, New York, 1964), Chap. 3

16. K. Gottfried: Quantum Mechanics (Benjamin, New York, 1966), p. 426
17. M.H. Mittleman: Phys. Rev. A 21, 79 (1980)
18. L. Rosenberg: Phys. Rev. A. 27, 1879 (1983)
19. H. Krüger and C. Jung: Phys. Rev. A 17, 1706 (1978)
20. H. Feshbach and D.R. Yennie: Nucl. Phys. 37, 150 (1962)
21. S.V. Bunkin and M.V. Fedorov: Sov. Phys. -- JETP (Eng. Transl.) 22, 884 (1966)
22. N.M. Kroll and K.M. Watson: Phys. Rev A 8, 804 (1973)
23. A. Weingartshofer, E.M. Clarke, J.K. Holmes, and C. Jung: Phys. Rev. A 19, 2371 (1979)
24. R. Shakeshaft: Phys. Rev. A. 28, 667 (1983)
25. J. Banerji and M.H. Mittleman: Phys. Rev. A 26, 3706 (1982)
26. L. Rosenberg: Phys. Rev A 30, 245 (1984)
27. P. Lambropoulos and P. Zoller: Phys. Rev. A 24, 379 (1981)
28. K. Rzazewski and J.H. Eberly: Phys. Rev. Lett. 47, 408 (1981)
29. G.S. Agarwal, S.L. Haan, K. Burnett, and J. Cooper: Phys. Rev. Lett. 48, 1164 (1982)

Multiphoton Effects During Collisions

K. Burnett*

Spectroscopy Group, Blackett Laboratory, Imperial College
London, SW7 2BZ, United Kingdom

J. Cooper

Department of Physics, University of Colorado and Joint Institute for Laboratory Astrophysics, University of Colorado and National Bureau of Standards, Boulder, CO 80309, USA

1. Introduction

We should like to present a brief progress report on multiphoton transitions occurring during collisions. The aim of the work is the development of techniques for studying collision dynamics using off-resonant excitation of atomic transitions in the presence of collisions [1]. We shall start with the now comparatively well understood subject of collisional redistribution, dealing with single-photon absorption during collisions [1,2]. The natural extension of this work to multiphoton effects is what we are pursuing. The first type of multiphoton effect we'll look at involves saturation of a two-level system: the Rabi problem of collision physics. This is an enormous topic that we shall discuss briefly and very naively [1,2]. We shall turn lastly to multilevel systems where much less is known and much more remains to be done. This report will use qualitative arguments. For more rigorous discussions the reader should consult the references given in the text.

2. Single photon absorption during collisions

Let's first establish a simple picture of absorption during a collision, which we shall use throughout this article [3]. Suppose we have an atom which interacts with a perturber. Its resonance transition frequency will be swept through a range of frequencies by a perturber passing by. Let us further suppose that a laser field, oscillating at a different frequency ω_ℓ from the natural frequency ω_0 of the atom, is present. In the absence of the collision the laser produces some small amplitude for finding the atom in its excited state. This amplitude gives rise to Rayleigh scattering, in the usual way. When a collision occurs a new process takes place. During the collision the atomic transition is brought momentarily into resonance with the incoming field (Fig. 1) (if, and only if, of course, the collisional shift is sufficiently strong and of the correct sign). Because of this the laser may produce a much larger amplitude in the excited state.

What is more, the amplitude is out of phase with respect to the incoming driving field, and can produce fluorescence at the atom's natural frequency. This process is termed collisional redistribution of radiation [1].

*A. P. Sloan Foundation Fellow 1982-84.

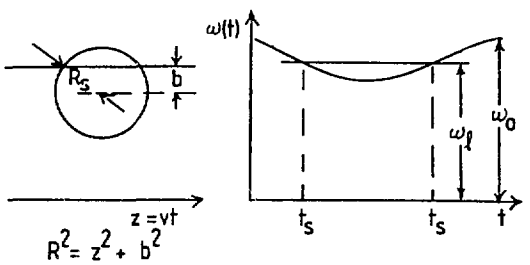

Fig. 1. Absorption during a collision: classical path approach in space and time

The amplitude for producing the excited state may be written thus [3]:

$$A = \int_{-\infty}^{\infty} dt \exp[i \int_{-\infty}^{t} dt'(\omega[t'] - \omega_\ell)] \quad . \qquad (1)$$

This result may be derived using a purely classical picture [3,4]. Note that the amplitude in equation (1) gives the contribution from a single encounter. The result needs summing over different impact parameters, and averaging over atom-perturber speeds and over times of closest approach. For large enough detunings the amplitude is dominated by the point where the transition is in resonance, i.e. when

$$\omega_\ell = \omega(t) = \delta V(R[t])\hbar^{-1} = [V_{excited} - V_{ground}]\hbar^{-1} \quad . \qquad (2)$$

There are two such times, one on the way in and one on the way out. We shall ignore the interference between the two points and consider these two points independently. How long is the transition in resonance? This question is important for two reasons. Firstly, because the time in resonance will determine the size of the amplitude. Secondly, because the time in resonance, t_R, must be much smaller than the duration of the whole collision $t_{D.C.}$ for us to use a localized picture.

The transition will be in resonance as long as it is not shifted out of phase with the incoming field [3]. This allows us to estimate the time in resonance, τ_R. It is given by

$$\int_{t_s}^{t_s+t_R} dt(\omega(t) - \omega_\ell) \sim 1 \quad , \qquad \text{i.e.} \qquad (3)$$

$$[\frac{d\omega}{dt}]_{t_s} t_R^2 \sim 1 \quad .$$

This gives us

$$t_R \sim \{[\frac{d\omega}{dt}]_{t_s}\}^{-1/2} \quad . \qquad (4)$$

If we use the crude estimate (see Ref. [4] for what happens when $[d\omega/dt]_{t_s} = 0$)

$$\left|\frac{d\omega}{dt}\right|_{t_s} \sim \frac{\omega_0-\omega_\ell}{t_{D.C.}} \tag{5}$$

we obtain

$$t_R \sim [t_{D.C.}/(\omega_0-\omega_\ell)]^{1/2} \quad . \tag{6}$$

For a localized picture to be valid we require

$$t_{D.C.} >> t_R \text{ , i.e. } (\omega_0-\omega_\ell)t_{D.C.} >> 1 \quad . \tag{7}$$

This is the usual quasi-static limit. In this limit we can think of localized absorption by a region length t_R around t_s. If the on resonance Rabi frequency for the problem is Ω the population produced will be of order Ωt_R. The cross section for excitation can then be written in the form

$$C|\Omega|^2 \langle v\pi b^2 \left[\frac{d\omega}{dt_s}\right]^{-1} \rangle \tag{8}$$

where v is the relative velocity. Here, the brackets denote the averaging process. This result can be converted, with certain assumptions, to the form

$$C \exp[-V_g(R_s)/kT]|\Omega|^2 \left[\frac{d\ \delta V}{dR}\Big|_{R_s}\right]^{-1} \quad . \tag{9}$$

This result is of utmost importance. It shows how measuring the frequency and temperature dependence of far-wing absorption can be used to study interatomic potentials [4,5]. There is another consequence of the localization of the excitation process which comes into play when there is more than one potential curve. We can populate a localized region inside a collision and then observe the asymptotic states produced by such a population. This enables us to observe the effect of fractional collisions in much the same way as photo-dissociation probes half-collisions [6].

We shall move on now to multiphoton effects, the first being the saturation of the single-photon absorption. The second effect, multistep absorption, will bring us back to the study of collision dynamics proper.

3. Saturation of a two-level system

The perturbation treatment used to obtain equation (8) will break down for $\Omega t_R \sim 1$ for then absorption may be followed by stimulated re-emission before the transition goes out of resonance [7]. We can deal with the problem of intense fields by solving the equations for the amplitudes to be in the states coupled by the laser. In the strong field limit the dressed state method is most useful [7,8]. In one form this is simply the Schrödinger picture for the combined system of atom plus radiation field. The behavior of the dressed state energy levels is shown in Fig. 2.

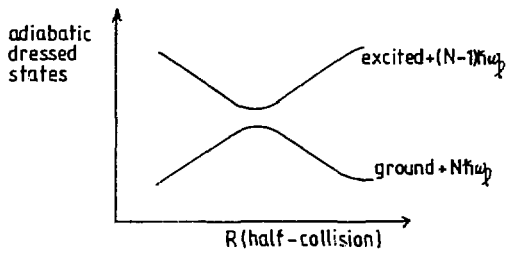

Fig. 2. Dressed state picture of absorption during a collision

Excitation during a collision comes about via the interaction of dressed states. This interaction is shown by the avoided crossing of the adiabatic dressed states in Fig. 2.

The probability for excitation during a single pass through "resonance" (there are, of course, two during a collision) is given qualitatively by the Landau-Zener expression [9]

$$P_{I\to II} = \{1 - \exp[-|\Omega|^2/|\tfrac{d\omega}{dt}|_{t_s}]\} \quad . \tag{10}$$

For small Ωt_R, i.e. for weak incoming fields, this reduces to the perturbation theory result.

For intense fields the dressed states avoid strongly and the transition is certain to happen [7]. Since there are two avoided crossings the cross section as a function of field strength looks qualitatively like the curve shown in Fig. 3. We can describe this behavior as saturation of the collision complex. It is not the same type of saturation as one usually considers in bound-bound transitions. Usually we would be interested in whether stimulated emission beats spontaneously back to the lower state.

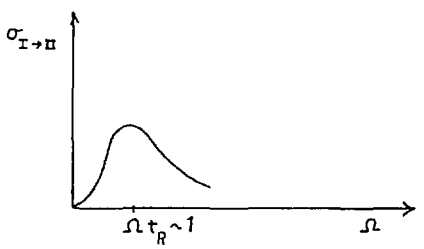

Fig. 3. Cross section for excitation during a collision as a function of field strength

In the case of the free-free transition the state is most likely to dissociate before it re-radiates spontaneously. For a bound state the atom-perturber molecule would return to the same point in phase-space where the transition occurs. Saturation of the type considered here, if present in a bound-bound system, will completely change the bound state spectrum [10].

There have only been a few observations [11,12,13] of saturation of absorption during collisions. All these observations have been qualitative, rather than quantitative. This is partly due to the difficulties inherent in strong-field experiments.

A typical collisional duration is $t_{D.C.} \sim 10^{-12}$ s. t_R is typically $\sim 10^{-13}$ s. For saturation we therefore need powers $\sim$100 MW/cm^2 (if we can couple to an allowed dipole moment).

In the presence of such field strengths many other processes, apart from collisional ones, can take place. Firstly, multiphoton ionization can take away the excited atoms you want to detect. Secondly, the energy in excited states can be stimulated out in a forward direction by four wave mixing. This can also be described in terms of transitions between dressed states (see Fig. 4). These effects can dramatically alter the populations in the dressed states and affect the measurements of collisional rates, especially in cells. Such effects are also very difficult to account for theoretically since they depend on the details of the frequency distribution of the laser.

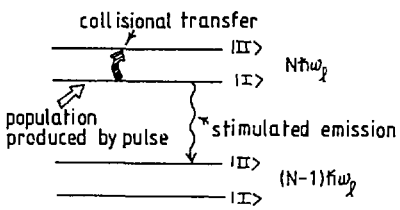

Fig. 4. Stimulated processes among the dressed states

Future quantitative studies on saturation effects will require molecular beam experiments. It is also likely that the most successful studies will exploit resonances and other means to increase Ω, and hence reduce the laser intensities needed [14].

4. Multiphoton transitions: multilevel systems

Let's suppose we've produced a population in a localized region on an excited potential surface during a collision. Ideally, we should like to follow this packet of population through the collision and watch it mixing with other states. To do this we could use a pump/probe technique, the probe being a second laser that can excite the population to a third level. We could then see whether the packet had crossed onto another potential surface as the collision proceeds. Under what conditions can we think of the populating and probing processes as independent?

Consider the model system shown in Fig. 5 [15]. In the following discussion we'll suppose that there is just one point of stationary phase for each transition (from ground to the first excited state and from this state to a third). Again we're just considering one half of the collision and ignoring interferences between the two parts.

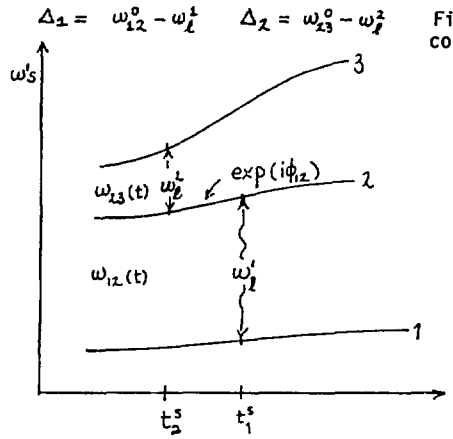

Fig. 5. Three-level system during a collision

The amplitude for excitation of level 3 has been calculated by Yeh and Berman [15]. This paper gives a thorough discussion of the three-level system with nondegenerate levels, during a single collision.

Even if we are in the limit where absorption is quasi-static for the transitions: Δ_1 and Δ_2 and the phase shift ϕ_{12} between the t_1^s and t_2^s is large, we still have to consider interference between the stepwise terms and direct two-photon absorption. The relative importance of these terms depends on the case in hand and it is not, in general, possible to think in terms of localized absorption followed by propagation and a subsequent absorption. We need to require

$$|\Delta_1 t_R^{12}| \gg 1 , \quad |\Delta_2 t_R^{23}| \gg 1 \quad \text{and} \quad |\phi_{12}| \gg 1 \quad .$$

We also need to have

$$|\Delta_1 + \Delta_2| \gg \left|\frac{d\omega_{13}}{dt}\right|^{+1/2} ,$$

in order to localize the direct two-photon absorption from state 1 to state 3. Thus, to decide whether the sequential resonant absorption picture is valid we need to know the lineshapes for the 1 → 2 and 2 → 3 transitions. A comprehensive theory of these processes including degeneracy effects has been developed by Alber and Cooper. This formalism, based on the techniques of Burnett and Cooper [1], deals consistently with events inside and outside collisions. Alber and Cooper's techniques also consider the effect of subsequent collisions on coherent and "incoherent" processes. The evaluation of the various terms for a realistic case will be important for experiments on three-level systems (such experiments are under way at JILA). We (Belsley, Burnett and Cooper) have also been extending work on fully off-shell T-matrices [16] to this problem where a considerable computational advantage exists (e.g. L. H. Beard and D. A. Micha have written a fully quantal code to calculate such things [17]). This has been combined

with our own work on uniform-semiclassical evaluations of the necessary quantities to give us physical insight into the overall amplitudes. Much work still needs to be done before multiphoton absorption can be used as successfully as single-photon absorption as a probe of collision dynamics. The field, however, seems to have plenty of physics in store.

Multiphoton processes during collisions has seen a great deal of theoretical activity in recent years. The experimental work to back it up is much slower in coming. We believe that the recently established advantages of collisional redistribution and photodissociation for probing collision dynamics direct us to the multiphoton generalizations.

It is too soon to give simple clear predictions of how fruitful the work will be: time will tell!

Acknowledgments

We should like to thank G. Alber, W. J. Alford, M. Belsley, N. Andersen, A. Gallagher, P. D. Kleiber, D. A. Micha, W. A. Molander and M. G. Raymer for helpful discussions. This work was supported by the A. P. Sloan Foundation, the United States National Science Foundation and the Science and Engineering Research Council of the United Kingdom.

[1] K. Burnett: "Collisional Redistribution of Radiation," Physics Reports (1984), in press. (This article contains a more or less comprehensive bibliography on the subject.)
[2] F. H. Mies: in "Theoretical Chemistry: Advances and Perspectives" (D. Henderson, ed.), Vol. 6B, Academic, New York (1981).
[3] H. Kuhn and F. London: Phil. Mag. XVIII, 983 (1934).
[4] N. Allard and J. Kielkopf: Rev. Mod. Phys. 54, 1103 (1982).
[5] R. E. Hedges, A. Drummond and A. Gallagher: Phys. Rev. A 6, 1519 (1972).
[6] J. Cooper: in "Spectral Line Shapes" (K. Burnett, ed.), p. 737, Walter de Gruyter, Berlin (1983).
[7] J. C. Light and A. Szoke: Phys. Rev. A 15, 1363 (1978).
[8] S. Reynaud: Ann. Phys. Fr. 8, 315 (1983).
[9] N. F. Mott and H. S. W. Massey: "The Theory of Atomic Collisions" 3rd edition, Oxford University Press (1965).
[10] A. D. Bandrauk and M. K. Sink: J. Chem. Phys. 74, 1110 (1981).
[11] A. M. Bonch-Bruevich, T. A. Vartanyan and V. V. Khromov: Sov. Phys.-JETP 51, 271 (1980).
[12] P. D. Kleiber, K. Burnett and J. Cooper: Phys. Rev. Lett. 47, 1595 (1981).
[13] P. D. Kleiber, K. Burnett and J. Cooper: Phys. Rev. A 25, 1188 (1982).
[14] T. F. George, et al., in "Collisions Atomiques et Moleculaires dans un Champ Laser," Colloques de C.N.R.S., Abbaye de Royaumont, March 1984.
[15] S. Yeh and P. R. Berman, Phys. Rev. A 22, 1403 (1980).
[16] K. Burnett and M. J. Belsley, Phys. Rev. A 28, 3291 (1983).
[17] L. H. Beard, Ph.D thesis, University of Florida, Gainesville, 1979 (unpublished).

Pressure Effects in the Multiphoton Ionization of Atoms and Molecules

Philip M. Johnson, Leping Li, and Richard N. Porter
Department of Chemistry, State University of New York
Stony Brook, NY 11794, USA

1. Pressure Reduction of the AC Stark Effect

Thirty years ago R. H. Dicke wrote "In the usual treatment of spontaneous radiation by a gas, the radiation process is calculated as though the separate molecules radiate independently of each other..... This simplified picture overlooks the fact that all the molecules are interacting with a common radiation field and hence cannot be treated as independent. The model is wrong in principle and many of the results obtained from it are incorrect."[1] Many subsequent results of magnetic resonance spectroscopy, and more recently of laser interactions have shown that Dicke stated a fundamental truth and that a collective treatment of molecules in a radiation field is often necessary. Notable examples in nonlinear optics include third harmonic generation and coherent antistokes Raman spectroscopy. We would like to present here another experimental effect which we feel is best explained by treating "non-interacting" molecules as a collective system. This effect is the quenching of the AC Stark shift upon an increase in the partial pressure of the molecule interacting with the radiation field.

The AC Stark effect is dramatically apparent in the multiphoton ionization spectra of atoms and molecules. The high intensity pulsed lasers used in these experiments produce electric fields in a focus region which cause Stark shifts of several wavenumbers even with intensities common to a pulsed dye laser. Because of the spatial and temporal variation of the light intensity interacting with the molecules, a great variety of Stark shifts are generally present in the ensemble of molecules and the experimental manifestation of the AC Stark effect is a characteristic asymmetric broadening of the spectral lines.

It was reported in 1980 that there is a pressure effect on the AC Stark broadening seen in multiphoton ionization spectra[2]. The system under study was nitric oxide, whose A state was being studied as a two-photon resonance in a four-photon ionization process. Whereas at low pressures the spectral lines are broadened to such an extent that the rotational structure blends together, at pressures of only a few torr the lines are completely resolved and become laser bandwidth limited (Fig. 1). This

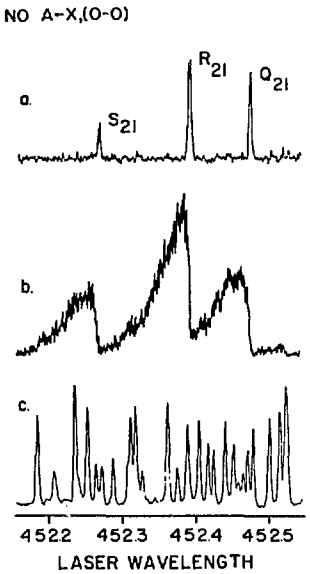

Figure 1: The spectrum of nitric oxide under three different conditions: a) at low laser intensity in a molecular beam, b) at high laser intensity in a molecular beam, and c) at the same laser intensity as b only in a room temperature cell at a few torr pressure

pressure narrowing has allowed the recording of high resolution MPI spectra which would have been completely useless if the AC Stark effect had not been quenched.

Subsequent work showed definitely that the low pressure broadening was due to the Stark effect to the exclusion of other processes[3] and it has been possible to precisely model the lineshape[4] for various focusing conditions. However, no model for the pressure narrowing which considered the molecules independently was justified quantitatively. Various possibilities were considered, including laser induced collisions, plasma formation in the focal region, self-defocusing of the gas, long range electrostatic interactions, etc. A new model which includes certain sets of molecules as a collective whole has been very successful quantitatively, and predicted a dependence of the pressure narrowing upon the laser bandwidth which was later verified by experiment[5]. Here we would like to present a brief description of the pressure narrowing theory and experiment.

In Fig. 1 it is seen that spectrum b is greatly broadened by the AC Stark effect, whereas this effect is quenched in the higher pressure spectrum c. Similar results to spectra a and b can be obtained in a static cell, but the supersonic beam apparatus provides better signal to noise at low pressure and a decrease in spectral congestion so the asymmetric broadening is more visible. It should be noted that the pressure narrowing only occurs when the partial pressure of nitric oxide itself is raised.

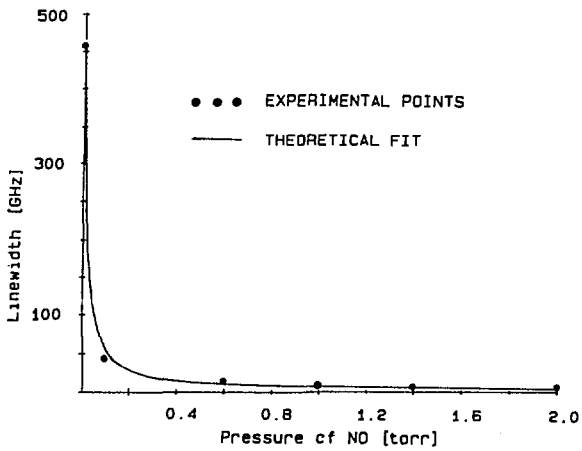

Figure 2: The width of a A↔X[0,0] MPI resonance line as a function of NO partial pressure at a fixed laser power

Pressurizing with a second gas has very little effect on the linewidth. Figure 2 shows a plot of the linewidth of the A↔X transition versus pressure at a given laser power. The point plotted at zero pressure was taken in a supersonic beam, while the other points are from a room temperature cell.

The standard formula for the shift of a molecular level $|a\rangle$ by radiation of frequency ν is

$$\Delta E_a^{(2)} = \sum_{c \neq a} \frac{\langle a|\underset{\sim}{\mu}^{(1)} \cdot \underset{\sim}{\mathcal{E}}^{o}|c\rangle\langle c|\underset{\sim}{\mu}^{(1)} \cdot \underset{\sim}{\mathcal{E}}^{o}|a\rangle}{(E_a - E_c)^2 - (h\nu)^2}[E_a - E_c] = \alpha I, \qquad (1)$$

where $\underset{\sim}{\mu}^{(1)}$ is the one-molecule dipole operator, $\underset{\sim}{\mathcal{E}}^{o}$ is the electric field of the radiation, I is the laser intensity and α is the AC Stark coefficient. The AC Stark shift is thus quantum mechanically represented by a cycling between the state of interest $|a\rangle$ and a virtual state.

While this formula is completely adequate for an isolated molecule in the laser focus, if there are a group of molecules which are indistinguishable in the laser field it is necessary to treat them as a collective whole. A key point is that no measurement is ever made which would determine that a given molecule is in $|a\rangle$, so in place of single-molecule kets $|a\rangle$ and $|c\rangle$ we must use normalized n-molecule kets $|A\rangle$ and $|C\rangle$ where the number n is determined from the gas pressure and an interaction volume which will be defined later. The single-molecule dipole operator $\underset{\sim}{\mu}^{(1)}$ in (1) must likewise be replaced by the n-molecule operator $\underset{\sim}{\mu}^{(n)} = \sum_{j=1}^{n} \underset{\sim}{\mu}_j^{(1)}$. Since energy differences are the same with or without the collective treatment because of energy conservation, it is possible to

rewrite (1) immediately as

$$\Delta E_A^{(2)} = \sum_{C\neq A} \frac{\langle A|\underset{\sim}{\mu}^{(n)}\cdot\underset{\sim}{\mathcal{E}}^{o}|C\rangle\langle C|\underset{\sim}{\mu}^{(n)}\cdot\underset{\sim}{\mathcal{E}}^{o}|A\rangle}{[E_A-E_C]^2-(h\nu)^2}\,[E_A-E_C]\ , \tag{2}$$

If we assume that n_a of the n collectively treated molecules are in $|a\rangle$, then the expression for $|A\rangle$ contains a total of $(n!/n_a!w_a)$ orthogonal equally weighted terms where w_a is the number of permutations of the $(n-n_a)$ molecules among states other than a the normalization constant for $\langle A|$ is thus $(n_a!w_a/n!)^{1/2}$. Choosing one of the dipole operators, $\mu_j^{(1)}$, there are $[(n-1)!/(n_a-1)!w_a]$ terms in which $\langle A|$ contributes to $\langle A|\mu_j^{(1)}\cdot\mathcal{E}^o|C\rangle$ if the jth molecule is assigned to a. This is the number of ways to assign the remaining states to the other molecules. There is at most one term in $|C\rangle$ in which j is assigned to c for any given term in $\langle A|$ because of the orthogonality of the one-molecule bras. There are thus $[n!/(n_a-1)!1!w_a]$ terms in $|C\rangle$ since this is the number of ways of assigning the (n_a-1) states a, the state c, and the remaining $n-n_a$ states to the n molecules. The normalizing constant for $|C\rangle$ is thus $[(n_a-1)!w_a/n!]^{1/2}$. The contribution of the jth term in $\mu^{(n)}$ to the left bracket in (2) is therefore

$$\begin{aligned}\langle A|\underset{\sim}{\mu}_j^{(1)}\cdot\underset{\sim}{\mathcal{E}}^{o}|C\rangle &= \left\{\frac{n_a!w_a}{n!}\right\}^{1/2}\frac{(n-1)!}{(n_a-1)!w_a}\left[(n_a-1)!w_a/n!\right]^{1/2}\langle a|\underset{\sim}{\mu}_j^{(1)}\cdot\underset{\sim}{\mathcal{E}}^{o}|c\rangle e^{i(\phi_c-\phi_a)_j}\\ &= (\sqrt{n_a}/n)\langle a|\underset{\sim}{\mu}_j^{(1)}\cdot\underset{\sim}{\mathcal{E}}^{o}|c\rangle\, e^{i(\phi_c-\phi_a)_j}\ ,\end{aligned} \tag{3}$$

where the phase difference $(\phi_c-\phi_a)_j$ is random for each molecule j. By similar reasoning we obtain for the right bracket

$$\langle C|\underset{\sim}{\mu}_k^{(1)}\cdot\underset{\sim}{\mathcal{E}}^{o}|A\rangle = [\sqrt{n_a}/n]\langle c|\underset{\sim}{\mu}_k^{(1)}\cdot\underset{\sim}{\mathcal{E}}^{o}|a\rangle\, e^{-i(\phi_c-\phi_a)_k}\ . \tag{4}$$

Since the energy difference in (2) is $E_A-E_C=E_a-E_c$, we get

$$\Delta E_A^{(2)} = [n_a/n^2]\sum_{j,k}\sum_{c\neq a}\frac{\langle a|\underset{\sim}{\mu}_j^{(1)}\cdot\underset{\sim}{\mathcal{E}}^{o}|c\rangle\langle c|\underset{\sim}{\mu}_k^{(1)}\cdot\underset{\sim}{\mathcal{E}}^{o}|a\rangle}{(E_a-E_c)^2-(h\nu)^2}(E_a-E_c)\delta_{jk} \tag{5}$$

where δ_{jk} results from the averaging over the random relative phase factors: $\langle e^{i(\phi_c-\phi_a)_j}xe^{-(\phi_c-\phi_a)_k}\rangle = \delta_{jk}$. This represents the physical idea that an excitation on one molecule cannot be accompanied by a deexcitation on another molecule. Therefore from (1) and (5) for a given n_a and n

$$\Delta E_A^{(2)} = [n_a/n]\Delta E_a^{(2)} = [n_a/n]\alpha\bar{1}\ . \tag{6}$$

This equation demonstrates that for a group of indistinguishable molecules the AC Stark shift is diluted according to the fraction of the molecules in that state. This fraction n_a/n is dependent upon the degree of excitation of the sample and the volume V_I in which the molecules can be considered to be indistinguishable. At very low pressures, where there is

only one molecule to be found in any such volume, there is never a ground state molecule to accompany an excited molecule so the normal shift (or broadening) is obtained. At higher pressures where there are n molecules in the interaction volume but the excitation rate is low enough that the probability of having an excited molecule in any volume is much less than one, then the shift is very pressure-dependent because the density affects the denominator of the ratio n_a/n but not the numerator. Finally, when the number of excited molecules is substantial in V_I, n_a and n are both affected by pressure proportionally, so there is no pressure dependence, but the shift is diminished from its single molecule value according to the ratio of molecules excited.

All of this can be taken into account by considering the joint Poisson distribution[6] for finding n_a and $n-n_a$ molecules in the volume V_I. One can then obtain the result[5],

$$\Delta E_A^{(2)} = [\eta_a + (1-\eta_a)\frac{1-e^{-(V_I/kT)P}}{(V_I/kT)P}]\alpha I \ , \qquad (7)$$

where η_a is the fraction of molecules that are in the state a.

There remains to define the volume V_I over which the molecules can be considered to be indistinguishable. Clearly two molecules in very different intensity regions of the laser focus can be considered to be distinguishable because they will have different Stark shifts and therefore be represented by different resonant frequencies. On the other hand, if the Stark shifts of two molecules do not differ by more than the laser bandwidth, that is $|I-I'| < \Delta(h\nu)/\alpha$, the experiment cannot chose between them. Therefore the interaction volume is determined by the spatial inhomogeneity of the electromagnetic field and the laser bandwidth. While the calculation of this volume is very complex for a general region inside a focused gaussian beam, it is possible to obtain an estimate for the very center volume where the intensity is maximum and the MPI and Stark effect dominate. This is the volume where the maximum intensity I_o drops off to $I_o-h\Delta\nu/\alpha$. From the well-known formulae for a gaussian beam, this volume can be derived to be

$$V_{I_0} = 2\pi r_0^2 z_0 (h\Delta\nu/\alpha I_0)^{3/2} \ , \qquad (8)$$

where the constants r_o and z_o are determined by the focal length l, and wavelength λ, and the unfocused beam diameter d: $z_o=2\pi r_o^2/\lambda$ and $r_o=2^{1/2}\lambda l/\pi d$.

The dye laser used in our experiments was a Littman double-grating type[7], operating in two or three longitudinal modes. The single-shot width of each of these well separated modes is estimated to be 0.3GHz. Other parameters are l~90mm, d~3.9mm, λ~4.5X10^{-5}cm and the observed[3,8]

value of α is ~60GHz/GW/cm^2, and I_o ~2.5X10^5[W/πr_o^2]. The numerical value of V_{I_e} is thus ~2.3X10^{-15}cm^3 and for T=300K, this gives V_{I_e}/kT~72torr^{-1}, which is the number of molecules contained in the interaction volume. Assuming that η_a<<1, the best fit of (7) to the experimental linewidth vs. pressure data gives V_I~80torr^{-1}, a somewhat fortuitously close agreement with the theory considering that the laser beam deviates considerably from a gaussian profile.

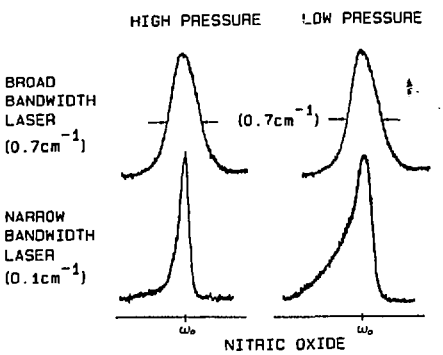

Figure 3

Since the theory predicts a variation of the line broadening with laser bandwidth, an experiment was devised whereby a dye laser was pressure tuned, with and without an intracavity air-spaced etalon, through a Stark broadened resonance. Whereas at a laser resolution of ~0.1cm^{-1}, asymmetric broadening is quite apparent in the lineshape (Fig. 3), at a lower resolution of about 0.7cm^{-1} there is no detectable broadening at the same laser power, in qualitative agreement with the prediction.

In thinking about the pressure-narrowing effect one must keep in mind that the molecules are indistinguishable in the interaction volume, so that it is incorrect to describe the excitation as being on any given molecule as long as no measurement is ever made on the excited state population. In an MPI experiment only the ion population is measured so the energy need not be localized until the ionization event. The $|A\rangle$ state can therefore be regarded as a collective virtual state of the system in which two photons have been absorbed from the field. The only pressure region in which the linewidth changes dramatically with density is when the probability of having an excitation in a given volume is less than 1/n where n is the total number of molecules in the volume. Therefore, at most one molecule in a region is excited and doubling the density does not double the number of excited molecules in any interaction volume, but only doubles the number of interaction volumes which have a single excitation.

If one thinks about the overall polarization vector of a region in which one molecule out of n is excited, and the excited state is much more

polarizable than the ground state, there are two ways to compose the vector, either by summing one excited molecule and n-1 ground state molecules or by summing n equivalent molecules which are slightly more polarizable than the ground state. The former is not allowed as long as no measurement is made on the excited state. We are left with the picture that when two photons are absorbed from the radiation field in an interaction volume, no given molecule is as polarizable as a localized excited state and therefore the Stark effect, which is a measure of this polarizability, is a factor of n less than it would be if the energy were localized. The absorption of two more photons by this virtual state then can localize the energy and ionize one of the molecules.

As the number of excited states represented in the superposition state increases, the polarizability of this state also increases. This is the high intensity limit and the Stark effect will return there even at high pressures. This is seen experimentally in that at intensities approaching saturation, lines begin to broaden before they are absorbed into the background continuum arising from direct four-photon ionization.

It is clear that the scheme described here is a very basic one of very low order of the number of photons involved. One could envision other schemes involving third harmonic generation, another collective effect, which may also cause a diminution of the AC Stark effect through the quenching of the three photon virtual level. However this would be at least a fifth order process and could only augment the fundamental mechanism described above. Most schemes involving collisions can be discarded because of the fact that the narrowing is dependent only upon the partial pressure of nitric oxide without regard to any buffer gas present. We would therefore conclude that since the collective excitation model describes all of the qualitative and quantitative features of the experiments we have been able to perform, and has essential aspects which must be present in any quantum mechanical system, this treatment represents a new manifestation of interference and collective excitation which should be considered in many nonlinear optical pathways.

2. Argon MPI Pressure Dependence

Several years ago a report from this laboratory[9] described the MPI spectra of xenon taken at pressures of a few torr using visible light. These spectra showed a series of broad resonances uncharacteristic of atomic spectra in addition to some narrow resonances. Most of these features were pressure-dependent and close examination revealed that the peaks of the broad resonances occurred at wavelengths corresponding to transitions between excited atomic states. Similar resonances had been seen in the resonant ionization of cesium and termed hybrid resonances[10]. Another anomalous feature in the xenon spectra was the absence of any ionization at wavelengths corresponding to the 6s resonances. This effect

was later studied experimentally[11,12] and theoretically[13,14,15], which led to an understanding of the nonappearance in terms of third-harmonic generation and a cancellation of the polarization of the medium at the first and third harmonic frequencies.

Despite the success in understanding the quenching of the 6s resonances in terms of a coherent effect, many of the effects of the higher pressure spectra remain quantitatively unexplained, including the occurrence of pressure-induced transitions between excited states. The standard explanation of hybrid resonances is that they are transitions that take place during an atomic collision, so that the interatomic interaction changes the excited state energy to bring it into resonance. To our knowledge, no one has examined this hypothesis quantitatively. Later we will make a few comments about the viability of these ideas.

With the current availability of high power lasers tunable in the ultraviolet it has become possible to study the resonance MPI spectrum of argon at various pressures. It is hoped that experiments on this atom with simpler electronic structure will enable development of a theory which can quantitatively explain the broad resonances appearing in the spectra.

The spectra in Fig. 4, which demonstrate the large changes with pressure, were taken in a room-temperature cell with parallel plate electrodes. The bias voltage was kept on a plateau region so that ion-electron recombination is not thought to be a factor in the overall signal. Argon was flowed slowly through the cell in order to maintain a constant pressure and to prevent the influence of outgassing impurities. Approximately 8mj of laser power from a frequency doubled YAG-pumped dye laser was focused into the cell by a 85mm lens.

As is obvious at first glance, the spectrum is anything but constant with respect to pressure. At low pressure the spectrum is dominated by two continua which lie just to the blue of the positions where the 4s and 4s' resonances would be expected to appear. Superimposed on these continua are some fairly sharp peaks at energies corresponding to four photon resonances to 9p states and to the $np'(3/2)_2$ autoionization series. It is interesting that the autoionizing resonances show Fano lineshapes etched out of the background continuum.

As the pressure is increased, the four-photon resonances are replaced by peaks at energies corresponding to transitions from the 4s levels to the same states which previously appeared as four-photon resonances. Simultaneously the continua associated with each 4s level move to higher energy and the more intense resonant peaks always correspond to the more intense part of the continuum. It is not just that the hybrid resonances are becoming stronger but as the pressure increases, the lower energy four-photon resonances actually decrease. Finally, at the highest pressures, the

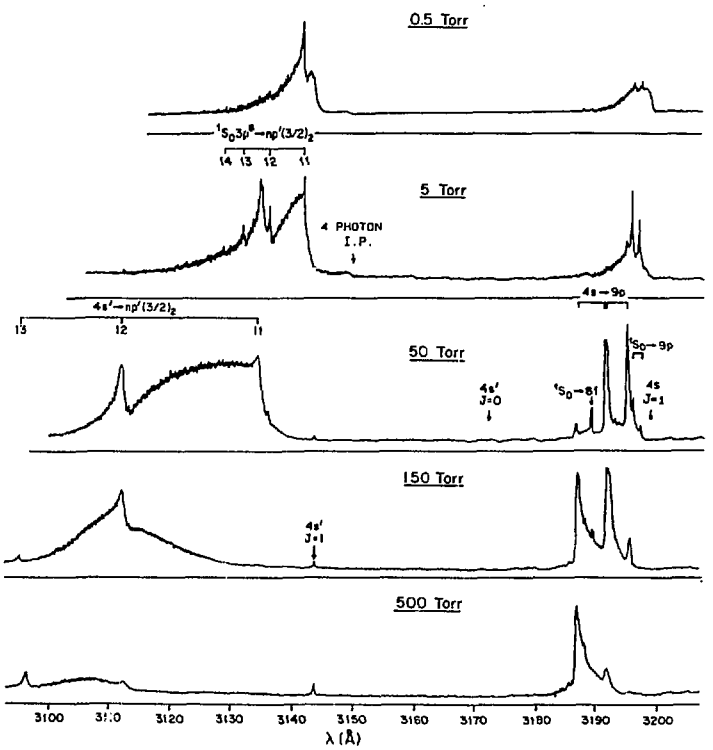

Figure 4: MPI spectra of argon at various partial pressures in the vicinity of the three photon 4s resonances as well as the four photon ionization potential

continua also start to decrease and eventually disappear. Pressurizing with neon instead of argon causes a decrease in the higher energy part of the continua and a quenching of the four photon resonances with respect to the hybrid resonances.

As was expected from the previous work on xenon the 4s resonance is never seen in a single beam experiment. The 4s' resonance starts to be seen at higher pressures however. An experiment with counterpropagating beams shows these resonances strongly at all pressures, in direct agreement with the previous xenon results[12,14,15]. The 4s' resonance intensity is relatively independent of pressure in this type of experiment and was used to calibrate the intensity of the pressure-dependent parts of the spectrum. The results, shown in Fig. 5, demonstrate that the overall intensity of the pressure-dependent features decreases at high pressures while the spectrum shifts to higher energy.

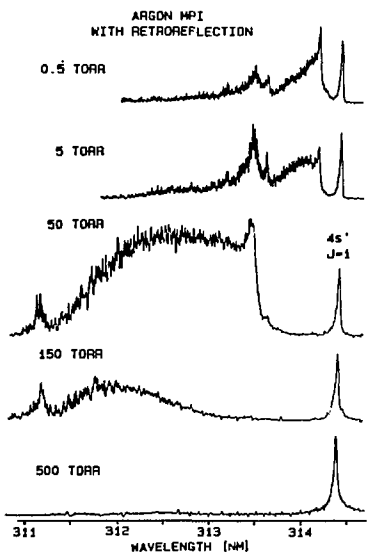

Figure 5: Argon MPI spectra showing the reappearance of the 4s' resonance upon retroreflecting the laser beam through the cell

In light of these results, let us examine the hypothesis of hybrid resonances, that all the features result from transitions of atoms undergoing a collision so that the spectra are representative of diatomic-like molecules. First of all, since the four-photon resonances are obviously pressure-dependent, they would have to be included in any logical description of the process, and whatever perturbation which induced these transitions would have to become unimportant at higher pressures.

It is quite easy to calculate that the most probable nearest neighbor distance at one torr pressure is about 165Å. It is obvious from this number that the majority of atoms are not interacting at any instant of time. However the atoms have a considerable velocity at room temperature so the probability of collision must be integrated over the time of a laser pulse. Using an interaction radius of 5Å, a pulse length of 10ns and a pressure of one Torr, it is found that the probability of collision for each argon atom during the laser pulse is 0.6.

Given the above information, it seems highly likely that most features seen in the spectra are indeed due to collisions. However, that does not appear to explain all of the changes with respect to pressure. One would expect that collisions with low impact parameter are responsible for the features with a large energy shift and vice versa. Then as the pressure is increased there would appear more intensity at a larger shift because low impact parameter collisions become more probable. However, even though the hard collisions become more probable at high pressure, so do soft

collisions, so one would also expect the small shift features to grow in intensity as the pressure is raised. This is not seen to be the case,and the observed shifts of the continua are very large, amounting to several hundred wavenumbers over the pressure range used in these experiments. Shifts in the absorption maxima are also seen in standard pressure broadened spectra, but they are much smaller and appear at much higher pressure.

We have seen that all the features in a single beam MPI spectrum of argon are pressure-dependent, including the four-photon resonances. The strengths of these features do not increase with increasing pressure, however, but each goes through a maximum. A quantitative explanation of this effect is not available, but may have something to do with ternary collisions destroying the phase of the continuum vibrational wavefunctions or possibly to off-resonant third-harmonic generation competing with ionization in a manner similar to that seen on the 4s resonances. If this latter were the case,the mechanism must be consistent with the fact that counter-propagating beams do not have any effect on the pressure-dependence of the pressure-induced features. It is hoped that these experiments on argon, where excited states potentials of some quality are available, will provide an incentive for a quantitative theory of the pressure effects in the MPI spectra of rare gases.

This work was supported by the U.S. National Science Foundation.

References

1. R. H. Dicke: Phys. Rev. 93, 99 (1954).
2. R.E. Demaray, C. Otis, K. Aron, and P.M. Johnson: J. Chem. Phys. 72, 5772 (1980).
3. C.E. Otis and P.M. Johnson: Chem. Phys. Lett. 83, 73 (1981).
4. Leping Li, Bingxin Yang and P.M. Johnson: "AC Stark Effect Lineshapes in Multiphoton Ionization Spectra", (submitted to JOSA B).
5. Leping Li, R.N. Porter and P.M. Johnson: "Pressure Narrowing of AC Stark-Broadened Multiphoton Spectra", (submitted to Phys. Rev. Lett.)
6. W. Feller: An Introduction to Probability Theory and Its Applications , Vol. 1 3rd ed. (Wiley, New York, 1968) pp. 156ff.
7. Michael G. Littman: Optics Letters 3, 138 (1978).
8. P.M. Johnson and C.E. Otis: Ann. Rev. Phys. Chem. 32, 139 (1981).
9. Kenneth Aron and P.M. Johnson: J. Chem. Phys. 67, 5099 (1977).
10. D. Popescu, C.B. Collins, B.W. Johnson, and I. Popescu: Phys. Rev. A 9, 1182 (1974).
11. J.C. Miller and R.N. Compton: Phys. Rev. A 25, 2056 (1982).
12. J.H. Glownia and R.K. Sander: Phys. Rev. Lett. 49 21 (1982).
13. J.C. Miller, R.N. Compton, M.C. Payne, and W.W. Garrett: Phys. Rev. Lett. 45, 114 (1980).
14. D.J. Jackson and J.J. Wynne: Phys. Rev. Lett. 49, 543 (1982).
15. J.J. Wynne: Phys. Rev. Lett. 52, 751 (1984).

Part III

Multiphoton Processes in Molecules and Surfaces

Infrared Multiphoton Absorption and Decomposition*

D.K. Evans and Robert D. McAlpine

Atomic Energy of Canada Limited, Research Company, Chalk River Nuclear Laboratories, Chalk River, Ontario, Canada K0J 1J0

1. Introduction

The discovery of infrared laser induced multiphoton absorption (IRMPA) and decomposition (IRMPD) by Isenor and Richardson in 1971 [1] generated a great deal of interest in these phenomena. This interest was increased with the discovery by Ambartzumian, Letokhov, Ryabov and Chekalin that isotopically selective IRMPD was possible [2]. One of the first speculations about these phenomena was that it might be possible to excite a particular mode of a molecule with the intense infrared laser beam and cause decomposition or chemical reaction by channels which do not predominate thermally, thus providing new synthetic routes for complex chemicals. The potential applications to isotope separation and novel chemistry stimulated efforts to understand the underlying physics and chemistry of these processes. At ICOMP I, in 1977 and at ICOMP II in 1980, several authors reviewed the current understandings of IRMPA and IRMPD as well as the particular aspect of isotope separation [3,4]. There continues to be a great deal of effort into understanding IRMPA and IRMPD and we will briefly review some aspects of these efforts with particular emphasis on progress since ICOMP II.

2. Outline of Theory

The absorption of many photons leading to decomposition has been modelled in terms of excitation through three energy regimes of the molecule being excited.

For the low energy region, E_1, excitation occurs via a coherent, resonant pumping of a ladder of levels of the resonant mode which are only weakly coupled to the background states (that is those due to other modes of the molecule). Anharmonicity in the pumped mode causes the spacings in the ladder to go off resonance with the laser photons as the molecule is excited through E_1. Phenomena such as power broadening [5], degeneracy splitting [6], participation of rotational levels [7], and collisions [8] have been suggested as means of overcoming the anharmonicity "bottle-neck".

Region E_2 is characterized by a density of background states sufficiently large to form a "quasicontinuum". The pumped levels are strongly coupled to the background states and further excitation of the molecule is possible within the quasicontinuum, almost without regard to the photon energy and with anharmonicity no longer causing a bottle-neck. At this point in the excitation, the molecule loses memory of the nature of the mode initially pumped.

Region E_3 occurs for excitation above the onset of a decomposition channel and the decomposition of the molecule is described by the

*Issued as AECL-8574

statistical RRKM theory. The IRMPA and IRMPD cross-sections are mainly functions of four parameters, $\sigma(\lambda,\phi,P,\Delta\tau)$: laser wavelength, λ, fluence, ϕ, pressure, P, and laser pulse duration, $\Delta\tau$. Experiments performed on SF_6 (9) indicated that σ was more controlled by ϕ than on intensity, $\phi/\Delta\tau$. The dependence on λ is, of course, exploited in isotope separation. Recent experimental work has tested this theory and the extent to which it may be applied,as well as generating the basis of an improved understanding of these processes.

3. Experimental Studies of IRMPD

3.1 Interaction of the Parameters

A major concern in designing experiments is the possibility of two parameters of the system, which are being changed simultaneously, both influencing the effect being measured. Such a possibility exists, for example, in studies for which ϕ and $\phi/\Delta\tau$ are simultaneously varied.

Another potentially confusing interaction of parameters can arise from changing $\Delta\tau$ since this also changes the number of collisions during the pulse (proportional to $P\Delta\tau$). An example of this potential problem is observed for the IRMPD of methanol studied in our laboratory [10]. For values of $P\Delta\tau$ < 40 kPa•ns, CH_3OH decomposes by a collisionless IRMPD process with a decomposition probability independent of P. However, for $P\Delta\tau$ > 40 kPa•ns, a collisionally assisted IRMPD process dominates for which the decomposition probability is proportional to pressure. Studies carried out at 1.0 kPa for $\Delta\tau$ = 6 and 60 ns result in collisionless IRMPD for $\Delta\tau$ = 6 ns and a collisionally assisted IRMPD for $\Delta\tau$ = 60 ns. Without a detailed study of the effects of both P and $\Delta\tau$ and their interaction the observed differences might be erroneously attributed to an intensity dependence for IRMPD. No such intensity dependence was in fact observed for measurements of the decomposition probability of methanol.

An example of a molecule showing both an intensity dependence and a pressure dependence in IRMPD is CH_3NH_2 [11,12]. For this molecule, Fig. 1 shows that the effect of increasing intensity seven fold (changing $\Delta\tau$ from 40 to 6 ns) was a thirty fold increase in hydrogen yield for P = 0.267 kPa, but only a five fold increase for P = 0.667 kPa. In this case, pressure or

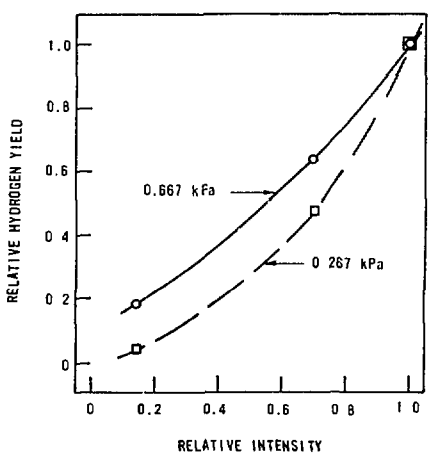

Fig. 1. The effect of both intensity ($\phi/\Delta\tau$) and pressure (P) on the relative yield of hydrogen for IRMPD of CH_3NH2.

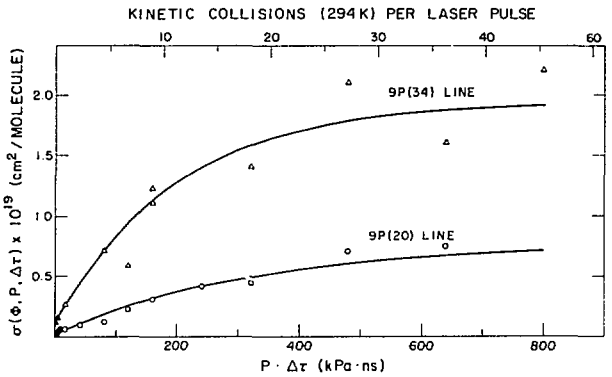

Fig. 2. The dependence of σ for IRMPA of the CO_2 9P(34) (▲ and △) and 9P(20) (● and ○) on PΔτ in the methanol molecule. Solid and open symbols correspond to Δτ=6 and 60 ns respectively.

collisions and intensity have opposing effects on the production of hydrogen and the intensity dependence could be seriously underestimated if no correction was made for the increased number of collisions when the longer pulse was used.

In Fig. 2, a plot of σ versus PΔτ is shown [13] for methanol. Separate measurements over a broad range of ϕ, P and Δτ show that $\sigma(\phi, P, \Delta\tau) = \sigma(\phi, P\Delta\tau)$. This dependence of σ on PΔτ for methanol can be fitted to a simple rotational hole filling model of the form:

$$\frac{\sigma(\phi,P\Delta\tau)-\sigma(\phi,o)}{\sigma(\phi,\infty)-\sigma(\phi,o)} = 1-\exp(P\Delta\tau/\tau_0) \qquad (1)$$

where $\sigma(\phi,o)$, $\sigma(\phi,\infty)$, and τ_0 are the low pressure value, the high pressure limit and the decay constant respectively. The curves shown in Fig. 2 are the fit of this equation to the observed results. The results of similar studies on fluoroform [14] and cyclobutanone [15] can be described by the same model. At any instant, the laser beam is resonant with only that fraction of the molecules in the appropriate rotational states and rotational relaxation occurs during the pulse to bring a greater fraction of the molecules into resonance with the laser beam. The increase in absorption observed is not due to an increase in the cross-section of each molecule but rather is due to an increase in the number of molecules interacting with the same beam. In Fig. 2, the 9P(18) and 9P(20) laser lines are absorbed by an R-branch transition while the 9P(34) line is absorbed into the Q-branch. At any instant a greater fraction of the molecules interact with the 9P(34) line and relaxation is more efficient as can be seen by higher intercept and the steeper initial rise for the Q-branch absorption (larger $\sigma(\phi,o)$ and smaller τ_0). This observation is only valid for excitation of methanol at fluences well below the threshold for IRMPD, and a comparison of decomposition probabilities at high fluence shows no measurable differences for the laser lines used. The IRMPA of fluoroform also follows this simple relaxation model at low fluences (0.08 J/cm^2) but at 50 J/cm^2 a plot of σ versus PΔτ, while still a smooth curve, has a more complicated shape [14]. At this higher fluence, we are at a level of excitation which is above the change in the power law describing the

dependence of σ on ϕ and the effect of collisions on the magnitude of this change can be seen. Cyclobutanone is a more complicated example [15]. For this molecule, the IRMPA results for two pulse lengths and fluences high enough for decompositon fit the same curve of $\langle n \rangle$, the average number of photons absorbed per molecule versus $P\Delta\tau$; however, in IRMPD measurements there is an increase in decomposition probability which is roughly proportional to the laser intensity. This has been interpreted as showing an intensity dependence of the distribution of the absorbed energy, which would not be expected if the randomization model could be used to describe this molecule.

As a final example, the IRMPA of NH_3 mixed with N_2 has been studied in an effort to understand the increased efficiency of the NH_3 laser when N_2 is added [16]. The increase in laser efficiency was found to be due to increased absorption of the pumping CO_2 laser photons. Whether this is due to the energy being stored in the nitrogen or by the N_2 collisionally assisting IRMPA by the NH_3 in a similar manner to the collisionally assisted IRMPA seen in many other molecules, was not determined. If there is collisionally assisted IRMPA, then many levels must be considered in the description of the NH_3 laser and also the potential for new lasing transitions between higher lying levels may exist. Morrison, Reid and Garside have achieved lasing in NH_3 on the $2 \rightarrow 1$ transition, but not with a single pumping laser [17].

3.2 Molecular Structure

The structure or complexity of the molecule may have an important influence on IRMPA and IRMPD. This is demonstrated by a study of HF laser induced IRMPA for a series of alcohols, ROH, where R = CH_3, CD_3, C_2H_5 and CF_3CH_2 [18]. The HF laser is resonant with the highly anharmonic -OH chromophore, and as the complexity of the R group is increased the rate at which the density of background states varies with excitation is increased. The observed IRMPA divides the alcohols into two groups according to the "size" and "complexity" of R. For the first group of "small" molecules, CH_3OH and CD_3OH, the absorption of three or four photons is required to reach E_2 and thus there is significant anharmonic bottle-necking. Under collisionless conditions, σ decreases with increasing ϕ meaning that absorption of the second and subsequent photons is more difficult than absorption of the first photon. As collisions were allowed to occur, σ became independent of ϕ thus demonstrating that collisions can efficiently overcome anharmonicity bottle-necking. For the second group of "large" molecules, C_2H_5OH and CF_3CH_2OH, E_2 is reached by absorption of only one or two photons and σ increases as ϕ is increased. Thus the second and subsequent photons are absorbed more easily than the first, and anharmonicity bottle-necking is not important for these molecules. Collisions have little or no effect on IRMPA for molecules in the second group.

At about the same time as the IRMPA study described above, IRMPA and IRMPD studies of CH_3OH were carried out using both CO_2 and HF lasers [19-21]. In these studies collisional processes occurred and it was impossible to determine whether IRMPD depended on the laser chosen. A recent study done in our laboratory with very short CO_2 laser pulses (10 and 60 ns) when compared to the HF laser experiments showed that, in the absence of collisions (even though four times as many CO_2 laser photons as HF laser photons must be absorbed to reach the same level of excitation), IRMPD of methanol is several orders of magnitude easier for CO_2 than HF laser pumping [10].

The search for tests of the theory has involved looking at molecules with fewer atoms. To date, there have not been any reports of IRMPA or IRMPD of diatomic molecules and only two triatomics have been reported to undergo IRMPD: OCS and O_3 [22]. The anharmonicity for these molecules is very small and very high fluences were used to induce IRMPD. Two studies on formaldehyde, a four atom molecule, have been reported [23,24]. In one case, excitation using a DF laser operating nearly simultaneously on all lines was compared to photolysis using many single lines sequentially. For the former experiment the simultaneous use of many lines overcame the anharmonicity by providing different frequencies which were fortuitously in resonance with different steps in the excitation ladder. Even with this means of overcoming the anharmonic barrier, collisions were found to increase the decomposition probability (while decreasing the selectivity) and the expected reaction pathway was not completely followed. The simple IRMPD reaction (2) was not the only chemistry that occurred.

$$H_2CO \rightarrow H_2 + CO \qquad (2)$$

The ratio of carbon monoxide to hydrogen was not unity, but typically about 20. Presumably many of the formaldehyde molecules, which were insufficiently excited to undergo IRMPD, reacted by some other mechanism. For CO_2 laser excitation, only the hydrogen product was monitored, which was isotopically enriched in deuterium. In the photolysis of D_2CO with a CO_2 laser we found CO/D_2 was again about 20. From these two sets of experiments, it seems possible that the hydrogen product is due to IRMPD, but that a lot of energy and formaldehyde are consumed by another reaction.

Borsella et al [25] measured the IRMPA of CF_3I and CF_3Br using a continuously tunable high pressure CO_2 laser. They observed some structure in the laser spectrum not present in the low intensity spectrum which they concluded might be due to true multiphoton resonances. Their calculation of the absorption by these molecules indicated that IRMPD using several single lines of a CO_2 laser could show a dependence on laser pulse intensity. We have studied these molecules using our variable pulse length laser and found a weak intensity dependence for one laser line for each of them. As well, this study looked at lines in which Quack and Seyfang [26] observed an intensity dependence of IRMPD in CF_3I. The results of these experiments are reported in another paper at this conference.

3.3 Multilaser Experiments

The IRMPD of formaldehyde induced by a DF laser (all lines), discussed above, can be considered as a multilaser experiment [23]. The use of many laser lines to compensate for the anharmonicity bottle-necking allowed more decomposition than was possible with just a single laser line.

Ambartzumian and Letokov used two CO_2 lasers in a study of the quasicontinuum of SF_6 [27]. A weak laser was tuned to be in resonance with the 1←0 transition and the frequency of the other laser varied. The resonant laser alone does not cause IRMPD but just pumps the SF_6 to its quasicontinuum. The non-resonant laser then probes the excitation of a molecule in its quasicontinuum. They found that the quasicontinuum of SF_6 has a broad resonance of 150-200 cm^{-1} full width. The low fluence or intensity required of the resonant laser means that power broadening is reduced from the case of single laser decomposition and thus higher selectivity is possible especially for laser isotope separation of heavy elements which have small isotope shifts in their spectra.

Ambartzumian and coworkers excited OsO_4 with two lasers tuned to different transitions [28]. They were able to study absorption in the quasicontinuum by pumping with a weak beam tuned to be on resonance but with insufficient energy to decompose the OsO_4. The other laser wavelength was then varied, as was the delay between pulses. A larger decomposition probability for the OsO_4 was observed with two lasers, even though the total laser energy was lower than when a single laser was used.

The two-laser excitation of UF_6 was studied by Tiee and Wittig [29] and by Rabinowitz, Kaldor, Gnauck, Wooden and Gethner [30]. In the first case, CF_4 and CO_2 lasers were used and in the other, two Raman shifted CO_2 lasers were used. In each case, IRMPD was augmented by the second frequency; however, one pumped two different modes of the UF_6 and the other pumped different levels of the same mode.

4. Concluding Remarks

Since IRMPA and IRMPD were discovered, experimental work and theoretical development have advanced to give a qualitative understanding of these phenomena and for some special cases to be able to consider application. For isotope separation, the attraction of spending separative effort on only the species carrying the desired isotope continues to be attractive and at least for carbon, selective IRMPD has been demonstrated to be competitive with conventional isotope separation processes [31].

Before we can apply IRMPA and IRMPD we need an understanding sufficient to allow prediction of the conditions necessary for decomposition of a molecule. To do so will require a larger base of results which have measured all aspects of IRMPA and IRMPD under a broad range of experimental parameters. Today, photoacoustic spectroscopy gives us a powerful tool to measure the average excitation of a system; however, we need to know the fraction of the molecules in resonance at a particular pressure and laser pulse fluence or intensity and the distribution of excitation among those molecules that are absorbing. This knowledge is important for testing the various models that have been proposed and to understand the chemistry which often occurs after the pulse is over. Experiments on molecules such as cyclobutanone which have several closely spaced decomposition channels will give us information about the molecular dynamics and energy distribution among molecules above the threshold for decomposition. Knowledge about the competition between intramolecular energy rearrangement and the rate of pumping the molecules is necessary to determine whether mode selective chemistry is possible and if so, under what conditions.

Research using several different wavelengths is a useful means of obtaining more detailed information about absorption as the molecule is being excited and more studies of this type will help to increase our understanding of IRMPA and IRMPD. Certainly, the lower total fluence required for IRMPD will make any application of these processes far more likely.

Our understanding has greatly increased in the last thirteen years, but there is still a lot to be learned about the fundamental physics involved. Increased understanding will come when carefully designed experiments, in which wide ranges of many parameters are studied, are used to test and improve detailed theories.

References

1. N.R. Isenor and M.C. Richardson, Appl. Phys. Lett. 18, 224 (1971).
2. R.V. Ambartzumian, V.S. Letokhov, E.A. Ryabov and N.V. Chekalin, ZhETF Pis. Red. 20, 597 (1974) [JETP Lett. 20, 273 (1974)].
3. Multiphoton Processes, Proceedings of an International Conference at the University of Rochester, Rochester, New York, 1977, June 6-9, eds. J.M. Eberly and P. Lambropoulos, Wiley, New York, 1978.
4. Second International Conference on Multiphoton Processes, Budapest, Hungary, 1980 April 14-18.
5. N. Bloembergen, Opt. Commun. 15, 416 (1975).
6. C.D. Cantrell and H.W. Galbraith, Opt. Commun. 18, 513 (1976).
7. R.V. Ambartzumian, N.P. Furzikov, Yu.A. Gorokhov, V.S. Letokhov, G.N. Makarov and A.A. Puretsky, Opt. Lett. 1, 22 (1977).
8. D.K. Evans, R.D. McAlpine, H.M. Adams, J. Chem. Phys. 77, 3551 (1982).
9. P. Kolodner, C. Winterfeld and E. Yablonovitch, Opt. Commun. 20, 119 (1977).
10. D.K. Evans, R.D. McAlpine, J.W. Goodale and H.M. Adams, to be published.
11. (a) G. Hancock, R.J. Hennesy and T. Villis, J. Photochem. 9, 197 (1978).
    (b) M.N.R. Ashfold, G. Hancock and G. Ketley, Faraday Disc. Chem. Soc. 67, 204 (1979).
12. D.K. Evans, R.D. McAlpine, H.M. Adams and A.L. Creagh, Chem. Phys. 80, 379 (1983).
13. D.K. Evans, R.D. McAlpine and H.M. Adams, Israel J. Chem., in press.
14. R.D. McAlpine, D.K. Evans and H.M. Adams, J. Chem. Phys. 78, 5990 (1983).
15. R.A. Back, D.K. Evans and H.M. Adams, Can. J. Chem., in press.
16. I.M. Waller, D.K. Evans and R.D. McAlpine, Appl. Phys. B 32, 75 (1983).
17. H.D. Morrison, J. Reid and B.K. Garside, to be published.
18. R.D. McAlpine, D.K. Evans and F.K. McClusky, J. Chem. Phys. 73, 1153 (1980).
19. R. Bhatnagar, P.E. Dyer and G.A. Oldershaw, Chem. Phys. Lett. 61, 2061 (1977).
20. S.E. Bialkowsky an W.A. Guillory (a) J. Chem. Phys. 67, 2061 (1977), (b) J. Chem. Phys. 68, 3339 (1978).
21. R.D. McAlpine, D.K. Evans and F.K. McClusky, Chem. Phys. 39, 263 (1979)
22. D. Proch and H. Schroder, Chem. Phys. Lett. 61, 426 (1979).
23. D.K. Evans, R.D. McAlpine and F.K. McClusky, Chem. Phys. Letts. 65, 226 (1979).
24. G. Koren, M. Okon and U.P. Oppenheim, Opt. Commun. 22, 351, (1977).
25. E. Borsella, R. Fantoni, A. Giardini-Guieni, D.R. Adams and C.D. Cantrell, Chem. Phys. Lett. 101, 86 (1983).
26. M. Quack and G. Seyfang, Chem. Phys. Lett. 93, 442 (1982).
27. R.V. Ambartzumian and V.S. Letokhov in "Chemical and Biochemical Applications of Lasers, Vol. III" ed. C.B. Moore, Academic Press, New York (1977).
28. R.V. Ambartzumian, V.S. Letokhov, G.N. Makarov and A.A. Puretsky, Opt. Commun. 25, 69 (1978).
29. J.J. Tiee and C. Wittig, Opt. Commun. 27, 377 (1978).
30. P. Rabinowitz, A. Kaldor, A. Gnauch, R.L. Woodin and J.S. Gethner, Opt. Lett. 7, 212 (1982).
31. (a) A. Outhouse, P. Lawrence, M. Gauthier and P.A. Hackett, Appl. Phys. in Press.
    (b) M. Gauthier, A. Outhouse, Y. Ishikawa, K.O. Kutschke and P.A. Hackett, Appl. Phys., in Press.

A Physical Explanation of Quasiperiodic Motion and the Onset of Chaos in Nonlinear Systems

Howard S. Taylor

Department of Chemistry, University of Southern California
Los Angeles, CA 90089, USA

The reader may have noticed that the subject broadly called classical and quantum nonlinear dynamics has lately gained considerable attention in many fields of physics and chemistry [1-4]. Of particular interest is the dynamics of systems of many oscillators coupled by nonlinear interactions. Such systems are used to model widely spread phenomena, for example, molecular vibrations, intra-molecular energy transfer, unimolecular reaction, and laser-matter interactions. In the latter case, the laser is viewed, using the classical idea of extended phase space, or quantum field theory, as an oscillator. Hence, multiphoton excitations of atomic, molecular and plasma systems are described using oscillators coupled in a nonlinear manner. In a completely different area we find the motion of galaxies is also modeled by nonlinear oscillators [5]. Recently the physics of light traveling in fibers (fiber optics) has been shown to obey similar equations. Atomic and molecular physics is far from left out. The nature of electronic excited states (e.g. doubly excited Rydberg states) and the whole question of the ability to assign quantum numbers to states and to corresponding spectra involves nonlinear ideas. The unusual behavior of electronic states in strong external fields is essentially governed by nonlinear equations.

One could well ask what is it that makes the nonlinear dynamics in coupled oscillator systems so general? At first thought the ability of a few model coupled oscillator systems to illuminate so many special fields seems unprecedented and shocking to the intellect. Actually it has plenty of precedents. Consider that engineers, chemists, classical physicists, quantum physicists, biologists, etc. all include in their studies a narrow range of model systems; for example, the harmonic oscillator (and driven oscillator), the rotor, and the Kepler problem (or hydrogen atom). These are so basic that they are the building blocks for more complicated models in all of these fields. The reason for this is simple. These systems supply basic qualitative physics for n degree or n uncoupled degree of freedom motion in real space and time. A similar role is played by models of nonlinearly coupled oscillators and rotors. They supply the basic qualitative physics for coupled many (two or more) degree of freedom motion. In both one and many (n) degree of freedom systems, concepts of orbits, period, frequency, etc. arise. In coupled n degree of freedom systems new concepts such as regular (quasiperiodic or periodic, localized) and irregular (chaotic, delocalized, random) motion enter. Generally speaking, in different fields, physicists are interested in different features of nonlinear motion. Plasma physicists interested in plasma heating desire that the system of plasma plus the periodic laser heater be driven to chaos so that the heat moves throughout the plasma, doesn't stay localized and certainly does not leave the plasma and go back into the laser field. High laser intensities will assure the desired chaotic motion. Spectroscopists usually desire regular, quasiperiodic and localized motion. This type of motion assures that states have quantum numbers for electronic or vibrational spectral lines. Atomic and molecular

physicists are interested in both regularity and irregularity. For the former, they want general dynamic models that explain the nearly separable motion which underlies regularity. The regular motion supplies nearly separable quantum numbers for naming and sequencing the exact states. Some of the most general methods for doing this will be given in this paper. For the latter, chaos and irregularity is of great importance and the question is how to recognize that it exists when observing spectra and how in the absence of a full set of quantum numbers to extract information from the spectra about the chaotic dynamics. In statistical mechanics [6] the desire is to assure chaos in very large N systems and to avoid regularity, so as to assure that the mixing property, needed to justify the ensemble theories of equilibrium, holds. For non-equilibrium conservative systems, chaos underlies the linear laws of transport [7]. Regular motion in systems studied by statistical mechanics in some sense would be disaster.

Chemists seek mode selective chemistry [8-9], that is, how to pump selected parts of the molecule so as to specify the exact bonds that break on initiate reaction. To do this they must understand not only how to pump the molecule selectively but also which parts of a molecule might hold its energy in place (no energy transfer) long enough for a build up of energy. The question is "Does the energy stay in one or several spots (regular motion) or move chaotically (statistically-RRKM) throughout the whole molecule"? This is of great interest to the chemist in his desire to understand reactions. In atom transfer reactions, especially in beam experiments, the existence of regular motion causes resonances and transition states and greatly modifies cross sections. The chemical bond itself as we shall see below is a perfect example where the ideas of regular motion have triumphed. This will be discussed here in detail. In fact our ideas developed from our realization that the chemical bond, as justified by the BORN-OPPENHEIMER approximation [10] and the self consistent field orbital theory, and the quantum numbers developed there, was a resolution, known for many years, of the question of what causes regular motion. With all the above we hope it is clear why we chose to study the mechanism of regular motion.

In principle, classical regular motion is explained by the KAM theorem [11-13]. The main result of the KAM theorem states that for sufficiently small perturbation most of the trajectories generated by the perturbed Hamiltonian are still conditionally periodic (quasiperiodic, i.e. QP) and local actions can be computed (assigned) for them. The quantum analogue of the classical KAM theorem recently given by HOSE and TAYLOR [14] provides a criterion of a unique transformation between eigenstates of integrable and nonintegrable Hamiltonian. This criterion determines the ability to assign local quantum numbers to the eigenstates of nonintegrable Hamiltonian and explains localization phenomena. The localized wavefunctions, which are also called regular, strongly resemble the regular trajectories when the potential has a good classical-quantum correspondence. Both in quantum mechanics and in classical mechanics, therefore, regular motion is justified by the small perturbation acting on a simple regular system. Our view of the onset of chaos will be that it occurs when one is unable to find such simple regular system. This brief discussion sets the scene for asking the question such as how to find the simple separable system. Our studies suggest that associated with every regular motion, a family of regular motions is a particular coordinate system in which the perturbation is small. In this system the best methods to find the unperturbed Hamiltonian and the dynamic potential which explains the spatial localization of the regular motion are the Born-Oppenheimer and the self consistent field approximations (BOA and SCF). With two examples, one from quantum mechanics, the Stadium, and the other from classical mechanics, the librating motion of the Henon-Heiles potential, we will show how we

obtain the zero order models that could verify the above assumption. In an associated paper, it is shown that these two systems supply the simple regular motion needed to assure the KAM perturbation theorem and its quantum analogue.

It should be mentioned that the details of formal KAM perturbation procedure are not covered in this paper, neither is the problem of finding the coordinate system in which the separations are to be carried out. For the two examples here, the choice of coordinates is simple; for a discussion of the general method of crossing coordinates see ref. 15.

We now proceed to our two examples and finish with a summary justified by our referred papers and admittedly not completely by the two examples given here.

I. CLASSICAL ADIABATIC (BORN-OPPENHEIMER) APPROXIMATION

In this section we illustrate our idea by explaining the physics behind the existence of one well known example of regular motion, the librator of the HENON-HEILES commensurate potential [3-5]. Figure 1 shows this regular quasiperiodic trajectory and in particular we note it is highly localized relative to the equipotential. This localization should be contrasted to a chaotic trajectory, an example of which will be given in the next section where it will be seen to fill the potential.

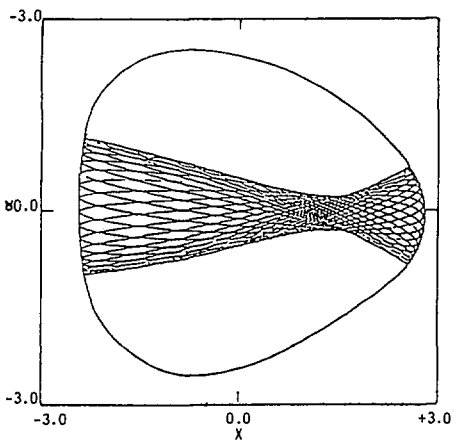

Fig. 1. Librating quasiperiodic trajectory that is confined to the Henon-Heiles potential valley along the x axis

The question is, how can one explain the localization since there are no obvious forces holding the trajectory in place. In this sense the localization is surprising. KAM theory explains this motion by assuring us that two (equal to the degrees of freedom) local actions do exist for the torus over which the trajectory lies in phase space. The question then is, what do these actions physically represent and what are the mysterious forces and potentials. Here we claim they are approximated by the actions and forces given by the classical Born-Oppenheimer Approximation (BOA).

The inspiration for this approach that focuses on localization and delocalization is twofold. First, the chemical bond is explained in the quantum mechanics in terms of an adiabatic decoupling and adiabatic dynamic po-

tentials. These potentials serve to explain localization of the electrons and nuclei in bonds. This localization would have never been anticipated from the static Coulomb potentials of the total Hamiltonian. Second are quantum studies of non-integrable model systems, which have revealed that the states with wavefunctions localized in the same configuration space regions as regular classical motions could be well approximated by the adiabatic energies and wavefunctions. This suggests that the classical limit of the adiabatic potentials that localize the wavefunction also localize the trajectory. These observations have led to the idea to explain localization of classical QP trajectories in terms of dynamic adiabatic potentials.

Here, in general, a Hamiltonian can be written in the form:

$$H = \frac{1}{2}(P_x^2 + P_y^2) + V_1(x) + V_2(x,y) \tag{1}$$

In the case of the Henon-Heiles model the explicit forms of both potentials are

$$V_1(x) = \frac{1}{2} w_x^2 x^2 - \frac{\lambda}{3} x^3 \tag{2}$$

$$V_2(x,y) = \frac{1}{2} w^2(x)\, y^2 = (\frac{1}{2} w_y^2 + \lambda x)\, y^2 \tag{3}$$

In the BOA one variable is adiabatically fixed as a parameter and other motion is obtained. The resulting energy, paramerized by the fixed variable, is then used as an added potential for the latter variable. This procedure depends on the choice of coordinate system and the parametric variable. For the librators, the intuitive idea is that the y motion, being of smaller range than the x should be averagable for fixed x due to the smaller error incurred than for the opposite choice. As such, a Hamiltonian for the y motion Hy(x) can be defined by dropping Px and $V_1(x)$ in (1). The parametric nature of x is emphasized by replacing the comma in the potential $V_2(x,y)$ by a semicolon:

$$Hy(x) = \frac{1}{2} p_y^2 + V_2(y;x) = Ey(x) \tag{4}$$

To determine Ey(x), the action for y motion is assumed to be an adiabatic invariant of the x motion:

$$Iy(x) = \frac{1}{2\pi} \oint Py(x)\, dy = \text{const} = J_1 \tag{5}$$

Iy(x) can be expressed explicitly as

$$J_1 = \frac{1}{\pi} \int_{y_1(x)}^{y_2(x)} \{2[Ey(x) - V_2(y;x)]\}^{1/2} dy \tag{6}$$

where $y_1(x)$ and $y_2(x)$ are turning points for a given x. The assumption (5) gives a unique form of Ey(x) and consistently $y_i(x)$ for any particular value of J_1. The curves $y_i(x)$ are given by the equation

$$Ey(x,J_1) - V_2(y;x) = 0 \tag{7}$$

$$Ey(x,J_1) = J_1 w(x) = J_1 (w_y^2 + 2\lambda x)^{1/2} \tag{8}$$

$$y_2(x,J_1) = -y_1(x,J_1)$$

$$= \sqrt{2J_1}\; w^{-1/2}(x) = \sqrt{2J_1}\; (w_y^2 + 2\lambda x)^{-1/4} \tag{9}$$

In general, numerical methods are necessary for inversion of (17) with respect to $Ey(x)$.

The function $Ey(x)$ together with $V_1(x)$ supplies a potential for the x variable (exactly as in QM):

$$V^{BO}(x,J_1) = V_1(x) + Ey(x,J_1) \tag{10}$$

and the Hamiltonian describing this variable reads

$$H^{BO}(J_1) = \frac{1}{2} p_x^2 + V^{BO}(x,J_1) = E^{BO}(J_1) \tag{11}$$

At this point the dynamic potentials are determined: $V_2(y;x)$ is always the same in CM and QM as nothing is actually done to modify its functional form. $Ey(x,J_1)$ in principle differ in the two mechanics even for quantized values of J_1. In our example, however, this is not the case due to the harmonic nature of $Hy(x)$ for any fixed x.

For a particular value of the adiabatic total energy $E^{BO}(J_1)$ for a given value J the second action can be determined from the formula

$$J_2 = \frac{1}{\pi} \int_{x_1(J_1)}^{x_2(J_1)} \{[E^{BO}(J_1) - V^{BO}(x,J_1)]\}^{1/2} dx \tag{12}$$

Again for given values of J_1 and J_2 both the values of E^{BO} and the turning points $x_1(J_1)$ and $x_2(J_1)$ can be determined from (12). The rectilinear intervals on the xy plane given by the equation

$$x = x_1(J_1,J_2), \; x = x_2(J_1,J_2) \tag{13}$$

and the curves given by

$$y = y_1(x,J_1), \; y = y_2(x,J_1) \tag{14}$$

determine the region in which (within the considered approximation) the trajectory should stay. The potentials $V^{BO}(x)$ and $V_2(y;x)$ as well as the "box" bounded on the sides by (13) and (14) are shown schematically in Figure 2.

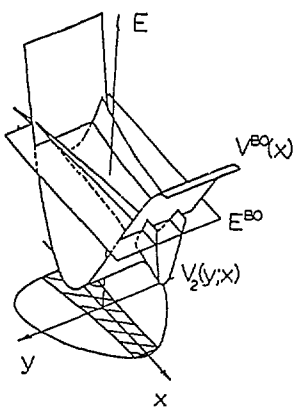

Fig. 2. Adiabatic potentials: $V_2(y;x)$ and $V^{BO}(x)$. The localization region inside the equipotential curve shown as shaded

Approximate values of J_1 and J_2 that are known from other works to give localized (QP) trajectories are used, the adiabatic box explains the localization well and the $V_2(y;x)$ and the $V^{BO}(x,J_1)$ serve to localize the motion as in separable cases. This is true in the case of both equal (Fig. 3a) and unequal frequencies (Fig. 3b), the former being surprising and the latter not from the point of view of "fast" and "slow" motion.

In (15) the range of J_1 and J_2 that admits librator motion is qualitatively determined by minimizing the correction to the BOA with respect to $J_1 + J_2$. The ranges found agree with the known results from computing trajectories. Note that here we have not calculated a single trajectory.

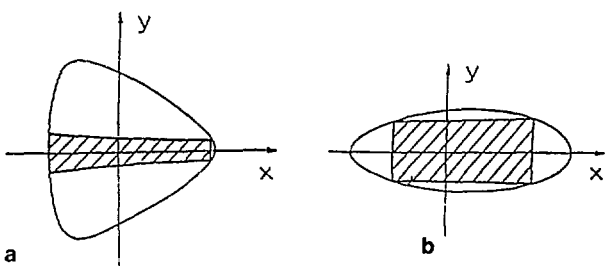

Fig. 3. Adiabatic localization regions in the Henon-Heiles potentials: a) with $w_x = w_y$, b) with $w_x < w_y$ (compare fig. in [2])

II. LOCALIZATION IN QUANTUM STADIUM

We shall use the 'Stadium' as an example to illustrate our ideas in quantum mechanics.

The classical stadium, a billiard with boundaries composed of two semicircles of the radius R connected by two parallel, equal, rectilinear intervals of length 2a (this model is directly related to the modes of a drumhead, the quantum mechanics of a particle in a two dimensional infinite well, or the transverse modes in an electromagnetic cavity or waveguide) has been proven to be [16], as other Bunimovich billiards, a mixing system with exponentially diverging trajectories, i.e. a K system (see Fig. 4); as such, according to BERRY [17] and ZASLAVSKY [18], its quantum counterpart should have: 1) a Wigner anticlustering distribution of spacings between eigenvlaues, and 2) irregular wavefunctions with uniformly distributed but erratically oriented nodal curves, the manifestation of an isotropic distribution of the wavevectors.

Fig. 4. Typical example of a chaotic trajectory in the stadium boundary with specular reflection

Contrary to the previous quantum studies which indicated that the Stadium is a totally chaotic mixing system, several regular states have been found not only in the low [19] but also high energy region [20]. Figs. 5a and 5b illustrate two types of wavefunction nodal patterns in the energy region about 150 levels up from the bottom. 90% of the states show similar behavior to 5b which is random and irregular, 10% of the states are similar to 5a which is regular in the rectangular region of the stadium. The question is, what causes these latter states to be regular? What are these good quantum numbers and what keeps most of the probability density out of the semicircle? The answer will again be given by the BO dynamics.

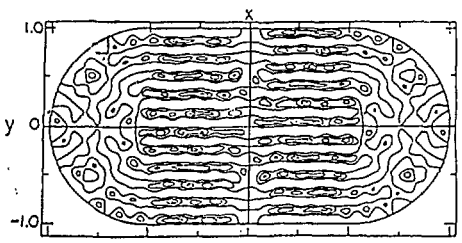

Fig. 5a. The exact regular wavefunction eigenvalue is Ke=52.2547

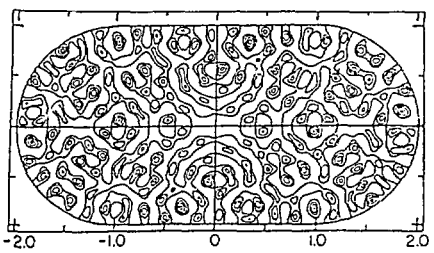

Fig. 5b. An irregular wavefunction with an eigenvalue K=52.3816 is shown for a comparison. Figs. 5a and 5b from (7)

The adiabatic approximation is discussed in detail below: First, we chose the longitudinal x coordinates as "slow"-averagable (or "vibrational") variables, and the transverse y as "fast"-parametric (or "electronic") variables. Several reasons for such a choice can be given. The first is that the smaller amplitude of the y motion is roughly equivalent to a higher frequency of the motion. The other two are of a practical nature. With the proposed breakup no approximation at all is introduced in the separable rectangular region. Secondly, in the semicircular regions where the boundary couples the variable x and y the adiabatic boundary conditions are automatically compatible with the original ones within the Born-Oppenheimer approximation, i.e. without first order diagonal corrections. The adiabatic Hamiltonian for the y variable parametrized by x has the form (all quantitative results are given for $\hbar$=m=1, a=R=0.66325):

$$Hy(x) = \frac{\hbar^2 d^2}{2m_{dy}^2} + V(y;x) \quad \text{where} \tag{16}$$

$$V(y;x) = \begin{cases} \infty & y < y_1(x) \\ 0 & y_1(x) < y < y_2(x) \\ \infty & y > y_2(x) \end{cases} \tag{17}$$

$$y_2(x) = -y_1(x) = \begin{cases} R, & -a < x < a \\ \sqrt{R^2 - (|x| - a)^2}, & a < |x| < a+R \end{cases} \tag{18}$$

The corresponding Schrodinger equation for the electronic motion

$$(Hy(x))\,\varphi_n(y;x) = Ey(x)\,\varphi_n(y;x) \tag{19}$$

has the eigenfunction:

$$\varphi n(y;x) = \frac{1}{\sqrt{y_2(x)}} \sin[\frac{n\pi}{2}\,(\frac{y}{y_2(x)} + 1)] \tag{20}$$

and the eigenvalues:

$$Ey(x) = \frac{(\pi\hbar n)^2}{8my_2^2(x)} \tag{21}$$

The Hamiltonian for the x variable in turn is

$$H = -\frac{\hbar}{2m}\frac{d^2}{dx^2} + Ey(x) \tag{22}$$

and the corresponding Schrodinger equation is:

$$H^{BO}Xnv(x) = E^{BO}Xnv(x) \tag{23}$$

E^{BO} is a total adiabatic energy of the state with quantum numbers n and v. The total wavefunction of the nv state is given by:

$$\Phi nv(x,y) = \varphi n(y;x)Xnv(x) \tag{24}$$

As can be easily noticed from (21), for increasing "electronic" quantum number n, the energy of the bottom (lying over the rectangular region) of the adiabatic potential Ey(x) increases as n. What's more, the steepness of the walls of Ey(x) over the semicircular regions increases even more rapidly, as the narrow boxes have intrinsically larger energy spacings which continue to separate as n (see Fig. 6). As such these walls for large n are so steep that low "vibration" states can hardly penetrate such an adiabatic potential Ey(x) from the infinite well over the rectangular region (Fig. 6). As a result, adiabatic wavefunctions for low "vibrational" states of high "elec-

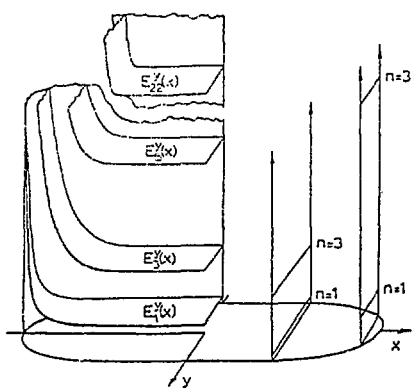

Fig. 6. Adiabatic potentials for n=1,3,5,22 shown in a cross section in the left part of the figure. The scheme for obtaining them can be seen from the right part

tronic" potentials (i.e. if v << n holds) are localized over the rectangular region, and have only very low amplitude over the semicircular regions. From the above analysis, one can predict where exact regular states for the stadium can be expected.

Consider the situation in which all the adiabatic wavefunctions were used as a basis set to diagonalize the Hamiltonian of the original system. Many of the low "vibrational" states of high electronic potentials turn out to be the dominant projections of the exact eigenfunctions. This is so because each of them has very low amplitude in the semicircular region. These regions give the only contribution to the coupling (as the adiabatic breakup leads to a zero coupling in the rectangular region). As such the above states mix very weakly with delocalized adiabatic states and with each other.

Clearly the exact problem should have many regular states, each very close in energy and with eigenfunction overlapping more than 50% with a single adiabatic state characterized by n >> v. As an example, we show the results for n=22, v=2. The adiabatic wavevector $K_{nv} = \sqrt{2E_{nv}}$ for this state is $K_{22,2}$=52.2405. The exact numerically calculated regular state was found to have K=52.2547. The contour plots of corresponding wavefunctions are shown in Fig.7. It is apparent that both are highly localized in the rectangular region. This localization is made even more obvious by the plot of $X_{22,2}(x)$ and $X_{1,2}(x)$ shown in Fig. 8. The wavefunction $\Phi_{22,2}(x,y)$ shown in Fig.7 overlaps the exact regular wavefunction by 80.7%.

It should not be surprising that in both energy regions studied by McDONALD [21] (k=50 and k=100) about 10% of the states found by him exhibited the rectangular localization and regularity. Thus the existence of regular, rectangular localized states for high energies is demonstrated. Their existence

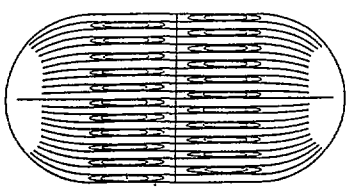

Fig. 7. A contour plot of the adiabatic wavefunction for n=22, v=2 is shown.

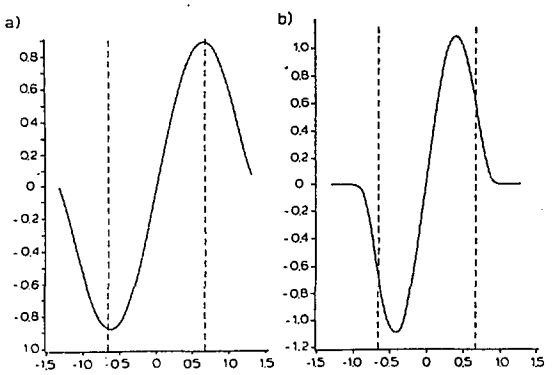

Fig. 8a,b. Wavefunctions X1,2(x) and X22,2(x). The latter is apparently localized over the rectangular region (bounded by the vertical dashed lines)

should continue to high energies. This would be so because the density of adiabatic states should not differ too much from those of a rectangular infinite well and this is approximately constant. Wavefunctions for the lowest v in very high n are even more localized in the rectangular region, i.e. even more weakly coupled to other adiabatic states.

Several low energy states of the Stadium are found, here and in (19), to be regular. They are not localized over the rectangular region but they and the corresponding eigenvalues agree well with the exact eigenvalues and still overlap considerably with the exact eigenfunctions. In this case again the regularity can be explained by weak mixing of adiabatic states. This is, however, due to the relatively large separation in energy of these basis states and not due to localization in the rectangular region. Also, importantly, the regularity in the semicircles is due to the fact that at this low energy the de Broglie wavelength does not allow detailed observation of the relation between x and y imposed by the boundary. To emphasize the difference between the degree of "rectangular" localization for low energy and higher energy states, Table 1 compares energies of the exact and the adiabatic states to those for states of the rectangular well. The comparison is made for adiabatic states: n=1, v=1,3,5; n=3, v=1,3; n=5, v=1,3 and n=22, v=2. Clearly the states (3,1), (5,1) and (22,2) agree well both with the exact and the rectangular ones as would be expected since the adiabatic wavefunctions are almost restricted to the rectangle. The other adiabatic states agree well with the exact only for the reasons just discussed and not because of localization.

Table 1. Eigenvalues for several adiabatic states compared with corresponding eigenvalues for the rectangular well and exact states of the stadium.

Adiabatic quantum numbers n,v	Adiabatic k_a	Rectangular k_r	Eigenvalues+ Exact k_e
1,1	2.6690	3.3405**	2.6925
1,3	4.3759	7.4696**	4.4669
1,5	6.4988	12.0444**	6.6153
3,1	7.2313	7.4696	7.2616
3,3	8.2538	10.0215*	8.3146
5,1	11.9136	12.0444	11.9802
5,3	12.6804	13.7744*	12.7821
22,2	52.2405	52.3182	52.2547

* poor approximation by a rectangular eigenvalue.
** approximation by a rectangular eigenvalue meaningless due to the lack of localization of adiabatic wavefunction.

+) $E = \frac{k^2}{2}$ ($\hbar = m = 1$)

It has now been clearly demonstrated how to explain regularity in the quantum stadium and how to assign quantum numbers, and which effective forces are keeping the regular states localized.

Let us summarize our concepts. In short our basic point of view is that in both CM and QM, if coordinates can be found in which methods like self consistent field and/or the BOA can be used to give a good zero order description, localized motion is explained (not always predicted). The explanation simply says that the good actions and quantum numbers are approximated by those of

the chosen model, BOA or SCF. Consequently the potentials of the separated BOA or SCF equations are the confining potentials that cause localized motion. In general, without knowing the exact trajectories or wavefunctions, the process of minimizing the perturbations to the separable model as a function of the actions or quantum numbers will give the qualitative ranges where these quantities describe the motion. The confining separable potentials make the reason for the local motions easily visualizable. In our view, it is the localization and delocalization of the trajectory or wavefunction that characterize regular and irregular motion respectively. Quasiperiodicity and chaos are companions of classical localized and delocalized motion respectively. They do not exist in QM as the de Broglie wavelength forbids them from being seen. Delocalization and its companion, classical chaos, occur when the separable methods referred to above fail or cannot be found. Different types of quasiperiodic motion appear in the same systems. For each of these it is seen that a different separation is needed.

The separable models fit well into the KAM and Hose-Taylor framework as follows. In CM a knowledge of the separable actions allows the definition of a F_2 generator which transforms the Hamiltonian into a canonical one. In this new Hamiltonian there is an easily identifiable, integrable, zero order part $H_0(J)$ and a perturbation $V(J,\theta)$. In QM representation of H spectrally in the separable basis corresponds to the F_2 transformation. The H_0 is simply the diagonal term. In a true sense the transformation is a renormalization.

Since a separable model has been picked that describes the motion, it is anticipated on physical ground that it supplies the integrable $H_0(j)$ or H_s and the "small" perturbation V called for as the starting point of a convergent forms of the KAM and the H-T perturbation methods, which in turn give rigour to the procedure.

The theory fails to do two important things. First, it ignores the dynamic details of chaos in CM systems. It really only treats regularity and says chaos is what one gets without regularity. Secondly, the theory needs in principle to "know the answer" before it can be sure that it has found all coordinates in which the system is locally separable. The procedures for finding, in general cases, the coordinates require a knowledge of the trajectories or wavefunctions. In this sense the theory "explains" but does not predict the motion. This is not a big fault and is a feature of many theories which start by separating the system into two parts, i.e. the part having a simple model of the phenomena to be explained and the correction. Chirikov's theory needs this to guess the $H_0(J)$ that in turn defines what is called resonant and non-resonant tori. In Feshbach's general theory of resonances the physical impact comes in choosing Q and P projections that assure that widths and shifts are small. Our theory and these theories, short of being pushed to the limit where they become just another way to solve the exact problem, rely on physical impact to define these models, which then give explanations of what the exact computations and presumably nature is showing us.

We note a historical observation that stresses the idea that we are seeing here. It is the qualitatives of coupled motion. As we have sketched here, the separality needed to assign quantum numbers and to explain localization is not always that gotten by trying to separate the Hamiltonian into an H_0+V such that H is a sum of one degree of freedom problems that were the above-referred to traditional models of one degree of freedom mechanics (rotor, harmonic oscillator, Kepler problem). For example, products of normal mode wavefunctions of one electron SCF orbitals often do describe the qualitatives of the regular motion. But often they don't. We need to incorporate models that use coordinates and methods (BOA, SCF) not envisioned in one degree of freedom

studies. The new coordinates used to separate the problem appear only upon observing coupled motion. Our training, which limits us to model in one degree of freedom, has caused much of the surprise generated when new foci of regular trajectories and wavefunctions have appeared in the journals of recent years. The examples of this short article, because of space restrictions, do not allow this point to be made clearly and the reader is referred to (15) and other papers of the group in the references.

III. AN APPLICATION TO LASER SPECTROSCOPY

The ideas about the nature of highly executed states, in particular the abilty to have families of localized states interspersed among themselves, and large numbers of delocalized states, have implications for the modeling of lasers with atomic and molecular systems. Clearly a smooth structureless quasicontinuum cannot be assumed. It has been shown [9] using quantum Floquet methods, that for the Henon-Heiles model discussed here that the precessor family of localized high angular momentum states (which to within a deviation of less than 2%, are equal in energy) can act as a localized ladder upon which multiphoton dissociation can occur. If the frequency of the laser is near the precessor spacing and the intensity not too high, the system stays on the ladder well into the dissociation region. If the intensity is increased, this effect disappears, as essentially the laser becomes part of the system and remixes the local and nonlocal states resulting in total delocalization. Under these conditions or under nonresonant frequency conditions the multiphoton climb is via the "smooth" quasicontinuum. Of course the ladder climb (even if it doesn't go all the way to dissociation) enhances efficiency as the localized states have higher oscillator strengths.

Generalizations of these ideas to real polyatomic molecules and how they are modified and how they help explain known experiments are given elsewhere [22].

ACKNOWLEDGEMENT:

This work was supported by the National Science Foundation through Grant No. CHE-8207152.

1. D.W. Noid, M.L. Koszykowski & R.A. Marcus, Ann. Rev. Phys. Chem. 32, 267 (198
2. G. Hose, H. Taylor & Y.Y. Bai, J. Chem. Phys. 80, 4363 (1984)
3. S. Rice, Adv. Chem. Phys. 47, 117 (1981)
4. G. Hose & H. Taylor, J. Chem. Phys. 76, 5356 (1982)
5. M. Henon & C. Heiles, Astron. J., 69, 73 (1973)
6. J. Lebowitz &). Penrose, Phys. Today, Feb. 23 (1973)
7. G. Casati, J. Ford & F. Vivaldi, Phys. Rev. Lett. 52, 1861 (1973)
8. Y.Y. Bai, G. Hose, W. McCurdy & H. Taylor, Chem. Phys. Lett. 99, 342 (1983)
9. R. Wyatt, G. Hose & H. Taylor, Phys. Rev. A 28, 815 (1983)
10. M. Shapiro & M. Child, J. Chem. Phys. 76, 6176 (1982)
11. A.N. Kolmogorov, Dokl. Akad. Nauk. USSR 98, 527 (1954)
12. V.I. Arnold, Usp. Mat. Nauk. 18, 13 (1963)
13. J. Moser, Nach. Akad. Wiss. Gottingen 1, 1 (1962)
14. G. Hose & H. Taylor, Phys. Rev. Lett. 51, 947 (1983)
15. K. Stefanski & H. Taylor, Phys. Rev. A (submitted)
16. S.W. McDonald & A.N. Kaufman, Phys. Rev. Lett. 42, 1189 (1979)
17. M.V. Berry, J. Phys. A 10, 2083 (1977)
18. G.M. Zaslavsky, Zh. Eksp. Theor. Fiz. 73, 2089 (1977)
19. M. Shapiro, R.D. Taylor & P. Brumer, Chem. Phys. Lett. 106, 325 (1984)
20. R.D. Taylor & P. Brumer, Faraday Dis. 75, 117 (1983)
21. S.W. McDonald, Ph.D. thesis (1983)
22. G. Hose & H. Taylor, Chem. Phys. 84, 375 (1984)

Theoretical Studies of Resonantly Enhanced Multiphoton Ionization Processes in Molecules

S.N. Dixit, D.L. Lynch, and V. McKoy

Arthur Amos Noyes Laboratory of Chemical Physics*,
California Institute of Technology, Pasadena, CA 91125, USA

I. Introduction

Multiphoton absorption and ionization processes add a new dimension to the study of excited state dynamics in atomic and molecular systems. The extreme energy- and state-selectivity achieved through the use of lasers enables one to access specific excited states which would otherwise be inaccessible in single photon spectroscopy due to the lack of appropriate light sources or due to dipole selection rules. Photoionization out of these excited states combined with photoelectron energy analysis yields detailed information about the excited state and the ionization continuum. Recent experiments [1-14] on multiphoton ionization of diatomic molecules H_2, N_2, NO and CO have revealed several interesting features, such as the state selectivity in the residual ion, non-Franck-Condon behavior, Rydberg-valence mixing, rotational and vibrational state dependence of photoelectron angular distributions, and vibrational and rotational autoionization. Multiphoton ionization has also been used to study van der Waal's complexes of rare gas atoms [15].

In spite of the increasing availability of such data, little quantitative theoretical work exists on the understanding of the features observed in these experiments. The theoretical analysis of multiphoton ionization of these systems is nontrivial with complexities arising from the molecular aspects and from the multiphoton nature of the process. Even for the simplest of the diatomics, H_2, very few calculations [16,17] exist in the literature. Recently, we have developed a general formalism [18] for analysis of resonantly enhanced multiphoton ionization (REMPI) processes in diatomics. In a (n+m)-type REMPI process, n-photons are absorbed by a molecule causing a transition from its initial state to some resonant excited state. The molecule in this state is subsequently ionized by absorption of additional m photons. Our approach consists of viewing a (n+m)-type REMPI out of an isotropic initial state as a m-photon ionization from an oriented, resonant, intermediate state. The orientation in this state, created because of the absorption of the first n-photons, carries within it the signature of the latter. Subsequent m-photon ionization simply probes this orientation. If m is greater than one, accidental resonances could occur in the m-photon ionization of the resonant state which would further influence the resulting ion/electron signal. A (n+1) REMPI process is, therefore, attractive both theoretically and experimentally as the probing of the resonant state is 'clean'.

As a first application of the formalism, we have analysed the vibrational branching ratios resulting from a (3+1) REMPI of H_2 via the $C^1\Pi_u$ state. The

*Contribution No. 7106

motivation for choosing this particular scheme of ionization was the recent experiment by PRATT et al. [12] who analyzed the photoelectron energy spectrum resulting from a three-photon resonant four-photon ionization of H_2 via the $C^1\Pi_u$ state. This resonant state, Rydberg in character, overlaps in energy with the valence $B^1\Sigma_u^+$ state. The Π^+ component of this $C^1\Pi_u$ state interacts with the $B^1\Sigma_u^+$ state via Rydberg-valence mixing while the Π^- component is unaffected. PRATT et al. [12] were able to select only the Π^- component of the $C^1\Pi_u$ state as the resonant intermediate state by tuning the laser frequency in resonance with the three-photon Q(1) transition line. This illustrates the tremendous selectivity achievable in REMPI processes. The kinetic energy of the photoelectrons ejected from this resonant intermediate was analyzed. This data provides the branching ratios for ionization out of a specific vibrational state v' of the $C^1\Pi_u$ state into different vibrational states v^+ of the $X^2\Sigma_g^+$ state of H_2^+. These vibrational branching ratios deviated significantly from the appropriate Franck-Condon factors. Possible reasons for this behavior are the energy and the internuclear distance dependence of the electronic transition moment, autoionization and perturbations with overlapping, allowed transitions. Autoionization and perturbations are less probable due to other considerations [12].

To assess the influence of the energy and internuclear distance dependence of the electronic transition moment on the vibrational branching ratios, we have studied this same (3+1) REMPI process in H_2 [12], i.e.,

$$H_2(X^1\Sigma_g^+,\ v'',\ J_0=1) \xrightarrow{3h\nu} H_2^*(C^1\Pi_u,\ v',J_i=1) \xrightarrow{h\nu} H_2^+(X^2\Sigma_g^+,\ v^+) + e^-. \qquad (1)$$

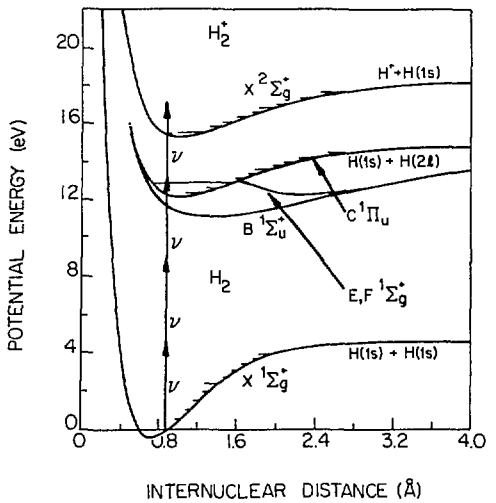

Fig. 1. Energy level diagram of H_2 relevant to the (3+1) REMPI process via the $C^1\Pi_u$ state

This process is illustrated in Fig. 1. Comparison of the preliminary results [19] for the vibrational branching ratios with the experimental data confirms certain important trends although some differences remain. In this report, we present additional results on the photoelectron angular distributions which show surprising non-Franck-Condon variations with the ionic vibrational state.

II. Theory

An analysis of REMPI cross sections and the related angular distributions requires molecular parameters such as transition moments and transition frequencies and their incorporation into the dynamics equations. As the general framework for the analysis of the dynamics has been presented elsewhere [18], we shall restrict ourselves in the present paper to the specific case of the three-photon resonant-four photon ionization of H_2 via the $C^1\Pi_u$ state. This is the same process as studied by PRATT et al. [12]. Calculation of the vibrational branching ratios and photoelectron angular distributions for this process shown in (1) can be divided into two parts: (a) the calculation of the alignment created in the $C^1\Pi_u$, J_i=1 state due to three-photon absorption from the $X^1\Sigma_g^+$, J_0=1 state. Mathematically, this is represented by the density matrix elements $\rho_{ii'}$, defined as

$$\rho_{ii'} \equiv < J_i M_i | \rho | J_i M_{i'} > ; \tag{2}$$

and (b) the coupling of this population in the C state to the ionization out of it. Denoting by $\Gamma_{i',i}$ the generalized photoionization rates, this leads to the following expression for the photoelectron angular distribution

$$\frac{dP(\theta)}{dt} = \sum_{i,i'} \Gamma_{i'i} \rho_{ii'} \cdot \tag{3}$$

We now discuss the calculation of $\rho_{ii'}$. The various channels contributing to the REMPI process through the three-photon Q(1) line excitation to the $C^1\Pi_u$ state for linearly polarized light are shown in Fig. 2. This diagram can be generated by successive application of the single-photon dipole selection rules [20]

$$\Delta J = 0, \pm 1, \quad \Delta K = 0, \pm 1, \quad \oplus \leftrightarrow \ominus \tag{4a}$$

and, additionally, for homonuclear molecules,

$$g \leftrightarrow u, \quad s \leftrightarrow s, \quad a \leftrightarrow a. \tag{4b}$$

In the above equation, J denotes the total angular momentum of a given state, K its projection along the internuclear axis, and $\oplus$,$\ominus$ specifies the parity of the total wave function. Note that $\oplus$,$\ominus$ depend explicitly on the rotational state and should not be confused with the $\pm$ superscript used in electronic state labelling which refer only to the electronic wave function. The selection rules given in (4a) therefore apply to the 'circle-plus' and 'circle-minus'. For homonuclear diatomic molecules, additional selection rules (4b) pertaining to the symmetry of the electronic wave function under inversion through the origin (g and u) and to the symmetry of the total wave function under the exchange of nuclei (s and a) also arise. It is clear from this figure why only the π^- component is selected during the excitation via the Q(1) branch. For linearly polarized light assumed here and used in the experiment of PRATT et al. [12], the M quantum number remains unchanged and equal to that in the initial J_0=1 state. Furthermore, in the absence of M-mixing interactions, ionization through each $|J_i M_i >$ forms an independent channel. This implies $\rho_{ii'}$ is diagonal in M_i and (3) then reduces to

$$\frac{dP(\theta)}{dt} = \Gamma_{11} \rho_{11} + \Gamma_{00} \rho_{00} + \Gamma_{-1-1} \rho_{-1-1} \cdot \tag{5}$$

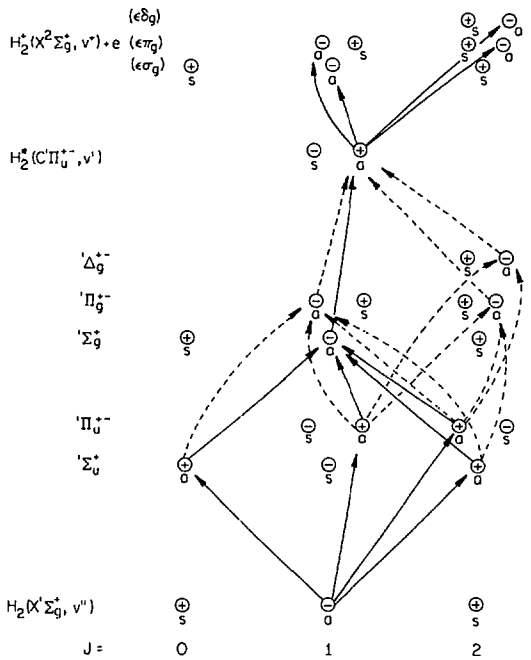

Fig. 2. Channel diagram for the (3+1) REMPI process of (1). Due to off resonant conditions states at one-and two-photon level are virtual and, therefore, only their symmetries are indicated. Note that ignoring the Π_g and Δ_g states removes channels containing dotted lines

Under the weak field excitation conditions of Ref. 12, ρ_{ii} is given by

$$\rho_{ii}^{\alpha} \sum_{M_0} \left| \sum_{\substack{|J_1M_1> \\ |J_2M_2>}} \frac{< J_iM_i|\vec{\mu}\cdot\vec{\varepsilon}|J_2M_2>< J_2M_2|\vec{\mu}\cdot\vec{\varepsilon}|J_1M_1>< J_1M_1|\vec{\mu}\cdot\vec{\varepsilon}|J_0M_0>}{(E_{J_1}-E_{J_0}-h\nu)\,(E_{J_2}-E_{J_0}-2h\nu)} \right|^2 . \tag{6}$$

In the above equation $|JM>$ denotes the complete rotational-vibrational-electronic wave function for a given molecular state. Within the Born-Oppenheimer approximation this can be written as

$$|\psi_{\gamma JMK}> = \sqrt{\frac{(2J+1)}{8\pi^2}}\, \psi_{\gamma}^{(e)}\,(\{\vec{r}_i,;R)\; \chi_v(R)\; D_{MK}^{(J)} \tag{7}$$

where $\psi_{\gamma}^{(e)}$, χ_v and $D_{MK}^{(J)}$ denote, respectively, the electronic, vibrational and rotational wave functions. For rotational wave functions, J denotes the total angular momentum, K and M its projections along the internuclear axis and along a space-fixed z-axis, respectively. With these wave functions a

dipole matrix element of the type appearing in (6) is given by (see Ref. 18 for details)

$$< J_i M_i | \vec{\mu}\cdot\vec{\varepsilon} | J_2 M_2 > \equiv e < \psi_{\gamma_i J_i M_i K_i} | \sum_s \vec{r}_s \cdot \vec{\varepsilon} | \psi_{\gamma_2 J_2 M_2 K_2} >$$

$$= e \left(\frac{4}{3}\pi\right)^{\frac{1}{2}} \sqrt{(2J_i+1)(2J_2+1)} \begin{pmatrix} J_i & 1 & J_2 \\ -M_i & \mu_0 & M_2 \end{pmatrix}$$

$$\sum_\mu \begin{pmatrix} J_i & 1 & J_2 \\ -K_i & \mu & K_2 \end{pmatrix} (-1)^{\mu - K_i + \mu_0 - M_i} \overline{r_{i2}^{(\mu)}} \qquad (8)$$

where μ_0 is the index for light polarization (0 for linear polarization) and

$$\overline{r_{i2}^{(\mu)}} = \int dR\ \chi^*_{v'}(R)\ r_{i2}^{(\mu)}(R)\ \chi_{v_2}(R) \qquad (9)$$

with $r_{i2}^{(\mu)}(R)$ denoting the electronic transition moment for a fixed inter-internuclear separation

$$r_{i2}^{(\mu)}(R) = < \psi^{(e)}_{\gamma_i}(\{\vec{r}_i'\};R) | \sum_s r_s\ Y_{1\mu}(\hat{r}_s')\ | \psi^{(e)}_{\gamma_2}(\{\vec{r}_i'\};R) > . \qquad (10)$$

It is clear from Fig. 2 that starting from the $X^1\Sigma_g^+$ initial state, the dipole allowed intermediate states at the one-photon level are of Σ_u^+ and Π_u symmetry while those at the two-photon level are of Σ_g^+, Π_g, and Δ_g symmetry. For an overall three-photon Q(1) transition, $J_0 = J_i = 1$ which restricts J_2 to be 1 or 2. Of these allowed states, the $J_2 = 2$ state contributes only if the electronic state is of Π_g or Δ_g type. In H_2, the lowest states of Π_g and Δ_g symmetry are, respectively, the $I^1\Pi_g$ and $J^1\Delta_g$ which lie at about 14-15 eV above the ground state [21]. The $E, F\ ^1\Sigma_g^+$ state, on the other hand, is about 12 eV from the ground state. For photon energies $h\nu \sim 4$ eV the detuning $(E_{J_2} - E_{J_0} - 2h\nu)$ for these Π_g and Δ_g states is about 6 eV while that from the $E, F\ ^1\Sigma_g^+$ state is about 4 eV. Hence, in the results presented here, we neglect the contribution to $\rho_{i'i}$ from states $|J_2 M_2>$ other than those of Σ_g^+ symmetry. Such contributions will be included in later studies. This removes the channels containing dotted lines in Fig. 2. Furthermore, neglecting this contribution eliminates the need to calculate any $\rho_{ii'}$, if one is interested only in the relative branching ratios. This comes about since the three-j symbol in (8) containing M_i, μ_0 and M_2 vanishes for $J_i = J_2 = 1$ and $M_i = \mu_0 = M_2 = 0$ which in turn implies $\rho_{00} = 0$. Furthermore, $\rho_{11} = \rho_{-1-1}$, and $\Gamma_{11} = \Gamma_{-1-1}$ which, combined with (5), imply

$$\frac{dP(\theta)}{dt} \propto \Gamma_{11}(\theta) . \qquad (11)$$

In the absence of saturation, as assumed here, the solution of the above equation is,

$$P(\theta) = (\text{constant})\cdot\Gamma_{11}(\theta) . \qquad (12)$$

Since we are only interested in relative contributions, we shall set the constant in the above equation to unity and use, hereafter,

$$P(\theta) = \Gamma_{11}(\theta) \ . \tag{13}$$

In the same spirit, we also ignore factors like the laser intensity in the expression for $\Gamma_{11}(\theta)$ (see Eq.(29) of Ref. 18).

Hence, to investigate relative branching ratios and photoelectron angular distributions all we need to calculate is $\Gamma_{11}(\theta)$. $\Gamma_{11}(\theta)$ can be expanded in spherical harmonics [18] as

$$\Gamma_{11}(\theta) = \sum_{\substack{L=0 \\ \text{even } L}}^{L_{max}^{(\Gamma)}} \gamma_{L0;11} \, Y_{L0}(\theta,\phi) \tag{14}$$

where $L_{max}^{(\Gamma)} = 2J_i+2 = 4$. Therefore, the four-photon REMPI angular distribution $P(\theta)$ can be expanded in terms of Legendre polynomials as

$$P(\theta) = \sum_{L=0,2,4} \beta_L \, P_L \, (\cos \theta) \tag{15}$$

where β_L is related to $\gamma_{L0;11}$ through

$$\beta_L = \gamma_{L0;11} \sqrt{\frac{(2L+1)}{4\pi}} \ . \tag{16}$$

The detailed expressions for $\Gamma_{11}(\theta)$ given in Ref. 18 show that $\gamma_{L0;11}$ (and hence β_L) depend on bound-free electronic transition matrix elements of the type

$$\bar{r}_{fi}^{(\mu)} = \int \chi_{v^+}^{*}(R) \, \chi_{v'}(R) \, r_{fi}^{(\mu)}(k;R) \, dR \quad \text{where} \tag{17}$$

$$r_{fi}^{(\mu)}(k,R) = \langle \psi_{\gamma_f}^{(e)}(\{\vec{r}_i'\};R) | \sum_S r_S \, Y_{1\mu}(r_S') | \psi_{\gamma_i}^{(e)}(\{\vec{r}_i'\};R) \rangle \tag{18}$$

denotes the transition moment for the i→f transition at a given internuclear separation R and electron momentum k. In our studies of the non-Franck-Condon effects on vibrational branching ratios, we adopt the following notation:

(a) Franck-Condon (FC): $r_{fi}^{(\mu)}(k,R)$ inside the integral in (17) is replaced by its value at some $k^2 = k_0^2$ and $R = R_e$. $r_{fi}^{(\mu)}$ then simplifies to a product of $r_{fi}^{(\mu)}(k_0;R_e)$ and the Franck-Condon overlap between the v^+ vibrational state of the ion and the v' vibrational state of the $C^1\Pi_u$ state.

(b)non-Franck-Condon (non-FC): $\bar{r}_{fi}^{(\mu)}(k;R)$ in (17) is replaced by $r_{fi}^{(\mu)}(k_0;R)$ and is retained inside the R integral. These calculations assess the effect of the R dependence of the transition matrix element on the branching ratios.

(c) Full: Here both the k and R dependences of $r_{fi}^{(\mu)}(k;R)$ are retained. For a fixed photon energy $h\nu$, selecting v' and v^+ fixes k^2 by the energy conservation equation (in atomic units)

$$E_{v'} + h\nu = E_{v^+} + \frac{k^2}{2} . \tag{19}$$

These results include both the energy dependence as well as the R dependence of the cross sections and should, therefore, be most complete.

Further analysis requires actual values of the bound free transition matrix elements r_{fi}^{μ}. In our calculations the $C^1\Pi_u$ wave function was obtained using the improved virtual orbital (IVO) technique [22]. The energies of the $C^1\Pi_u$ state obtained this way are within 5% of the correct values [21]. The continuum wave functions for the photoelectron in σ_g, π_g and δ_g channels were obtained by solving the Hartree-Fock equations using the iterative Schwinger variational technique [23]. $r_{fi}^{(\mu)}(k;R)$ was then calculated at R=1, 1.4,2,3 and 5 a.u. and for a range of k (0.05-0.45 a.u.). Interpolation was performed in R and in k to obtain the required $r_{fi}^{(\mu)}(k;R)$. For part (a) R_e = 1.4 a.u. The value of k_0^2 for parts (a) and (b) was determined from (19) with $v' = v^+$ and ν taken from Ref. 12 for excitation to the Q(1) branch of $C^1\Pi_u(v')$ state. For part (c), the correct value of k is determined from (19) for each v^+. Finally, the vibrational wave functions $\chi_{v'}$ and χ_{v^+} were calculated using the finite element method of MALIK et al. [24] with the potential curves of SHARP [21].

III. Results

In Fig. 3 we compare the branching ratios calculated at the various levels of approximation (a), (b) and (c) with the experimental results of PRATT et al. [12]. As in the experimental data, we plot P(θ=0). The results are normalized such that the $v' = v^+$ peak in all three approximations and in the experiment is of unit height. (Note the break in the graph for $v' = v^+$ peak). As expected, the $v' = v^+$ peak is dominant. This is due to the Rydberg character of the $C^1\Pi_u$ state which makes the potential surface for the $C^1\Pi_u$ state nearly identical to (but shifted in energy from) that of the $X^2\Sigma_g^+$ state of H_2^+. The theoretical branching ratios decrease rapidly for $v^+ \neq v'$. The results of approximations (a), (b), and (c) reveal an interesting feature: the branching ratios decrease for $v^+ < v'$ as the R and k dependences of $r_{fi}^{(\mu)}$ are included and increase for $v^+ > v'$ with these dependences included. The difference between 'non-Franck-Condon' and 'full' results is simply a reflection of the increasing of the cross section for decreasing energy which skews the branching ratios towards higher v^+ values. Note that, since v^+ is increasing to the left, k increases to the right as indicated by (19). The difference between Franck-Condon and non-Franck-Condon results arises from the particular R dependence of the photoionization cross section for the $C^1\Pi_u$ state. This difference is probably specific for the photoionization process under study and may be different for other states and molecules.

We now compare the results of our studies with the data of PRATT et al. [12]. For $v' = 0$ and $v' = 1$ excitations, the agreement between theory and experiment seems quite good. For $v' = 2$ to 4 the experimental branching ratios for $v^+ \neq v'$ are much larger than the theoretical predictions. In particular, for $v' = 4$, the $v^+ = 3$, 5, and 6 experimental peaks are all of about equal height, while theory predicts the $v^+ = 3$ and 6 peaks to have 0.11 and 0.2 times the height of $v^+ = 5$ peak (which is $\sim$ 18% of $v^+ = 4$ peak). A similar discrepancy exists in the $v' = 3$ and $v' = 2$ excitation data as well. These differences may be due to autoionization, accidental resonances at the

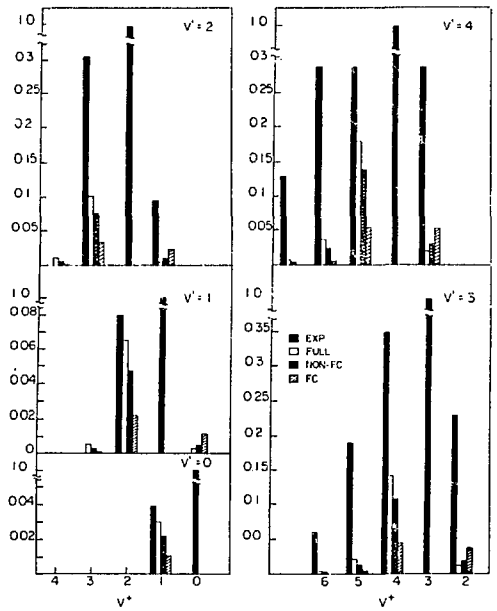

Fig. 3. Vibrational branching ratios in (3+1) REMPI via the $C^1\Pi_u$ state. v' denotes the vibrational state of the $C^1\Pi_u$ state and v^+ that of the $X^2\Sigma_g^+$ state of the ion.

three-photon excitation level, and the contribution of the Π_g and Δ_g states to the three-photon excitation amplitude which is neglected in our present studies. Of these, autoionization seems to play no role as the results of Ref. 12 are insensitive to changes in photon frequency. To analyze the contribution of Π_g and Δ_g states to the excitation, we have calculated Γ_{00} in (5) and observe that the branching ratios in $\Gamma_{00}(\theta=0)$ are very similar to those quoted here. Thus the inclusion of the $\Gamma_{00}\rho_{00}$ term in (5) will not significantly alter the relative branching ratios. The existence of accidental resonances with the P branch of some high vibrational level of the $B^1\Sigma_u^+$ state can also be ruled out for all v' states except v' = 3 [12]. Another improvement in our calculations would be the inclusion of correlation effects. Such studies are currently underway.

The non-Franck-Condon effects in the REMPI process are exhibited even more dramatically in the photoelectron angular distributions (AD). In Fig. 4 we plot these for various ionic vibrational states when the three-photon excitation proceeds via the v' = 4 level of the $C^1\Pi_u$ state. All the angular distributions are normalized to unit area ($\beta_0 = 0.5$ in (15)). Within the FC approximation, the AD is independent of v^+. The NFC and 'full' normalized AD's are also identical for a given v^+ as any scaling of the cross section due to its dependence on energy drops out upon normalization. However, it is very clear from the figure that inclusion of the R dependence introduces dramatic variations of the AD's with ionic states. Such variations, the details of which depend on the variation of the electronic transition matrix elements with the internuclear separation, are sensitive probes of non-Franck-Condon effects and can be used to assess their importance. In

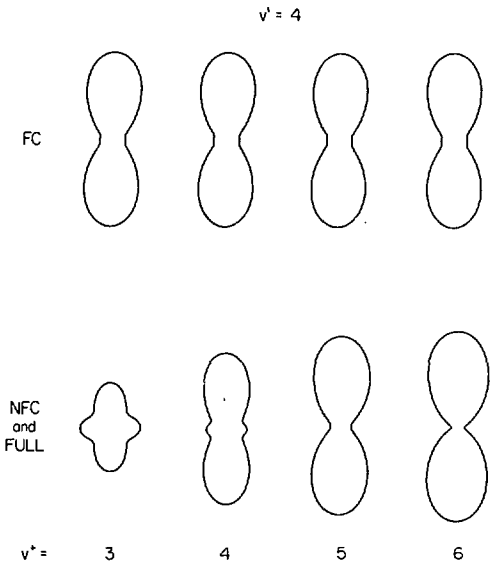

Fig. 4. Normalized photoelectron angular distributions. v' and v^+ have the same meaning as in Fig. 3. Angle θ is measured with respect to the vertical. See the text for details of various approximations.

a recent (2+1) REMPI experiment probing the E, F $^1\Sigma_g^+$ state of H_2 [11] such changes of the AD with the final vibrational state of the ion have been observed.

IV. Summary and Future Work

In this report, we have presented the results of studies of the vibrational branching ratios and photoelectron angular distributions resulting from a three-photon resonant four-photon ionization of H_2 via the $C^1\Pi_u$ state. Comparison of the calculated branching ratios with those measured in the recent experiment of PRATT et al. [12] shows good agreement for excitations through the lower ($v' < 2$) vibrational levels of the $C^1\Pi_u$ state while differences remain for excitation through higher vibrational states. Photoelectron angular distributions exhibit very interesting variations with ionic vibrational states when non-Franck-Condon effects are introduced. Such a variation is an unequivocal demonstration of non-Franck-Condon features since in the absence of these there would be no variation of the angular distributions with the ionic vibrational state. These variations can be used as a probe in estimating the strength of such effects.

The present analysis demonstrates the feasibility of theoretical studies of REMPI processes at the level of accuracy of current experiments. Of course, the present calculations have not dealt with states showing strong Rydberg-valence mixing or autoionization. Incorporation of such features will reveal new and interesting effects. Work is currently underway in our group to analyze REMPI processes in other molecules such as NO, N_2 and CO where several experiments have revealed effects due to Rydberg-valence mixing and autoionization. Results of such theoretical studies will aid in our understanding of molecular multiphoton ionization processes.

Acknowledgments

This research was supported by the National Science Foundation under Grant No. CHE-8218166. The research reported in this paper made use of the Dreyfus-NSF Theoretical Chemistry Computer which was funded through grants from the Camille & Henry Dreyfus Foundation, the National Science Foundation (Grant No. CHE-7820235), and the Sloan Fund of the California Institute of Technology.

References

1. J. C. Miller, R. N. Compton: J. Chem. Phys. 75, 22 (1981)
2. J. Kimman, P. Kruit, M. J. Van der Wiel: Chem. Phys. Lett. 88, 576 (1982)
3. M. G. White, M. Seaver, W. A. Chupka, S. D. Colson: Phys. Rev. Lett. 49, 28 (1982)
4. J. C. Miller, R. N. Compton: Chem. Phys. Lett. 93, 453 (1982)
5. S. T. Pratt, E. D. Poliakoff, P. M. Dehmer, J. L. Dehmer: J. Chem. Phys. 78, 65 (1983)
6. S. T. Pratt, P. M. Dehmer, J. L. Dehmer: J. Chem. Phys. 78, 4315 (1983)
7. S. T. Pratt, P. M. Dehmer, J. L. Dehmer: J. Chem. Phys. 79, 3234 (1983)
8. Y. Achiba, K. Sato, K. Schotabake, K. Kimura: J. Chem. Phys. 78, 5474 (1983)
9. M. G. White, W. A. Chupka, M. Seaver, A. Woodward, S. D. Colson: J. Chem. Phys. 80, 678 (1984)
10. S. T. Pratt, D. M. Dehmer, J. L. Dehmer: J. Chem. Phys. 80, 1706 (1984)
11. S. L. Anderson, G. D. Kubiak, R. N. Zare: Chem. Phys. Lett. 105, 22 (1984)
12. S. T. Pratt, P. M. Dehmer, J. L. Dehmer: Chem. Phys. Lett. 105, 28 (1984); see also P. M. Dehmer. J. L. Dehmer, S. T. Pratt in this volume
13. J. Kimman, M. Lavollée, M. J. Van der Wiel: preprint
14. See, for example, papers A3, P10, P11, P12, P13, D2: in the book of abstracts for the Third International Conference on Multiphon Processes
15. K. Sato, Y. Achiba, K. Kimura: J. Chem. Phys. 81, 57 (1984)
16. B. Ritchie, E. J. McGuire, J. M. Peek, C. W. Band: J. Chem. Phys. 77, 877 (1982); see also S. N. Dixit, V. McKoy: J. Chem. Phys. 80, 5867 (1984) for comments on this paper
17. K. R. Dastidar, P. Lambropoulos: Chem. Phys. Lett. 93, 273 (1982), and Phys. Rev. A 29, 183 (1984)
18. S. N. Dixit, V. McKoy: submitted to J. Chem. Phys.
19. S. N. Dixit, D. L. Lynch, V. McKoy: submitted to Phys. Rev. A-Rapid Communications
20. G. Herzberg: Molecular Spectra and Molecular Structure II. Spectra of Diatomic Molecules (Van Nostrand Reinhold, Princeton, 1950)
21. T. E. Sharp: Atomic Data 2, 119 (1971)
22. W. J. Hunt, W. A. Goddard III: Chem. Phys. Lett. 24, 464 (1974)
23. R. R. Lucchese, G. Raseev, V. McKoy: Phys. Rev. A 25, 2572 (1982)
24. D. J. Malik, J. Eccles, D. Secrest: J. Comp. Phys. 38, 157 (1980)

Photoionization of Excited Molecular States[1]

Dup

P.M. Dehmer, J.L. Dehmer, and S.T. Pratt
Argonne National Laboratory, Argonne, IL 60439, USA

1. Introduction

Rapid advances in laser and detector technologies are making it possible to investigate molecular photophysics and photochemistry in powerful new ways. For example, resonantly enhanced multiphoton ionization (REMPI) measurements, in which the total (or the mass selected) ion current is monitored as a function of laser wavelength, have yielded extensive and often novel information on the spectroscopy of the resonant intermediate states [1]. With the addition of photoelectron spectrometry (PES) to analyze the kinetic energy of the ejected electrons, it is possible to determine the branching ratios into different electronic, vibrational, and rotational levels of the product ion and to focus directly on both the dynamics of the multiphoton ionization process and the photoionization of excited state species [2-9]. In the present paper, we report several REMPI/PES studies of H_2 and N_2. The results reflect both the spectroscopy and the dynamics of photoionization of excited molecular states and are discussed in terms of the selection rules for photoionization and the relative probabilities of photoionization from Rydberg and valence states. In some cases, in accordance with the Franck-Condon principle, the results demonstrate that resonant multiphoton ionization through Rydberg states may be a powerful technique for the production of electronic, vibrational, and rotational state selected ions. However, in other cases, systematic departures from Franck-Condon behavior are observed, which reflect the more subtle dynamics of excited state photoionization.

2. Experimental

The apparatus used to perform these studies consists of a Nd:YAG pumped dye laser (Molectron MY34-10/DL18P), a time-of-flight mass spectrometer, and a hemispherical electron energy analyzer [3,10]. The dye laser output is frequency doubled in a KDP crystal and the resulting UV light is separated from the fundamental by multiple reflections on dichroic beamsplitters, which reduce the visible light by a factor of 10^4. In all of the measurements reported here, the photoelectron spectrometer was operated with 1 mm entrance and exit slits, and with a 2 eV energy of analysis, resulting in an energy resolution of approximately 35 meV. All spectra were recorded along the polarization axis of the laser. The transmission function of the electron spectrometer in the energy range 0.0-3.3 eV was determined by measuring the HeI photoelectron spectrum of the O_2^+ b $^4\Sigma_g^-$ and B $^2\Sigma_g^-$ bands. The estimated error in the relative intensities of the photoelectron peaks

[1] Work supported by the U. S. Department of Energy and the Office of Naval Research.

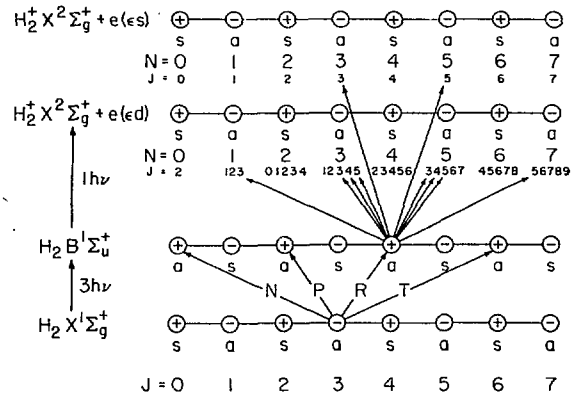

Fig. 1. Schematic diagram of the allowed transitions for (3+1) resonant multiphoton ionization of H_2 via the B $^1\Sigma_u^+$ state. Only those transitions from J"=3 of the ground state and J'=4 of the intermediate state are shown.

in the energy range 0.5-3.3 eV is ~30%. The estimated error for peaks in the energy region 0.0-0.5 eV is greater and is somewhat difficult to assess. However, peaks at energies below 0.25 eV are outside the dynamic range of the analyzer and their intensities are accurate only to within a factor of 2-3.

3. Photoionization of the B $^1\Sigma_u^+$ and C $^1\Pi_u$ States of H_2

Our (3+1) REMPI/PES studies on H_2 via the B and C states[2] [4,7] both illustrate the power of the method for the study of photoionization dynamics of excited molecular states [4,7] and demonstrate the possibility of producing ions in single electronic, vibrational, and rotational states using selective multiphoton ionization [7]. Figure 1 summarizes the selection rules for both the excitation and ionization steps for REMPI of H_2 via the B intermediate state. For the transition from the ground electronic state to the B state, the three photon selection rules based on symmetry properties are identical to those for single photon transitions (g↔u, +↔-, and s↔a) [11]. In addition, for a three photon transition, $\Delta J \leq 3$; however, transitions having $\Delta J=3$, i.e., the N and T rotational branches shown in Fig. 1, have been found to be weak or absent in a number of cases [12].

The determination of the rotationally resolved photoelectron spectra obtained by pumping individual rotational transitions will yield important information on the dynamics of the photoionization process from the B excited state, just as the analogous single photon studies have yielded important information on the dynamics of the photoionization process from the ground state of molecular H_2 [13]. The selection rules governing this transition are illustrated in the upper half of Fig. 1. Owing to the g↔u

[2] Molecular term symbols are abbreviated according to the following example -- B $^1\Sigma_u^+$, v' = 0 is written B, v' = 0. A double prime on the vibrational quantum number (v") denotes the ground state, a single prime (v') denotes the resonant intermediate state, and a plus (v^+) denotes the ion.

selection rule, the outgoing electron must have an even value of ℓ. Only s and d partial waves need be considered, since higher partial waves will be excluded by their large centrifugal barrier. It is seen that the ionizing transition must obey the selection rule $N(H_2^+ X)-J(H_2 B)=\pm1,\pm3$. It should be noted that, in the angular momentum transfer (j_t) formulation [14-16], the ejection of an s electron can lead only to a j_t value of 1, while the ejection of a d electron can yield j_t values of 1, 2, and 3. The j_t value of 2 is parity unfavored, and only values of 1 and 3 are important. The photoelectron spectra obtained by pumping the P(3) and R(3) rotational transitions of the B, v'=7, ← X, v"=0 band are shown in Fig. 2. These spectra show partially-resolved rotational structure and clearly demonstrate that higher angular momentum transfers are not observed. One of two conclusions may be drawn from these observations -- either the ejection of a d-wave or an angular momentum transfer of 3 is strongly discriminated against. From various considerations, we believe the latter is more likely to be correct, although this has not been rigorously demonstrated. Experiments such as this are of great fundamental importance, since the quantum state at each of the three stages of the overall process is precisely specified in terms of electronic, vibrational, and rotational degrees of freedom.

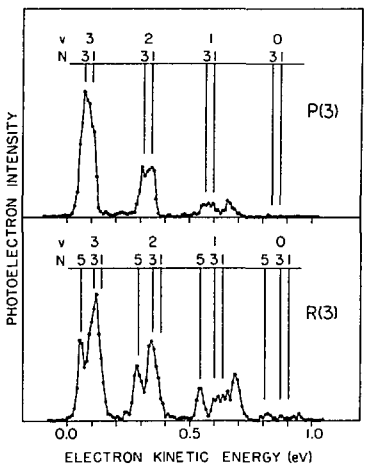

Fig. 2. Photoelectron spectra of H_2 following (3+1) ionization via the B $^1\Sigma_u^+$, v'=7, J'=2 [P(3)] and J'=4 [R(3)] levels. The unassigned peaks at 0.69 eV in the R(3) spectrum and at 0.67 eV in the P(3) spectrum are believed to result from photoionization of H(2ℓ) formed by photodissociation of B $^1\Sigma_u^+$.

In a companion (3+1) REMPI/PES study of H_2 via the resonant intermediate C state [7], two issues were addressed. First, to what degree can vibrational state selected ions be prepared by photoionization of a Rydberg state. Second, what can we learn about the more subtle dynamical effects in excited state photoionization from a comparison of the observed vibrational branching ratios with accurate Franck-Condon factors. The photoelectron spectra obtained at the wavelengths of the three photon Q(1) transitions of the C, v'=0-4 ← X, v"=0 bands are shown in Fig. 3. The most striking aspect of the photoelectron spectra is the dominance of the photoelectron peak corresponding to the X, v^+ = C, v' transition, indicating that the Rydberg electron is ionized while the vibrational state of the ionic core remains largely undisturbed. In addition, the weaker peaks with greatest intensity are those adjacent to the v^+=v' peak. This agrees with expectations based on Franck-Condon factor calculations. However, while

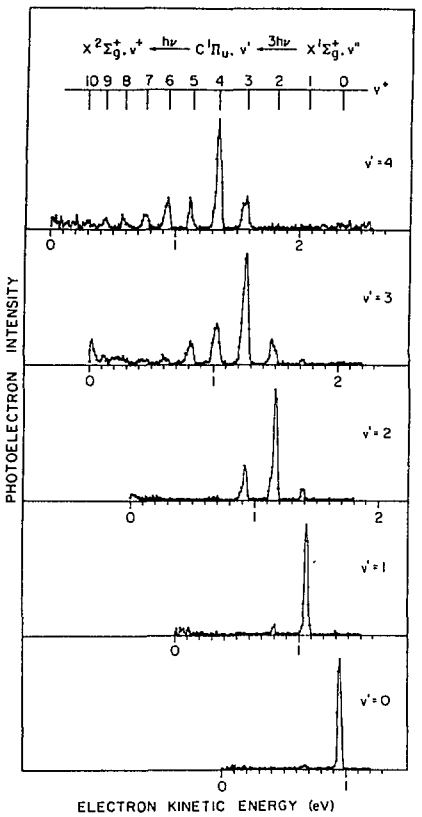

Fig. 3. Photoelectron spectra of H_2 following (3+1) ionization via the $C\,^1\Pi_u$, v'=0-4 levels.

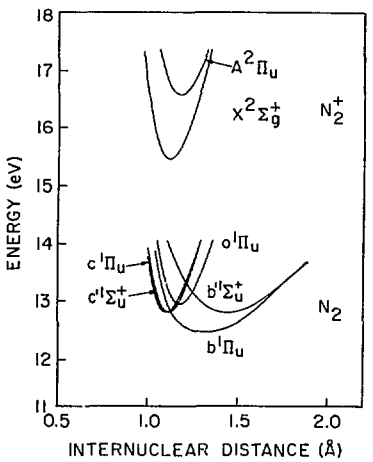

Fig. 4. Potential energy curves of N_2 and N_2^+.

the qualitative agreement with the calculations is very good, the quantitative agreement is poor. For example, in the spectrum obtained via the C, v'=4 level, the relative intensities of the v^+=3, 5, and 6 peaks are too large by factors of 3, 2, and 23, respectively, and the intensity of the v^+=4 peak accounts for only 43% of the total, rather than the predicted 90%. The most likely causes of such deviations are: (1) a kinetic energy dependence of the electronic transition matrix element, which must be taken into consideration even within the Franck-Condon approximation [17]; (2) an R-dependence of the same electronic transition matrix element, which, by definition, constitutes a breakdown of the Franck-Condon approximation; and (3) a v^+-dependence of the photoelectron angular distribution [2h]. Further experimental studies on this system that will help determine which of the above points is of major importance include determinations of the angular distributions of the photoelectrons and the wavelength dependence of the vibrational branching ratios. In addition, these data represent a well defined case for theoretical investigation of excited state photoionization. DIXIT and McKOY [18] have recently made significant progress in assessing the importance of the dynamical effects mentioned above for the present data.

4. Photoionization of $^1\Sigma_u^+$ and $^1\Pi_u$ Rydberg and Valence States of N_2

Since the first excited state of the N_2^+ ion can be accessed in the ionization step of the REMPI process, electronic as well as vibrational and rotational branching ratios may be determined. Furthermore, since the neutral excited states of N_2 have been very well characterized both experimentally and theoretically [19], N_2 is a particularly attractive system for study using REMPI/PES techniques. The recent vibronic analysis of the $^1\Sigma_u^+$ and $^1\Pi_u$ states by STAHEL et al. [20] provides a useful framework for understanding photoelectron spectra from these levels by providing a breakdown of the strongly perturbed intermediate vibronic levels in terms of deperturbed diabatic states with well defined Rydberg or valence character. However, in some instances, the situation is complicated further by strong local perturbations and predissociations that affect the rotational structure of these bands, as well as the photoelectron branching ratios. These cases require going beyond the vibronic approximation.

Photoelectron spectra have been obtained by single-color (3+1) REMPI via the b $^1\Pi_u$, c $^1\Pi_u$, c' $^1\Sigma_u^+$, and o $^1\Pi_u$ states. The relevant N_2 and N_2^+ potential energy curves are shown in Fig. 4. The c and c' states are the $3p\pi_u$ and $4p\sigma_u$ Rydberg states, both of which converge to the X $^2\Sigma_g^+$ ground state of the ion; the o state is the $3s\sigma_g$ Ryberg state that converges to the A $^2\Pi_u$ state of the ion; and the b state is a valence state having two primary electron configurations, both of which differ from the X and A states of N_2^+ by two orbitals [19]. In this energy region, the b and c states are strongly mixed by a homogeneous perturbation, as are the b' and c' states (the former is also a valence state). Hence, it is possible to study photoionization from Rydberg states (including core-excited Rydberg states), valence states, and certain perturbed levels that are complex mixtures of these.

Two of the simplest photoelectron spectra are shown in Fig. 5 and were obtained following (3+1) multiphoton ionization of N_2 via the o, v'=1,2 levels [6], which are relatively unperturbed. This photoionization process leads to the production of N_2^+ A, v^+=1,2, respectively, with greater than 90% purity. Hence, the ionizing transition strongly favors the removal of the outer $3s\sigma_g$ electron, preserving both the electronic and vibrational levels of the ion core. This is the first experimental evidence in a molecular system showing the degree to which the electronic excitation of the ion core is retained following photoionization of a Rydberg state. Similar effects have been observed in the photoionization of the rare gas atoms (i.e., in all of the observed transitions, the spin-orbit state of the ion core was preserved) [21].

Photoelectron spectra obtained following photoionization from various vibrational levels of the b state are more complicated and are shown in Fig. 6. According to the analysis of STAHEL et al. [20], the b, v'=0-2 vibronic levels contain very little c character, and are therefore relatively unpertubed. As is expected, photoionization from these levels populates a broad distribution of vibrational levels, in qualitative although not quantitative agreement with the calculated Franck-Condon factors [8]. Beginning with the b, v'=1 photoelectron spectrum, the A, v^+=0 state of N_2^+ becomes energetically accessible and is observed with a large intensity, as it is in the b, v'=2 photoelectron spectrum. Unfortunately, relative intensities in this (near zero) electron kinetic energy region are not reliable, making it difficult to accurately compare the intensities of the A, v^+=0 ← b, v'=1 and X, v^+=0 ← b, v'=1 ionizing transitions.

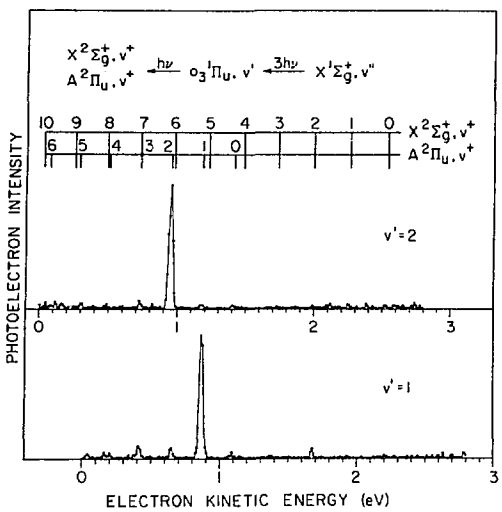

Fig. 5. Photoelectron spectra of N_2 following (3+1) ionization via the o $^1\Pi_u$, v'=1,2 levels.

Unlike the b, v'=0-2 photoelectron spectra, which exhibit a number of intense peaks, the b, v'=3-5 photoelectron spectra each display a single intense X, v^+=0 peak, with very little intensity in any of the other peaks. This is somewhat surprising since the Franck-Condon factors predict a number of other moderately intense peaks [8]. The single intense v^+=0 peak suggests that photoionization from these levels may be dominated by a v'=0 Rydberg state component in the wavefunction of the intermediate state, since photoionization from a Rydberg level is expected to preserve the vibrational quantum number of the intermediate state. The analysis of STAHEL et al. [20] shows that the b, v'=3-5 wavefunctions contain 5.8%, 16.0%, and 22.1% c, v'=0 character, respectively, and this admixture could account for the intense v^+=0 peak observed in the b, v'=3-5 photoelectron spectra.

The c, v'=0 photoelectron spectrum shown in Fig. 7 can be understood by assuming that photoionization from a Rydberg level preserves the vibrational quantum number and the electronic state of the ion core; however, the c, v'=1 photoelectron spectrum cannot be understood in this way. Although the latter spectrum does display a prominant X, v^+=1 peak, the A, v^+=0 peak is equally intense. The appearance of the strong A, v^+=0 peak can be rationalized by the existence of 7% o, v'=0 state character in the c, v'=1 wavefunction [20]. Similarly, the appearance of the A, v^+=1 peak in the photoelectron spectrum may be due to the existence of 2% o, v'=1 character in the c, v'=1 wavefunction. However, the large relative intensity of the A peaks with respect to the X peaks is more difficult to understand, since production of the A electronic state from the c state requires a two electron transition in the ionization step.

The c', v'=0,1 photoelectron spectra shown in Fig. 8 also show signficant complications. The X, v^+=0 peak is the most intense in the c', v'=0 photoelectron spectrum (in agreement with the Franck-Condon factor

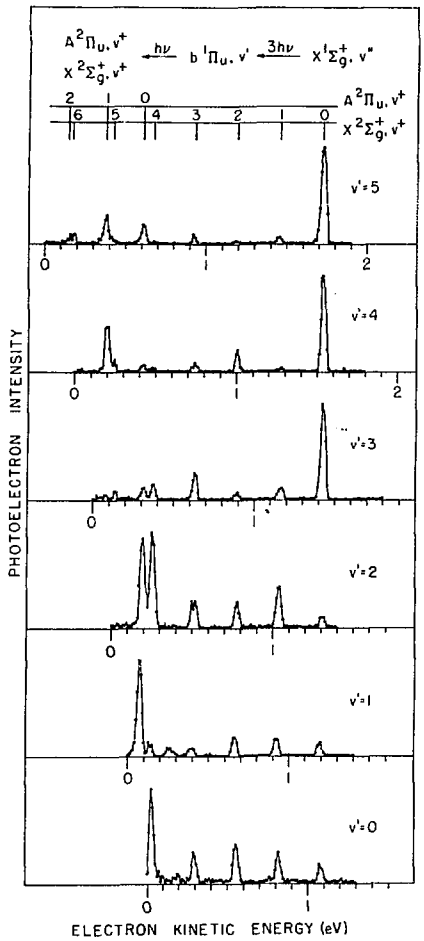

Fig. 6. Photoelectron spectra of N_2 following (3+1) ionization via the b $^1\Pi_u$, v' = 0-5 levels. The impurity peaks at 0.26 eV and 0.50 eV in the v'=1 spectrum are due to (2+1) ionization of O_2.

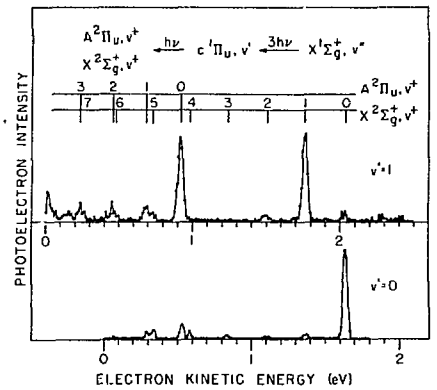

Fig. 7. Photoelectron spectra of N_2 following (3+1) ionization via the c $^1\Pi_u$, v'=0,1 levels.

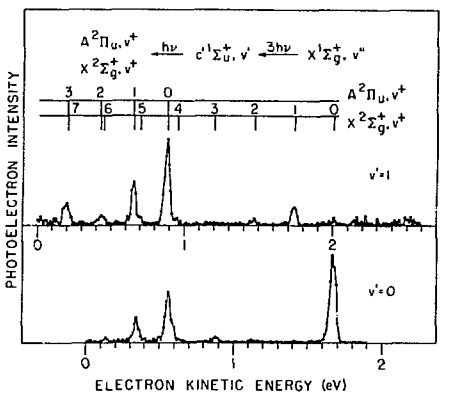

Fig. 8. Photoelectron spectra of N_2 following (3+1) ionization via the c' $^1\Sigma_u^+$, v'=0,1 levels.

calculations [8]); however, the A, v^+=0,1 photoelectron peaks are much larger than expected for photoionization from a Rydberg state converging to the X state of N_2^+. This indicates that the c', v'=0 Rydberg state ion core does not act like a spectator in the ionizing transition as it does in photoionization of the o state. The c', v'=1 photoelectron spectrum in Fig. 8 is even more intriguing, as the X, v^+=1 peak is completely overshadowed by the intense A, v^+=0,1 peaks. According to the analysis of

STAHEL et al. [20], the c', v'=1 level contains 14% b, v'=4 character and 2% b', v'=3 character, while the c', v'=0 state contains less than 2% total b' character. A large A ← b' electronic transition matrix element would help account for the strength of the A, v^+=0,1 peaks, but it is difficult to imagine that it is so much larger than the corresponding X ← c' matrix element. In addition, the Franck-Condon factors for the A, v^+=1 ← b', v'=3,4 transitions are three and two times larger, respectively, than those for the A, v^+=0 ← b', v'=3,4 transition [8], while the observed A, v^+=0 peak is nearly twice as intense as the A, v^+=1 peak. A second possibility (which may also be applicable to the c, v'=1 photoelectron spectrum) is the presence of autoionizing resonances at the four photon energy. In order to examine this possibility, we determined the photoelectron spectrum from the c', v'=1 state prepared by a two step process. The first laser pumped a two photon transition to the a $^1\Pi_g$, v=1, J=4 level, and a second laser was tuned to the wavelength of the c', v'=1, J'=5 ← a, v"=1, J"=4 transition. Ionization occurred by absorption of one photon of the first laser wavelength. Although the total energy is 140 cm^{-1} removed from the four photon energy in the single laser experiments, the photoelectron spectrum obtained is nearly identical to that of Fig. 8. This indicates that the observed branching ratios are not due to sharp autoionizing resonances, although the effects of a broad autoionizing resonance cannot be ruled out.

5. Summary

The present studies represent some of our early attempts to exploit the technique of resonantly enhanced multiphoton ionization to probe the photoionization dynamics of the excited states of small molecules that are theoretically tractable. Another aspect of REMPI is that it allows the selective ionization of one component of a complex mixture. Thus, state preparation of ions and the study of their subsequent reactions could be performed in the same region of space. This would allow the study of reactions of ions in relatively short-lived electronic states without interference from extraneous ionization products. However, the present studies illustrate that one cannot rely, a priori, on the Franck-Condon principle to predict the vibrational state distributions following REMPI.

6. References

1. See, for example, P. M. Johnson and C. E. Otis: Ann. Rev. Phys. Chem. 32, 139 (1981)
2. For examples of REMPI studies of small molecules using photoelectron spectroscopy, see (a) J. C. Miller and R. N. Compton: J. Chem. Phys. 75, 22 (1981); (b) M. G. White, M. Seaver, W. A. Chupka, and S. D. Colson: Phys. Rev. Lett. 49, 28 (1982); (c) J. Kimman, P. Kruit, and M. J. van der Wiel: Chem. Phys. Lett. 88, 576 (1982); (d) J. H. Glownia, S. J. Riley, S. D. Colson, J. C. Miller, and R. N. Compton: J. Chem. Phys. 77, 68 (1982); (e) Y. Achiba, K. Sato, K. Shobatake, and K. Kimura: J. Chem. Phys. 78, 5474 (1983); (f) S. R. Long, J. T. Meek, and J. P. Reilly: J. Chem. Phys. 79, 3206 (1983); (g) W. G. Wilson, K. S. Viswanathan, E. Sekreta, and J. P. Reilly: J. Phys. Chem. 88, 672 (1984); (h) S. L. Anderson, G. B. Kubiak, and R. N. Zare: Chem. Phys. Lett. 105, 22 (1984); and (i) K. Kimura: Adv. Chem. Phys. (in press)
3. S. T. Pratt, E. D. Poliakoff, P. M. Dehmer, and J. L. Dehmer: J. Chem. Phys. 78, 65 (1983)
4. S. T. Pratt, P. M. Dehmer, and J. L. Dehmer: J. Chem. Phys. 78, 4315 (1983)
5. S. T. Pratt, P. M. Dehmer, and J. L. Dehmer: J. Chem. Phys. 79, 3234 (1983)

6. S. T. Pratt, P. M. Dehmer, and J. L. Dehmer: J. Chem. Phys. 80, 1706 (1984)
7. S. T. Pratt, P. M. Dehmer, and J. L. Dehmer: Chem. Phys. Lett. 105, 28 (1984)
8. S. T. Pratt, P. M. Dehmer, and J. L. Dehmer: J. Chem. Phys. (in press)
9. S. T. Pratt, J. L. Dehmer, and P. M. Dehmer: (in preparation)
10. J. L. Dehmer: Argonne National Laboratory Radiological and Environmental Research Division Annual Report, July 1974-June 1975, ANL-75-60, Part I, pp. 61-63.
11. G. Herzberg: Molecular Spectra and Molecular Structure II. Spectra of Diatomic Molecules (Van Nostrand Reinhold, Princeton, 1950)
12. J. B. Halpern, H. Zacharias, and R. Wallenstein: J. Mol. Spectrosc. 79, 1 (1980)
13. (a) J. E. Pollard, D. J. Trevor, J. W. Reutt, Y. T. Lee, and D. A. Shirley: J. Chem. Phys. 77, 34 (1982) and references therein; (b) J. E. Pollard, D. J. Trevor, J. E. Reutt, Y. T. Lee, and D. A. Shirley: Chem. Phys. Lett. 88, 434 (1982); and (c) M. W. Ruf, T. Bregel, and H. Hotop: J. Phys. B. 16, 1549 (1983)
14. U. Fano and D. Dill: Phys. Rev. A 6, 185 (1972)
15. D. Dill: Phys. Rev. A 6, 160 (1972)
16. D. Dill: in Photoionization and Other Probes of Many-Electron Interactions, edited by F. J. Wuilleumier (Plenum, New York, 1976), p. 387
17. Y. Itikawa: Chem. Phys. 28, 461 (1978); 30, 109 (1978)
18. S. Dixit and V. McKoy, private communication.
19. A. Lofthus and P. H. Krupenie: J. Phys. Chem. Ref. Data 6, 113 (1977)
20. D. Stahel, M. Leoni, and K. Dressler: J. Chem. Phys. 79, 2541 (1983)
21. (a) J. Ganz, B. Lewandowski, A. Siegel, W. Bussert, H. Waibel, M. W. Ruf, and H. Hotop: J. Phys. B. 15, L485 (1982); (b) A. Siegel, J. Ganz, W. Bussert, and H. Hotop: J. Phys. B 16, 2945 (1983); and (c) K. Sato, Y. Achiba, and K. Kimura: J. Chem. Phys. 80, 57 (1984); (d) R. F. Stebbings, F. B. Dunning, and R. D. Rundel: in Atomic Physics Volume 4, edited by G. zu Putlitz, E. W. Weber, and A. Winnacher (Plenum, New York, 1975), p. 713

Resonant Two-Photon Ionization and Dissociation of the Hydrogen Atom and Molecule

Karl H. Welge[1,2] and H. Rottke

Fakultät für Physik, Universität Bielefeld
D-4800 Bielefeld, Fed. Rep. of Germany

1. Introduction

In this paper we report on two experimental studies: A) the ionization of the H atom in strong external electric fields around the ionization limit by state-selective two-photon, one-photon resonant excitation through single sublevels of the n = 2 Stark manifold as intermediate step, and B) the two-photon, one-photon resonant ionization and dissociation of the H_2 molecule through selected rotational-vibrational levels of the $B^1\Sigma_u^+$ electronic state as intermediate step.

A) The interaction of atoms with strong external electric and magnetic fields, that is, where the field strength is comparable with, or larger than, the internal binding forces, has gained considerable attention in recent years [1]. At laboratory field strengths the strong interaction situation is always given in the vicinity of ionization limits, that is, in high Rydberg states and the adjacent continuum. While the extensive theoretical work in this field is based largely on the hydrogen atom, experimental studies have been performed almost exclusively with non-hydrogen atoms [1]. In fact, no experiments are known with the H atom in strong magnetic fields, that means, with the diamagnetic interaction dominating. In electric fields experiments have been carried out by Koch and collaborators who used a method of fast atomic beam laser spectroscopy combined with Stark tuning levels into resonance with fixed frequency CO_2 laser lines [2,3]. They have performed precise measurements on the energy and ionization rate of discrete, quasi-stable states at energies above the classical field ionization saddle point, $E_{sp} = -2\sqrt{F}$ a.u., and well below the zero field ionization limit, $E < 0$.

A conceptually straightforward and versatile method, widely used in studies on high Rydberg atoms in strong fields, is the state-selective excitation with field ionization in atom beam arrangements [1]. Experimental obstacles have prevented so far the application of this technique to the hydrogen atom. In this work we have essentially overcome these obstacles by two-step excitation of the atoms using tunable VUV laser light in the Lyman-α line wavelength range for the first, resonant step and tunable UV laser light for the second, ionizing step:

$$H(n=1) + VUV \rightarrow H(n=2) + UV \rightarrow H^+ + e \quad .$$

[1] Joint Institute for Laboratory Astrophysics, University of Colorado and National Bureau of Standards, Boulder, CO 80309, USA
[2] JILA Visiting Fellow, 1983-84. Permanent address: Department of Physics Universität Bielefeld, Fed. Rep. of Germany

The objectives of this work were 1) to develop the two-photon technique of state-selective excitation of high Rydberg states of the atom in a crossed laser atomic hydrogen beam, 2) photoionization spectroscopy of H in electric fields 1000 V/cm $\lesssim F \lesssim$ 8000 V/cm through single Stark levels of the n = 2 manifold at energies from below the classical field ionization saddle point, $E_{sp} = -2\sqrt{F}$ a.u., into the ionization continuum region, E > 0,3)observation and investigation of the oscillations in the ionization cross section around the zero field ionization limit, which have been observed first with Rb [4] and later also with other atoms [5-7]. Our first observation of these oscillations with the H atom has been reported previously [8,9]. Another reason for these experiments was to use them as a preparatory stage for analogous studies with the H atom in strong magnetic fields, now carried out in our laboratory.

B) Elementary photophysical and collisional processes of the hydrogen molecule are of basic interest and importance in many areas of physics and chemistry. Only in recent years, however, have laser techniques been developed to the point where the molecule can be excited state-selectively with tunable laser radiation by single- or multi-photon absorption to its lowest electronic states in the far vacuum ultraviolet. References to work until about 1983 may be taken from a paper by Rottke and Welge [10], which was concerned with the two-photon (VUV + UV) resonant photoionization of the molecule. Other recent studies have been carried out on: a) (3+1) MPI-PES via the $B^1\Sigma_u^+$ three-photon resonant intermediate state [11], b) (2+1) MPI-PES via the $E,F\ ^1\Sigma_g^+$ two-photon resonant intermediate state [12], c) one-photon excitation of the $B^1\Sigma_u^+$ state at 1058-1068 A monitored by LIF [13], d) state distribution measurements of H_2 in the $H-H_2$ reaction monitored by E,F state (2+1) MPI [14].

In this paper, we report experiments on the two-photon (VUV + UV) ionization and dissociation spectroscopy of H_2, where the molecule is excited state-selectively via

$$H_2(X^2\Sigma_g^+, v''=0, J'') \xrightarrow{VUV} H_2(B^2\Sigma_u^+, v', J') \xrightarrow{UV} H_2^* \quad ,$$

with both the VUV and UV laser radiation tunable independently. In contrast to previous experiments [10], the VUV was tuned to and kept fixed at a selected X-B transition while the UV was scanned at energies so that the total photon energy, $h\omega_{VUV} + h\omega_{UV}$, covered ranges around the ionization limits of $H_2^+(X^2\Sigma_g^+, v^+=0, N^+)$ and $H_2^+(X^2\Sigma_g^+, v^+=1, N^+)$. The adiabatic energy limits for the dissociation into H(n=1) + H(n=2) and the ionization H_2 $(X^2\Sigma_g^+, v^+=0, N^+=0) + e^-$ are 118,443 cm^{-1} and 124,417.2 cm^{-1} [15], respectively. First such state-selective photodissociation and photoionization spectroscopy studies with H_2 by two-photon excitation have been reported by us previously [9,16].

2. Two-Photon Ionization of H in Strong Electric Fields

2.1 Experimental

The experimental arrangement consisted essentially of two parallel field electrodes and an electron multiplier placed behind the positive electrode which carried a wire mesh through which electrons from the field region could pass and be detected by the multiplier. The arrangement is, except for the hydrogen atom beam arrangement, similar to that used in the H_2 experiments (Fig. 5). The VUV and UV laser beams passed, anti-collinearly, through the field, such that the pulses (~8 ns duration, 10 Hz repetition

rate) arrived simultaneously at the center of the field. Hydrogen atoms, produced in a microwave discharge, entered the field region in an atomic beam with a two-stage vacuum pumping arrangement. The beam was well collimated by a skimmer between the two stages to an effective, perpendicular Doppler width of ~2 GHz at 121.6 nm. The axes of the atomic beam, of the laser beams, and of the electric field intersected each other at right angles. The field electrode arrangement was enclosed in a cryogenically cooled (~14 K) metal housing provided with the appropriate openings for the atomic and laser beams, as well as for the electrons to reach the multiplier, positioned outside the housing. The VUV was generated by frequency tripling in krypton, $h\nu_{VUV} = 3\ h\nu_{UV}$ [17]. As opposed to the previously employed procedure [17], the fundamental VUV at ~3648 A was obtained from a tunable ultraviolet dye laser pumped by an excimer laser at 308 nm. The UV fundamental leaving the krypton tripling cell was separated from the VUV by a 30° lithium-fluoride prism. This was necessary in order to prevent the intense UV fundamental from photoionizing the H(n=2) atoms [17]. The excimer laser also pumped simultaneously a second dye laser which produced the tunable UV light for the second-step excitation. More detail of the experimental setup and procedure will be published elsewhere [18].

2.2 Results and Discussion

Experiments have been carried out in the energy range from the classical saddle point energy, E_{sp}, through the zero field ionization limit, E = 0, (IP_0 = 109678.77 cm^{-1}) into the continuum region, E > 0. While the VUV wavelength was kept fixed at a given Stark line in the H(n=1) → H(n=2) transition manifold (Fig. 2), the UV laser was scanned and the electron signal recorded as a function of the UV wavelength.

As the excitation-ionization cross section essentially depends on the spatial quantization [19,20], the polarization of both laser beams had to be well defined with respect to the electric field direction. In these experiments both parallel (π) and perpendicular (σ) polarization have been used in both excitation steps, yielding the four polarization combinations: (π,π), (π,σ), (σ,π), and (σ,σ). By the same token, the H(n=1) → H(n=2) transition around 1216 A had to be excited at a resolution such that, of the four Stark sublevels in the n=2 manifold, only single levels were populated. Figure 1 shows the theoretical Stark splitting in the n = 2 state manifold as a function of the electric field strength. The Stark sublevels are labeled on the left side of the figure by the low-field quantum number notation and on the right side by parabolic quantum numbers $\{n_1,n_2,m_L,m_S\}$, appropriate for high fields. Taking the state $^2P_{3/2}$ $|m_j| = 1/2$ (low-field notation) as an example, expansion of this state wave function, $\psi_i^{\pm}$, in the parabolic functions $|n_1,n_2,m_\ell\rangle|m_s\rangle$ at an electric field strength F = 5714 V/cm (used in the experiments below), yields $\psi_i^{\pm} = 0.985|1,0,0\rangle\ |\pm1/2\rangle - 0.111|0,1,0\rangle|\pm1/2\rangle - 0.156|0,0,\pm1\rangle|\mp1/2\rangle$. This shows that the orbital part of the intermediate state is nearly of pure $|1,0,0\rangle$ parabolic character. The admixtures from the other parabolic states total in this case to only about 3%. In the following, we identify therefore the n = 2 states by their parabolic quantum number notation.

Figure 2 shows a measurement of the Stark splitting in n = 2 at a field of F = 5465 V/cm. The effective resolution is ~3 GHz width at half maximum. It results from the combined contributions of the laser bandwidth at 121.6 nm and the effective perpendicular Doppler line width of the atomic beam. This measurement has been made with the resonant two-step photoionization technique previously applied by us to the H atom [17].

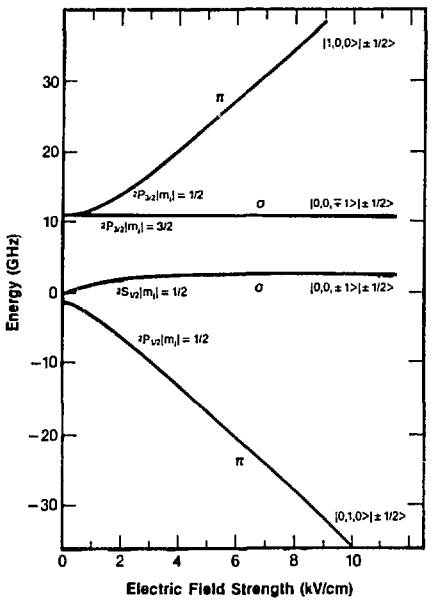

Fig. 1. Theoretical Stark splitting of the H(n=2) state as a function of the electric field. State labeling by low (left) and high field (right) notation. π and σ, parallel and perpendicular, polarization directions of the excitation laser light, with respect to the electric field.

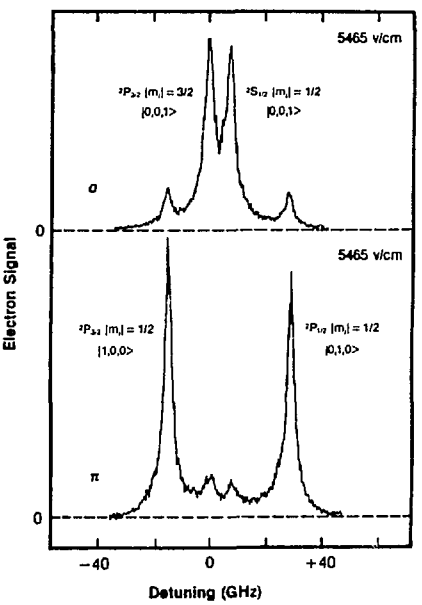

Fig. 2. Stark splitting of the H(n=1) → H(n=2) transition in an electric field of 5465 V/cm, observed by two-photon (VUV + UV) excitation, with crossed atomic and laser beams.

However, different from the previous experiments, the ultraviolet radiation, obtained from the second laser, had here a wavelength such that the total energy of the two photons was well above (~3000 cm^{-1}) the zero field ionization limit, where the ionization cross section could be assumed to be practically constant and not be affected by the electric field. At F = 5465 V/cm only the two strongest lines ought to be present in the respective σ and π spectra. The appearance of two low-intensity satellites is attributed to imperfect linear polarization of the VUV laser light.

Ionization spectra have been taken and investigated at different field strengths, with all four polarization combinations and from all four Stark sublevels. Figure 3 shows two examples obtained at F = 5715 V/cm: (a) with (π,π) and (b) with (π,σ) polarization. In both spectra, the intermediate state in the n = 2 manifold was the highest one, i.e. |1,0,0>. The saddle point energy which corresponds to F = 5715 V/cm and the zero field limit, E = 0, are marked in the figures.

To discuss the photoionization in an electric field, three energy regions may be distinguished: (A) $E < -|E_{sp}|$, (B) $0 \gtrsim E \geq -|E_{sp}|$, and (C) $E \gtrsim 0$. In region (A) the lifetime of the states is practically determined by spontaneous emission, the tunneling rate being negligibly small, except very close to the saddle point. In fact, no ionization was observed in

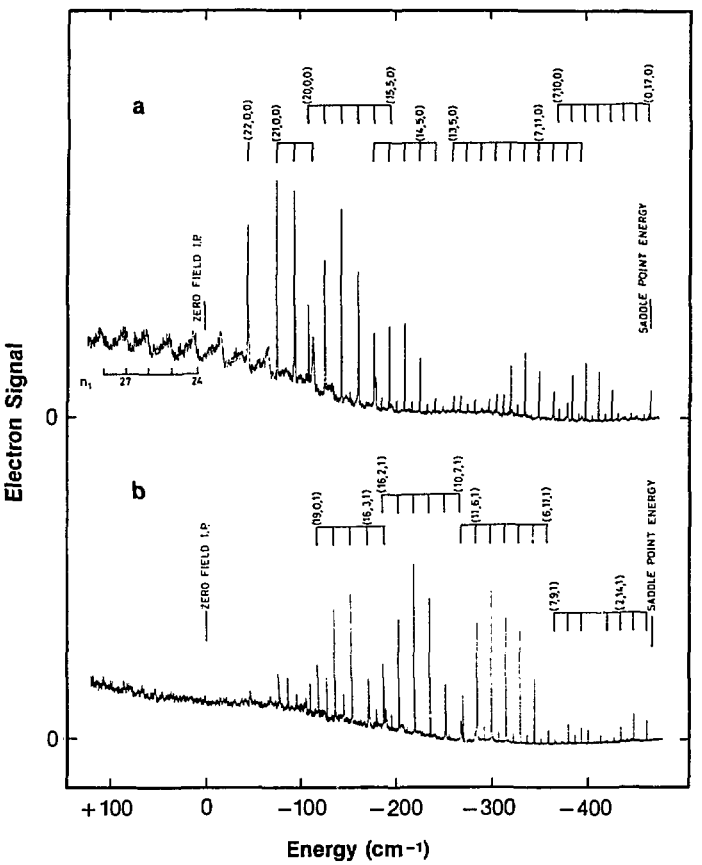

Fig. 3. Ionization spectra of the H atom in an electric field (5714 V/cm) from the $|1,0,0\rangle$ intermediate Stark level of the n = 2 manifold. Excitation of the $|1,0,0\rangle$ state from the $|0,0,0\rangle$ ground state with π polarized VUV light. Polarization of the ionizing light: (π) in spectrum (a), perpendicular (σ) in spectrum (b). Labeling lines by parabolic quantum number notation $(n_1,n_2,|m|)$. Spectrum (a): Calculated energy positions, E_{n_1}, of oscillation minima indicated by parabolic quantum number: $n_1 = 24,\ldots,28$.

these experiments below the classical saddle point since the ionization rate there dropped rapidly below the experimental detection limit of $\sim 10^{+5}\ s^{-1}$, given by the residence time of the excited atoms in the effective observation region between the field plates.

The strong mixing of Rydberg states with the external electric field in the region (B) results, as is well known from theory [1,19-23] and previous experiments [2,3], in quasi-stable quantum states with ionization lifetimes ranging over many orders of magnitude from $\sim 10^{-5}$ s to $<10^{-12}$ s, where they disappear in the continuum. This structure of discrete lines

is clearly exhibited by the spectra shown. The lines are identified by the parabolic quantum numbers of the respective upper, ionizing states, $|n_1,n_2,|m|>$ grouped according to $n = n_1+n_2|m| + 1$, where n is the principal quantum number. The assignment has been achieved theoretically by calculating the state energy, according to the perturbation method previously developed and employed [2,21,22]. We have made the computations to an approximation such that the theoretical state energies reached a precision comparable to the experimental accuracy to which the line positions were measured, which was ~0.8 cm^{-1} for the absolute and ~0.1 cm^{-1} for the relative energies. The intermediate state was assumed to be of pure $|1,0,0>$ character and the ionizing light to be purely π or σ polarized. Both assumptions did not fully apply, causing the appearance of additional low-intensity resonances that are not assigned.

The spectrum (a) clearly exhibits the sought-for oscillator structure growing out of the sharp resonances at energies below the zero field limit, $E < 0$, well into the continuum region, $E > 0$. At $E = 0$ the modulation degree is about 30%, where the modulation is defined by $(S_{max}-S_{min})/S_{max}$, with S_{max} and S_{min} being the adjacent maximum and minimum signals of an oscillation period. The spectrum (b), taken from the same intermediate state $|1,0,0>$, but with σ polarized ionizing UV light, does not show oscillations within the precision of these measurements, that is, a modulation must be less than a few percent.

Spectra (not shown in this paper) have also been taken and investigated from the other three Stark components of the $n = 2$ manifold, again with the UV radiation π and σ polarized. They all showed the resonant structures of quasi-stable states as clearly as in the spectra of Fig. 2, but none of them contained noticeably the oscillation.

We have measured the energy spacing of the adjacent maxima (or minima) of the oscillation closest to the zero field ionization limit $E = 0$ as a function of the electric field strength F. The experimental results are given in Fig. 4 by the open circles. Also shown in Fig. 4 (solid line) is the $F^{3/4}$ dependence of the oscillation spacing, according to the approximate theoretical relation for the distance between adjacent resonance maxima at $E = 0$,

$$\left.\frac{dE}{dn_1}\right|_{E=0} = 2\sqrt{\pi}\,\frac{\Gamma(\frac{1}{4})}{\Gamma(\frac{3}{4})}\,(\frac{F}{4})^{3/4} \quad ,$$

as given by Rau [23], Kondratovich and Ostrovskii [24], and Rau and Lu

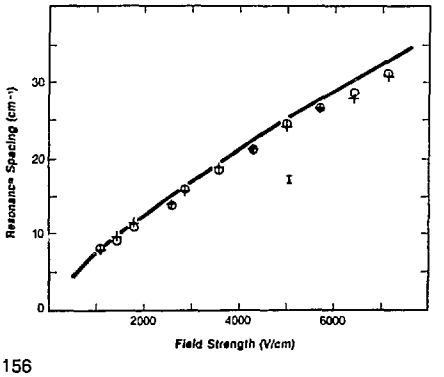

Fig. 4. Dependence of oscillation spacing period on the electric field strength. Open circles: measured results; solid line: approximate theoretical model (giving $F^{3/4}$ dependence) [23-25]; crosses: results of theoretical calculation (this work).

[25]. The measured points deviate slightly but systematically and beyond the experimental error limit from the theoretical $F^{3/4}$ dependence. The deviation is due to the fact that a maximum normally does not occur exactly at E = 0 and two adjacent maxima occur, of course, at somewhat different energies.

Following essentially the theoretical work of Kondratovich and Ostrovskii [24], Harmin [20], and Luc-Koenig and Bachelier [19], we have theoretically calculated the energies E_{n_1} of the maximum (and minimum) positions. The results of the calculation are shown in Fig. 3 for the field strength of F = 5714 V/cm, where the calculated minimum positions are indicated in the scale by the parabolic quantum numbers n_1 = 24,..., 28. In Fig. 4 the results are shown by the crosses. As can be seen, the agreement is within experimental error. The calculations will be presented in detail elsewhere [26].

3. Two-Photon Dissociation and Ionization Spectroscopy of H_2

3.1 Experimental

Figure 5 shows schematically the experimental arrangement. Hydrogen gas was introduced as an effusive beam through a capillary into the region between two parallel electric field plates P_1 and P_2. The pulsed VUV and UV laser beams (~8 ns pulse duration, 10 Hz repetition rate) passed anticollinearly through the system, with the laser axis at right angles to the molecular beam axis. The spontaneous radiative lifetime of the $H_2(B^1\Sigma_u^+)$ state being ~0.6 ns, both laser pulses were synchronized at the molecular beam intersection. The VUV and UV laser beam diameters at the intersection were of the order of ~1 mm and ~5 mm, respectively. Ionization in the intersection region was monitored by the electrons formed. They were extracted by the electric field through the fine mesh grid in one of the electrodes and accelerated onto the cathode of the electron multiplier SEM. The apparatus was pumped by a diffusion pump. The interaction region with the electrodes was enclosed in a metal housing (C), which was cooled cryogencally to ~14K. In this way the interior of the housing

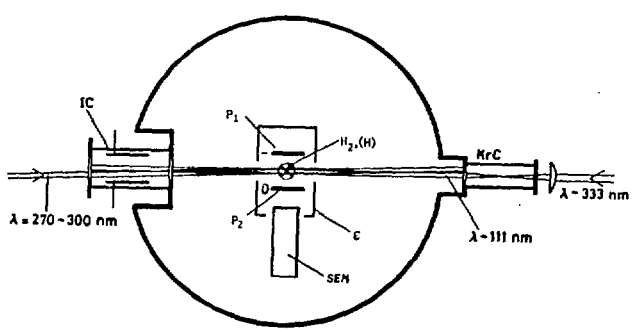

Fig. 5. Experimental arrangement. P_1,P_2: plane parallel electrodes for electric field; C: cryogenically cooled housing; SEM: electron multiplier; H_2,(H): molecular (or atomic) hydrogen beam perpendicular to plane; KrC: krypton cell for frequency tripling ($\lambda \sim 333$ nm + $\lambda \sim 111$ nm); IC: acetone ionization cell.

with the beam interaction region was pumped very efficiently, such that it was practically free of any background gas, as indicated by the absence of a noticeable signal background when no H_2 gas was admitted, or with H_2 present but the VUV not being in resonance with a $H_2(B \leftarrow X)$ transition.

The experiments reported here have been carried out from the ($B^2\Sigma_u^+$, v'=0,J'=0) state which was excited at the P(1) line (90,085.01 cm^{-1}) from the ($X^2\Sigma_g^+$,v"=0,J"=1) ground state at 1110.06 A. This wavelength was generated by frequency tripling of the corresponding fundamental of 3330.18 A in a krypton cell. The 3330 A light was obtained directly from a tunable ultraviolet dye laser (~7 mJ/pulse) pumped by a 308 nm excimer laser. The VUV, together with the UV fundamental were passed through the interaction chamber. These two light beams alone did not produce a noticeable ionization signal, either with or without H_2 gas admitted, as the energy of the 1110 A and 3330 A photons together was below the H_2 ionization limit. The VUV light was monitored by an ionization cell (IC) with acetone. The ultraviolet radiation for the second-step excitation entered the system through the ionization cell provided with quartz (Q) and LiF (L) windows. Neither the 3330 A fundamental for the VUV light nor the ionizing UV caused ionization in the acetone cell.

The tunable ionizing UV light was generated by frequency doubling the output of the second dye laser, pumped by the same XeCl excimer laser that pumped the 3330 A generating dye laser. In these experiments, we have worked with the ionizing UV in a tuning range ~2700-3000 A. The bandwidths of the VUV and the UV lasers were ~0.4 cm^{-1} and ~0.2 cm^{-1}, respectively.

The spectra, shown below, have been taken with absolute wavelength calibration of the ionizing UV radiation. The calibration was performed in the visible scanning range (~5400-6000 A) by means of the Ne hollow-cathode optogalvanic technique, providing reference wavelengths, combined with interferometric interpolation. The interferometer (etalon) used had a free spectral range of 1.6931 ± 0.0009 cm^{-1}.

It is important to note that during the VUV + UV laser excitation pulse no electric field existed between the electrodes P_1,P_2. As was expected, and observed in preliminary experiments, electric fields profoundly affected the excitation mechanism through strong interaction with the high-lying states in the region of the ionization thresholds, an effect well studied with atoms [1]. An electric field, F, was however applied in a pulsed form after the laser excitation (delay ~100 ns). This field served two purposes: (1) field ionization of highly excited H_2^* molecules, specifically ones in high Rydberg states, which otherwise would not have been observable because of too long field-free ionization lifetimes and (2) extraction of the electrons from the ionization zone, particularly the ones originating from field-free ionization.

2.2 Results

At room temperature, where the experiments have been carried out, most of the H_2 population is contained in the v" = 0, J" = 0, 1 and 2 levels of the electronic ground state, $X^1\Sigma_g^+$. From these states J' = 0, 1, 2 and 3 levels can be reached in the $B^1\Sigma_u^+$ state, according to the $\Delta J = \pm 1$ selection rule for the homonuclear molecule. As an example, Fig. 6 shows a laser excited fluorescence spectrum of the X-B, (0,0) band obtained with room temperature hydrogen at a pressure of about 10^{-4} Torr [27]. The signal intensity distribution corresponds within the experimental error limit of a few degrees (K) to the room temperature Boltzmann rotational equilibrium distribution.

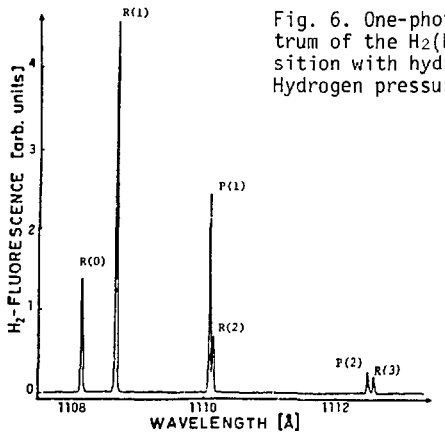

Fig. 6. One-photon laser excited fluorescence spectrum of the $H_2(B^1\Sigma_u^+, v'=0, J' \rightarrow X^1\Sigma_g^+; v''=0, J'')$ transition with hydrogen at room temperature in bulk. Hydrogen pressure $\sim 10^{-4}$ Torr.

In this paper, we present spectra obtained from the B,v'=0,J'=0 level, excited at the P(1) line:

$$H_2(X^1\Sigma_g^+, v''=0, J''=1) \xrightarrow[P(1)]{VUV} H_2(B^1\Sigma_u^+, v'=0, J'=0) \xrightarrow{UV} H_2^* \quad .$$

The UV tuning covered two energy regions of final H_2^* states: (I) ~123,500-125,000 cm^{-1} and (II) ~126,000-127,000 cm^{-1}. Region (II) includes the adiabatic ionization limit for $H_2^+(X^2\Sigma_g^+, v^+=0, N^+=0)$ and (II) the H_2^+ $(X^2\Sigma_g^+, v^+=1, N^+=0)$ limit. Figures 7 and 8 show spectra in these regions. They have been composed from a number of spectra taken on much larger signal and wavelength scales. The signal scaling factors for the various spectral sections are indicated in the figures. The energy positions of the ionization limits for $H_2^+(v^+=0, N^+=0,1,2)$ and $H_2^+(v^+=1, N^+=0,1,2)$ are also shown.

To discuss the spectrum in Fig. 7, we divide it into three energy regions: a) $E \gtrsim 124{,}430\ cm^{-1}$; b) $124{,}430\ cm^{-1} \gtrsim E \gtrsim 124{,}400\ cm^{-1}$; c) $E \lesssim 124{,}400\ cm^{-1}$. In region a) lies a well-developed series of high Rydberg states which were detectable only through field ionization. Corresponding to the external field, F, the ionization thresholds are lowered, classically, by $E_{sp} = -2\sqrt{F}$ a.u. Figure 9 shows the region b) on an enlarged scale; in the upper part again for F = 178.5 V/cm and in the lower part for 35.7 V/cm. With the exception of the line at 124,422 cm^{-1}, all Rydberg states in this region are evidently field ionized, leading to $H_2^+ + e$.

The spectrum in region a) consists of autoionization line structures on a continuum background, not affected by the electric field. Experiments, not presented in this paper, with mass-selective ion detection using a mass filter, showed that the spectrum in a) and b) results from ionization to $H_2^+ + e$. In region c), however, the spectrum was found to be due to H^+ ion formation. The occurrence of atomic H^+ ions in this region is accounted for by predissociative decay $H_2^* \rightarrow H(n=1) + H(n=2)$ and subsequent photoionization of the H(n=2) atoms by the UV radiation $H(n=2) + UV \rightarrow H^+ + e$. The photoionization of H(n=2) atoms has been observed by us previously [17].

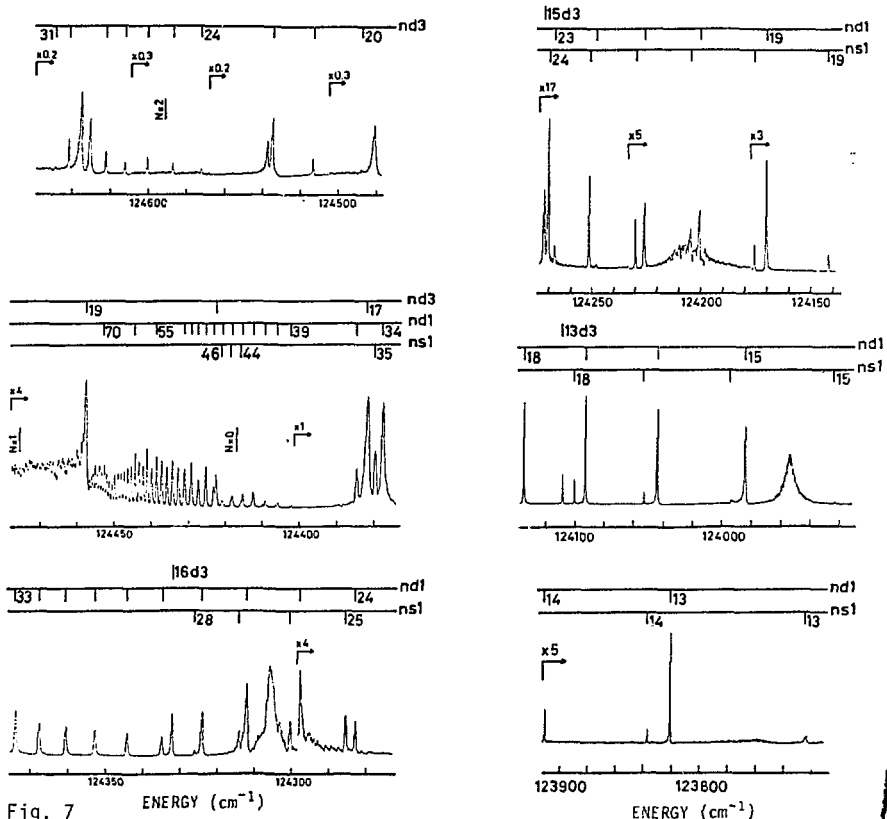

Fig. 7

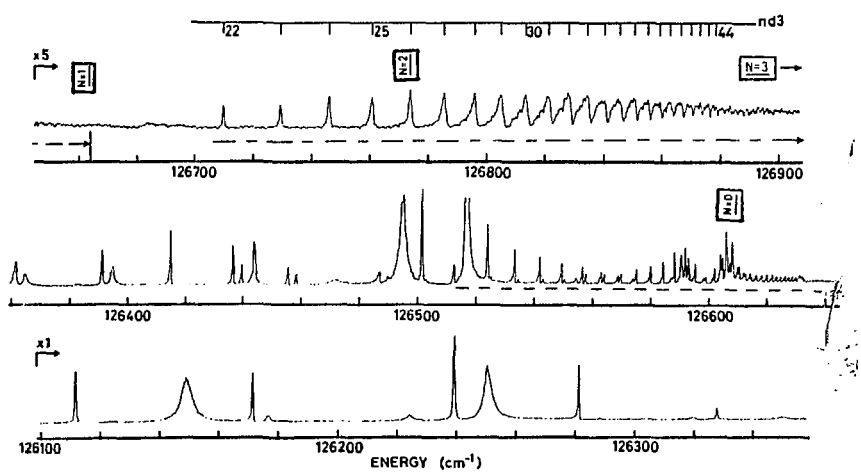

Fig. 8

Figure captions see opposite page

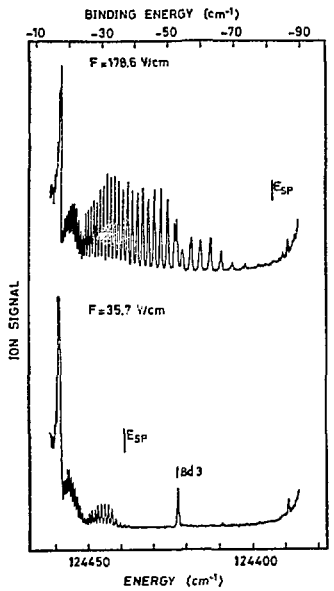

Fig. 9. Field ionization of high Rydberg states in the (nd1) series converging toward the $H_2^+(X,v^+=0, N^+=1)$ + e (εd) limit. Electric field strength: upper spectrum F = 178.6 V/cm, lower spectrum F = 35.7 V/cm.

Using the quantum defect theory we have been able to analyze parts of the spectra. As indicated in Fig. 7, three Rydberg series are identified: ns1, nd1 and nd3, the first two converging toward the $H_2^+(X^2\Sigma_g^+,v^+=0,N^+=1)$ + e and the other one toward the $H_2^+(X^2\Sigma_g^+,v^+=0,N^+=3)$ + e limit. From the J'= 0 level in the intermediate $B^1\Sigma_u^+$ state the total angular momentum of the final H_2^* states must be $J^* = 1$, which allows for the $H_2^+(N^+=1)$ ionization limit only (εs) and (εd) and for $H_2^+(N^+=3)$ only (εd) electrons. Transitions to states converging to the limits $N^+ = 0$ and 2 are not allowed, and in agreement with this not observed. Some of the features in the spectrum have not yet been identified, particularly the broad ones peaking at 124,306, 124,208, 123,955 and 123,760 cm^{-1}. They likely result through perturbations from levels of lower electronic states.

Figure 8 shows a section in the region around the $H_2^+(X^2\Sigma_g^+,v^+=1,N^+=0, 1,2,3)$ + e limits. Here, the ionizing field had no effect on the spectrum, which means all spectral features are due to field-free direct or auto-ionization. Again only final states with $J^* = 1$ can be reached. Accordingly, Rydberg series converging to $N^+ = 1$ and 3 limits are observed. This spectrum, like the one in Fig. 7, shows unidentified lines that do not belong to the $v^+ = 1$; $N^+ = 1,3$ Rydberg series. Like all other

---

Fig. 7. Photodissociation-ionization spectrum of H_2 from the $B^1\Sigma_u^+,v'=0$, J'=0 level in the vicinity of the adiabatic ionization limit, $H_2^+(X^2\Sigma_g^+,v^+=0)$ + e. $H_2(B,v'=0,J'=0\leftarrow X,v''=0,J'=1)$ excitation at P(1) line at 90085.0 cm^{-1}.

Fig. 8. Photoionization spectrum of H_2 from the $B^1\Sigma_u^+,v'=0,J'=0$ level in the vicinity of the ionization limit for $H_2^+(X^2\Sigma_g^+,v^+=1)$ + e. Excitation of (B,v'=0,J'=0) as in spectra in Fig. 7. Underlined parts of spectrum indicate Rydberg series converging toward $N^+=1$ and 3 limits.

lines, they are not found in the one-photon H_2 spectroscopy, since they involve final states of equal parity with the ground state.

4. Conclusions

In the first part of this work we have studied the ionization of the H atom around the ionization threshold in strong electric fields from selected levels of n = 2 Stark manifold, using tunable VUV to excite these intermediate levels. In the ionization spectra the quasi-stable level structure has been observed and investigated in the energy region between the classical field ionization saddle point and the zero-field limit. Also, the oscillatory structure of the ionization cross section around the zero-field and in the continuum region has been observed and studied. The experimental results have been theoretically analyzed and full agreement between experiment and theory is found, as was to be expected for the H atom in electric fields. The studies show the feasibility of analogous experiments with the H atom in strong magnetic fields with dominating diamagnetic external forces. Such experiments, not previously performed, are in progress in our laboratory.

The second part of the work was concerned with first experiments on the photoionization and also photodissociation spectroscopy of the H_2 molecule from selected vibrational-rotational levels in the $B^1\Sigma_u^+$ electronic state. Tunable VUV laser radiation of ~1110 A was employed to excite the intermediate levels in the first step. From there, tunable UV excited the molecules in the second step to the ionization and dissociation region. In this paper, ionization-dissociation spectra are presented in regions of the ionization limits $H_2^+(X^2\Sigma_g^+, v^+=0, N^+=0,1,2,3)$ + e and $H_2^+(X^2\Sigma_g^+, v^+=1, N^+=0,1,2,3)$ + e. The spectra exhibit a wealth of autoionization and predissociation line structures, including also well-developed Rydberg series with states up to n ~ 70. Field ionization has been used to observe part of the high-lying Rydberg states. Rydberg series converging to the ionization limits of $H_2^+(X;v^+=0;N^+=1,3)$ and $H_2^+(X;v^+=1;N=1,3)$ have been analyzed. Other parts of the spectra remain to be analyzed. Since final states of equal parity with the ground state are excited, the spectra, of course, differ essentially from the well-known one-photon He spectroscopy. While one-photon excitation leads to np electrons, the two-photon absorption excites ns and nd electrons in the final states.

References

1. The field has been reviewed extensively. See, for instance: a) J. Phys. Colloque C-2, 43 (1982) on "Atomic and molecular physics close to the ionization threshold in high fields." b) S. Feneuille, P. Jacquinot, Adv. Atom. Mol. Phys. 17, 99 (1981). (c) "Rydberg states of atoms and molecules," eds. R. F. Stebbings and F. B. Dunning, Cambridge Univ. Press (1983). d) C. W. Clark, K. T. Lu, A. F. Starace, Progress in At. Spectr., Part C, eds. H. J. Beyer and H. Kleinpoppen, Plenum, New York (1984).
2. P. M. Koch, Phys. Rev. Lett. 41, 99 (1978).
3. P. M. Koch and D. R. Mariani, J. Phys. B 13, L645 (1980); P. M. Koch and D. R. Mariani, Phys. Rev. Lett. 46, 1275 (1981).
4. R. R. Freeman, N. P. Economou, G. C. Bjorklund and K. T. Lu, Phys. Rev. Lett. 41, 1463 (1978); R. R. Freeman and N. P. Economou, Phys. Rev. A 20, 2356 (1979).
5. W. Sandner, K. A. Safinya and T. F. Gallagher, Phys. Rev. A 23, 2448 (1981).

6. T. S. Luk, L. DiMauro, T. Bergemann and H. Metcalf, Phys. Rev. Lett. 47, 83 (1981).
7. B. E. Cole, J. W. Cooper and E. B. Saloman, Phys. Rev. Lett. 45, 887 (1980).
8. K. H. Welge and H. Rottke, AIP Conference Proceedings No. 119, pp. 213-219 (1984); "Laser Techniques in the Extreme Ultraviolet," eds. S. E. Harris and T. B. Lucatorto, Am. Inst. Phys., OSA, Boulder, CO (1984).
9. H. Rottke and K. H. Welge, XIII Inter. Quant. Electr. Conf., June 18-21, 1984, Anaheim, CA; Technical Digest TUGG5, p. 21 (1984).
10. H. Rottke and K. H. Welge, Chem. Phys. Lett. 99, 456 (1983).
11. S. T. Pratt, T. M. Dehmer and F. L. Dehmer, J. Chem. Phys. 78, 4315 (1983).
12. S. L. Anderson, G. D. Kubiak and R. N. Zare, Chem. Phys. Lett. 105, 22 (1983).
13. F. J. Northrop, J. C. Polanyi, S. C. Wallace and F. M. Williamson, Chem. Phys. Lett. 105, 34 (1984).
14. E. E. Marinero, C. T. Rettner and R. N. Zare, J. Chem. Phys. 80, 4142 (1984).
15. G. Herzberg and Ch. Jungen, J. Mol. Spectr. 41, 425 (1972).
16. H. Rottke and K. H. Welge; Proceedings of CoII. Int. "Collisions Atomiques et Moleculaires dans un Champ Laser," Abbaye de Royaumont, France, March 27-30, 1984 (in press).
17. H. Zacharias, H. Rottke, J. Danon and K. H. Welge, Opt. Comm. 37, 15 (1981).
18. H. Rottke, A. Holle and K. H. Welge, to be published.
19. E. Luc-Koenig and A. Bachelier, J. Phys. B 13, 1743 (1980); ibid., 1769 (1980).
20. D. A. Harmin, Phys. Rev. A 24, 2491 (1981); ibid., 26, 2656 (1982).
21. H. J. Silverstone and P. M. Koch, J. Phys. B 12, L557 (1979).
22. R. J. Damburg and V. V. Kolosov, J. Phys. B 12, 2637 (1979); ibid., 9, 3149 (1976); ibid., 14, 829 (1981).
23. A. R. P. Rau, J. Phys. B 12, L193 (1979).
24. V. D. Kondratovich and V. N. Ostrovskii, JETP 52, 198 (1980).
25. A. R. P. Rau and K. T. Lu, Phys. Rev. A 21, 1057 (1981).
26. H. Rottke and K. H. Welge (to be published).
27. This spectrum is from work by W. Maier, H. Rottke, H. Zacharias and K. H. Welge (to be published).

Multiphoton Ionization Photoelectron Spectroscopy for Excited-State Atoms and Molecules

Katsumi Kimura
Institute for Molecular Science, Okazaki, 444, Japan

1. Introduction

Multiphoton ionization (MPI) is remarkably enhanced, when atoms and molecules are pumped to resonant excited states by visible and UV lasers [1-3]. On the other hand, a photoelectron spectroscopic technique using resonant MPI has been developed to study photoelectron spectra of electronically excited states in this laboratory [4-6] and others [7-11] in the early 1980's. Such laser photoelectron spectroscopy makes it possible to obtain excited-state photoelectron spectra which are very useful for studying dynamic behavior of excited states and ionic states from a new spectroscopic point of view.

One of the remarkable characters of resonant multiphoton ionization is that one-electron ionization transition is always allowed from any excited states. In other words, photoelectrons can be ejected from any excited states by one-electron ionization, if an appropriate laser system is used. In this sense, the range of excited states studied by this method seems to be much wider compared with other spectroscopic methods available for excited states.

Resonant multiphoton ionization under mild laser conditions even by a single laser source may be regarded as a stepwise process, as shown in Fig. 1(a). In this case, it is considered that ionization takes place independently from a specific excited state pumped by the same laser.

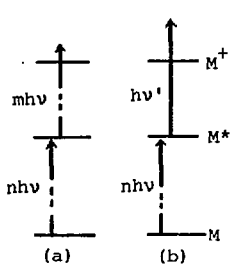

Fig. 1. Resonant multiphoton ionization. (a) One-color (n+m) resonant ionization, and (b) two-color resonant ionization in which the second step is due to a single-photon absorption

Such two-step ionization has been clearly demonstrated from previous MPI photoelectron studies [12-14]. It is desirable to use a single photon for the second step as shown in Fig. 1(b), since if two or more photons are absorbed in the second step

there would always be a possibility of further resonance at a higher excited state. In this sense, two-photon experiments are much more desirable to follow dynamics of excited states.

In this paper I want to emphasize the advantages of multiphoton ionization photoelectron spectroscopy of atoms and molecules, using various examples mostly obtained in this laboratory [12-22].

2. Experimental Technique

The experimental method developed in this laboratory has been reported in detail elsewhere [14,15]. Briefly, the main part of the laser photoelectron spectrometer consists of (1) a main vacuum chamber with a nozzle beam source for introducing a gas sample into the ionization region, (2) a laser system for excitation and ionization, (3) a photoelectron energy analyzer, (4) other detection devices for the total ion current and mass spectrometry, and (5) a data acquisition system. The experimental setup of laser photoelectron spectroscopy is schematically shown in Fig. 2.

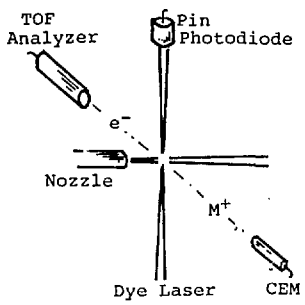

Fig. 2. Schematic drawing for experimental setup of laser photoelectron spectroscopy

In our experiments, tunable dye lasers (5 nsec) pumped by a Nd-YAG laser or a nitrogen laser are used for excitation and ionization in one- and two-color experiments. A time-of-flight energy analyzer (10-12 cm long) is used for photoelectons. Calibration for the photoelectron energy is performed with reference samples, Xe, NO, and atomic Fe [13,14].

3. MPI Ion-Current and Photoelectron Spectra

When the n-photon energy is in coincidence with the energy of a specific excited state, an MPI ion-current spectrum shows a peak which corresponds to a resonant excited state. At the same time, photoelectrons are ejected of course. A photoelectron spectrum thus obtained reflects ionization transition between the resonant state and the ionic state. This situation is demonstrated in Fig. 3. In this paper we mostly consider the process in which ionization takes place by a single photon from the resonant state. If the resonant excited state is too low to ionize by a single photon, two lasers must be used separately for excitation and ionization.

One of the advantages of two-color experiments is that the photoelectron energy can be changed arbitrarily without chang-

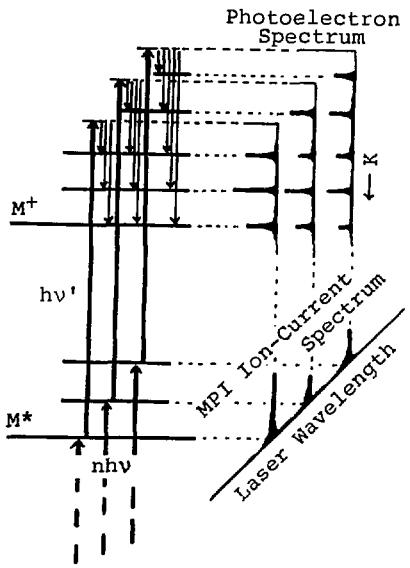

Fig. 3. MPI ion-current spectrum and photoelectron spectra

ing the wavelength of the first, excitation laser. In two-color experiments, photoelectrons due to the first laser alone are more or less mixed with photoelectrons attributed to combination of the two lasers. In actual two-color experiments, therefore, photoelectrons due to the first laser alone and the second laser alone should be subtracted from the whole photoelectrons.

Another important advantage of two-color photoelectron experiments is that autoionization may be distinguished from direct ionization by scanning the second laser wavelength. In other words, it is possible to find out a super-excited autoionizing state from photoelectron spectra by changing the second laser wavelength.

It is definite that MPI ion-current and photoelectron measurements provide very complementary information about resonant multiphoton ionization for atoms and molecules in the gas phase.

4. Number of Photons in Resonant MPI

From photoelectron energies, it is possible to determine the number of photons absorbed in resonant MPI. The number of photons absorbed in ionization is not always the minimum, depending on the laser power used. It is essentially important to know the photon number for identifying ionic states, as well as for interpreting photoelectron spectra. Under mild laser conditions, photoelectrons due to the minimum photon number have been observed in resonant MPI [6-22]. However, this is not self-evident unless photoelectron measurements are carried out.

If the energy of the minimum photons of ionization is in accordance accidentally with a super-excited state of the

parent species, absorption of an additional photon is enhanced to produce further photoelectrons with the energy of K + hν, where K is the photoelectron energy due to the minimum photons.

Let us here mention an example for such double resonance. When NO molecule is ionized through a specific vibrational rotational level of the two-photon resonant B state (for example, $v' = 9$, Q_{22}, $J' = 6\ 1/2$), a photoelectron band due to $v^+ = 6$ is observable by additional photon absorption from the super-excited state (assigned to the Rydberg N state at the $v'=6$, $N'=6$ level located above the ionization threshold, in addition to a series of photoelectron bands of $v^+ = 0$, 1, and 2 produced by the three, minimum photons [22]. It has also been indicated that the photoelectron band intensity due to double resonance is more sensitive to the laser power than the intensities of normal photoelectron bands.

Hydrogen sulfide (H_2S) is ionized by three photons through two-photon resonant Rydberg excited states in the laser wavelength region 420 - 455 nm. From a photoelectron study [12], it has been suggested that ionic photofragmentation of this molecule to HS^+ and S^+ takes place by additional photon absorption from the ground-state ion (H_2S^+) at vibrational levels of $v^+ = 0$ and 1, respectively.

5. Identification of Resonant Intermediate States

Resonant excited states in MPI are not always determined unambiguously from MPI ion-current spectra. In resonant three-photon ionization, for example, it is sometimes not possible to distinguish the processes of (1 + 2), (2 + 1), and (1 + 1 + 1) from one another. The third process is due to an accidental double resonance. However, these processes may clearly be distinguished by carrying out two-color photoelectron experiments.

As mentioned before, one-electron direct ionization from a resonant intermediate state probably provides a simple, but important idea to identify the resonant state on the basis of well-defined ionic states.

The photoelectron spectrum of resonant ionization for a molecule is governed by Franck-Condon factors between the resonant and the ionic state. If the equilibrium geometry of the ionic state is almost the same as that of the excited state, a selection rule of $\Delta v \approx 0$ ionization transition is expected to hold. Thus there should always exist a vibrational correlation between the ionic and the excited state for any molecule. Such vibrational correlation is also important to identify the resonant excited state.

Molecular ionic states for a great number of compounds have been already identified from HeI photoelectron spectroscopic studies [23]. These informations should be useful for identification of resonant excited states in MPI.

6. Identification of Ionic States

The advantage of photoelectron spectroscopy is that information about ionic states can be obtained directly from photoelectron energies and intensity distributions. Let us consider a single-photon ionization of a resonant excited state. As shown in Fig.

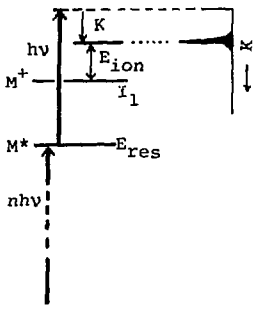

Fig. 4. Energy level diagram relevant to resonant MPI photoelectron spectroscopy

4, the kinetic energy of a photoelectron (K) is simply converted to the internal energy of the corresponding ionic state (E_{ion}) with respect to the first ionization potential (I_1) by the relationship $K = h\nu - I_1 - E_{ion} + E_{res}$, where E_{res} is the energy of the resonant state. For molecules, I_1 means the adiabatic ionization potential.

On the other hand, the intensity of a photoelectron band directly depends on the ionization cross-section for producing an ionic state, involving the electronic and vibrational wavefunctions of both the resonant and the ionic state. The probability of producing an identical ionic state is generally different from one resonant state to another, depending on selection rules of ionization transition. If we select a specific excited state as a resonant state in MPI, then we may selectively produce a specific ionic state that may not be produced from the neutral ground state by conventional VUV photoelectron spectroscopy.

Ionization of a Rydberg electron in an atom and molecule gives rise to the ion which has the same electron configuration as the core of the Rydberg state. It would also be possible to remove another electron from an inner shell in a Rydberg excited state. In this case, it should be mentioned that an excited-state ion is produced which cannot be formed by one-electron direct ionization from the nuetral ground state. A similar situation also occurs in the case of direct ionization from a valence excited state.

Information about vibrational modes and frequencies of ionic states for molecules can also be obtained in detail from laser photoelectron spectroscopy, if the vibronic level selected as a resonant state is well identified. Various vibrational levels of ionic states thus may selectively be studied by this technique. Such studies have been reported on benzene and its related compounds [24,25].

7. Ionization Selectivity

Ionization selectivity is itself not a special selection rule, but there are many interesting features for ionization transitions of electronically excited states. In this section, let us mention a few examples for ionization selectivity in resonant MPI.

When Xe is ionized by VUV radiation from the ground state, it is known that two ionic states $^2P_{3/2}$ and $^2P_{1/2}$ are produced [23]. However, when Xe is ionized at a laser wavelength of 363.9 nm by

(3+1) resonant ionization through the $5d[2\ 1/2]^0_3$ Rydberg state which has the $^2P_{3/2}$ core, a single photoelectron peak due to the $^2P_{3/2}$ ionic state is observed [16]. This fact suggests that removal of the Rydberg electron does not induce relaxation of the core electrons. This is consistent with the consideration of single-electron ionization.

The second example to be mentioned is the (2+1) resonant ionization of NO molecule through the B state which is the excited valence state expressed by $(5\sigma^2 1\pi^3 2\pi^2)$. The ground state of NO^+ is expressed by $(5\sigma^2 1\pi^4)$, so that formation of the ground-state ion requires such a two-electron transition in which one electron is removed and another electron excited. Actually the ground-state NO^+ is not formed by direct ionization from the B state of NO, but produced only by autoionization, if we select a vibrational level of $v' = 9$ of the B state as a resonant state [22], since there is no appreciable mixing with other electronic states.

Another interesting example is the resonant ionization of an organic molecule, which has both π and nonbonding (n) orbitals. When the molecule is ionized through the $n\pi^*$ and the $\pi\pi^*$ excited states, it is expected that the ionic states of n^{-1} and π^{-1} are mainly produced by one-electron direct ionization scheme. This correlation may be very useful for identifying $n\pi^*$ excited states in many organic compounds.

Spin-orbit splitting in laser photoelectron spectra has been clearly seen for atomic iron which is produced by photodecomposition of $Fe(CO)_5$ molecule [13]. Removal of an electron from, for example, the 5s orbital of the excited e^7D_3 state gives rise to photoelectron peaks due to the J = 5/2, 7/2, and 9/2 levels of the a^6D_J of Fe^+. The strongest photoelectron peak appears at $J = J' - (1/2)$, where J' is the J number of the excited state [13].

Vibrational photoelectron pattern in a photoelectron spectrum of an excited state is governed by the Franck-Condon principle which correlates vibrational functions between the resonant excited and the ionic state. Photoelectron spectra obtained by (3+1) resonant ionization of ammonia molecule through different vibrational levels of the Rydberg C' state show sharp prominent peaks due to $\Delta v = 0$ ionization transitions [14]. This is a typical case in which the equilibrium geometry of the excited state is almost the same as that of the ionic state.

8. Applications

(A) Autoionization Very recently, a laser photoelectron spectroscopic study of NO molecule has been carried out to study autoionization pathway through dissociative super-excited valence states [22]. Many rotational levels of the $v'=9$ vibrational state of the valence excited $B\ ^2\Pi$ state (designated hereafter B-9) of NO were selected as two-photon resonant states. The B-9 state was selected to remove a possibiltiy of direct ionization of producing the ground-state NO^+ ion for the reason already mentioned. The following results have been obtained [22].

An ion-current spectrum for the B-9 region shows several intensity-anomalous rotational lines as well as normal Q-branch

rotational lines. A photoelectron spectrum obtained for one of the normal rotational line shows three energetically accessible vibrational bands with branching ratios of 0.65 ($v^+ = 2$), 0.30 ($v^+ = 1$) and 0.05 ($v^+ = 0$), whereas a photoelectron spectrum obtained for the intensity-anomalous rotational line indicates a relatively high yield of the $v^+=0$ ion in addition to the $v^+=0$, 1, and 2 bands. From these results the following conclusions have been deduced.

The overall process of producing the normal rotational lines is represented by $X + 2h\nu \rightarrow B\text{-}9$; $B\text{-}9 + h\nu \rightarrow I^* \longrightarrow NO^+$, where I^* is the super-excited valence I state and $\longrightarrow$ indicates electronic autoionization forming the ground-state ion. On the other hand, the ionization scheme of producing the intensity-anomalous rotational lines is expressed by $X + 2h\nu \rightarrow B\text{-}9$; $B\text{-}9 + h\nu \rightarrow N\text{-}6 \longrightarrow B'^* \rightsquigarrow NO^+$, involving an accidental double resonance, where N is the Rydberg N state, B'^* is the valence excited B′ state, and $\rightsquigarrow$ means an electronic coupling between the Rydberg and the valence states. Therefore, it has been found that an additional one-photon absorption from the two-photon resonant B-9 state leads selectively to production of the specific super-excited valence state at which autoionization takes place [22].

(B) Intramolecular Vibrational Redistribution (IVR) The IVR process can also be studied by means of the resonant MPI photoelectron technique. A recent photoelectron study [17] for (1+1) resonant ionization of benzene through its excited S_1 state indicates the following results: (1) Vibrationally resolved bands are observed by excitation through low vibronic S_1 levels. (2) The spectrum becomes broad with increasing excitation energy. (3) The vibrational structure mostly disappears for vibronic levels above ca. 5000 cm^{-1}.

From these results, it is suggested that the excitation of benzene at the vibronic levels above the onset of the "channel three" is followed by IVR within the S_1 state [17]. There seem to be no decay channels faster than this IVR process up to 5000 cm^{-1} at the first decay stage. Furthermore, the ionization rate of the S_1 state of benzene has been estimated to be the order of $10^{10\text{-}11}$ s^{-1} under experimental conditions used [17].

Since the up-pumping ionization transiton from resonant intermediate states should in principle compete with IVR proceses, it will be possible to study rapid picosecond processes by using a nanosecond pulse laser under suitable laser power conditions [15,17].

An evidence for fast IVR within the E_{1u} state has also been obtained from laser photoelectron spectroscopy [15]. When benzene is ionized by four photons through the two-photon resonant B_{2u} state, single prominent photoelectron bands due to $\Delta v=0$ ionization transitions are observed, and the prominent peak is shifted with increasing photon energy by $K = h\nu$ - const. This simple relationship suggests that the third photon is resonant with another excited state which is assignable to the E_{1u} state from energy consideration. Therefore, it has been concluded that fast IVR takes place at the third-photon states within the E_{1u} state, followed by the ionization from vibrationally relaxed levels [15].

Naphthalene molecule has been studied by (1+1) resonant ionization through various vibronic levels of the S_1 and S_2 states [21]. Different vibrational patterns have been observed in photoelectron spectra, depending on the vibronic character of the optically prepared states. The conclusions deduced are the following. (1) For fairly low vibronic levels (< ca. 2000 cm^{-1}) of S_1, vibrational bands of the cation are observed, due to $\Delta v = 0, \pm 1, \ldots$ ionization transitions from the optically prepared S_1 levels. (2) For higher vibronic levels (>ca. 2000 cm^{-1}), broad photoelelctron bands are observed which cannot be explained by ionization from the optically prepared vibronic levels. It is suggested that IVR competes with ionization under the laser conditions used. (3) For the origin region of S_2, a broad photoelectron band appears, suggesting that the electronic relaxation faster than ionization from the optically prepared S_2 state occurs to produce vibrationally redistributed S_1 vibronic levels.

(C) van der Waals Complex and Hydrogen Bonded Complex Photoelectron spectra for (2+1) resonant ionization of Ar-NO van der Waals complex through the Rydberg C state have been studied in a supersonic free jet [18]. An ion-current spectrum obtained for Ar-NO in the laser wavelength region 383-385 nm shows a vibrational progression attributable to the resonant excited state expressed by $Ar\text{-}NO^*(C)$, slightly shifted to the longer wavelength compared with the corresponding spectrum of free NO molecule. From the photoelectron spectra obtained at the ion-current peaks, the adiabatic ionization potential of Ar-NO has been determined to be 9.148 ± 0.005 eV. Furthermore, the dissociation energies of $Ar\text{-}NO^*(C)$ and $Ar\text{-}NO^+(X)$ have been found to be 0.058 ± 0.001 and 0.132 ± 0.005 eV, respectively [18].

It has also been found that no photoelectron spectra are detected for the Rydberg A state, $Ar\text{-}NO^*(A)$, under the laser conditions used [18]. This is in contrast to the Rydberg C state. Dissociation of $Ar\text{-}NO^*(A)$ is considered to be much faster than ionization, since its potential curve is probably shifted so that the repulsive wall lies above the minimum of the ground-state potential.

Several hydrogen bonded complexes of phenol and 7-azaindole in a supersonic jet have been studied by (1+1) photoelectron spectroscopy through the S_1 states,as well as by two-color ionization threshold spectroscopy [19]. For the phenol-$(H_2O)_n$ clusters, where $n = 0$, 1, and ≥ 4, the observed adiabatic ionization potentials (I_a) are 8.49, 8.09, and 8.05 ev, respectively. The observed reduction of I_a due to complex formation has been ascribed to stabilization of the ionized cluster [19].

Similar laser photoelectron spectroscopic studies on simple molecules such as H_2 and CO have been reported in detail [26,27]. A photoelectron angular distribution also provides important information on resonant MPI. In the course of the MPI photoelectron studies of atoms and molecules in this laboratory [13, 14,16], angular distribution measurements have also been carried out, although not mentioned here. Photoelectron angular distribution of resonant MPI has been reviewed in detail from a theoretical point of view [28].

9. Conclusions

The technique of resonant MPI photoelectron spectroscopy is a highly selective analytical diagnostic tool for excited-state atoms and molecules, and applicable to higher excited states which cannot be studied by fluorescence spectroscopy. The time-of-flight electron analyzer has a good resolution (several meV) for the low-energy photoelectrons which are mostly produced in laser photoelectron spectroscopy. Therefore, this technique has a high ability for molecular spectroscopy of excited states. Although a ns laser has so far been used for excitation and ionization, the use of a ps laser will make it possible to follow faster processes of excited states with ps lifetimes.

Acknowledgments

The author would like to thank Dr. Y. Achiba and Mr. K. Sato, for their patient cooperation for the development of the laser photoelectron spectroscopy of resonant multiphoton ionization.

References

1 P. M. Johnson, Acc. Chem. Res. 13, 20 (1980)
2 P. M. Johnson and C. E. Otis: Ann. Rev. Phys. Chem. 32, 139 (198)
3 V. S. Letokhov: Nonlinear Laser Chemistry (Springer-Verlag, Berlin 1983)
4 Y. Achiba, K. Shobatake, and K. Kimura: "Construction of an Apparatus for Studying Multiphoton Ionization Electron and Mass Spectroscopy", in Annual Review (Institute for Molecular Science, Okazaki, 1980), p.100
5 Y. Achiba, K. Sato, Y. Shindo, and K. Kimura: "Construction of a Time-of-Flight Electron Analyzer for Laser Ionization Photoelectron Spectroscopy", in Annual Review (Institute for Molecular Science, Okazaki, 1981), p. 105
6 Y. Achiba, K. Sato, K. Shobatake, and K. Kimura: J. Photochem. 17, 53 (1981)
7 R. N. Compton, J. C. Miller, A. E. Carter, and P. Kruit: Chem. Phys. Lett. 71, 87 (1980)
8 F. Fabre, P. Agostini, G. Petti, and M. Clement: J. Phys. B 14, L677 (1981)
9 J. T. Meek, R. K. Jones, and J. P. Reilly: J. Chem. Phys. 73, 3503 (1980)
10 G. J. Fisanick, A. Gedanken, T. S. Eichelberger IV, N. A. Kuebler, and M. B. Robin: J. Chem. Phys. 75, 5215 (1981)
11 P. Kruit, J. Kimman, and M. J. van der Wiel: J. Phys. B. 14, L597 (1981).
12 Y. Achiba, K. Sato, K. Shobatake, and K. Kimura: J. Chem. Phys. 77, 2709 (1982)
13 Y. Nagano, Y. Achiba, K. Sato, and K. Kimura: Chem. Phys. Lett. 93, 510 (1982)
14 Y. Achiba, K. Sato, K. Shobatake, and K. Kimura: J. Chem. Phys. 78, 5479 (1983)
15 Y. Achiba, K. Sato, K. Shobatake, and K. Kimura: J. Chem. Phys. 79, 5213 (1983)
16 K. Sato, Y. Achiba, and K. Kimura: J. Chem. Phys. 80, 57 (1984)
17 Y. Achiba, A. Hiraya, and K. Kimura: J. Chem. Phys. 80, 6047 (1984)
18 K. Sato, Y. Achiba, and K. Kimura: J. Chem. Phys. 81, 57 (1984)

19 K. Fuke, H. Yoshiuchi, K. Kaya, Y. Achiba, K. Sato, and K. Kimura: Chem. Phys. Lett. 108, 179 (1984)
20 K. Kimura: Adv. Chem. Phys. (in press)
21 A. Hiraya, Y. Achiba, N. Mikami, and K. Kimura: J. Chem. Phys. (to be published)
22 Y. Achiba, K. Sato, and K. Kimura: J. Chem. Phy. (to be published)
23 K. Kimura: Handbook of HeI Photoelectron Spectra of Fundamental Organic Molecules (Japan Scientific Societies Press, Tokyo; Halsted Press, New York, 1981)
24 S. R. Long, J. T. Meek, and J. P. Reilly, J. Chem. Phys. 79, 3206 (1983)
25 S. L. Anderson, D. M. Ridev, and R. N. Zare, Chem. Phys. Lett. 93, 11 (1982)
26 S. T. Pratt, E. D. Poliakoff, P. M. Dehmer, and J. L. Dehmer, J. Chem. Phys. 78, 65 (1983)
27 S. T. Pratt, P. M. Dehmer, and J. L. Dehmer, J. Chem. Phys. 78, 4315 (1983)
28 S. N. Dixit and P. Lambropoulos, Phys. Rev. A 27, 861 (1983)

2-Step Photoionization of Benzene: Mechanism and Spectroscopy

G. Müller, K.L. Kompa, and W.E. Schmid
Max-Planck-Institut für Quantenoptik, D-8046 Garching, Fed. Rep. of Germany

J.L. Lyman
Los Alamos National Laboratory, Los Alamos NM 87545, USA

S. Trushin
Institute of Physics, BSSR Academy of Sciences, Minsk, USSR

Some results are summarized on the UV-laser-induced resonant 2-photon-ionization of the benzene molecule. The discussion starts with the general excitation and fragmentation behaviour including some work with psec laser pulses and goes on to spectroscopic information obtained by measurements of fluorescence from the intermediate (1 photon-resonant) states and comparative measurements of ion currents.

1. Introduction and Background

Resonant 2-photon ionization is the simplest and at the same time most efficient multiphoton ionization process. Absorption of the first photon leads to a real electronic state from which the second photon produces an ion. In the common notation of molecular spectra the process reads $S_o \xrightarrow{h\upsilon_1} S_1 \xrightarrow{h\upsilon_2}$ ion. Fluorescence from S_1 back to S_o competes with the second step as well as radiationless relaxation and possibly photochemistry of S_1. The ion thus formed can usually again undergo photon absorption changing its spectroscopic state and even its chemical identity. Since no virtual states are involved in all the excitation steps high ion yields are the rule. At least in the first step state selective excitation is possible.

The ionization energy of the benzene molecule is $E_{ion} \cong 9.241$ eV $\sim 74000\ cm^{-1}$ and S_1 lies at approximately half this energy. We therefore consider 2-step ionization of benzene with wavelengths $h\upsilon_1, h\upsilon_2$ around 260 nm. The first experiments with the use of UV lasers (although dealing with molecules other than benzene) were reported by Rockwood et al. /1/. This was extended to a mass spectrometric study by Reilly et al. /2/ looking mainly at secondary fragmentation processes in a time-of-flight mass spectrometer and determining the experimental parameters for optimum ion yields. The rather simple experimental scheme and a typical result are reproduced in Fig. 1. The lasers used there were simple KrF and ArF excimer lasers. The observed mass spectra exhibit certain characteristics not found in conventional mass spectra. These properties may be utilized potentially in the development of a mass spectrometric ion source based on this principle. While other groups did more extensive work along this direction /3,4,5/ a contribution to be mentioned here concerns the use of a psec laser which eliminates some of the complications with secondary ion fragmentation. Mass spectra were recorded with a 20 psec (quadrupled Nd-YAG) UV laser source. This experiment was suggested by theoretical treatments of the process /6,7,8/, among other approaches using a phase space model /8/. As expected by RRKM considerations of fragmentation timescales the sequence of ion photodissociation events can be intercepted by sufficiently short laser pulse durations. Fig. 2 exemplifies this point.

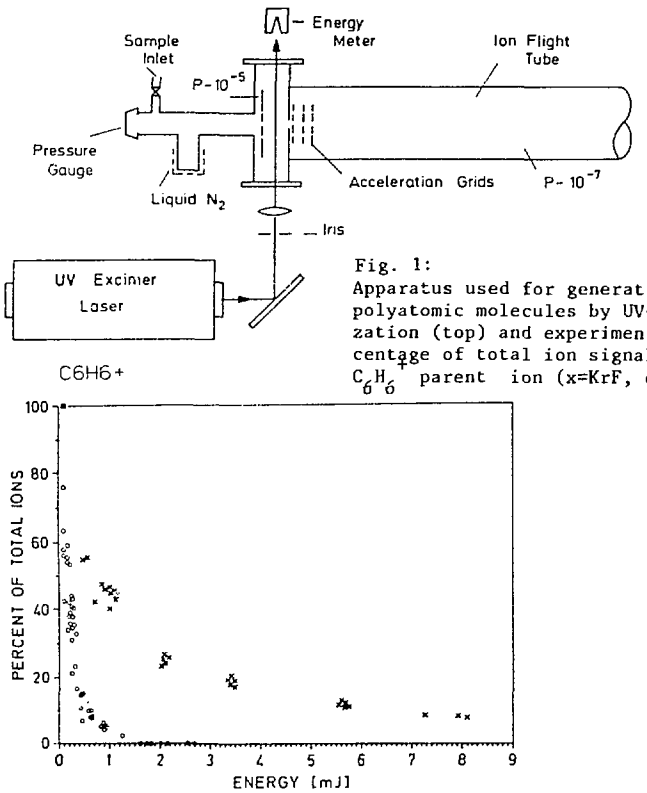

Fig. 1:
Apparatus used for generating mass spectra of polyatomic molecules by UV-laser-induced ionization (top) and experimentally observed percentage of total ion signal represented by the $C_6H_6^+$ parent ion (x=KrF, o=ArF laser)

The results at this point suggest the use of laser-induced 2-photon ionization of polyatomic molecules as a technique in

(1) molecular spectroscopy (spectral dependence of ionizing step, lifetimes of intermediates)
(2) mass spectrometry (ion yield, spectral dependence, fragmentation pattern, predictability of ionization characteristics)
(3) photochemistry (cold ions, well defined ionic states, role of neutral fragments in addition to ions).

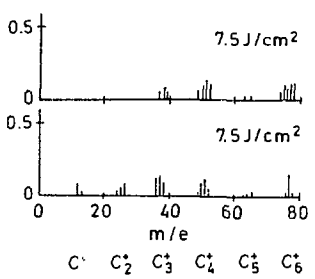

Fig. 2:
Mass spectra of benzene induced with single or multiple Nd-YAG laser pulses. Top spectrum 1 pulse, 20 psec, bottom spectrum 4 pulses. The upper spectrum shows the absence of smaller mass peaks due to missing secondary fragmentation. The lower spectrum closely resembles the results obtained with nsec lasers /9/

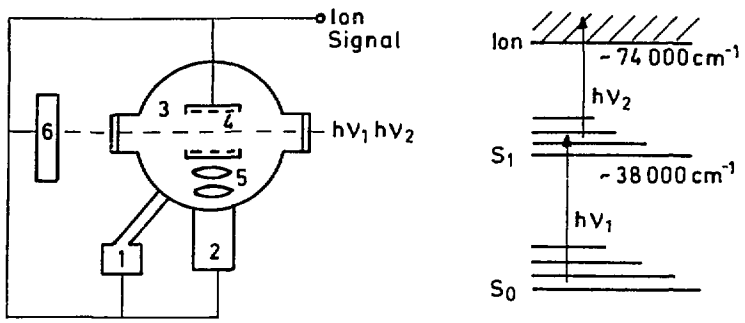

Fig. 3: Experimental diagram and principal spectroscopic scheme for ionization spectroscopy of benzene with one or two (excimer-laser-pumped) dye laser frequencies (1 manometer, 2 photomultiplier, 3 gas cell containing ~ 10^{-3} mbar of benzene, 4 electrodes with shielding, 5 collecting optics, 6 linear diode array as beam detector)

The experiment to be described in the next paragraph consists of a measurement of fluorescence and ion currents as function of the two wavelengths $h\upsilon_1$ and $h\upsilon_2$. A schematic diagram is shown in Fig. 3.

2. Results and Discussion

A rate equation treatment may be used in a first attempt to quantify the relationship between excitation, fluorescence and ionization:

$$\frac{dN_o}{dt} = -\sigma_{ex}^r \cdot I(t)/h\cdot r \cdot (N_o - N_1)$$

$$\frac{dN_1}{dt} = \sigma_{ex}^r \cdot I(t)/h\cdot r\cdot(N_o - N_1) - (k_r + k_{nr})N_1 - \sigma_{ion}\cdot I(t)/h\cdot r\cdot N_1$$

$$\frac{dN_2}{dt} = \sigma_{ion} \cdot I(t)/h\cdot r\cdot N_1 \ .$$

$N_{o,1,2}$ are the corresponding population densities, σ_{ex}^r and σ_{ion} are the real absorption and the ionization cross section, $k_{r,nr}$ are the radiative and non-radiative rate constants and I(t) is the intensity profile in time of the laser. This set of rate equations cannot be solved in closed form. However, approximate solutions can be given if saturation effects may be excluded. Based on this approach a direct evaluation of σ_{ion} was possible for excitation on the $6_o^1 16_1^1$ transition in $S_o \rightarrow S_1$. The phenomenological absorption cross section there is $\sigma_{ex}^{ph} = 1.3\cdot10^{-18}$ cm^2. Figs. 4a and b show the measured plots of fluorescence and ion signal. The fluorescence shows the linear behaviour expected on the basis of the above equations while the ion signal shows neither linear dependence as function of pressure nor quadratic dependence as function of energy. This is explainable on the assumption that less than the original number of ions is seen, which points to substantial ion-electron recombination. The only way to consider this effect within the boundary conditions of the experiment is by numerical compensation. We will skip the details of this treatment here and report that the cross section for ionisation from 6'16' in S_1 at λ = 260.08 nm is

$$\sigma_{ion} = 2.5 \pm 0.5 \cdot 10^{-17} \text{ cm}^2 \ .$$

This is a remarkably high value and maybe compared on the one hand to an

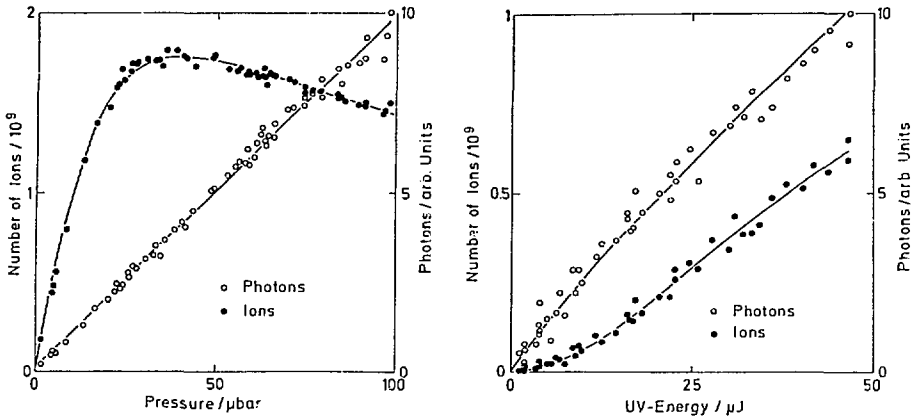

Fig. 4: Plots of measured fluorescence and ion signals as function of benzene pressure (a) and UV laser energy (b)

estimate for benzene ionization with KrF laser light (248 nm) of $\sigma_{ion} \sim 2 \cdot 10^{-18}$ cm^2 /10/. On the other hand a figure for aniline has been given with $\sigma_{ion} = 3.5 \pm 0.8 \cdot 10^{-17}$ /11/ which is somewhat closer to our measurement.

The ionization cross sections for threshold ionization are wavelength dependent. This question will be addressed below. Before, however, a comparison between fluorescence and ion spectra in the band 6_1^o appears appropriate (see Fig. 5).

It is apparent that with the appropriate corrections the LIF and ion spectra agree very well in this wavelength range. This is an important

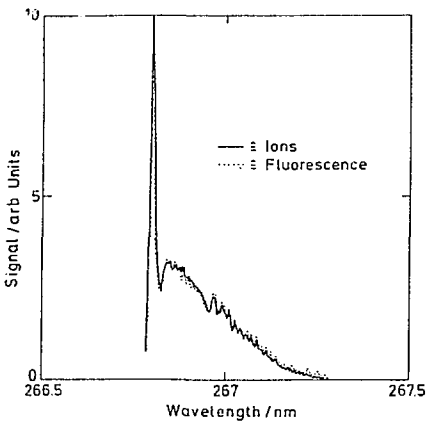

Fig. 5: LIF spectrum and corrected 2-step ionization spectrum of the rovibronic band 6_1^o of the $S_o \rightarrow S_I$ transition

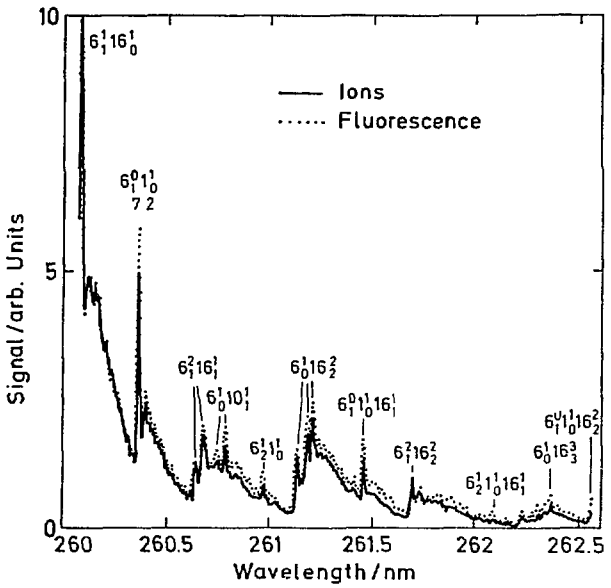

Fig. 6: LIF and ionization spectrum of benzene in the wavelength range 260 - 262.5 nm

conclusion demonstrating that the spectral structure is determined solely by the first excitation step and that the ionizing step adds no particular spectral dependence. This identity of LIF and ion spectra, however, does not prevail in all wavelength ranges as can be seen by looking at the range 260 - 262.5 nm (Fig. 6). While the number and positions of the bands is still the same in both cases their respective intensity is different. Reasons for that may be suspected in the influence of S_1 radiational lifetimes or fluorescence quantum yields as well as in an intrinsic variation of the ionization cross section with the S_1 vibrational levels. In an enlarged part of Fig. 4 (Fig.7) it becomes apparent that ionization is less probable from S_1 vibrational levels with υ_1 participation. Strongly increased ion signals are observable in the region of $6_1^2 16_2^2$ and there is a stronger variation in comparison to LIF for the angular momentum components within a given band (e.g. $6_1^2 16_2^2$). Skipping all the details here we wish to suggest a possible explanation for the observed effects in Franck-Condon type arguments concerning the potential minima of the states with respect to each other and the bonding nature of the electron liberated in the ionization process (Fig.8). The alternative suggestion would consider autoionization contributions for instance from Rydberg states. Since the observed effects in Figs. 6 and 7, however, are due to 2-step excitation by the same laser wavelength such an accidentally resonant process is highly unlikely. In the then assumed direct ionization the probability of ionization, going from states V'' in S_1 to V' in the ion, is ($E'_{vib}(V') < E_{ex}$)

$$P = \sum_{v} \langle v'v'' \rangle \ .$$

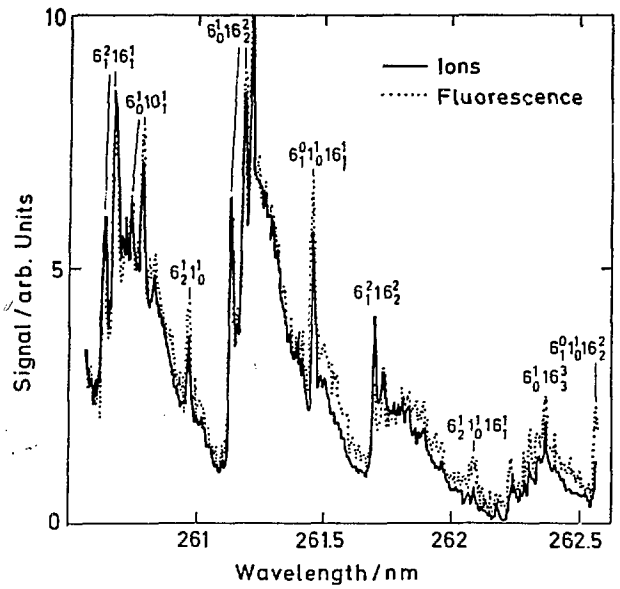

Fig. 7: Blow up of part of Fig. 6 showing the diminished ionization from υ_1 vibronic states.

This makes P a monotonically growing function of E_{ex}, lim(P) = 1. Taking the electron out of the highest occupied valence orbital in the neutral molecule leaves an unpaired e_{1g} electron which defines the symmetry of the ion as e_{1g}. Perturbation by Jahn-Teller forces must be considered. The distorted structure may have point group D_{2h} rather than D_{6h}. Such potential shifts are only possible in the direction of totally symmetric coordinates ($\upsilon_1, \upsilon_2, \upsilon_6, \upsilon_7, \upsilon_8, \upsilon_9$). In a recent paper on photoelectron spectroscopy of benzene Jahn-Teller parameters for the mode υ_6 in the ion were reported /12/.

Although the vibronic potential surface for the benzene ion is not known in any degree of detail some information can be obtained with regard to the υ_1 normal coordinate by comparing suitable bands, e.g. 6_1^0 and $6_1^1 1_0^1$ which show no Jahn-Teller effects in S_1. The vibrational frequency of υ_1 in the ion is 976 cm^{-1}, rather similar to the ground state vibration (993.1 cm^{-1}) while in S_1 it is only υ_1 = 923 cm^{-1}. The measured (and corrected) ratio of the ionization cross sections for the two bands mentioned above $6_1^1 1_0^1$ and 6_1^0 is 0.80 ± 0.05. The corresponding excess energies in the ion are 2890 cm^{-1} and 1040 cm^{-1}. This can be rationalized in terms of a potential shift in going from S_1 to the ion (Fig. 8). This is to say that Franck-Condon overlap becomes small for vibrations influenced by the bonding character of the excited electron. While in S_1 this electron is antibonding (pointing to a weak bond or large internuclear separation in this case, see Fig. 8) it becomes non-bonding in the ion, reversing the bond energy trend again.

The results reported here exemplify the possibility to obtain spectral information on molecular ions and to study ionization mechanisms. Be-

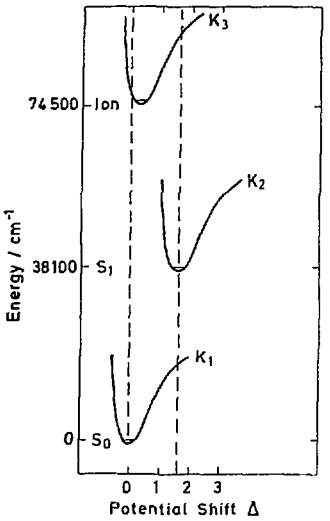

Fig. 8

Fig. 9

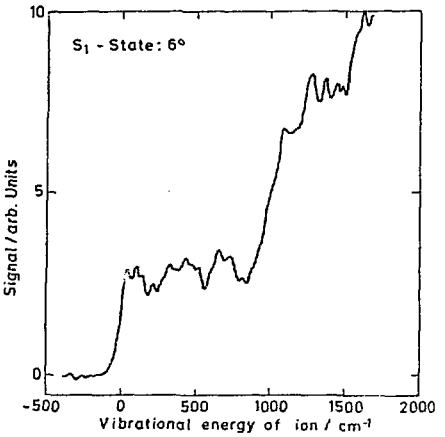

Fig. 8: Relationship of υ_1 potential surfaces in S_o, S_1 and ion

Fig. 9: Ionization spectrum of benzene from state 0° in S_1. The increasing ion yield as function of accessibility of increasing number of ion vibrational levels is obvious

sides this spectroscopic perspective there is clearly the possibility to introduce this highly selective and sensitive ionization technique into mass spectrometry. Experiments are in progress in both directions. As an outlook to these studies a recent result will be mentioned where the single laser (Fig. 3) used so far is replaced by two independently tunable sources. One laser then populates a defined vibronic level in S_1, the second one is tuned to vary the ion excess energy from threshold up to any desired value. The two lasers can also be delayed with respect to each other. The remaining experimental details are as shown in Fig. 3. First results confirm the dominating direct ionization and the influence of Jahn-Teller distortion in the mode υ_6. A photoionization spectrum of benzene out of 0° in S_1 is given in Fig. 9. A detailed discussion is beyond the scope of this brief summary but the vibrational structure of the ion to be correlated with the steps in the plot of ion yield versus excess energy is apparent /13/.

Based on these results an cold beam ion source has also been constructed and will be employed in LIF studies of ions as well as in the study of ion molecule reactions. Results will be published at a later date /14/.

References

1 S.D. Rockwood, J.P. Reilly, K. Hohla, K.L. Kompa, Opt. Comm. 28, 175 (1979)

2 J.P. Reilly, K.L. Kompa, J. Chem. Phys. 73, 5468 (1980)
3 D.A. Lichtin, L. Zandee, R.B. Bernstein, in Lasers in Chemical Analysis, Ed. by G.M. Hieftje, J.C. Travis, F.E. Lytle, The Humana Press, Clifton, N.J., 1981
4 V.S. Antonov, V.S. Letokhov, Appl. Phys. 24, 89 (1981)
5 U. Boesl, H. Kühlenwind, H.J. Neusser, E.W. Schlag, this volume
6 J. Silberstein, R.D. Levine, J. Chem. Phys. 75, 5735 (1981)
7 W. Dietz, H.J. Neusser, U. Boesl, E.W. Schlag, S.A. Lin, Chem. Phys. 66, 105 (1082)
8 F. Rebentrost, A. Ben-Shaul, J. Chem. Phys. 74, 3255 (1981) F. Rebentrost, in Laser Applns. in Chemistry, Eds. K.L. Kompa, J. Wanner, Plenum Publishing Corp., 1984
9 P. Hering, A.G.M. Maaswinkel, K.L. Kompa, Chem. Phys. Lett. 83, 222 (1981)
10 V.S. Antonov, V.S. Letokhov, A.N. Shibanov, Zh. Eksp. Theor. Fiz. 78, 2222 (1980)
11 J.H. Brophy, C.T. Rettner, Chem. Phys. Lett. 67, 351 (1979)
12 J.T. Meek, K.S. Viswanathan, E.Sekreta, J.P. Reilly, this volume
13 G. Müller, J.Y. Fan, J.L. Lyman, W.E. Schmid, K.L. Kompa, to be published
14 D. Proch, T. Keiderling, K.L. Kompa, T. Trickl, to be published

Multiphoton Ionization Spectroscopy of Surface Molecules

Vladimir S. Antonov and Vladilen S. Letokhov

Institute of Spectroscopy, USSR Academy of Sciences
SU-142092 Troitsk, Moscow Region, USSR

1. Introduction

The method of resonant multiphoton ionization (MPI) of molecules, which has been extensively developed in the last few years, is now widely used for the purposes of spectroscopy and detection of free molecules in the gas phase [1,2]. On the other hand, investigations into the laser-induced surface processes (production of free ions in particular) are constantly gaining in importance to the spectroscopy and analysis of surface. As applied to surface studies, most experiments involving the use of laser radiation were conducted in conditions of intense surface heating, wherein free ions were formed as a result of thermal and chemical ionization [3]. In this respect, laser resonant molecular photoionization is an alternative approach which, thanks to its high efficiency, could have considerable promise for the spectroscopy of surface. This is borne out by the high rise of ion and electron signal intensities observed in MPI experiments whenever the laser radiation happened to get onto a surface containing the molecules under study [4-7]. In view of the fact that such observations were made under a great variety of experimental conditions (laser pulse durations and energies, adsorbed molecules or molecular crystals, weak or strong applied electric fields etc.), there is, in all likelihood, no universal mechanism responsible for the production of free ions upon irradiation of a surface by a laser light tuned to resonance with the electronic transitions of the surface molecules. As regards the laser pulse duration τ_{las} the following two productions regimes for free ions may be distinguished.

(1) $\tau_{las} \gtrsim \tau_{therm} = 10^{-9}$ to 10^{-10} s, where τ_{therm} is the thermalization time for the energy absorbed by the molecules in the surface layer. It was shown in our experiments that the process dominating the production of free ions in weak electric fields is the MPI near the surface of the neutral molecules desorbed under the action of the leading edge of the ionizing laser pulse (the molecular desorption in most cases being of thermal nature), despite the fact that the MPI of molecules directly on the surface, followed by the desorption through repulsive states of the ions thus produced [5], is, in principle, possible. In contrast, in strong ($\sim$ 0.1 V/Å) electric fields the photostimulated detachment of ions directly from the surface becomes dominant [10].

(2) $\tau_{las} < \tau_{therm}$. In these conditions, on the surface there may form highly excited states as a result of absorption

of a few photons by some surface molecules, so that the molecules or their fragments, or else ions, may detach from the surface without its being heated until thermal equilibrium is established [11].

In this paper, we will consider (a) the production of free ions upon irradiation of a surface by nanosecond laser pulses /regime (1)/ in a weak electric field, special attention being paid to the use of the IR-UV laser desorption/MPI technique for the detection of surface molecules, and (b) the MPI-stimulated desorption of ions in a strong electric field.

2. Detection of Surface Molecules by IR-UV Laser Desorption/MPI Technique

In surface experiments, the specimen is usually placed directly inside the ion source of a mass spectrometer. This allows the photoions produced to be mass-analyzed. In the simplest case, the specimen, which may be a microquantity of a solid organic substansce (molecular crystals or adsorbed molecules), is irradiated by a single UV-laser pulse. By virtue of the fact that the production of ions is preceded by the thermal evaporation of surface molecules where nanosecond laser pulses are used, the ion signal intensity N_{ion} is proportional to the product of the desorption probability P_{des} and the multiphoton ionization yield η_{mp}:

$$N_{ion} = N_0 \cdot P_{des} \cdot \eta_{mp} \qquad (1)$$

where N_o is number of irradiated molecules. The absorption of radiation in the surface layer causes the temperature of the layer to rise by an amount ΔT which is easy to estimate considering that all the absorbed energy has converted to heat and that the laser pulse duration $\tau_{las} \simeq 10^{-8}$ s is too short for the heat to have enough time to spread into the bulk of the specimen. The molecular desorption rate W_{des} strongly depends on the surface temperature T and is described by the Arrenius -type formula

$$W_{des} = \omega \exp\ (-E_{ads} / kT) \qquad (2)$$

where $\omega = 10^{11}$ to $10^{13} s^{-1}$ is the characteristic vibration frequency of the surface molecules and E_{ads} the adsorption energy. Obviously, the molecular desorption probability is

$$P_{des} = 1 - \exp\left[- \int_0^{\tau} W_{des}\ (t)\, dt \right] \qquad (3)$$

To improve the sensitivity of analysis, it was suggested in [12] that use should be made of a double-frequency IR-UV laser scheme providing for the separation of laser radiation functions as to the evaporation and photoionization of molecules. With this scheme, surface molecules desorb under the effect of the first, IR-laser pulse irradiating the surface and then undergo ionization at some distance from the surface under the resonant action of the

second , UV-laser pulse (Fig.1). Such a functional separation, firstly, allows optimizing the energy of the first, desorning laser pulse to attain a maximum desorption yield (overheating of the surface may cause molecular decomposition) and that of the second, ionizing laser pulse to achieve a maximum photoionization efficiency. Secondly, the use of IR radiation to effect the desorption of surface molecules enables one to avcid undesirable photochemical processes on the surface that may be caused by the UV radiation.

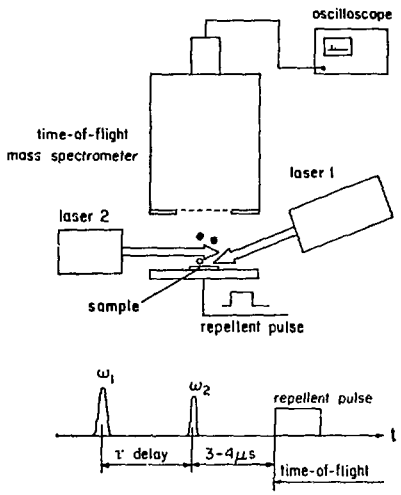

Fig. 1. Experimental setup for pulsed desorption/MPI of molecules

In the approach under consideration, one of the main factors governing the sensitivity of detection of adsorbed molecules is the maximum fraction of surface molecules that can be desorbed without their being decomposed. We have investigated this point using naphthalene and anthracene molecules adsorbed on the surface of graphite.

Figure 2 shows the relationship between the photoion signal intensity for the naphthalene and anthracene molecules and the fluence of the pulsed CO_2 laser irradiating the surface. The fluence dependence of the desorption yield features a plateau in the fluence range 0.05 to 0.3 J/cm^2 for naphthalene molecules and a less distinct plateau in the fluence range 0.15 to 0.3 J/cm^2 in the case of anthracene molecules. In the IR-laser fluence region above 0.3 J/cm^2, a decline of the molecular ion yield, attended by the appearance of the ions of molecular fragments and substrate material, C^+ and C_2^+, is observed for both kinds of molecules. Also observed in this laser fluence region is a bright glow of the substrate, which is indicative of the surface heating to a temperature $T \gtrsim 1000$ K. This causes the decomposition of molecules both on the surface and in a close proximity to it under the effect of the evaporating substrate material.

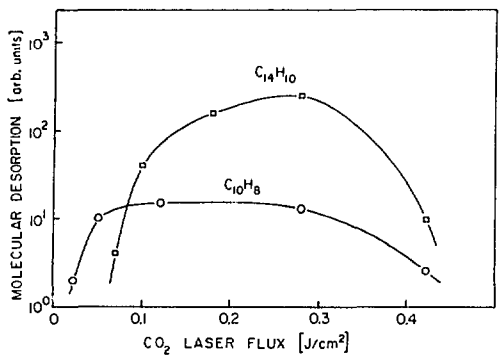

Fig. 2. The dependence of molecular photoionization signal of naphthalene and anthracene adsorbed on graphite (T_{substr} = 200 K) on desorbing laser flux. The ionizing KrF excimer laser flux was fixed to $1.5 \cdot 10^{-2}$ J/cm2

The plateau in Fig.2 corresponds to the saturation of pulsed desorption:

$$W_{des}\ \tau_{las} = \tau_{las}\ \omega \exp(-E_{ads}/kT) \simeq 1 \qquad (4)$$

In this case, it is an easy matter to estimate the sensitivity of surface molecules detection in so far as the efficiency of MPI for the free molecules is known. In our experimental conditions, it comes to 2% for naphthalene molecules [12]. The 10^3-ion /pulse naphthalene signal intensity observed in the experiment in the case of complete desorption of the surface molecules corresponds to 10^6 molecules/cm^2.

The existence of pulsed desorption makes it possible to readily measure the adsorption energy of molecules in conditions of equilibrium between the surface and the gas phase:

$$n_{surf} / \tau_{ads} = n_{gas} v_o / 4 \qquad (5)$$

where n_{surf} and n_{gas} are the respective concentrations of molecules on the surface and in the gas, $\tau_{ads} = 1/W_{des}$ is the time of molecular adsorption on the surface, and v_o the average thermal velocity of the molecules in the gas. According to (5), the value of τ_{ads} can be found by measuring the ratio between the photoion signal intensity N_{surf} in the case of complete desorption of surface molecules (which is proportional to n_{surf}) and the photoion signal intensity N_{gas} from the gas phase in the absence of surface irradiation ($N_{gas} \propto n_{gas}$). In the case of naphthalene [12], measurements of N_{surf}/N_{gas} yielded $\tau_{ads} = 5 \cdot 10^{-3}$s. Substituting into (2) $\omega = 10^{12}$ s^{-1} and T = 200K for estimation purposes, one can easily find the adsorption energy for naphthalene on graphite:

$$E_{ads} = kT \ln(\omega \tau_{ads}) = 0.43 \text{ eV} \quad (6)$$

Substituting this value of adsorption energy into (4) gives the surface temperature corresponding to complete desorption of surface molecules during the time that the CO_2 laser pulse lasts:

$$T = E_{ads}/k \ln(\omega \tau_{las}) = 390 \text{ K} \quad (7)$$

Thus, the experiment demonstrated that under favorable conditions the IR-UV pulsed laser desorption/MPI technique enables one to detect with confidence ultrathin layers (10^{-10} to 10^{-8} monolayer) of surface molecules. This determined further studies into the sensitivity of the technique in the trace analysis of organic and bioorganic molecules in conditions of an ordinary analytical specimen preparation procedure. Tryptophan was chosen as the test substance [13]. Specimens were prepared using (0.02 - 20)- ng/ml aqueous tryptophan solutions. Half a microliter of the solution was applied onto a stainless steel substrate which was dried in air and then placed into the ion source of a time-of-flight mass spectrometer.

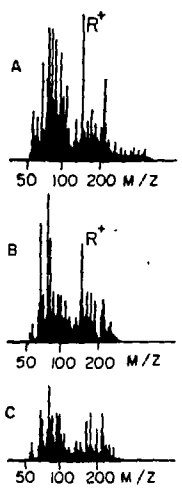

Fig. 3. Laser desorption/MPI spectra of sample containing 10^{-14} g of tryptophan measured in three successive laser shots with constant CO_2 desorbing laser flux 0.3 J/cm^2 and XeCl ionizing laser flux 0.1 J/cm^2

Figure 3 presents time-of-flight (TOF) spectra for the substrate treated with 0.5 μl of a tryptophan solution (20 pg/ml). The TOF spectra (a)-(c) represent a sequence of three laser pulses irradiating one and the same substrate. Since no special measures were taken to purify the solvent and protect the substrate against contamination with solid particles and aerosols from the atmosphere, there is a substantial background noise signal present at the given level of sensitivity. Nevertheless, the intensity of the signal corresponding to the characteristic tryptophan mass m = 130 AMU (indol chromophore) is, in the case of the

first laser pulse, irradiating a substrate with 10^{-14} g of tryptophan, several times in excess of the background noise level.

3. Photostimulated Desorption of Ions in a Strong Electric Field

The adsorption energy of an ion on the surface of a metallic or dielectric substrate is increased by an amount equal to the ion-image potential (3 to 5 eV) for the metal or the polarization energy (0.2 to 1 eV) for the dielectric. It is this fact that materially impedes the desorption of surface ions at low substrate temperatures, as compared with that of neutral surface molecules (E_{ads} = 0.1 - 0.5 eV). However, in the presence of a strong electric field the surface-binding energy of ions may be lowered so that ions may be effectively field-desorbed [14]. In these conditions, the production of surface ions as a result of MPI may, apparently, cause quantum (rather than thermal) effects stimulating the desorption of the ions, and our tentative experimental results [10] favor this assumption.

The experiment on the MPI-stimulated desorption of ions was performed with naphthacene molecules vacuum deposited in a thick layer (10 - 100 monolayers) onto a razor blade (Schick). The blade with the sample substance was placed into the ion source of a time-of-flight mass separator and a positive voltage of 4-11 kV was applied to the blade. It is known from field-ionization experiments that blades of this type provide for an electric field strength of the order of 10^7 V/cm in close proximity to the cutting edge at a blade potential of around 10 kV [15]. The cutting edge of the blade was irradiated with a pulsed KrF excimer laser (λ = 248 nm, E = 0.5 - 5 mJ/cm^2), the radiation being directed in the plane of the blade at an angle of 7° to the edge. The ion desorption signal was recorded by means of an electron multiplier and a storage oscilloscope triggered by the laser pulse.

Figure 4 shows the dependence of the ion signal intensity on the laser fluence. The observed square-law fluence dependences of the ion yield for various blade voltages, along with the strong dependence of the ion signal intensity on the magnitude of this voltage (Fig.5), are the main factors pointing to the fact that, firstly, the ions are field-desorbed and, secondly, the laser stimulation of desorption is of a non-thermal origin.

To interpret the results obtained, we suggest a model explaining the photostimulation of field desorption of molecules from the surface of a dielectric through their photoionization on the surface. Figure 6 presents simplified potential-energy curves for a neutral molecule and an ion in the vicinity of a dielectric surface. Figure 6a illustrates the usual field desorption in a strong (0.1 - 1 V/Å) electric field as a result of deformation of the ionic potential curve and its intersection with the ground neutral state at the coordinate X_c. Neglecting the surface-binding energies of the ion and molecule at the point X_c for qualitative estimation purposes, the threshold condition for

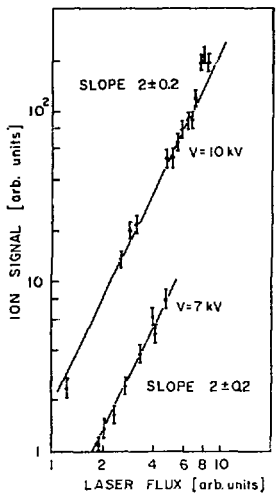

Fig. 4

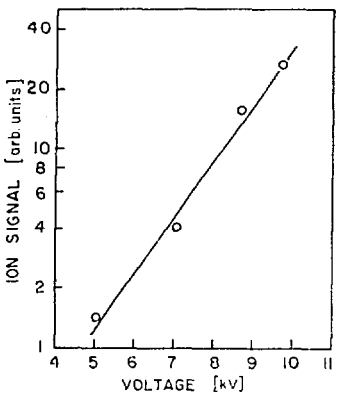

Fig. 5

Fig. 4. The dependence of naphthacene ions desorption yield on KrF excimer laser flux for two different voltages applied to the sharp blade

Fig. 5. The dependence of naphthacene ions desorption yield on the voltage applied to the sharp blade

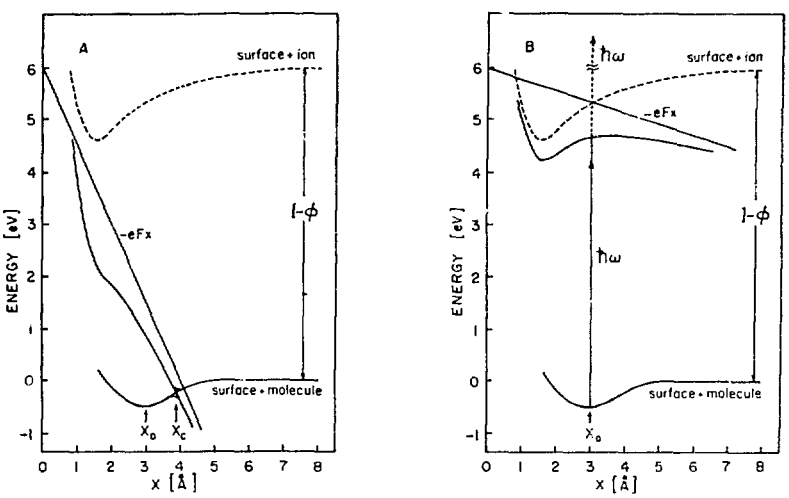

Fig. 6a,b. Ion desorption processes in the presence of strong electric field: (A) field desorption due to interception of neutral and ionic molecular states at X_c [14]; (B) field desorption stimulated by two photon Franck-Condon transition to the repulsive ionic state. F is the electric field strength, I the ionization potential of the free molecule and φ the work function of dielectric

field desorption may be expressed as

$$eFX_c = I - \varphi \simeq 5 - 8 \text{ eV} \qquad (8)$$

where e is the electric charge, F the electric field strength, I the ionization potential of the free molecule, and φ the work function of the dielectric medium. In the case of molecular photoionization on the dielectric surface, the threshold condition for ionic desorption corresponds to the vertical Franck-Condon transition into the saddle point of the ionic potential curve (Fig.6b). By virtue of the fact that the potential of polarization interaction between the ion and the dielectric medium rapidly drops with the increasing coordinate X, and the equilibrium distance between the physisorbed molecule and the surface is greater than that between the ion and the surface, the surface-binding energy of the ion at the point X_o can differ but by a few tenths of an electron-volt from the adsorption energy E_{ads} of the neutral molecule. This allows an immediate estimation of the threshold electric field strength:

$$eFX_o \simeq E_{ads} = 0.2 - 0.5 \text{ eV} \qquad (9)$$

Comparison between (8) and (9) shows that in the case of photoionization of surface molecules, their effective desorption can take place in the presence of substantially lower electric fields. Thus, the photoionization of surface molecules in the presence of a strong electric field may (a) materially lower the critical electric field strength value and (b) change qualitatively the nature of field desorption: photoionization yields ions in a repulsive state, and so no thermal activation is, in principle, required for their detachment. In the case of a metallic surface, the rapid neutralization of the ion consequent upon the transition of an electron from the conduction band, may greatly lower the probability of ionic desorption.

The square-law fluence dependence of the ion yield observed in the experiment is, apparently, attributable to the resonant two-photon ionization of surface molecules, because the ionization potentials of the free naphthacene molecule, I = 6.95 eV, and crystal, I_{cr} = 5.26 eV, are higher than the energy of a single laser photon, $\hbar\omega$ = 5 eV. To estimate the threshold electric field strength, we substitute into (9) X_o = 3 Å and E_{ads} = 0.5 eV to get $F \simeq 2 \cdot 10^7$ V/cm. Further experimental measurements of the spectral dependence of photoion yield will enable us to gain a better insight into the observed phenomenon.

References

1. V.S.Antonov, V.S.Letokhov, A.N.Shibanov: Usp.Phiz.Nauk . (Russian) 142, 177 (1984)
2. U.Boesl, H.J.Neusser, E.W.Schlag: Acc.Chem.Res. 16, 355, (1983)
3. F.Hillenkamp: In "Ion Formation from Organic Solids", ed. by A.Benninghoven. Springer Series in Chemical Physics, Vol. 25 (Springer, Berlin, Heidelberg, New York, 1983) p.190.

4. V.S.Antonov, V.S.Letokhov, A.N.Shibanov: Pis'ma Zh.Exp.Teor. Fiz.(Russian) 31, 471 (1980)
5. V.S.Antonov, V.S.Letokhov, A.N.Shibanov: Appl.Phys. 25, 71 (1981)
6. D.M.Lubman, R.Naaman: Chem.Phys.Let., 95, 325 (1983)
7. R.B.Opsal, J.P.Reilly: Chem.Phys.Lett. 99, 461 (1983)
8. S.E.Egorov, A.N.Shibanov: Kvantovaya Elektronika (Russian) 11, 1397 (1984)
9. V.S.Antonov, V.S.Letokhov, Yu.A.Matveetz, A.N.Shibanov: Laser Chem. 1, 37 (1982)
10. V.S.Antonov, E.V.Moskovetz: Poverkhnost: Fiz.Chim.Mech.(Russian) to be published
11. V.S.Antonov, S.E.Egorov, V.S.Letokhov, Yu.A.Matveetz, A.N. Shibanov: Pis'ma Zh.Exp.Teor.Fiz. (Russian) 36, 29 (1982)
12. V.S.Antonov, S.E.Egorov, V.S.Letokhov, A.N.Shibanov: Pis'ma Zh.Exp.Teor.Fiz. (Russian) 38, 185 (1983)
13. V.S.Antonov, V.S.Letokhov, A.N.Shibanov: Laser Chem. to be published
14. R.Gomer: J.Chem.Phys. 31, 341 (1959)
15. H.D.Beckley: "Principles of field ionization and field desorption mass spectrometry", Intern.Series in Ananlytical Chem., vol.61 (1977) p.61

Experimental Investigation of the Possibilities of the Optical Tunnelling of Electron from a Metal Surface Induced by Strong CO_2 Laser Pulses

Gy. Farkas
Central Research Institute of Physics, H-1525 Budapest 114, POB.49, Hungary

S.L. Chin
Laboratoire de Recherce en Optique et Laser, Département de Physique
Faculté des Sciences et de Génie, Université Laval, Quebec, G1K 7P4, Canada

1. Introduction

According to the fundamental laws of the intense field QED, the general processes governing the laser-induced electron emission from atoms or solids "traditionally" may be interpreted as two complementary limiting interaction processes of the same phenomenon. The first is the "multiphoton" type process, when the electron interacts only with several well determined small number of photons (quantum limit), the second is the "tunnelling" type, when the number of the interacting photons is increasingly high (classical limit). While practically all research activity was concentrated both theoretically and experimentally to the "multiphoton" questions, less attention was paid to the "tunnelling" case, in spite of the fact that the early beginning of the intense field QED started with the pronunciation of this latter.

After a short summarizing formulation of the topics, we describe several experiments performed by us at the Laval University for the study of the laser induced tunnelling. The surface photoeffect of gold proved to be a good experimental tool for these studies giving complementary results to the experiments carried out by us for the tunnel ionization of gas atoms.

2. Brief Formulation of the Topics

Although the questions to be summarized here can be found in nearly every work dealing with multiphoton problems (e.g.Ref.1), for the easy treating and interpreting of the experiments we outline them here.

When a strong laser beam interacts with atoms or solids, electron emission may occur. Many theories have been proposed to describe this process since the early work of KELDYSH [3] leading to different conclusions [2 to 7]. The Keldysh type theories treat this process by calculating the transition probability from the fundamental state as an initial state into a Volkov's final state [9] (Fig.1). The result obtained in this way may analytically be treated very well (Fig.2) as the occurrence of two alternative processes: "traditionally" one uses the so called "Keldysh-type parameter" γ to distinguish the "boundary" between the multiphoton approach ($\gamma>>1$) and the optical tunnel approach ($\gamma<<1$), here $\gamma\equiv\omega\sqrt{2mA}/eE$, where ω and E are the angular frequency and peak electric field of the laser radiation respectively; "A" denotes the ionization potential of the atom or metal (=work function) and e and m are the charge and mass of the electron, respectively. In the first case, which is the higher order perturbation approach, the number of the emitted electrons, or the photocurrent $j\propto|E|^{2n_o}\propto I^{n_o}$ where I is the laser intensity, $n_o\equiv[A/\hbar\omega+1]_{integer}$ is the order of the perturbation. In the second case, when $\gamma<<1$, $j\propto\varphi(E)\exp(-const/E)$ is the optical tunnel current, which reminds one of the static field tunneling formula; here the $\varphi(E)$ preexpo-

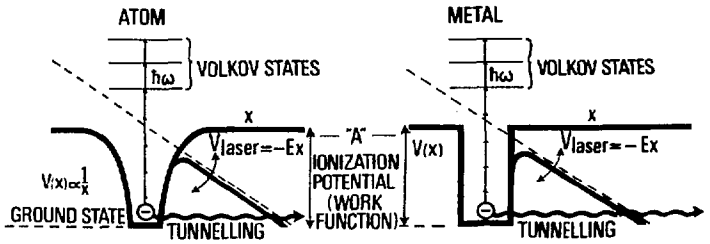

Fig.1 Characteristic parameters of the laser induced electron emission processes

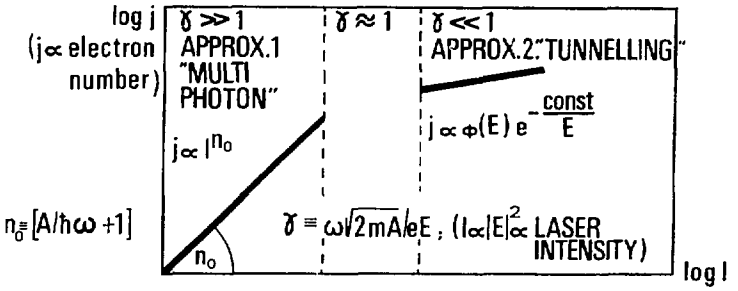

Fig.2 The qualitative summary of the theoretical expectations

nential factor is not very important. It can easily be seen that γ is essentially the parameter, which is characteristic for the validity of the perturbation calculation: $\gamma^2 = A/E_{osc}$ where $E_{osc} = e^2E^2/2m\omega^2$ is the oscillation energy of the electron in the laser field. In other terms $\gamma = \tau\omega/2\Pi = \tau/T$, where τ is the tunnelling time of the electron through the potential barrier narrowed by the laser light of oscillation half period T.

It should be noted that both $\gamma \ll 1$ and $\gamma \gg 1$ cases may be experimentally realized practically in two ways: by changing either E or ω. The two ways are not equivalent. If one varies E by keeping ω constant (visible or near i.r.), $\gamma \gg 1$ during most of the laser pulse temporal envelope, except near the peak where γ starts to be less than 1. Therefore the multiphoton contribution may strongly exceed or mask the low probability tunnel contribution which may occur only around the maximum, where $\gamma \ll 1$ (Fig.3).

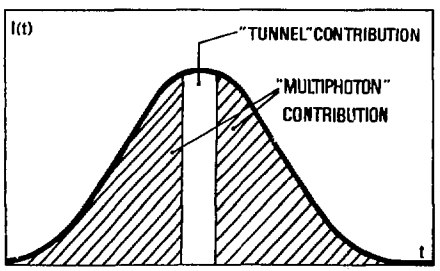

Fig.3 The multiphoton and the tunnelling contributions to the emission

Therefore it is reasonable to use lasers of small ω to realize the condition $\gamma<<1$ for the whole duration of the pulse, when only the tunnel contribution exists.

It can be seen that in principle both atoms and metal surfaces can be used for studying multiphoton and tunnel mechanisms. Here we deal with metal surfaces only; our experiments concerning atoms will be presented in a separate lecture at this Conference.

In the case of metals, however, the occurrence of an additional process may be expected. Electron inside the metallic potential well may dynamically acquire more energy during the laser pulse either by electron heating [10, 11,12] or by inverse Bremsstrahlung [13] considering the very high probability of the latter at a low frequency (e.g. with CO_2 laser). Any of these two effects may change the Fermi distribution without any thermionic emission. These short lifetime high energy electrons, however, having already the new $\gamma'(t)=\omega\sqrt{2mA'}/eE<\gamma=\sqrt{2mA}/eE$ may now escape by a certain "dynamic" tunnelling (Fig.4). This possibility will be discussed below. (It is interesting to note here, that a very similar theoretical suggestion for atoms has been published just recently [14] to realize the above mentioned "dynamic" tunnelling. For the realization of the $\gamma'(t)<<\gamma$ condition the radiation of a laser with relatively great ω will dynamically raise the electron above the fundamental level to an intermediate level, from where another low frequency laser radiation may cause the tunnelling easily.)

At last we note that both in the multiphoton and in the tunnelling cases the laser coherence properties play a predominant role. While, however, the effects of the coherence properties in the multiphoton case are very well known first of all due to the fundamental works of P. LAMBROPOULOS [15], in the case of the tunnelling, only one qualitative attempt can be found [32], although the coherence properties must have a very important role here too.

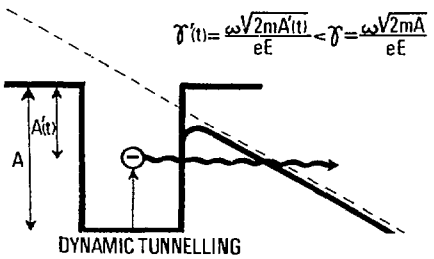

Fig.4 The qualitative model of the "dynamic" tunnelling process

3. Preliminary Experiments

Preliminary experiments have been tried for both gas atoms and metals to demonstrate the possible tunnelling. The experiments concerning gases will be discussed in a separate lecture, therefore we make here only several remarks. In the first experiments [16,17] when the condition $\gamma<1$ was realized using CO_2 laser, no detectable tunnelling was observed probably due to the low detection-efficiency. In another experiment [18] RF radiation and highly excited atoms were used: owing to the many competing multiphoton mechanisms occurring here no definite conclusion could be drawn. With Nd laser at $\gamma<1$ in the experiment [19] only background signals were detected, while in another experiment [20] the $j\propto I^{no}$ multiphoton dependence was always found both for $\gamma>1$ and $\gamma<1$. As we mentioned, in the latter case it is possible that the very weak tunnelling could not be detected in the presence of the multiphoton background, but as we shall see it from the lectures of P.

Agostini and M.J. van der Wiel, the so-called "above-threshold ionization" may also furnish some explanation. At last we succeeded in demonstrating the atomic optical tunnelling at the Laval University [21].

As for metals, the $\gamma \ll 1$ condition could not be achieved with the generally used Nd picosec laser pulses because the high laser intensity needed for this condition exploded the metal. Therefore only the $\gamma \lesssim 1$ condition was approached, consequently the multiphoton current was always predominant. It is known [22] that the photoeffect may exist in two forms: 1) in form of the surface photoeffect when the photocurrent j depends only on the $|E_\perp|$ component perpendicular to the metal surface of the total laser electric field strength $|E|$. 2) in form of the volume photoeffect when j depends only on $|E|$.

The experiments showed that at very high intensities (but still at $\gamma \lesssim 1$) the $j \propto |E_\perp|^{2n_0} \propto I^{n_0}$ perturbation power law [23] passes into the predicted [24,25] $j \propto I^n$ dependence with $n \lesssim n_0$, in the case of surface photoeffect [26,27], while in the case of volume photoeffect [12,28,29,30] with $n > n_0$. These experimental facts have led to the conclusion [28] that during the picosec interactions the energy increase of the Fermi-electrons due to heating supports the multiphoton mechanism ("thermal assisted multiphoton photoeffect" [28]) in the case of volume-effect. On the contrary, for surface photoemission, this effect has not occurred in contrast to the other theoretical expectations [12], manifesting itself rather with the experimentally found $n \lesssim n_0$ result; this fact may also suggest the existence of some possible "thermally assisted" type of very weak tunnelling process. That the occurrence of such a mechanism in principle may be expected follows from the works of KÖRMENDI [31], who has illuminated a metal tip with a continuous laser: applying a high outer static electric field to the tip, they could measure the change of the Fermi distribution due to the laser heating by detecting the increased tunnel current. Being only $E_\perp$ effective in the case of the optical tunnelling, the occurrence of the effect may be expected clearly only in the case of the surface (and not for the volume) photoeffect.

4. Summary of the Predictions for the Experiments

The theoretical works predict relations between measurable quantities on the basis of which the experimentally found mechanism can be identified. Among these the most usual and practical is to determine the $j=f(I)$ relation. The determination of the absolute value of j is difficult and is not necessarily important, the experimental determination of the $n \equiv d(\log j)/d(\log I)$ relation is practically sufficient.

As it was mentioned in the Introduction the occurrence of the two following processes can be expected on the basis of Keldysh's general work [3] and from its application to the case of Au metal ($A=4.679$ eV) and of CO_2 laser ($\lambda=10.6\mu$; $\hbar\omega=0.117$ eV) by BUNKIN and FEDOROV [23], when the laser beam is falling onto the metal surface at a grazing angle and its electric field is perpendicular to this surface (we denote it as $E_\perp$):

1) Optical tunnel emission if $\gamma \ll 1$, then n decreases monotonically with increasing $I=|E_\perp|^2$.

2) In the case of $\gamma > 1$ and $n=n_0[A/\hbar\omega+1]_{integer}=40$, even though the 40th order multiphoton surface photoeffect is rather low, it cannot be excluded in principle. In this case $n=n_0=40$, independent of I.

Beside these pure QED processes in the case of relatively long laser pulses and high I values, the simple Richardson-emission may also occur [10] for which n increases with I, then after passing through a maximum, it decreaes.

Furthermore, as we have mentioned, one can imagine the combined situation, where during the laser pulse, the electrons are raised above the Fermi-level and then ejected by the laser field $E_\perp$ (dynamic optical field emission, si-

milar to BLOEMBERGEN's [26] thermally assisted multiphoton photoeffect) due to the realization of $A'(t) \ll A$, or $\gamma' \ll \gamma$. In this situation n decreases monotonically with I.

Furthermore, we note that the theories [3,23] are working with single-mode laser radiation. At the same time it is well known that the transition from the use of single-mode to multimode laser presents an ($n_0!$) increase [15] in the j value for the pure multiphoton interactions which may have many orders of magnitude. We can not exclude the possibility of similar effect for the optical tunnelling either for multimode laser radiation; this effect (if it exists) - strongly increasing the probability of the otherwise very weak process - may facilitate its observation.

5. Experimental Results

In the first experiment [33] we demonstrated the first observation of the characteristics of the surface electron emission from An surface (A=4.679 eV) induced by strong 4 nsec CO_2 laser pulses (γ=10.6 μ; $h\omega$=0.117 eV). The 4 nsec laser pulse was created by first chopping the smooth output pulse from a hybrid TEA-CO_2 laser oscillator, using an extra-cavity electro-optical switch (CdTe Pockels cell). The chopped-out 4 nsec pulse had a signal-to-noise contrast of about one thousand to one. It was then amplified by a double discharged TEA-CO_2 amplifier using a double pass configuration. The light was slightly focussed by a f=2 m NaCl lens onto a well prepared [26,27,33] and polished ~2 mm thick polycrystalline gold cathode (at a distance of 85 cm from the lens) at a near grazing incidence in the interaction chamber at $\sim 10^{-7}$ Torr. The 10^{-7} Torr proved to be an optimum value: our (and other) former experiments [26,27,28,33] showed that ascending from $\sim 10^{-10}$ Torr up to $\sim 10^{-6}$ Torr, the atomic monolayer evaporated immediately from the surface after the first 2-3 strong laser shots; these first somewhat irregular electron pulses changed their shapes to very regular reproducible shapes. Furthermore, a direct experiment with electron microscopic observation [34] revealed by applying 2-3 laser shots, of a low as 30 MW/cm^2 intensity that atomically clean surfaces might have been produced; our intensities far exceeded the 30 MW/cm^2 value. The polarization direction of the laser electric vector was almost perpendicular to the Au surface ($\equiv E_\perp$). The electrons were collected by another (Ni) electrode kept at +3000 V. Both the laser pulse (detected by a photon drag detector) and the electron signal (detected without an electron multiplier) were swept and photographed simultaneously on a 400 MHz bandwidth fast oscilloscope. Figure 5 shows the typical 4 nsec laser pulse shape (curve "a") and the electron signal shape (curve "b"). It can be seen

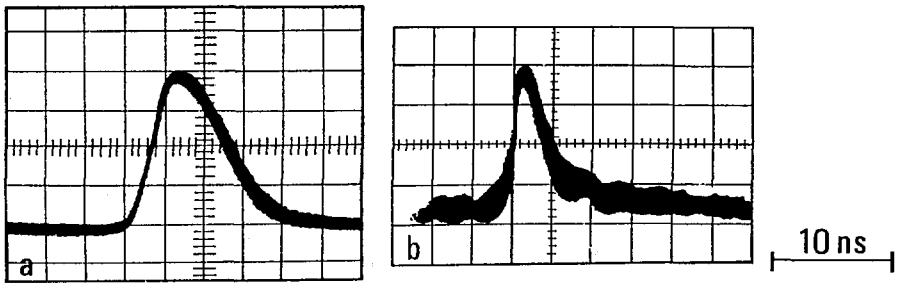

Fig.5 a) The pulse shape of the laser pulse. Horizontal scale 2 nsec/cm. b) The pulse shape of the electron emission signal. Half width: ≤4 nsec. Peak current intensity: 30 mA/cm^2 (The photos are traced for clarity)

that the electron signal duration is a little shorter than that of the laser signal, apart from the superimposed rapid small ripple due to the imperfect electronics. When the laser was adjusted such that the laser electric field was parallel to the gold surface, long (~μs) irregular signals were observed at times after the appearance of the laser pulse characterizing the pure thermionic effect.

The $j=f(I)$ dependence was investigated in the laser intensity range 60 MW/cm^2<I<4 GW/cm^2. The experiment consisted of measuring the slopes n at different I values in this range. The results are n=10, 5 and 2 around I=0.06, 0.12 and 4 GW/cm^2 respectively. Figure 6 shows a typical log-log plot of j versus I while Fig.7 given n versus I in a log-log scale. It can be seen that the measured values of n (points) decrease strongly with I, similar to the theoretically predicted [3,23] "tunnelling" decreasing character. Due to the small values of n found in this experiment, the pure n_0=40 order multiphoton photoeffect (line (c)) and its slight modification $n \leq n_0$ predicted in [24,25] may be discounted. Similarly, the pure thermionic emission due to the heating of the gold cathode by the laser is also excluded: using [10] we calculated the slopes n of the laser-induced pure Richardson-current using a 4 nsec square pulse at 10.6 μm (Fig.7 line (a)). This shows a strong increasing tendency of slope with increasing I, in contrast to that of our experimental points.

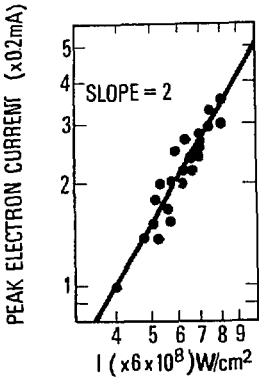

Fig.6 A typical example for the slope determination from the experimental points for n=2

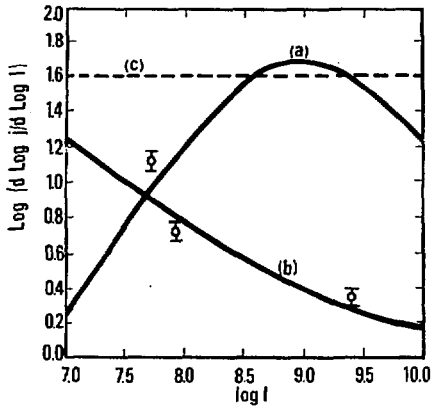

Fig.7 Experimental (points with error bars) and theoretical (full lines) intensity dependence of slope n for different processes

The absolute values of our observed slopes, however, according to the theories [3,23] in the case of pure "tunnelling", is expected to occur at much higher I values. How is it possible at all to get a "tunnelling" character in our relatively low intensity range (where, e.g. γ=6.68 at 4 GW/cm^2)?

According to our remarks made in 4., we may give an explanation on the basis of the occurrence of the "dynamic tunnelling" outlined there. A numerical fit of our experimental points to the tunnelling theory [3] was thus carried out. The best fit (Fig.7 curve (b)) corresponds to a "dynamic" work function A'=0.112 eV. After the formation of A', subsequent "thermally assisted" multiphoton emission can be excluded because the condition of $\gamma \gg 1$ for multiphoton emission valid in [28] does not hold here; also $n \ll n_0$ is true in our case. (This unusual extremely high precision of the work func-

tion is not meaningless considering the new work function measuring method using just the resonance multiphoton photoeffect of Au [35] at high laser intensities.)

In a subsequent experiment [36] carried out by using a train of mode-locked CO_2 laser pulses, we checked further these observations. First of all, if thermionic emission were possible, then due to a possible accumulation effect of the successive pulses (FWHM of ~2 nsec) of such a train, it ought to manifest itself in the lengthening and delaying of the electron pulses with respect to the laser pulses. Secondly, if this heating did not exist, using a pulse train, which presumably contains better pulse-to-pulse coherence stability within the train, the former results [33] obtained with individual pulses would be confirmed further. The experimental setup was the same as in the former [33] experiment, except that we used a different TEA-CO_2 laser mode-locked acoustooptically. A typical pulse train pair is shown in Fig.8, where the curve "a" is the laser pulse train and curve "b" is that of the electron current signal (both traced for clarity). Two aspects were observed in the electron signal. Firstly, the electron current pulse train resembles the laser train showing no significant heating: no delay or lengthening of the individual pulses with respect to the laser pulses occurred. Secondly, the log-log plot of the peak electron current versus the peak laser intensity using the respective pairs of electron and laser pulses of a train shows two different slope values for the ascending and descending parts of the train, respectively. Figure 9 shows a typical plot. The left part of the plot corresponds to the descending, part of the laser pulse train and follows a straight line of slope n=2.2. This slope did not vary much from shot to shot. The right hand part corresponds to the ascending part of the laser train and has steeper slope, varying strongly for different shots. This "double slope" phenomenon is well known in the case of multiphoton photoelectric emission using a mode-locked picosecond Nd: glass 1.06 μ laser pulses [26]. In this latter case it was pointed out that the pulses in the ascending part of the mode-locked train gave rise to photoelectron current that fitted the theory very well [3], because the laser pulses are bandwidth-limited here. The pulses of the descending part of the train gave rise to a higher slope than predicted theoretically; this was attributed to the irregular pulse structures of the subsequent pulses in the descending

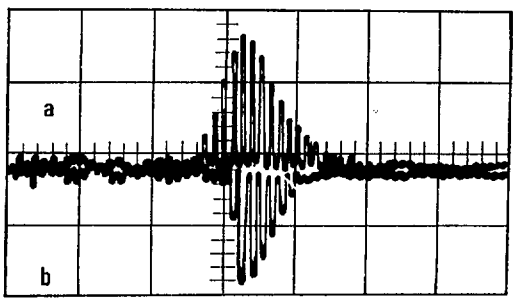

Fig.8 Typical mode-locked CO_2 laser pulse train (top, a) containing ~2.5 nsec pulses separated by 25 nsec and the corresponding electron current pulse train (bottom, b). (Traced for clarity)

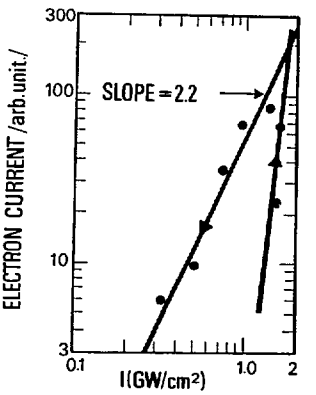

Fig.9 A typical plot of electron peak current vs. laser peak intensity using one pair of pulse tranins shown in Fig.1

part of the train. As for our present case it seems to be therefore reasonable that the mode-locked CO_2 laser pulses in the ascending part of the train are irregular, while those in the descending part are regular. We see thus a reverse situation as compared to the [26] Nd: glass laser's case. (We note, that in contrast to the single photon linear detection, only the higher order processes, e.g. the multiphoton photoeffect or the optical tunnelling are sensitive to the detection of the higher order coherence properties of the laser light, which thus furnishes a useful detection method.) Our most important conclusion is, however, that comparing our recent results using mode-locked CO_2 pulses with those [33] using independent 4 nsec CO_2 pulses, we see that for the same $I \sim 10^9$ W/cm^2 laser intensity value, the slope values n=2.2 and n=2 for the mode-locked case and for the individual pulse case, respectively, coincide even numerically. This means that the data obtained at the descending part of the mode-locked train can be explained again by the dynamic tunnelling.

In conclusion, we have experimentally confirmed both with single CO_2 pulses [33] and pulse trains, that short (nanosecond scale) CO_2 laser pulses at near grazing incidence and at $E_\perp$ polarization induce a non-thermal electron emission from a gold surface which can be explained by a dynamic tunnelling model, and this emission process is to some extent analogous to the pure optical tunnelling predicted [3,23] long ago, and observed by us [21] recently.

Detailed experiments are in progress to study this new phenomenon using shorter pulses in the higher intensity (~100 GW/cm^2) range, where even the "static" $\gamma \ll 1$ condition is valid.

Acknowledgement

We would like to thank the following persons for their help in some of the experiments: P-A. Bélanger, P. Galarneau, I. Grégoire, Z-Y. Niu and F. Yergeau.

References

1. Gy. Farkas, in Multiphoton Processes, Eds. J.H. Eberly and P. Lambropoulos (Wiley, New York, 1978) pp.81-100
2. F.V. Bunkin, A.M. Prokhorov, Sov. Phys. JETP, 22, 844 (1964)
3. L.V. Keldysh, Sov. Phys. JETP, 1307 (1965)
4. S. Geltman, M.R. Teague, J. Phys. B 7, L 22 (1974)
5. J.I. Gersten, M.H. Mittleman, Phys. Rev. A 10, 74 (1974)
6. G.J. Pert, J. Phys. B 8, L 173 (1975)
7. P. Kostic, M.H. Mittleman, Phys. Rev. A 25, 1568 (1982)
9. D.M. Volkov, Z. für Phys. 94, 250 (1935)
10. J. Lin, T.F. George, J. Appl. Phys. 54, 382 (1983)
11. N. Bloembergen, Rev. Mod. Phys. 54, 685 (1982)
12. S.I. Anisimov, N.A. Inogamov, Yu.V. Petrov, Phys. Lett. 55A, 449 (1976)
13. N.M. Kroll, K.M. Watson, Phys. Rev. A 8, 809 (1973)

14. N.B. Delone, N.L. Manakov, A.G. Fainshtein, ZhETF 86, 906 (1984)

15. P. Lambroponlos, in Advances in Atomic and Molecular Physics, Vol. 12, (Academic, New York, 1976) pp.87-142

16. G. Mainfray, in Electronic and Atomic Collisions, Ed. G. Watel (North--Holland, Amsterdam, 1978) pp.699-712

17. J. Black. E. Yablonovitch, IEEE J. Quant. Elect. QE13, 117 (1977)

18. J. Bayfield, L. Gardner, P. Koch, Phys. Rev. Lett. 39, 76 (1977)

19. B.W. Boreham, "Europhysics Study Conference on Multiphoton Processes, Bénodet, France, June 18-22, 1979 (Private communication)

20. L-A. Lompré, G. Mainfray, C. Manus, C. Repoux, J. Thébault, Phys. Rev. Lett. 36, 949 (1976)

21. S.L. Chin, Gy. Farkas, F. Yergeau, J. Phys. B 16, L 223 (1983)

22. K. Mitchell, Proc. Roy. Soc, 146 A, 442 (1934)

23. F.V. Bunkin, M.V. Fedorov, Sov. Phys. JETP 21, 896 (1965)

24. A.P. Silin, Sov, Phys. Solid State 12, 2886 (1971)

25. A.M. Brodsky, phys. stat. sol. (b) 83, 331 (1977)

26. Gy. Farkas, Z.Gy. Horváth, Opt. Comm. 12, 392 (1974)

27. L-A. Lompré, J.Thébault, Gy. Farkas, Appl. Phys. Lett. 27, 110 (1975)

28. R.Yen, J. Liu, N. Bloembergen, Opt. Comm. 35, 277 (1980)

29. J.H. Bechtel, W.L. Schmidt, N. Bloembergen, Opt. Comm. 12, 392 (1975)

30. R. Yen, P. Liu, M. Dagenais, N. Bloembergen, Opt. Comm. 31, 334 (1979)

31. F.F. Körmendi, J. Phys. E 7, 1004 (1974)

32. J. Bergou, Gy. Farkas, Z.Gy. Horváth, Acta. Phys. Acad. Sc. Hung. 32, 319 (1972)

33. Gy. Farkas, S.L. Chin, P. Galarneau, F. Yergeau, Opt. Comm. 48, 275 (1983)

34. S.M. Bedair, H.P. Schmidt, J. Appl. Phys. 40, 4776 (1969)

35. L-A. Lompré, G. Mainfray, C. Manus, J. Thébault, Gy. Farkas, Z.Gy. Horváth, Appl. Phys. Lett. 33, 124 (1978)

36. Gy. Farkas, S.L. Chin, to be published.

Index of Contributors

Springer Series in Chemical Physics

Editors: **V.I. Goldanskii, R. Gomer, F.P. Schäfer, J.P. Toennies**

Volume 1
I.I. Sobelman

Atomic Spectra and Radiative Transitions

1979. 21 figures, 46 tables. XII, 306 pages
ISBN 3-540-09082-7

"... this book presents a wealth of information about the quantum mechanics of free atoms ... it is nearly a must." *Applied Optics*

Volume 5
W. Demtröder

Laser Spectroscopy

Basic Concepts and Instrumentation
2nd corrected printing. 1982. 431 figures.
XIII, 696 pages. ISBN 3-540-10343-0

From the reviews: "The scope of this book is most impressive. It is authoritative, illuminating and up-to-date. The 650 pages of text are supplemented by 34 pages of references, and many of the chapters are furnished with a selection of problems. It is strongly recommended for all spectroscopists of the laser era and will be valuable for research students entering spectroscopic laboratories." *Contemporary Physics*

Volume 10

Lasers and Chemical Change

By A. Ben-Shaul, Y. Haas, K.L. Kompa, R.D. Levine
1981. 245 figures. XII, 497 pages
ISBN 3-540-10379-1

Contents: Lasers and Chemical Change. - Disequilibrium. - Photons, Molecules, and Lasers. - Chemical Lasers. - Laser Chemistry. - References. - Author Index. - Subject Index.

Volume 22
V.S. Letokhov

Nonlinear Laser Chemistry

Multiple Photon Excitation
1983. 152 figures. XIV, 417 pages
ISBN 3-540-11705-9

Contents: Introduction. - Selective Photoexcitation of Atoms and Molecules. - Multi-Step Selective Photoionization of Atoms. - Selective Monomolecular Photoprocesses with Nonlinear Excitation of Electronic States. - Multi-Photon Monomolecular Photoprocesses in the Ground Electronic State. - Laser Photoseparation on an Atomic and a Molecular Level. - Selective Laser Detection of Atoms and Molecules. - Laser Photochemistry and Photobiochemistry. - Main Notations. - References. - Additional Reading. - Subject Index.

Volume 28
N.B. Delone, V.P. Krainov

Atoms in Strong Light Fields

1985. 49 figures. XII, approx. 345 pages
ISBN 3-540-12412-8

Contents: Introduction. - Time-Dependent Perturbation Theory. - The Resonance Approximation. - The Adiabatic Approximation. - Laser Radiation. - Experimental Aspects. - Nonresonant Phenomena. - Resonance Phenomena. - Conclusion. - Notation Index. - References. - Subject Index.

Volume 38

Ultrafast Phenomena IV

Proceedings of the Fourth International Conference Monterey, California, June 11-15, 1984
Editors: **D.H. Auston, K.B. Eisenthal**
1984. 370 figures. XVI, 509 pages
ISBN 3-540-13834-X

Contents: Part I: Generation and Measurement Techniques. - Part II: Solid State Physics and Nonlinear Optics. - Part III: Coherent Pulse Propagation. - Part IV: Stimulated Scattering. - Part V: Transient Laser Photochemistry. - Part VI: Molecular Energy Redistribution, Transfer, and Relaxation. - Part VII: Electronics and Opto-Electronics. - Part VIII: Photochemistry and Photophysics of Proteins, Chlorophyll, Visual Pigments, and Other Biological Systems. - Index of Contributors.

Springer-Verlag
Berlin
Heidelberg
New York
Tokyo

Coherent Nonlinear Optics

Recent Advances

Editors: **M.S. Feld, V.S. Letokhov**
1980. 2 portraits, 134 figures, 18 tables.
XVIII, 377 pages. (Topics in Current Physics, Volume 21). ISBN 3-540-10172-1

Contents: *M.S. Feld, V.S. Letokhov:* Coherent Nonlinear Optics. – *M.S. Feld, J.C. MacGillivray:* Superradiance. – *V.P. Chebotayev:* Coherence in High Resolution Spectroscopy. – *G. Grynberg, B. Cagnac, F. Biraben:* Multiphoton Resonant Processes in Atoms. – *C.D. Cantrell, V.S. Letokhov, A.A. Makarov:* Coherent Excitation of Multilevel Systems by Laser Light. – *A. Laubereau, W. Kaiser:* Coherent Picosecond Interactions. – *M.D. Levenson, J.J. Song:* Coherent Raman Spectroscopy.

Excimer Lasers

Editor: **C.K. Rhodes**
2nd enlarged edition. 1984. 100 figures.
XII, 271 pages. (Topics in Applied Physics, Volume 30). ISBN 3-540-13013-6

Contents: *P.W. Hoff, C.K. Rhodes:* Introduction. – *M. Krauss, F.H. Mies:* Electronic Structure and Radiative Ttransitions of Excimer Systems. – *M.V. McCusker:* The Rare Gas Excimers. – *C.A. Brau:* Rare Gas Halogen Excimers. – *A. Gallagher:* Metal Vapor Excimers. – *D.L. Huestis, G. Marowsky, F.K. Tittel:* Triatomic Rare-Gas-Halide Excimers. – *H. Pummer, H. Egger, C.K. Rhodes:* High-Spectral-Brightness Excimer Systems. – *K. Hohla, H. Pummer, C.K. Rhodes:* Applications of Excimer Systems. – List of Figures. – List of Tables. – Subject Index.

Springer-Verlag
Berlin
Heidelberg
New York
Tokyo